„Role of unphosphorylated STAT5 in maintenance of Acute Myeloid Leukemia cells “

Dissertation

Zur Erlangung des Grades

Doktor der Naturwissenschaften

Am Fachbereich Biologie

der Johannes-Gutenberg-Universität Mainz

Jakub Szybinski

geb. am 1.09.1989 in Krakau, Polen

Mainz, 2018

Tag der mündlichen Prüfung: 18.02.2019

Abstract

Background

In its phosphorylated state, the Signal Transducer and Activator of Transcription 5 (STAT5) A and B form homo- or heterodimers, which bind to chromatin and activate expression of target genes. In leukemia models harboring FLT3-ITD, BCR-ABL or JAK2 mutations, constitutive phosphorylation of STAT5 activates key proliferation and survival transcriptional programs. Recent studies in mouse hematopoietic progenitor cells suggest a distinct function of unphosphorylated STAT5 (uSTAT5): via restricting the access of ERG to target genes uSTAT5 acts as a repressor of megakaryocytic transcriptional programs [1]. The goal of this study is to examine the biological role of uSTAT5A and B in acute myeloid leukemia (AML) and to explore their role as potential therapeutic targets.

Results

We initially screened a panel of human AML cell lines and patient samples for STAT5A and STAT5B expression and phosphorylation at defined tyrosine residues. Most of the samples displayed strong expression of both STAT5A and STAT5B. Phosphorylation of STAT5 proteins at tyrosine 694 (pSTAT5A) and 699 (pSTAT5B) residues was strongly dependent on the presence of FLT3-ITD mutations. To explore the role of uSTAT5A/B, we performed doxycycline-inducible, short-hairpin RNA (shRNA) mediated knock-down of STAT5A and STAT5B. Targeting STAT5A or STAT5B severely suppressed cell proliferation across the entire tested panel; nevertheless, differentiation assays revealed that only the suppression of uSTAT5B induced cellular differentiation. In line, gene expression profiling by high-throughput sequencing (RNA-seq), demonstrated enrichment of monocytic differentiation programs in the THP-1 cell line upon loss of uSTAT5B. To further assess the distinct effects of STAT5A and STAT5B, we performed SILAC-based mass spectrometry and identified several STAT5 interacting partners in AML cell lines. While uSTAT5A primarily was found to be associated with proteins involved in RNA processing and translation initiation pathways, uSTAT5B co-precipitated chromatin- and histone-binding proteins, such as the transcription factor ETV6 or the histone H3K4 demethylase KDM5C.

Finally, to elucidate the role of STAT5 on leukemic cell function in a mouse model, *Stat5*$^{fl/fl}$ or *Stat5*$^{fl/fl}$_Mx1-Cre bone marrow cells were transformed with a retroviral construct of *Mll/Af9* and transplanted into lethally irradiated mice. In the second round of transplantations, we performed a pIpC induction of Mx-1-Cre recombinase to explore, whether complete excision of *Stat5* can prevent leukemia development. Surprisingly, animals transplanted with *Stat5*-depleted MA9 cells died briefly after excision with median survival of 15 days, while median survival of the *Stat5*$^{fl/fl}$ control was 26 days. Bone marrow cells from both cohorts were investigated for the expression of CD11b and Gr-1, both markers of differentiated hematopoietic cells. Interestingly, the *Stat5*$^{fl/fl}$_*Mx1-Cre*-MA9-group, depleted of *Stat5,* showed a strong increase in the double-positive cells compared to control group suggesting a more mature phenotype.

Summary

In summary, our data indicate that uSTAT5B is involved in the regulation of differentiation through modulation of the epigenetic landscape and transcriptional programs of leukemic cells. Targeting of uSTAT5B or its downstream pathways might represent an interesting novel strategy in AML treatment.

Contents

List of abbreviations

Abbreviation	Explanation
AGM	aorta-gonad mesonephros
AML	acute myeloid leukemia
APC	antigen-presenting cells
APL	acute promyelocytic leukemia
AraC	cytosine arabinoside
ATRA	all-trans retinoic acid
BC	band cell
BM	bone marrow
BMT	bone marrow Transplantation
CART	chimeric antigen receptor-T
CD	cluster of differentiation
CFC	colony forming cell
ChIP	Chromatin Immunoprecipitation
CLP	common lymphoid progenitors
CML	chronic myeloid leukemia
CMP	common myeloid progenitors
CPM	counts-per-million
CR	complete remission
DEG	differentially expressed genes
DHE	Dihydroergotamine
DMEM	Dulbecco's Modified Eagle's Medium
DMSO	Dimethyl sulfoxide
DOX	Doxycycline
DSigDB	drug signatures database
EFS	event-free survival
FBS	Fetal Bovine Serum
FDA	Food Drug Administration
FLT3-ITD	fms-related tyrosine kinase 3 internal tandem duplication
FL	FLT3 ligand
GAS	γ-interferon-activated sequences
GH	growth hormone
GHR	growth hormone receptor
GM-CSF	Granulocyte-macrophage colony-stimulating factor
GMP	granulocyte and macrophage progenitors
GO	Gene Ontology
GPP	Genetic Perturbation Platform
GSEA	Gene Set Enrichment Analysis
HLA	human leukocyte antigen
HSC	hematopoietic stem cells
IP	Immunoprecipitation
IPA	Ingenuity Pathway Analysis
LMPP	lymphoid-primed multipotent progenitor
LSC	leukemic stem cells
LTC-IC	long-term culture-initiating cell
MDS	myelodysplastic syndrome

MEP	megakaryocyte and erythrocyte progenitor
MFI	Median Fluorescence Intensity
MM	Metamyelocyte
Mono	Monocyte
MPN	Myeloproliferative neoplasm
MPP	multipotent progenitors
MSigDB	Molecular Signatures Database
MTT	3-[4,5-dimethylthiazole-2-yl]-2,5-diphenyltetrazolium bromide
My	Myelocyte
MyB	myeloid progenitor with B cell potential
MyBT	myeloid progenitor with B cell and T cell potential
MyE	myeloid progenitor with erythroid potential
MyT	myeloid progenitor with T cell potential
nes	nuclear export sequence
NES	normalized enrichment score
NK	natural killer
NPM1	nucleophosmin 1
OS	overall survival
PBS	Phosphate-buffered saline
PCA	principle component analysis
pIpC	polyinosinic-polycytidylic acid
PM	Promyelocyte
PMN	polymorphonuclear cells
PSP	Proline-Serine-Proline motif
pSTAT5	phosphorylated STAT5
qRT-PCR	quantitative reverse-transcription PCR
RBC	Red Blood Cells lysis buffer
RIN	RNA integrity number score
RNA-seq	RNA-sequencing
ROS	reactive oxygen species
RPMI	Roswell Park Memorial Institute
Sca-1	stem cell antigen 1
SCCHN	squamous cell carcinoma of the head and neck
SD	standard deviation
sgRNA	single-guide RNA
SH2	Src Homology 2
shRNA	short haiprin RNA
SILAC	Stable Isotope Labeling by Amino acids in Cell culture
STAR	Spliced Transcripts Alignment to a Reference
STAT	Signal Transducer and Activator of Transcription
TCGA	The Cancer Genome Atlas
TLR	Toll-like receptor
uSTAT5	unphosphorylated STAT5
WBC	white blood cell
WHO	World Health Organization
WT	wild-type

Introduction

Hematopoiesis

Hematopoiesis - from Ancient Greek αἷμα (haima), "blood" and ποιεῖν (poesis), "to make"- can be described as combination of precisely orchestrated processes that govern the maturation of blood system cells.

Development of the hematopoietic system can be divided in the embryonic phase described as "primitive wave" of hematopoiesis that develops into "definitive hematopoiesis". In adults, definitive hematopoiesis becomes the exclusive way of blood production.

The primitive wave of hematopoiesis comprises the production of primitive erythroid and macrophage progenitors taking place in the yolk sac [2]. The following events contributing to embryonic blood production are not limited to one location, as this happens at a stage when the whole blood system is developing. During embryonic development hematopoietic stem cells (HSC) are first observed in an area surrounding the dorsal aorta termed the aorta-gonad mesonephros (AGM) region around E9.5, then migrate to the fetal liver around E12.5 and shortly before birth colonize the fetal thymus, spleen and finally the hematopoietic stem cell niche in the bone marrow (BM) [3], [4]. This is a final stage of the migration and their home throughout a life-time of an adult [5]. During the time of migration HSCs can be characterized as cycling cells, whereas after engraftment in the bone marrow niche they became mainly quiescent [6] and are maintained in a condition of relative hypoxia [7].

The definitive, mature hematopoiesis can be described as process that relies on small-number of self-renewing HSCs residing in the bone marrow niche of adults. By cellular divisions HSCs can give rise to a progenitor cells able to mature into a lineage specific functional blood cells or produces another HSC.

Functional transplantation assays in murine animal models revealed the ability of HSC to reconstitute the entire functional blood system for more than 24 weeks. In similar experiments the existence of multipotent progenitors (MPP) of limited re-population capacity and a finite self-renewal potential were identified [8]. In syngeneic transplantation experiments, HSC numbers in the BM were quantified applying limited dilution assays and estimated that 1 HSC cell can be found in 10.000 BM cells [9]. To properly define and further characterize the cells, scientists aimed at defining HSC surface markers in the past two decades. Today researchers know that murine HSCs express CD117 (c-Kit), stem cell antigen 1 (Sca-1) and are low in mature cell surface marker expression (lineage markers negative cells) [10]. By incorporation of SLAM family markers (CD150, CD244, and CD48) purification of murine HSC became even more efficient, yielding in 1 HSC in 1.3 analyzed cells [11].

Murine hematopoiesis reflects human in many ways, but the identification and purification of human HSC is more challenging and requires different surface markers [12]. First *in vitro* experiments to identify the surface markers - long-term culture-initiating cell assay (LTC-IC) were performed with hematopoietic BM cells cultured on a monolayer of feeder cells to identify progenitor cells being capable of producing hematopoietic cells for 5 weeks or longer. This resulted in the identification of a cell population defined as lineage negative, CD34 positive, in which the percentage of LTC-ICs is enriched 800-fold [13]. Further studies using the same model reported that long-term cultures initiated with CD34+CD38- cells from BM generated threefold to fourfold more progeny than previously observed [14]. To define the markers and function of human HSC more precisely researchers took advantage of *in vivo* models. McCune and colleagues used the SCID-hu mouse model to identify HSC

populations among Lin-CD34+CD90+ cells [15], whereas other groups reported that with help of the NOD/SCID mice model transplantation of Lin-CD34+CD38-/lo cells caused long-term multipotent human hematopoiesis in recipients and resulted in the ability to form secondary and tertiary transplantations [16]. In clinical trials, where population of Lin-CD34+CD90+ cells were transplanted, long-term engraftment was observed and confirm these findings. Majeti and colleagues expanded this view by utilizing in vivo transplantation studies and demonstrated the Lin-CD34+CD38-CD90+CD45RA- cord blood fraction to contain human HSC whereas the Lin-CD34+CD38-CD90-CD45RA- fraction comprises of human multipotent progenitors [17].

Classification/ Hierarchy

A classic hematopoiesis hierarchy assumes HSCs as the only self-renewing cell type that persists life-long, maintains it self-renewal activity and gives rise to all functional blood cells. Divisions of HSC can be described as either "asymmetric renewal" giving rise to a daughter HSC cell and a committed progenitor cell, or an occasional symmetric renewal division may take place leading to the generation of two daughter HSCs. Another possibility is an extinction division resulting in two progenitor cells and clonal extinction of the parental HSC [18], [19].

Over the past decades several models of hematopoietic cell hierarchies were proposed by different groups. By introduction of a bifurcation model (Fig. 1A) Weissman's group has identified two mutually exclusive populations: common lymphoid progenitors (CLPs - giving rise to B cells, T cells, and natural killer (NK) cells) and common myeloid progenitors (CMPs – giving rise to granulocytes, macrophages, erythrocytes, and platelets) in bone marrow and fetal liver [20], [21]. In this model announced eighteen years ago, HSCs give rise to MPPs which maintain differentiation potential into all lineages but lose the self-renewal capability of HSCs.

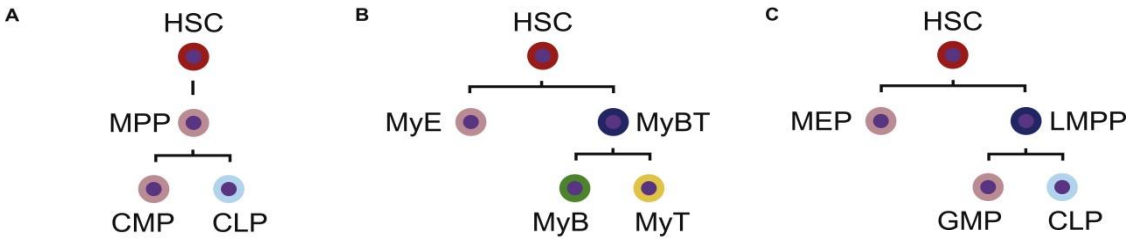

Figure 1. HSC differentiation models. Bifurcation (A), Myeloid-based (B), and LMPP (C) models of hematopoietic progenitors hierarchy. CLP = common lymphoid progenitor; CMP = common myeloid progenitor; GMP = granulocyte and macrophage progenitor; LMPP = lymphoid-primed multipotent progenitor; MEP = megakaryocyte and erythrocyte progenitor; MPP = multipotent progenitor; MyB = myeloid progenitor with B cell potential; MyBT = myeloid progenitor with B cell and T cell potential; MyE = myeloid progenitor with erythroid potential; MyT = myeloid progenitor with T cell potential. Adapted from Ema H, Experimental Hematology, 2014.

Another model, the myeloid-based theory (Fig1 B) proposed by Kawamoto et al., describes the existence of new progenitors: myeloid progenitor with erythroid potential (MyE), myeloid progenitor with B cell and T cell potential (MyBT) and others directly below in the hierarchy: MyB progenitors, and MyT progenitors. This model could not differentiate between HSCs and previously described progenitors, as the in-vitro assays design was unable to detect HSC [22].

Another model has been proposed by Jacobsen's group, which combines elements of the bifurcation and myeloid-based models (Figure 1C). They identified a novel lymphoid-primed MPPs (LMPPs) that

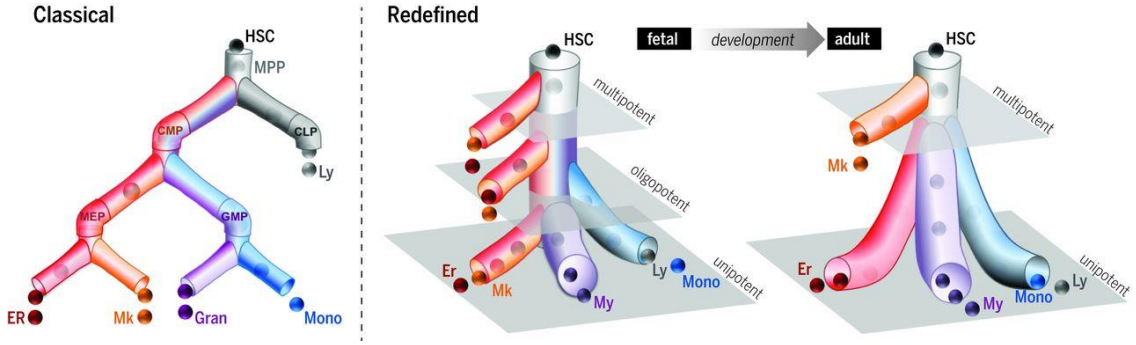

Figure 2. Roadmaps of human blood stem cell differentiation. HSC = hematopoietic stem cell; MPP = multipotent progenitor; CLP = common lymphoid progenitor; CMP = common myeloid progenitor; GMP = and granulocyte and macrophage progenitor; MEP = megakaryocyte and erythrocyte progenitor; My = myeloid cells, Er = erythroid cell; Mk = megakaryocyte cells; Mono = monocytes; Ly = lymphoid cells. From Notta F, Science 2016.

can give rise to either granulocyte and macrophage progenitors (GMP) or CLPs. Another progenitor branching from HSCs is the megakaryocyte and erythrocyte progenitor (MEP) [23].

With development of single-cell techniques and sequencing technologies detailed evaluation of the potential of each progenitor population became possible and allowed revision of the classic hematopoietic hierarchy. Notta and colleagues with help of fluorescent sorting purified populations known as MPPs, CMPs, and MEPs revealing substantial cellular heterogeneity within these populations. By assessing the reconstitution potential of these cell populations in mice the authors found that megakaryocytes were derived directly from HSCs (or MPPs), thereby obviating a lineage differentiation route via oligopotent CMPs and MEPs intermediates. On top of that, single-cell transcriptome analysis of cord-blood and adult BM failed to detect cells such as CMPs or MEP that express multiple lineage specific genes concluding that either these populations represent a highly transient cellular state, or they simply do not exist. In line with previous findings in the fetal development, analysis of hematopoietic cells in the fetal liver demonstrated erythroid/megakaryocytic progenitors reside in the stem cell compartment. To summarize these findings the authors, propose a new two-tier model of hematopoiesis assuming a highly multipotent HSC (and MPPs) in the top-tier, and committed unipotent progenitors in the bottom-tier, without lineage restricted multipotent intermediaries (Figure 2) [24].

Acute Myeloid Leukemia

Acute myeloid leukemia (AML) is a form of a cancer in which blood progenitor cells acquire genetic alterations and mutations that lead to their hyper-proliferation, increased self-renewal activity and a block in differentiation (Gilliland D, Tallman M, Cancer Cell 2002). AML was completely incurable 50 years ago, but nowadays can be cured in 35 to 40% of younger patients (<60 years old) and in 5-15% of older patients (>60 years old) [25]. Chances of induction of complete remission and adequate treatment choice made by clinicians are dependent on proper classification of the disease. Identification of prognostic markers and integration in clinical treatment decision was an area of intensive research in the past decades. Recent years also brought substantial advances in present treatments and (hopefully) breakthroughs in the future thanks to novel specific drugs. This chapter will summarize the classification, prognostic markers as well as current and future treatment strategies in AML.

Classification

Cytology (morphology assessment of BM and blood smears), cytogenetics and modern molecular approaches (e.g. sequencing of DNA to screen for selected molecular marker) are mandatory to classify AML into defined subtypes. The first classification of AML introduced in 1976 named the French–American–British (FAB) classification system defines eight subtypes of the disease (M0 through M7) and is based on morphological and cytochemical characteristics of the leukemic cells. In 2008, the World Health Organization (WHO) classified AML into 7 groups [26] and was revised recently in 2016. By incorporating genetic information with morphology, immunophenotype and clinical presentation, the current classification proposed 6 main categories presented in the table 1 [27].

	AML Categories
1	AML with recurrent genetic abnormalities
2	AML with myelodysplasia-related features
3	therapy-related AML
4	AML not otherwise specified
5	myeloid sarcoma
6	myeloid proliferation related to Down syndrome

Table 1. Classification of AML. Categories proposed by WHO in 2016 (Arber D, Blood 2016).

Prognostic markers

The prognosis of an individual patient can be estimated with help of patient related and disease related prognostic markers. On top of that, establishment of molecular genetic markers has been an active research area in the recent decades. Currently, three molecular markers used in clinical practice are nucleophosmin 1 (*NPM1)* and CCAAT/enhancer binding protein α (*CEBPA)* mutations and fms-related tyrosine kinase 3 (*FLT3)* internal tandem duplications [25]. Additionally, prognosis of patients can be estimated by cytogenetic profiles. The disease can be categorized into favorable (patients with the chromosomal rearrangements t(8;21), t(15;17) or inv(16)), intermediate (patients with normal karyotype), and adverse (complex karyotype - 3 or more chromosomal abnormalities, monosomy of 5

or 7, t(6;9)) prognostic risk [28], [29]. New ELN classification from 2016 extended this categorization by adding *NPM1*-mutated and *NPM1*-mutated-*FLT3*-ITD^{low} patients to the favorable prognostic risk group and *NPM1* mutated-*FLT3*-ITD^{high} as well as *RUNX1*, *ASXL1*, and *TP53* mutated patients to the group of adverse prognostic risk [30].

Current therapy

The current therapeutic approach remained substantially unchanged in the last 30 years. Eligible patients first undergo induction therapy to achieve complete remission (CR). The mainstay of induction therapy consists of the '7+3' regimen combining 7 days cytarabine (cytosine arabinoside or AraC) with 3 days of anthracycline. Around 60–80% of patients with *de novo* AML will achieve CR with induction therapy [31]. Standard post-remission (consolidation) strategies include conventional chemotherapy as well as hematopoietic stem cell transplantation for selected patients. In majority of patients disease relapse is observed within 3 years from diagnosis. Intensive salvage regimens contain chemotherapy and hematopoietic stem cell transplantation but will only applied if the patient is fit to undergo it. Alternatively, patient can be treated with new investigational therapies.

Acute promyelocytic leukemia (APL) is a leukemia subtype characterized by an accumulation of abnormal promyelocytes in the BM and an increased risk of bleeding. Majority of patients carry a chromosomal translocation t(15;17) [32] resulting in the leukemogenic PML-RARα fusion protein [33]. Disease was first approached with classic anthracycline based treatment [34], but patients failed to achieve CR. Introduction of all-trans retinoic acid (ATRA) by Huang and colleagues in late 80' led to first reported CRs in APL patients, but due to high relapse rate complete remission was still low [35]. To resolve this problem combinational therapies with chemotherapeutics were tested with different time and order of treatments and further increased the percentage of patients achieving a CR [36]. By combining ATRA and chemotherapy simultaneously, followed by two courses of chemotherapy alone and finally ATRA in combination with low doses of chemotherapy as a maintenance therapy for two years long-term survival was achieved in up to 90% of patients.

New therapies

FLT3-ITD inhibitors

One of the molecular markers associated with poor outcome and present in 25% of AML patients is an internal tandem duplication (ITD) of the FLT3 tyrosine kinase (FLT3-ITD) [37]. As a potential target for treatment it was subject of broad investigations in recent decades and several specific FLT3-ITD inhibitors were evaluated in clinical trials [38], [39], [40]. Unfortunately, single agent treatment with these inhibitors lead only to a transient decrease in BM blast percentage, was characterized by toxicity due to off-target effects and has been proven to cause resistance via mutations within FLT3 domains. Combination of standard therapy with sorafenib, a multityrosine kinase inhibitor, was beneficial for event-free survival (EFS) but not overall survival (OS) [41].

Another first generation FLT3 inhibitor with significant single-agent impact on AML cells is Midostaurin also known as PKC412 [42]. Recently, the results of a randomized, double-blind clinical trial of 717 patients with FLT3 mutations treated with PKC412 in combination with standard therapy were published [43]. Compared to a placebo control group, PKC412 treatment resulted in significantly higher OS and EFS, but no difference in the rate of complete remission was observed.

Currently there are clinical trials ongoing with second generation FLT3 inhibitors like quizartinib. It is designed to be exclusively specific to its target helping to reduce cytotoxic effects caused by off-target

activity. Although showing promising results in phase I and II clinical trials, quizartinib therapy has also led to the development of resistance [44]. Another second generation FLT3 inhibitor is crenolanib. In contrast to other FLT3 inhibitors, crenolanib was proven to be efficient in inhibition of resistance mutations within FLT3 caused by previous treatment with quizartinib [45]. Several clinical trials including crenolanib are ongoing.

IDH inhibitors

In approximately 20% of de novo AML cases there is present IDH1/IDH2 gain of function mutation [37]. There are several inhibitors (AGI-6780, AG-221) available to target this de-regulation and initial experiments proven their value *in vitro* and *in vivo* [46].

Other therapeutic approaches

Another approach of targeting leukemic blasts is a treatment with monoclonal antibodies targeted against antigens on the AML cells surface. The mechanism of action is either through an antibody-dependent cytotoxicity, or cytotoxic agents used as antibody conjugates. The most famous antibody broadly investigated for treatment of AML is Gemtuzumab ozogamicin recognizing CD33 trans-membrane protein present on the surface of cells of myeloid lineage. Initially approved by the Food Drug Administration (FDA) for the treatment of elderly AML patients, it was reported to cause increased fatal cytotoxicity without impacting the disease-free or overall survival [47]. Further studies showed a beneficial effect of Gemtuzumab in treatments combined with standard therapy [48].

Chimeric antigen receptors are synthetic T-cell receptors with antibody-like specificity. Created by synthesis of the variable fragment from a monoclonal antibody with the trans-membrane and intracellular domains of a T-cell receptor they allow for the *in vivo* creation of a host-derived population of chimeric antigen receptor-T (CART) cells directed against the antigen recognized by the antibody part of the receptor. CD19 (for B-cell lymphoma) and CD33 (for AML) are examples of antigens for which the CART therapy was already investigated. Unfortunately, as a healthy CD33 positive cells were targeted as well, treatments resulted in profound cytopenia [49]. Recently, effects of β member of the folate receptor family -specific CART cells therapy showed promising results both in vitro and in a xenograft model [50].

Last decades of research helped to optimize the existing therapies in terms of prognostic risk stratification, but the overall survival of patients remains poor. Big hopes lie in novel targeted therapies which offer the promise of effective anti-leukemic activity with reduced toxicity from off-target effects. Different novel inhibitors reviewed in the previous chapters are currently investigated in clinical trials, but its rather unlikely that any of these compounds, when used as single agents, will cure the disease [30]. There is a high need for new therapeutical targets, and surface markers that will be present exclusively on AML blasts, but not on healthy myeloid precursor cells of the patient. Intensive research in the direction of the pathways down-stream of the currently targeted and resistant kinases may shed a light on novel targets for therapy.

STAT family

The Signal transducer and activator of transcription (STAT) family consists of seven proteins referred to as STAT1-6 including the two STAT5 members - STAT5A and STAT5B [51], [52], [53], [54], [55], [56], [57]. Structurally, STAT proteins consist of a transactivation domain (TAD) - the most divergent part among STAT family located at the C-terminus of the protein. It is followed by a part of the molecule containing the tyrosine residue (Y694 for STAT5A) that becomes phosphorylated by JAKs and is located between the TAD and a Src-homology-2 (SH2) domain. The DNA binding domain located between residues 320 and 490 allows interaction with DNA and transcriptional activity of STATs. At the N-terminus of the protein, an α-helical coiled-coil domain extends possibilities for further interaction with other proteins. STAT molecules also contain two flexible loops, between the N-terminus and the core fragment and a second loop connecting the C-terminus to the core. These loops allow conformational changes during activation and dimerization of STATs (see also Figure 3 below).

STAT5A and STAT5B proteins

STAT5A, and a closely related protein, called STAT5B were firstly reported by 3 independent groups in 1995 [58], [56],[55]. STAT5A and STAT5B proteins share 96% of homology with the highest degree of divergence found in the C-terminal transactivation domain. *STAT5A* and *STAT5B* genes can be found on chromosome 11 in *Mus musculus* [59] or chromosome 17q11.2 in *Homo sapiens* [60] and belong to the same locus as the *STAT3* gene. Although the *STAT5A* and *STAT5B* gene promoters are juxtaposed and separated only by 10 kb they are not equivalently expressed, and the expression patterns are cell specific, for example STAT5A expression is prevalent in mammary tissue, whereas STAT5B is more abundant in liver [61], [62].

STAT5 residues responsible for protein activity

The composition of the cellular proteome comprised of all translated proteins must be tightly regulated. One of the regulation mechanisms relies on post-translational modifications of a protein. By adding or removing a modification protein may be either marked for degradation, its conformation may change allowing interactions with other proteins or activated to perform its canonical function. Modification at distinct protein residues may lead to different mechanisms of protein action, and therefore different biological outcome. This chapter will summarize the post-translational modifications reported on STAT5A and STAT5B (presented in the Figure 3) and their impact on the function of both proteins.

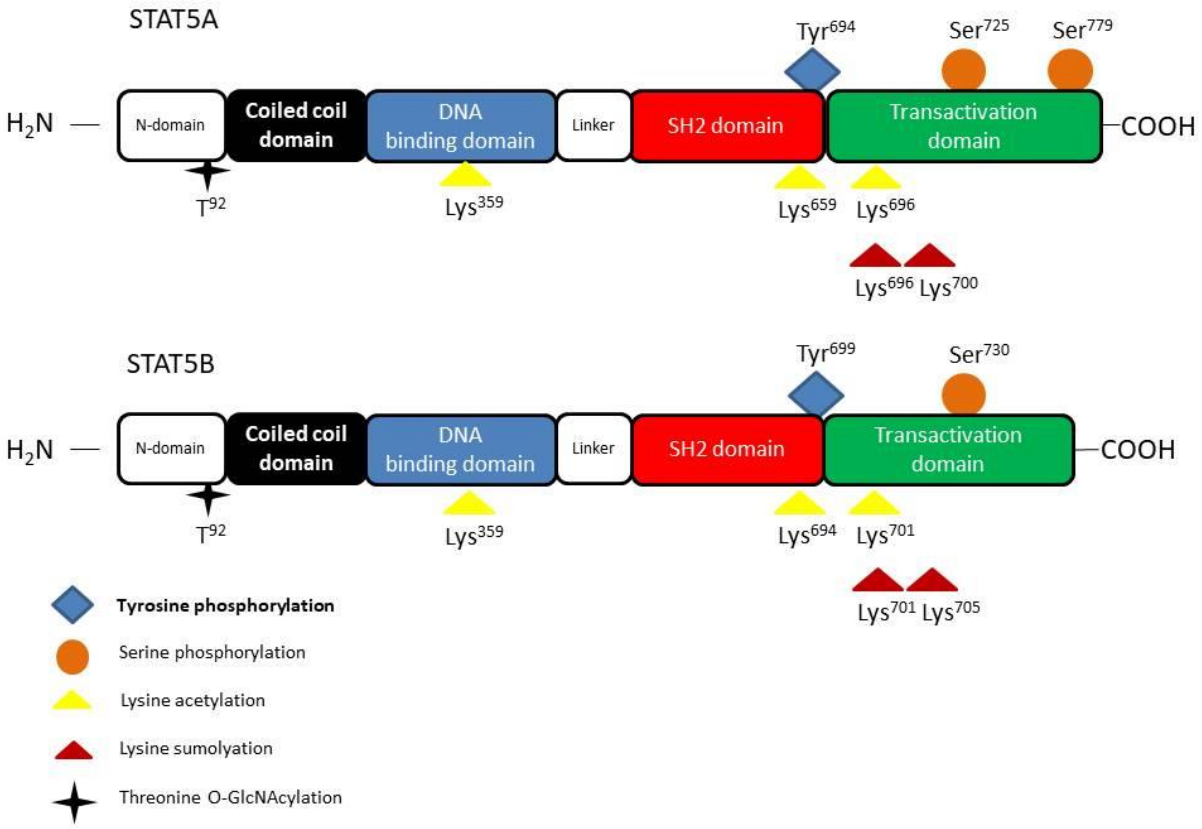

Figure 3. Structure of STAT5A and STAT5B proteins. Lys- Lysine, Ser- Serine, Tyr- Tyrosine, SH2 domain - Src-homology-2.

Tyrosine phosphorylation

Canonical STAT5 protein activation depends on phosphorylation of evolutionary conserved tyrosine residue within the SH2 domain. As reported by Gouilleux and colleagues, STAT5 can be phosphorylated at a tyrosine residue Tyr^{694} (STAT5A) or Tyr^{699} (STAT5B) followed by formation of homo- or heterodimers and translocation to the nuclear compartment [63]. Several reports demonstrated that overexpression of mutated, constitutively active STAT5 lead to increased proliferation and survival of cells [64], [65]. In addition, activated tyrosine-phosphorylated STAT5 dimers can further interact with other dimers leading to tetramerization of pSTAT5 molecules through its N-terminal domain residue lysine 70 (K70) further enhancing transcriptional activity [66]. Formation of STAT5 tetramers was proven to increase specificity of binding to promotors and to widen target gene spectra [66], [67]. Reconstitution of mice bone marrow, with cells expressing constitutively active, tetramer-forming mutants of Stat5a resulted in induction of acute leukemia, whereas the same mutant with exchange of the lysine 70 residue abolished tetramers formation and did not lead to leukemia development [68]. Further roles of tyrosine phosphorylated STAT5 in leukemogenesis will be described in the following chapters.

Serine phosphorylation

The serine residue of STAT5 is located within the Proline-Serine-Proline (PSP) motif (located in the TAD domain) analogical to other vertebrate STAT family members except STAT2.

Next to tyrosine phosphorylation, serine residues serve as another phosphorylation site located at Ser^{725} (Stat5a) and Ser^{730} (Stat5b). They were reported to be phosphorylated in both Stat5 proteins upon prolactin and IL-2 stimulation [69], or, in case of Stat5a, constitutively phosphorylated in fibroblast-like COS-7 cells [70].

To assess the biological function of STAT5 serine phosphorylation Yamashita and colleagues took advantage of point mutations and investigated its impact on prolactin-responsive promotors. They did not observe any changes in gene expression upon prolactin stimulation in mutant STAT5 expressing cells as compared to wild-type (wt) controls concluding that this phosphorylation site may not be responsible for transcription or regulation of expression of different gene-sets [70]. They also did not observe any changes in the ability of mutated Stat5 to bind DNA.

On the other hand, in a recently published report serine phosphorylation of Stat5 proteins was shown to influence leukemic transformation in erythroid and myeloid leukemia. Mutations of serine residues in these models prevented transformation and induced apoptosis [71], [72]. These reports demonstrate a role of serine STAT5 phosphorylation, but only in the context of malignancies with constitutive $STAT5^{Y694}$ phosphorylation. The role of serine phosphorylation in un-phosphorylated $STAT5^{Y694}$ remains elusive.

Lysine acetylation

STAT5 plays an important role in mammary gland development. There are several reports indicating STAT5s signaling via the prolactin receptor followed by transcriptional activity. Recently there was a report that shed light on the mechanism of this activation and demonstrated acetylation-mediated STAT5 activation in this model. The authors prove that STATs in general can be acetylated upon cytokine activation signal by the acetyl transferase CBP/p300 on multiple sites within different domains. Furthermore, they prove in an example of STAT5B that this modification leads to acetylation-dependent dimerization and transcriptional activation [73].

In line with this finding, another recent report showed that upon deletion of histone deacetylase 9 (HDAC9) in regulatory T-cells acetylation of STAT5 increased and was followed by activation of its target genes [74].

Interestingly, a recent publication indicates a direct mechanism of HDAC9 mediated STAT5 de-acetylation and its impact on transcriptional activity of STAT5. The authors provide evidences that targeting histone deacetylases blocked transcriptional activity in BaF3 model by interfering with the function of the BET family protein Brd2, preventing it from recruiting and stabilizing the transcriptional machinery. Furthermore, authors prove that STAT5 transcriptional activity is not directly correlated with acetylation of STAT5 lysine residues, but is required as an initial step in activation of STAT5 by tyrosine phosphorylation [75].

Lysine SUMOylation

In early lymphoid development, STAT5 SUMOylation was reported at two lysine residues (K^{696} and K^{700} of STAT5A) adjacent to the critical tyrosine of the protein. Van Nguyen and colleagues show that SUMO-specific protease 1 (SENP1) controls lymphoid development through regulation of the SUMOylation status of STAT5. As the same lysine residues can be either modified by SUMOylation or acetylation it emerges that SUMOylation of this lysine in the absence of SENP1 blocks acetylation resulting in inhibition of STAT5 activation and signaling. In other words, Nguyen and colleagues presented a model in which SUMOylation and acetylation antagonistically regulate STAT5 transcriptional activity. However, this effect seems to be highly cell specific as no SUMOylated STAT5 was detected in myeloid cells upon SENP1 depletion [76]. SUMOylation, unlike poly-ubiquitination was reported to rather regulate activity of proteins in on/off manner than promote proteasomal degradation [77].

O-GlcNAcylation

Another type of modification that influences phosphorylation of tyrosine residue and transactivation ability of STAT5 is O-GlcNAcylation at T^{92}. Located in the N-terminus T^{92} is conserved for both STAT5A and STAT5B. It has been shown that in $T^{92}A$ mutant STAT5B phosphorylation at Tyr^{699} is not affected [78]. In contrast, Freund and colleagues describe glycosylation at threonine 92 as a requirement for strong STAT5A tyrosine phosphorylation facilitating hematopoietic transformation. They overexpressed a mutant hyperactive STAT5A without O-GlcNAcylation and observed decreased tyrosine phosphorylation, diminished transactivation potential and most importantly complete loss of oncogenic transformation capacity [79].

Role of STAT5 proteins in growth and development

STAT5 is a member of an evolutionary conserved protein family. It plays an important role in basic developmental processes like proliferation and differentiation. In line with that, complete deletion of both *Stat5a* and *Stat5b* results in perinatal lethality due to severe anemia [80]. To reveal these critical roles of STAT5 in the hematopoietic stem/progenitor compartment researchers took advantage of loss-of-function experiments in mouse models.

STAT5A and STAT5B play essential redundant and non-redundant roles in orchestrating immuno-regulation and the development of immune cells. Notably, in the complete absence of STAT5, mice failed to develop T-, B-, and natural killer (NK)-cells [81]. STAT5 has also been demonstrated as the critical link between the IL-2/15 and FOXP3 pathways, essential for the development of regulatory T-cells [82]. In another report, BM cells from mice harboring homozygous deletions of both Stat5a and Stat5b genes (Stat5ab$^{-/-}$) were characterized for hematopoietic repopulating activities resulting in a major decrease in reconstitution in all lineages, however, leaving HSCs unaffected [83]. Work of Liu G and colleagues, using *Stat5ab*$^{-/-}$ mice completely lacking expression of STAT5 revealed that STAT5 was necessary for the development of HSCs, lymphocytes, and erythrocytes, but myelopoiesis was not affected in these animals [84]. Furthermore, Wang et al demonstrated that deletion of *Stat5* in a Mx1-Cre-inducible mouse model decreases the number, survival and quiescence of HSCs, indicating a role of STAT5 in the maintenance of HSCs under physiologic conditions but not in stress assays like bone marrow transplantations [85]. Additionally, a report from Kato and colleagues shows a beneficial role of STAT5-activation in expansion of multipotential progenitors and promotion of HSC self-renewal ex vivo [86]. Contrary, similar induction of STAT3 activation led to lineage commitment and differentiation of HSCs. The authors stress that this role could be a key to understand the maintenance of leukemic stem cells (LSC) and a hope for new therapeutical targets. Furthermore, it was found that the deletion of liver STAT5 resulted in impaired cell proliferation and development of fatty livers [87].

With then majority of manuscripts investigating the role of both STAT5A and STAT5B in double-deletion models, only few publications distinguish these two proteins by introducing single gene knock-downs and describing the functions of STAT5A or STAT5B independently. Research published by Liu and colleagues aimed at identifying the role of Stat5a upon deleting Stat5a, but not Stat5b. They observed attenuation of mammary alveolar development and milk secretion in mice suggesting that Stat5a acts as the principal mediator of mammopoietic and lactogenic signaling [61].

Additionally, deletion of both Stat5 genes in mice resulted in pronounced reduction of body growth [88], which was also linked to GH (Growth hormone and GHR (Growth hormone receptor) regulation [89]. This topic was further investigated by Udy and colleagues who showed that Stat5b depletion results in loss of sexual dimorphism of body growth rates in mice and proper gene expression in liver, contrary to depletion of Stat5a, which did not show the same effects [62]. In humans this phenotype has been also attributed to STAT5B function: in six patients with severe growth retardation disabling mutations in the *STAT5B* gene were described and linked to the regulation of GH-mediated postnatal growth [90].

Another report describes STAT5 as a master regulator in Natural killer (NK) cells. Upon loss of STAT5 expression, NK cells show diminished cytotoxic activity, but the most striking phenotype is that loss of pStat5b in healthy NK-cells led to overexpression of *Vegfa* and promoted tumor formation. In addition,

targeting of NK-cells with Ruxolitinib (JAK1/2 inhibitor) led to accumulation of uSTAT5B and tumorigenesis both in vitro and in vivo [91]. The authors stress here the importance of tumor monitoring in patients undergoing treatments with JAK inhibitors and interestingly similar effects have already been reported in this group of patients [92]. Finally, STAT5B mutations in human samples resulted in very low numbers of NK cells, confirming the observation in mice and supporting a role of STAT5B in this process [93], [94].

Canonical and non-canonical functions of STAT5 proteins

Canonical functions

STATs are the mediators of signals derived from cellular cytokine receptors. They are activated by phosphorylation of a critical tyrosine residue by Janus kinases (JAK), which are associated with membrane receptors. Upon activation, STATs form dimers via interaction of its SH2-domains, translocate to the nucleus and initiate target gene expression by binding to a specific DNA sequences containing γ-interferon-activated sequences (GAS) motifs. This transactivation process is known as the canonical pathway of STAT mediated signal transduction.

Among cell membrane receptors signaling via the receptor tyrosine kinase FLT3, activated by the FLT3 ligand (FL), results in tyrosine phosphorylation of STAT5. The role of Stat5a and Stat5b in Flt3 signal propagation was investigated in BaF3 cells and surprisingly only Stat5a was reported to be activated upon FL induction. Furthermore, the activation of Stat5a was not mediated by Jak, which remained inactive, but rather directly via Flt3 [95].

Various reports have shown the importance of STAT5 in self-renewal in mouse and human HSCs. To investigate the mechanisms behind this, Fatrai and colleagues performed genome-wide gene expression profiling and identified 32 pSTAT5 target genes in the HSC compartment, among them Hypoxia-inducible factor 2a (HIF2α). Upon down-regulation of HIF2α they observed reduced STAT5-induced cell proliferation, colony forming cell (CFC) numbers, and LTC-IC frequencies, but no impact on differentiation or apoptosis. In light of this, they concluded that the long-term phenotypes induced by STAT5 in HSCs are partly mediated via regulation of HIF2α expression [96].

Another study describing canonical signaling of pStat5a and pStat5b revealed novel target genes upon IL-3 activation in Ba/F3 murine pro B cell line. Using a ChIP-seq approach, the authors demonstrate clear differences between pStat5a and pStat5b target sites. They were able to identify known target genes like c-Myc, Id-1 or Bcl-x, but also confirm binding motifs within promotor regions of previously reported putative Stat5 targets: Cis, Socs1, Osm, IL-2Rα and Spi2.1. To confirm the novel targets and determine whether it is a pStat5a or pStat5b targeted gene, the authors performed shRNA mediated knock-down of pStat5a/b, pStat5a or pStat5b upon IL-3 stimulation. Common genes targeted by both, pStat5a and Stat5b, were Cish, Socs1 and Osm. Stat5a regulated expression of Spi2.1, whereas Stat5b alone targeted IL-2Rα, Wasp and Lama5. They also report 3 novel target genes of both Stat5b and Stat5b, namely TNFRSF13b, MKP-1 and C3ar1, all associated with tumorigenesis [97].

Mechanisms of pSTAT5 activated transcription were also investigated in a pro-B cell model with focus on pSTAT5A. Using a ChIP-seq. approach, putative genome binding regions were identified showing both pSTAT5A mediated gene induction and repression at these loci. Both types of transcriptional activity were linked with a GAS motif present upstream of gene promotor regions. Genomic binding sites of novel interacting partners of pSTAT5A, LSD1 and HDAC3 (revealed by mass spectrometry experiments) were investigated in the same model. Both proteins were shown to co-localize and physically interact with pSTAT5A in shared regions of the genome rich in GAS motif, but also in regions lacking this motif, which was associated with a weaker pSTAT5a binding. Interestingly, the authors observed strong pSTAT5A binding in intragenic regions suggesting a possible enhancer role of pSTAT5A [98]. Work presented within this paper shows a novel complex interacting together to modulate gene expression, however, the biological functions behind this remain unknown.

Finally, recent work of Zhen and colleagues compared pSTAT5A/B binding sites discovered in previous reports in mouse mammary tissue (Stat5a binding [99]), T helper cells (total STAT5 binding [100]) and liver (STAT5B binding [101]) and identified 183 pSTAT5-positive promoters shared in all 3 cell types and 74% of the promotors contained a GAS-motif. With total number of discovered binding sites ranging from 12,300 in liver cells to 16,000 sites in mammary tissue, the number of joint sites is surprisingly low. The authors further explored this area concluding that pSTAT5 regulates these two distinct gene categories through separate mechanisms, binding to distal enhancers in lineage-specific genes and to promoters in commonly expressed genes. They shed new light on the role of pSTAT5 as a master regulator of transcription promoting chromatin opening and binding of co-factors to enhancers of lineage-specific genes [102].

Non-canonical functions

In response to growth factor stimulation and phosphorylation, STATs shift to the nucleus and induce expression of target genes. Translocation between cytoplasmic and nuclear compartments is central to STAT biological functions. As the canonical pathway has been precisely investigated, increasing number of studies indicate other unphosphorylated STATs function in cytoplasmic and nuclear compartments. Consequences of these activities will be described in this chapter and referred to as non-canonical activation with focus on STAT5.

One of the assumptions of canonical STAT signaling claims that only activated proteins are recognized and translocated to the nucleus. Interestingly, several studies report that the coiled-coil domain of both unphosphorylated and tyrosine phosphorylated STAT5a is accessible for recognition by importin carrier proteins. Therefore, there could be a possibility of transporting unphosphorylated (at tyrosine residue) STAT5 (uSTAT5) to the nucleus. In fact, the crystal structure of an uSTAT5 dimer was obtained and shed light on the interactions of the proteins. uSTAT5 forms anti-parallel homodimers in which the interactions between monomers is stabilized by β-barrel of the DNA-binding domains. Following activation, tyrosine phosphorylated STAT5 (pSTAT5) forms anti-parallel dimers, but interaction between dimers occurs via the SH-2 domain and the phosphorylated tyrosine residue of the other dimer [103].

Another group developed an in-vitro based assay to define what proteins recognize the nuclear localization sequence (NLS) within uSTAT5 and pSTAT5 protein. They were able to show that importin-α3 is a primary binding adaptor of an unconventional STAT5 NLS, which is constitutively active

independent of tyrosine phosphorylation. They have also proven that siRNA-mediated silencing of importin-α3 or importin-β1 led to inhibition of nuclear transport. In a similar manner the authors decided to investigate the STAT5 protein structure for the presence of nuclear export sequence (NES). One NES sequence, indicating interaction with exportin Crm1 was found in the N-terminus of STAT5 and another sequence, a Crm1-independent NES, within the DNA-binding domain [104]. This finding shed a light on non-canonical signaling of STAT5 proteins. As a mediator of external signals, STAT5 proteins can be expressed on a high, endogenous level, ready to immediately forward signals from the cellular membrane to the nucleus and migrate between the compartments even without an activation signal. This way, they can wait for an activation either from cytoplasmic or nuclear located JAKs and react to a stimulus in a quicker manner. On the other hand, they could also perform novel non-canonical functions as uSTAT5 via protein-protein interactions within the nucleus.

In *Drosophila melanogaster*, where only one STAT protein has been reported, Shi and colleagues provided experimental confirmation of such a model. They demonstrated a direct interaction of uSTAT and heterochromatin protein (HP1) [105]. Follow-up investigations confirmed a role of uSTAT in the maintenance of genome stability by promoting heterochromatin formation (Figure 4) [106]. Further, Hu and colleagues demonstrated a dynamic interaction of HP1a and uSTAT5A in human cellular models. In addition, the authors showed that overexpression of uSTAT5A leads to growth inhibition of murine and human colon cancer cells [107].

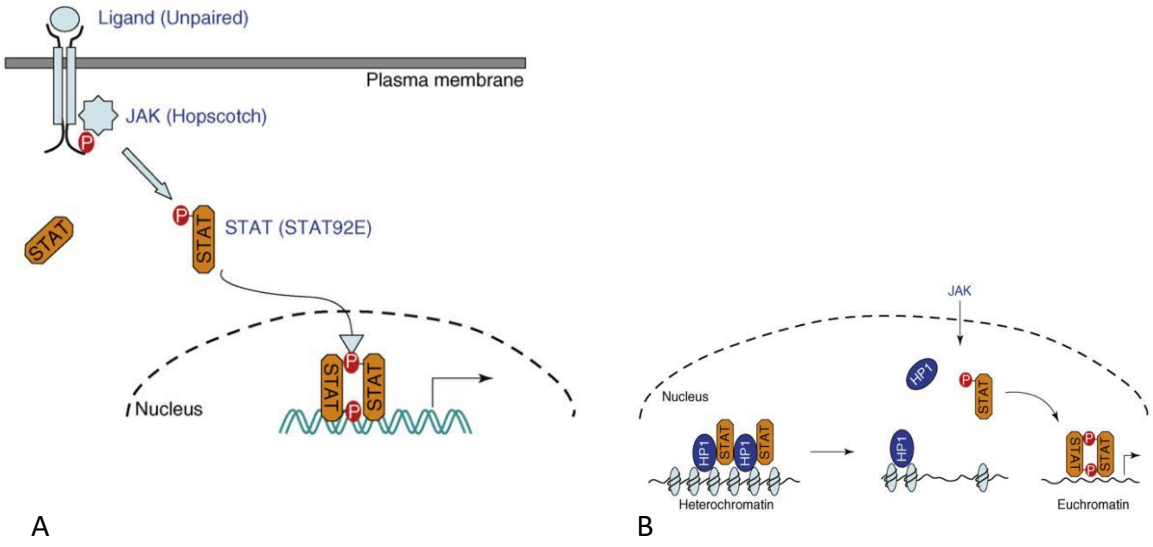

Figure 4. Graphic presentation of STAT canonical pathway (A) and non-canonical pathway (B).
Adapted from Lee WX, Trends in Cell Biology 2008.

Recently, Park and colleagues demonstrated a separate transcriptional program for uStat5 in mouse hematopoietic stem/progenitor cells. Upon cytokine-induced differentiation and activation of pStat5 these cells switch to a canonical pathway of STAT signaling. In the un-phosphorylated state uStat5 acts in a repressive manner interacting with ERG, FLI1, and SCL – key megakaryocytic transcription factor pre-occupying the same loci in the genome. Upon TPO activation and phosphorylation, pStat5 is lost

in these regions and ERG binds the same loci in a stronger manner leading to differentiation. Secondly, the authors demonstrated co-localization of uStat5 and CTCF indicating a new link between STAT signaling and nuclear topology. However, the direct interaction of CTCF and uStat5 was not proven and the mechanism of recruitment of uStat5 remains unknown.

Furthermore, comparison of uStat5 and pStat5 genomic binding performed in this model (murine stem cell line Hpc-7) revealed individual gene targets for each phosphorylation state. In the un-phosphorylated state Stat5 has more than 4000 binding sites, among them promotors of genes associated with megakaryocytic differentiation (e.g. Mpl, Gp6, Pf4 and Cd41). On the other hand, among genes targeted by TPO induced pStat5 (771 binding sites), they observed Cish, Bcl6, Pim2, and Socs2. It is striking that uStat5 covers more bindings sites on DNA and tyrosine phosphorylation causes redistribution to a low number of defined target genes. Unfortunately, the authors did not distinguish between Stat5a and Stat5b in their experimental design [1].

A STAT5 non-canonical function has also been reported during B lymphopoiesis. In B-cells that perform immunoglobulin kappa-chain rearrangements the process is tightly controlled by Stat5. Again, the authors did not distinguish between STAT5A or STAT5B, but they report a STAT5-mediated transcriptional repression by recruitment of histone methyl-transferase Ezh2 [108].

uSTAT5 has also been described to play a non-canonical function in the cytoplasmic compartment. Lee and colleagues discovered a novel role of un-phosphorylated Stat5a in the regulation of the Golgi apparatus and rough endoplasmic reticulum functions [109].

Effects of STAT5 inhibition in malignant disease

STAT5 is known to be involved in the maintenance of solid tumors, as well as hematological disorders where it acts down-stream of kinase-mediated constitutive phosphorylation. Several studies investigated the role of STAT5A and STAT5B in these models, for solid tumors also distinguishing between activated pSTAT5 and uSTAT5. Most of the studies in blood malignancy models evaluated the role of STAT5 without distinguishing the impact of STAT5A or STAT5B focusing exclusively on pSTAT5 functions. This chapter will summarize these findings.

pSTAT5 in solid cancer

In a glioblastoma model (U87-MG cell line) suppression of cell growth and a reduced cell number were observed following siRNA-mediated silencing of pSTAT5. The down-regulation of pSTAT5 caused changes in the cell cycle, which was arrested at the G1 stage [110]. Another group was able to provide evidence that Stat5b, but not Stat5a, contributes to tumor progression in a human squamous cell carcinoma of the head and neck (SCCHN) cancer. In their model, Stat5a expression and phosphorylation were similar in tumor tissue and control mucosa from subjects without cancer. On the other hand, Stat5b expression and phosphorylation was consistently enriched in SCCHN tumors but not in their epithelial counterparts. In addition, specific targeting of Stat5b abrogated tumor progression and target gene expression *in vivo*, whereas targeting Stat5a had no effect on tumor growth or gene expression. The authors explained these effects upon Stat5b knock-down with down-regulation of target genes that regulate cell cycle and apoptosis. Specifically, targeting of Stat5b resulted in decreased expression of Cyclin D1 and Bcl-x_L [111]. Another small study investigated the role of STAT5 in the esophageal carcinoma cell line Eca-109. siRNA mediated knock-down of STAT5 resulted in suppressed cell growth and G1 arrest in the cell cycle. The authors observed also a decrease in BCL2 and Cyclin D1 mRNA expression [112].

To sum up, malignant transformation mediated by constitutively phosphorylated STAT5 in most of the cases works through i) cell cycle regulators, such as the D-type cyclins [113] ii) DNA repair proteins, such as RAD51 [114] and iii) antiapoptotic proteins such as BCL-XL and BCL-2 [115].

uSTAT5 in solid cancer

Findings in human colorectal cancer cells (CRC) indicate that downregulation of STAT5 and pSTAT5 was associated with a decrease in cell viability and a G1 cell cycle arrest. These data are consistent with the upregulation of p16, p21 and p27 protein expression following suppression of STAT5, suggesting that the STAT5 pathway is involved in cell cycle regulation. Additionally, the authors provide an evidence that STAT5 may also play a role in tumor metastasis and invasion by regulating E-cadherin [116]. In line with this work, Gu and colleagues demonstrate the involvement of Stat5 in metastatic progression of human prostate cancer cells *in vivo* [117].

In another article, colorectal cancer (HCT116), breast cancer (T-47D), prostate cancer (PC-3), and epidermal carcinoma (A431) cell lines were transduced with short-hairpin RNA targeting STAT5A and B to evaluate the role of STAT5 proteins in these cancers. In line with other findings, the authors observed reduction in proliferation and viability independently of endogenous phosphorylation status of STAT5 in these cell lines [118]. Furthermore, upon STAT5-knockdown the cells showed cytoskeletal deformation and a round morphology like previous reports regarding non-canonical function of STAT5a implicating regulation of the Golgi apparatus and rough endoplasmic reticulum functions [109].

pSTAT5 in leukemogenesis

STAT5 has been shown as an essential signaling molecule down-stream of the fusion protein BCR-ABL, which causes chronic myeloid leukemia (CML) [119]. Mouse experiments using loss-of function STAT5 mutations in BCR-ABL-expressing cells showed that STAT5 is not essential for the leukemic transformation [120]. In contrast, genetic depletion using single null mutation of Stat5a showed slower CML progress [121], and cells with null mutations of both Stat5a and Stat5b were unable to generate leukemia in recipient mice following retroviral transduction with BCR-ABL [81].

In a recent paper direct comparison between STAT5 phosphorylation upon IL-3 stimulation or BCR-ABL oncogene expression has been presented in context of STAT5A and STAT5B separately. The authors show that STAT5 phosphorylation by BCR-ABL and the resulting dimerization of STAT5 proteins is weaker than in IL-3 treated cells. Furthermore, pSTAT5A translocation to the nucleus is reduced in BCR-ABL-positive cells as compared to IL-3. Instead, pSTAT5A accumulates at cell membrane close to the IL3R. Finally, siRNA mediated targeting of STAT5B and not STAT5A leads to increased sensitivity to imatinib treatment. In summary the data suggest different functions for STAT5A and STAT5B in the context of BCR-ABL [122]. Another study, by Weber and colleagues confirmed that STAT5 promotes survival of BCR-ABL mutated cells [123].

In a similar manner, phosphorylated STAT5 promotes an aggressive form of acute myeloid leukemia (AML) harboring FLT3-ITD [124]. Interestingly, another report presented only STAT5A as protein activated by FLT3-ITD [95].

Worth mentioning is also the role of STAT5 in various malignancies caused by a mutation within the upstream kinase JAK2. In a *Stat5*-deficient background neither JAK2-V617F nor the fusion protein TEL-JAK2 can cause a disease phenotype in vivo [125], [126]. Reconstitution of these mice with a BM containing constitutively activated STAT5A or overexpression of Oncostatin M (a STAT5 target gene) led to development of the disease [127].

In CML patients a canonical JAK2-STAT5 pathway was initially considered. However, it has been reported that BCR-ABL is able to directly phosphorylate STAT5, making JAK2 dispensable [128]. Based on this discovery, the authors claim that there is no biological rationale for using JAK2 inhibitors in CML patients.

Another interesting report shows that in CML cells, that developed resistance to imatinib treatment, the levels of STAT5A are elevated as compared to other CML cells. It is accompanied by an increase in reactive oxygen species (ROS) production with increased genomic instability and suggested as a source of mutagenesis for BCR-ABL mutations [129].

Epigenetics

Gene expression is a process strictly regulated at different levels. Starting from genetic information encoded in the DNA, through transcriptional regulation resulting in a corresponding mRNA transcript, to the functional protein many steps involving thousands of regulatory proteins and factors are necessary. Accessing and transcribing the information encoded in DNA is mediated by transcription factors and the transcriptional machinery recruited to the promotor region of a gene. Recent decades of research in this area helped to unravel many challenging questions regarding this straight forward model. For example, how do cells, residing in a completely different organ, but carrying the identical genetic information differ in gene expression programs? A branch of biology that investigates and helps to answer this and many other questions is called epigenetics. Initially this term was used to describe heritable changes in gene expression (phenotype) that were independent of DNA sequence alterations (genotype) (Waddington C, 1957; reviewed by Ferrell J [130]). Further investigations revealed that epigenetics serves as another layer of information encoded in DNA that influences switching on/off sets of genes and regulates their expression levels.

Among best investigated epigenetic modifications are modifications of DNA and histone proteins, which will be briefly described in this chapter. Furthermore, proteins that regulate post translational modifications are often mutated, linked to AML maintenance and represent potential therapeutic targets.

DNA methylation

An important modification of DNA is the methylation of cytosine nucleotides at carbon 5 position in the context of a 5'-cytosine-phosphate-guanine-3' (5'-CpG-3') dinucleotides. Methylated cytosine (5mC), particularly in CpG islands of promoters, is associated with heterochromatin and therefore with transcriptional repression [131].

This is one of the most important epigenetic modifications which is hereditary [132]. Regulation of DNA methylation is a dynamic process mediated by two predominantly de novo DNA methyltransferases, DNMT3A and 3B, and the maintenance methyltransferase DNMT1 [131], which can put the methylation mark on cytosine. Contrary, active cytosine demethylation is achieved by members of TET (ten eleven translocation) family of DNA dioxygenases, which initiate demethylation by a series of enzymatic reactions with methylated cytosine as a substrate and finally involvement of base excision repair pathways [133].

With its proven role in normal hematopoiesis (in absence of DNMT3A a differentiation block in HSCs is observed) DNMT family methyltransferases are also reported to be mutated in hematological malignancies including Myelodysplastic syndrome (MDS) and Myeloproliferative neoplasm (MPN) and are associated with an increased risk of progression to AML [134].

The most common mutation of DNMT3A is the substitution of arginine within the catalytic domain to histidine (Arg882His) resulting in loss of function [135]. In this scenario HSCs carrying this mutation may confer a self-renewal advantage leading to the development of leukemia if additional mutation is acquired over time [136].

Among the TET family of DNA demethylases, TET2 is mutated most frequently in lymphoid and myeloid hematopoietic malignancies, suggesting that mutations in TET2 occur in early hematopoietic progenitors [137]. Similarly to DNMT3A mutations, mutated TET2 is able to induce leukemia alone, but could be the first mutation in a multi-hit model of leukemogenesis and has been found to coexist with mutations of EZH2, DNMT3A and other [138].

Histone marks

To compress the 2-meter-long [139] DNA in a mammalian cell, which is about 10 μm in diameter, several mechanisms have been established during evolution. Most efficient compression is achieved by wrapping the DNA around proteins called histones (beads on string model). The nucleosome core complex is formed of two copies of four histone core proteins (H2A, H2B, H3, and H4) and, when DNA wrapped around the complex, is called chromatin. Historically chromatin has been thought to be present in two physical states: euchromatin or heterochromatin. While euchromatin describes chromatin in a more relaxed state open to bind proteins modulating gene expression (transcriptional machinery), heterochromatin is a more compact state facilitating gene repression [140]. While the core part of histone proteins is involved in maintaining the proper DNA compaction, the long histone tails are region of high importance. Lysine residues along the N-tails of histone 3 can be modified with so called histone marks. Different chemical modifications (e.g. addition of a methyl group) can have a completely different impact on the DNA and replication. Depending on the modification and lysine residue that carries it, the landscape of the nuclear DNA can be different. In most cases, the change of the mark will lead to higher accessibility of DNA in the proximity of the mark for transcription factors and machinery, formation of euchromatin, or decreased accessibility achieved by formation of heterochromatin. The most known modifications of histone tails are methylation, acetylation, phosphorylation (at serine and threonine residues), ubiquitination and ADP-ribosylation. The euchromatin region is marked with trimethylation at H3K4, H3K36, or H3K79 and high levels of histone acetylation, whereas the most common modifications promoting closed, heterochromatin structures include trimethylation of H3K9, K3K27, and H4K20 [141].

H3K4 tri-methylation

Among methylation marks indicating active chromatin, H3K4me3 has been shown to localize to the 5' end of active genes and mediates transcriptional activity by association with the RNA Pol II [142]. Potentially active genes are also known to be enriched in H3K4 di-methylation marks within the gene body [143],[144]. As discovered in a *S. cerevisiae* model all H3K4 methylation marks are set by a methyltransferase named Suv, Ez, and Trithorax domain 1 (SET1) [145]. In addition, the pattern of H3K4 tri-methylation is linked to the association of Set1 with a phosphorylated form of elongating RNA Pol II at the 5' regions of transcriptionally active genes [146]. While the correlation between H3K4 tri-methylation and transcriptional activity is high in all eukaryotes examined, there are exceptions indicating presence of "bivalent" marks, where H3K4 methylation is enriched at loci also enriched for silencing-associated marks such as H3K9 or H3K27 methylation [147]. This phenomenon could serve as a repression mechanism in which a balanced ratio between active and repressive histone marks poises expression of certain genes, which can be directly expressed upon stimuli or remain in the steady state.

H3K9 methylation

Formation of heterochromatin is strongly linked to the presence of tri-methylation at the lysine 9 residue on histone 3 in the same region. The methyltransferase with specificity for H3K9 and responsible for setting this mark is SUV39H1 [148]. In addition, SUV39H1 was reported to form a repressive complex with M31, a murine homologue of drosophila heterochromatin protein 1 (HP1) [149]. This complex is described to be evolutionary conserved, maintaining heterochromatin formation from yeasts models [150] to human cell lines [151].

Interestingly, the presence of H3K9 tri-methylation does not necessarily have to indicate transcriptional repression. It has been reported that in several mammalian cell lines the coding/ gene body regions of several active genes are enriched in H3K9 tri-methylation marks and co-localize with HP1γ protein [152]. It could be that H3K9 tri-methylation corresponds to heterochromatin and transcriptional repression of a gene only if located within the promotor region.

The process of epigenetic landscape regulation is modulated not only by the methyltransferases that write the H3K9 and H3K4 histone marks, but also by demethylases, which dynamically respond to stimuli and help regulating the chromatin accessibility and transcriptional activity. One example is lysine specific demethylase 1 (LSD1), which demethylates both H3K4 and H3K9 mono and di-methylation dynamically affecting transcriptional programs, acting either as a repressor or activator [84] [153]. Its over expression has been reported in many malignant models including solid organ tumors, e.g .bladder, lung and colorectal carcinomas, as well as myeloproliferative disorders [154], [155], [156].

Methods

AML cell lines used in the study

In this study we focus on acute myeloid leukemia (AML) cell lines originally derived from leukemia patients. The following cell lines were used in experiments (Table 2):

CELL LINE	LEUKEMIA TYPE	DRIVING MUTATION	FLT3 STATUS	CELL DEPOSITORY ID
MV4-11	acute monocytic leukemia	MLL-AF4	$FLT3^{ITD}$	ATCC® CRL-9591™
MOLM-14	Acute myeloid leukemia	MLL-AF9	$FLT3^{ITD}$	ACC 777
THP-1	acute monocytic leukemia	MLL-AF9	$FLT3^{WT}$	ATCC® TIB-202™
SKM-1	Acute myeloid leukemia	EZH2-Y641C	$FLT3^{WT}$	ACC 547

Table 2. AML cell lines used in the study.

To prepare lentiviruses for shRNA mediated gene knock-down or retro-viruses for *in vivo* experiments 293T adherent cell line was used as packaging cells (ATCC® CRL-3216™).

All cell lines had been validated and authenticated by Multiplexion GmbH (Ludwigshafen) and the summary can be found in Supplementary figure 1.

Culturing conditions

Validated cell lines were thaw from liquid-nitrogen general lab stock. All AML cell lines were cultured in suspension with Roswell Park Memorial Institute (RPMI) 1640 Medium supplemented with 1% v/v of L-Glutamine (final concentration of 20 mM). Additionally, RPMI medium was supplemented with Fetal Bovine Serum (FBS – 10% for MV4-11, MOLM-14, THP-1, or 20% for SKM-1 cells.

First, the thaw cells were expanded in 6-well plates and subsequently transferred to culture flasks after several passages. MV4-11 cells were cultured exclusively in 6-well plates. Cell were splitted to concentration of 0.4 x 10^6 cells/ mL and expanded for 2-3 days until next splitting.

293T adherent cells were cultured in Dulbecco's Modified Eagle's Medium (DMEM) containing 20 mM L-Glutamine. Additionally, DMEM medium was supplemented with 10% of FBS.

293T cells were seeded in 10cm dishes at concentration of 1 million cells per dish and splitted 1:10 every second day using Trypsin-EDTA for detaching.

After one week in culture part of cells were frozen back to maintain back-up vials and cellular lab stock. Briefly, 5 x 10^6 cells were centrifuged at 300g for 5 minutes, re-suspended in FBS supplemented with 10% of Dimethyl sulfoxide (DMSO), transferred to cryo-preservation vials in pre-cooled cryo-box and frozen at -80°C. After 24 h cells were transferred to N2 tank.

MTT

A colorimetric assay based on enzymatic reduction of 3-[4,5-dimethylthiazole-2-yl]-2,5-diphenyltetrazolium bromide (MTT) to MTT-formazan, by mitochondrial succinate dehydrogenase was formed to monitor the cell metabolic activity. Briefly, technical triplicates of 100 µl cell suspension were transferred to 96-well plate and incubated with MTT solution (Thiazolyl Blue, Carl Roth) for 4 h before adding MTT solubilization buffer (10% w/v SDS in 0.01M HCl) for an overnight incubation (37°C, 5% CO_2). Afterwards, plates were analyzed using the plate reader (FLUOstar Omega, BMG Labtech Germany).

Cell Cycle analysis

The impact of STAT5 knock-down on cell-cycle of the AML cell lines was assessed by PI staining using HFS buffer (3.87 mM Sodium Acetate (Roth), 0.075 mM PI(Sigma), 0.1% TritonX-100 (Sigma)). Briefly, $0{,}3\times10^6$ cells/mL were washed with 500 µl of cold PBS, re-suspended in 300 µl of the HFS buffer, vortexed and placed on ice. Cells were analyzed by Flow cytometry (FACS Canto II, Beckton and Dickinson) recording 10.000 events for each sample. The analysis of the data was performed using FlowJo 10 (FLOWJO, LLC). An example, showing the gating strategy is presented in Figure 5.

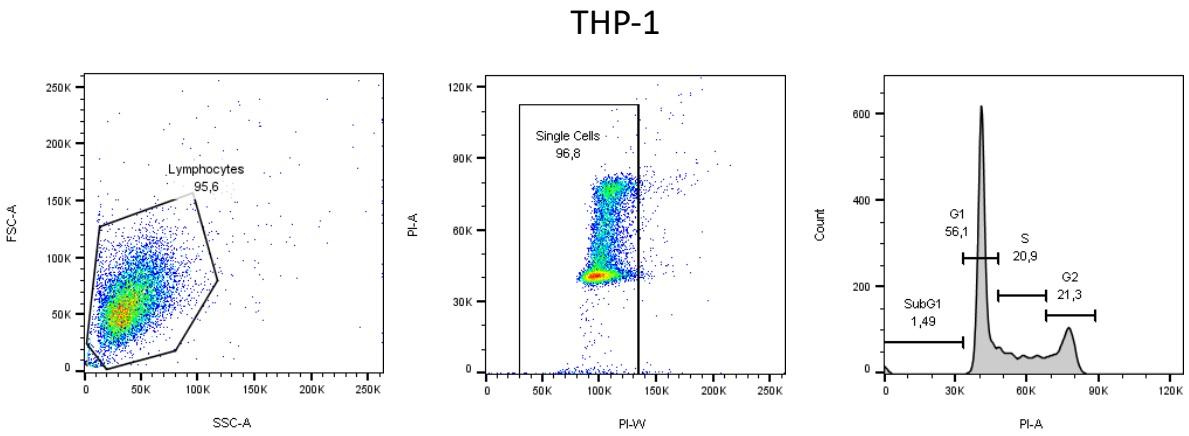

Figure 5. Strategy of gating for the cell cycle analysis via FACS in THP-1 cells

As the first step, the small events caused by cell debris were excluded, followed by gating out the events resulting from possible cell duplexes using the area and width parameters. Finally, the histogram of the PI-A was analyzed to group the cells into different cell-cycle phase based on the DNA amount [157].

Assesment of differentiation via FACS analysis and histological stainings.

Flow cytometry was also used to analyze cell cycle progression, as well as to monitor levels of CD11b and cKIT expression upon STAT5 downregulation. STAT5 knock-down and control cells were washed once with PBS, centrifuged and re-suspended in 300 µl PBS and 3 µl of a CD11b-PE-conjugated antibody (BioLegend 101212), a cKIT-APC- conjugated antibody (BioLegend 105812) or respective IgG controls. After 20 minutes of incubation at 4°C and in the dark, cells were washed 3 times with cold PBS and analyzed using flow cytometer recording 10.000 events for each sample.

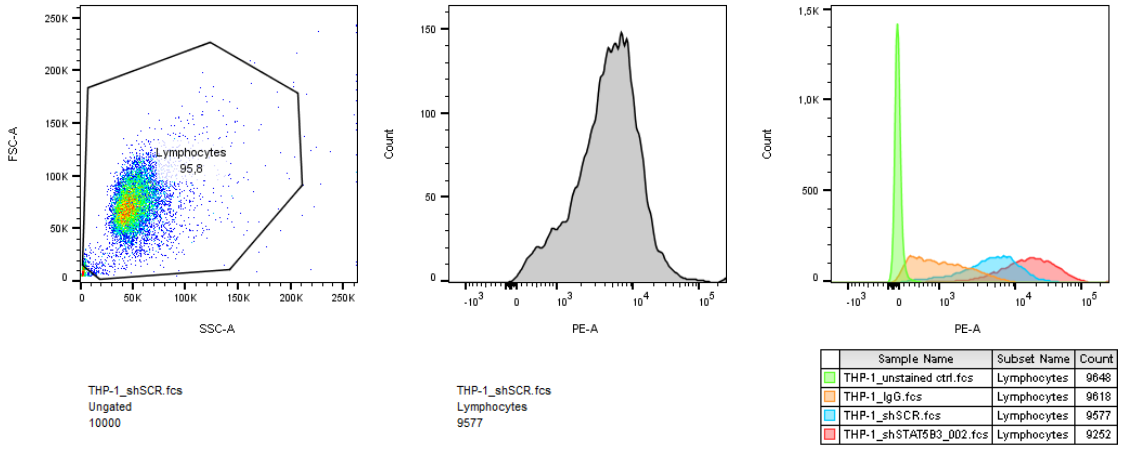

Figure 6. Strategy of gating for CD11b expression FACS measurement in THP-1 cells.

Figure 6 shows an example of the analysis for CD11b expression in THP-1 cells upon uSTAT5B knock-down. The first step was gating-out of cell debris. Afterwards the cells were checked and compared for the expression of CD11b. For each sample the Median Fluorescence Intensity (MFI) for the PE channel was calculated using FlowJo 10 software.

The effect of STAT5 knock-down on cell morphology was analyzed by May-Grünwald-Giemsa staining. AML cell lines and cells with and without STAT5 knock-down were washed once with PBS and smeared onto a microscopy slide. After drying, slides were stained with May-Gruenwald stain (Applichem GmbH) for 10 minutes, washed twice in water and stained with Giemsa solution (Merck, diluted 1:20) for 16 minutes. After one wash in water, the slides were left for drying and cell morphology was investigated using light microscopy.

Expression of STAT5A and STAT5B in AML parental cells assessed by RT-qPCR and western-blotting.

To analyze STAT5A and STAT5B mRNA and protein expression levels in AML cell lines we performed qRT-PCR analysis and western-blotting, respectively.

For qRT-PCR analysis total RNA was extracted using High Pure RNA extraction kit (Roche) and the reverse-transcription (RT) was performed according to the manufacturers protocol (Fermentas). The qRT-PCR reaction was performed with primers covering the genomic regions of exons 15 and 16 for STAT5A and exons 4 and 5 for STAT5B. GAPDH primers were used as a reference gene control. The primer sequences are listed in the Supplementary Figure S2. The reaction mix was composed as presented in the Table 3. As a template, 5 µl of cDNA pre- diluted (1:5) in water was used. The LightCycler® 480 SYBR Green I Master mix (Roche) was composed of SYBR Green I double-strand specific DNA dye, dNTPs and FastStart Taq DNA polymerase. Each sample was analyzed in technical duplicates.

	Volume [µl] per well
10 pmol/µl of Primer For	1
10 pmol/µl of Primer Rev	1
cDNA template 5x diluted	5
H_2O	3
LightCycler® 480 SYBR Green I Master	10

Table 3. Composition of qPCR reaction mix

To calculate relative changes in gene expression obtained from real-time PCR experiments we took advantage of the $2^{-\Delta\Delta Ct}$ method [158]. The equation below represents the way to calculate relative expression (R) assuming optimal doubling of the target cDNA in each qPCR cycle.

$$R = 2^{\Delta C_t} = 2^{(C_t sample - C_t reference\ gene)}$$

To quantify the relative expression of our genes of interest (e.g. STAT5A or STAT5B) compared to GAPDH (reference gene) we used "delta C_t" values.

The relative expression was used to plot the RNA expression levels of different AML cell lines. The changes in expression levels of STAT5 proteins were analyzed using western blotting. Briefly, equal numbers of cells were washed once with ice-cold Phosphate-buffered saline (PBS, Gibco), centrifuged and re-suspended in RIPA extraction buffer (50 mM Tris-HCL pH=7,5, 150 mM NaCl, 1 mM EDTA, 0,1% Na-deoxycholate, 1% NP-40, freshly supplemented with Complete protease inhibitors mix), vortexed and incubated on ice for 20 minutes. Cells were than centrifuged for 30 minutes at 13,000 rpm. Supernatants, containing whole cell lysates were transferred to clean

eppendorf tubes and protein concentration was assessed using Bradford Protein Assay (Biorad). Equal amounts of proteins (50-100 µg) were mixed with 4x Sample buffer (40% Glycerol, 240 mM Tris/HCl pH 6.8, 8% SDS, 0.04% bromophenol blue) supplemented with 20% β-mercaptoethanol, heated at 95°C for 5 min, loaded and separated in a SDS-PAGE gel for 3 h at 100 V. Separated proteins were blotted over-night at 20 V in the cold room using nitro-cellulose membrane (Amersham Protran 0.45 NC, GE Lifesciences). For blocking, membranes were incubated for 3 h in 5% milk (Roth) re-suspended in PBS-Tween (Sigma) and additionally in Net-G blocking buffer (50 mM TRIS, 150 mM NaCl, 5 mM EDTA, 0,04% Gelatine, 0,05% Tween-20) for one hour. Incubation with primary antibodies (antibodies listed in the Antibody List, Table S2) was performed overnight and after several washing steps the membrane was incubated with secondary antibodies coupled with the Horse-Radish Peroxidise for one hour. Washing steps were performed followed by incubation with the ECL substrate for the Horse-Radish Peroxidise enzyme (Pierce™ ECL Western Blotting Substrate, Thermo Scientific). Chemiluminescence signals were assessed using imaging machine INTAS (Intas Science Imaging Instruments GmbH).

Preperation and cloning of short hairpin RNA sequences into the pLKO-Tet-On plasmid

Short-hairpin RNA design

In order to perform siRNA-mediated gene knock-down experiments, we used the short-hairpin RNA (shRNA) approach. The shRNA sequences used in this project were determined with help of the Genetic Perturbation Platform (GPP) of the Broad Institute (https://portals.broadinstitute.org/gpp/public/) or using already existing RNAi target sequences from the Biosetta website (http://biosettia.com/) followed by adding oligonucleotide overhangs to make them suitable for the shRNA system.

Each of the shRNAs targeting sequences was analyzed for possible off-target effects by aligning them to the genome and transcriptome of *Homo sapiens* using blast (NCBI, NIH) and Ensembl blast (EMBL-EBI). The results of this control alignment are presented in Figure 7 and for the other shRNAs used in this study in supplementary figure 2.

1. TRCN000019304 aka shSTAT5A1
   Target sequence: GCTCTGAATTAGTCCTTGCTT

Show All entries | Show/hide columns (2 hidden) | Filter

Subject name	Gene hit	Subject start	Subject end	Subject ori	Genomic Location	Orientation	Query start	Query end	Length	Score
ENST00000588868.5	STAT5A	3028	3048	Forward	17:42311339-42311359 [Sequence]	Forward	1	21	21 [Sequence]	42.1
ENST00000345506.8	STAT5A	3697	3717	Forward	17:42311339-42311359 [Sequence]	Forward	1	21	21 [Sequence]	42.1
ENST00000621274.3	RAD17	2433	2446	Reverse	CHR_HSCHR5_2_CTG1_1:69414825-69414838 [Sequence]	Forward	4	17	14 [Sequence]	28.2

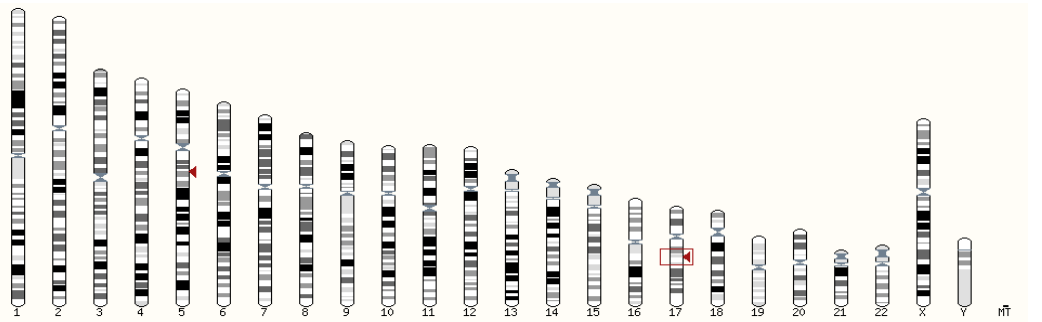

Figure 7. Control alignment of shRNA sequence to the genome and transcriptome of *Homo sapiens.* *STAT5A* is located on chromosome 17. The red arrow in the box indicates chromosomal locus with a highest alignment score of targeting by shRNA.

Control digestion

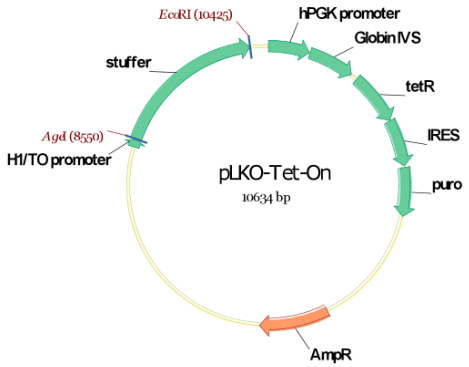

Figure 8. Map of the pLKO-Tet-On vector. Adapted from Dmitri Wiederschain, PhD

The pLKO-Tet-On vector (Figure 8) was was a gift from Dmitri Wiederschain (Addgene plasmid #21915) [159]. It is a one-vector system for production of the lentiviral particles, containing all elements necessary for the inducible shRNA-mediated gene-knockdown in target cells. The shRNA cloned in the vector will not be expressed in the absence of doxycycline, as the tetR element is blocking the shRNA promotor. Upon doxycycline substitution, shRNA expression is triggered and target genes are knocked-down.

The pLKO-Tet-On vector was enzymatically digested using AgeI and EcoRI enzymes (reaction mix see table 4). The reaction was carried out for 2 h at 37°C in thermoblock.

	Final concentration/amount	Volume
2.1 10x Buffer NEB	1x	10 µl
100x BSA	1X	1 µl
AgeI	40 U	8 µl
EcoRI	40U	2 µl
H_2O	Up to 100 µl	77,8 µl
pLKO-Tet-On vector [3650ng/µl)	4 µg	1,2 µl

Table 4. Composition of pLKO enzymatic digestion reaction.

The control for the digestion didn't contain the enzymes. The digestion sample was divided into two samples – a 10 µl reference and a 40 µl probe to be used for extraction from the gel. The control and digestion products were run on a 1% TAE agarose gel at 130 V for 1 h. The results are shown in the Figure 9.

Only the right part of the gel was initially exposed to UV light. The reference sample and negative controls were used to prove the efficacy of the reaction and to mark the region for gel extraction. The area was cut out using a surgical blade and the rest of the gel was than analyzed to check if the

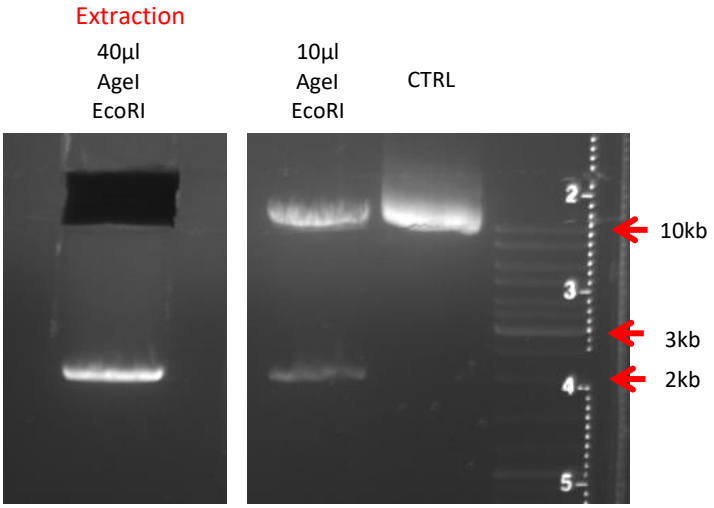

Figure 9. Results of pLKO enzymatic digestion

whole product was removed. The restriction digestion is expected to generate two products: stuffer of 1,8kb size and pLKO backbone >10kb, which corresponds to the obtained results (Figure 4). DNA was extracted from the gel using the Gel Extraction Kit (Qiagen).

In parallel, the annealing of top and bottom strands of shRNAs was performed. Top and bottom strands of oligonucleotides were diluted to a final concentration of 100 pmol/µl. For the annealing reaction, 11,25 µl of top and bottom strands were transferred to the PCR tube and 2,5 µl of the 10x annealing buffer (1 M NaCl, 100 mM Tris-HCl, pH=7,4) were added. Annealing was performed using thermo-cycler program as showed in the table 5:

Temperature	Time
95°C	5 minutes
80°C	5 minutes
72°C	5 minutes
68°C	5 minutes
65°C	5 minutes
0°C	forever

Table 5. Conditions of the shRNA annealing reaction.

The annealed oligonucleotides were immediately used for the ligation reaction. The reaction was performed with the TAKARA-kit (Takara Bio Inc.). The mix of annealed oligonucleotides was diluted 1:50 using 0,5x annealing buffer. 2 µl of the diluted annealed oligonucleotides were ligated with 20 ng of the digested pLKO-Tet-On backbone. The total volume was then mixed with 5 volumes of

reagent A and 1 volume of reagent B from the TAKARA kit and incubated over-night at 16°C. The digested-vector-only control was also included to monitor possible self-ligation of the vector.

The total volume of the ligation reaction was transformed into the DH5α bacteria (Invitrogen), plated on agar-plates supplemented with ampicillin (Carl Roth), and incubated for 16 h at 32°C. Single colonies were picked and collected into 5 ml of LB-medium containing ampicillin, followed by a 16 h incubation step.

From the resulting bacterial culture, 100 µl of the suspension was mixed with 100 µl of 87% glycerol and frozen at -80°C as a glycerol stock back-up. The rest was centrifuged and the DNA was isolated using the MINI- preparation kit (Qiagen). The pellet was dried over-night and re-suspended in 100 µl of 0.1 x TE buffer. For analysis of the ligation, 3 µl of the product were mixed with 2 µl of H1_seq#1-S (binding to the H1 promoter indicated in the vector map), pre-diluted to 10 pmol/µl and sent for sequencing. The obtained sequencing results were analyzed for presence of the shRNA sequence. An example of alignment is presented below (Figure 10) for a successful ligation of the shRNA directed against *STAT5A* (shRNA sequence TRCN0000232135).

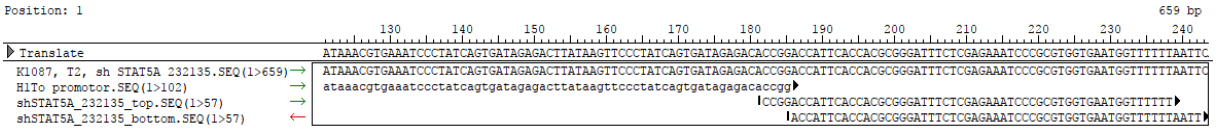

Figure 10. Result of sequencing of the H1 promotor region in the pLKO vector containing the STAT5A-shRNA.

The glycerol stocks for positive clones were used for inoculation of bacterial cultures in 200 ml of LB medium containing ampicillin and incubated over-night. After preparing new glycerol stocks, the DNA was isolated from the culture using the Maxi-preparation kit (Qiagen). Resulting DNA pellets were dried over-night and re-suspended in sterile RPLC water. The concentration of the plasmid DNA was assessed using a Nanodrop spectrophotometer (Thermo Scientific). Obtained plasmid-DNA was again sent for sequencing to confirm the shRNA sequences were cloned inside.

Production of viral soups

Production of the lentiviral particles was performed using 293T packaging cell line. Cells were seeded to reach the confluency of 50-60% and transfected with the pLKO-Tet-On vector containing the shRNA sequence together with the packaging plasmid (pSPAX2) and the envelope plasmid (pMD2.G) using TransIT-LT1 transfection reagent (Mirus). The TransIT transfection reagent (18 µl per plate) was diluted with RPMI1640 medium (270 µl per plate) and incubated for 5 minutes in room temperature. The packaging, envelope and expression plasmids were mixed together according to table 5, transferred to the tube containing diluted TransIT-LT1, re-suspended and incubated for 25 minutes at room temperature. The transfection mix (Table 6) was afterwards added to the culturing plate with 293T cells covered with 6 ml of DMEM medium and incubated for 16 h (37°C, 5% CO_2).

Reagent	Per 10 cm culture plate
Packaging plasmid (pSPAX2)	1,8 µg
Envelope plasmid (pMD2.G)	0,3 µg
pLKO-Tet-On shRNA plasmid	3 µg
RPMI1640 (clean)	20 µl

Table 6. Composition of the transfection mix.

The next day, medium was removed (S2-waste), replaced by 4 ml DMEM supplemented with 30% FBS and incubated for 24 h. Afterwards, the medium containing the viral particles was collected, transferred to a sterile 15 ml Falcon tube (BD) and centrifuged for 5 min at 400 g to pellet down the 293T cells. The supernatant was aliquoted in 1 ml cryo-tubes and stored at -80°C.

Transduction of the AML cell lines was performed in 6-well plates. One million of cells were seeded in 3 ml of RPMI1640 medium and 1 ml of the viral soup was added. The transduction plate also included a negative control with medium only. Plates were centrifuged at 3000 rpm at 30°C for 135 minutes followed by an over-night incubation in the S2 incubator (37°C, 5% CO_2). The next day, cells were spun down and the medium was replaced with RPMI1640 supplemented with 1-1.5 mg/ml of puromycin 24 h post transduction. The selection of transduced cells was performed until the cells in the non-transduced well were dead (approximately 1 week).

Control of knock-down efficacy and effects on transduced cells

Knock-down efficacy

AML cell lines transduced with control or targeting shRNA were treated with doxycycline for 3 days and the efficacy of knock-down was assessed by quantitative real-time PCR and western blot according to the protocols described in the first section. To compare the changes of mRNA levels upon induction of knock-down, relative expression calculated via qRT-PCR was normalized to the shSCR control and the Base-2 logarithm of the Fold Change was plotted.

Growth curves and proliferation assays

Cell lines transduced with control or targeting shRNA were treated with doxycycline for 3 days and seeded in T75cm suspension culture flask at a cell density of $0{,}3\times10^6$cells/mL. Cells were treated with doxycycline at the final concentration of 100 ng/mL. Concentration of cells was monitored for 4 days via cell counts (trypan exclusion assay) and confirmed by MTT assay performed on day 5.

Analysis of Cell cycle and differentiation.

The analysis of Cell cycle was performed by PI stainings and FACS measurements on day 6 of doxycycline induced STAT5 knock-down (day4 for SKM-1). Differentiation of cells was monitored by validation of CD11b and cKIT (both antibodies from Biolegend) expression with FACS on day 3 of knock-down induction. To follow morphology of AML cells upon STAT5 down-regulation, May Grunwald-Giemsa stainings were performed on day 7 of doxycycline administration.

Phosphorylation of STAT5A at Tyr694 and STAT5B and Tyr699

Immunoblotting and induction / inhibition of STAT5 phosphorylation

Phosphorylation of STAT5 at Tyrosine 694 is known as a mark for an active protein, which can translocate to the nucleus and induce the transcription of target genes. To compare the phosphorylation levels of STAT5A and STAT5B we performed immunoprecipitation (IP) experiments with $FLT3^{ITD}$-positive MV4-11 cells, which show constitutive STAT5 phosphorylation. In contrast, treatment with the FLT3-inhibitor PKC412 (midostaurin) causes de-phosphorylation of STAT5. Similarly, IPs were performed with protein lysates from cells that express uSTAT5 (THP-1 and SKM-1) at steady state levels or upon treatment with media supplemented with supernatants from 5637 cells, which produce Granulocyte-macrophage colony-stimulating factor (GM-CSF) (10% of 5637 supernatant in complete RPMI). GM-CSF is a known stimulator of the JAK-STAT pathway and causes strong STAT5 protein phosphorylation. Efficacy and kinetics of GM-CSF treatment were assessed by protein extraction at the different timepoints and western blotting analysis (Figure 11). For further experiments a 30 minutes timepoint of GM-CSF induction was used.

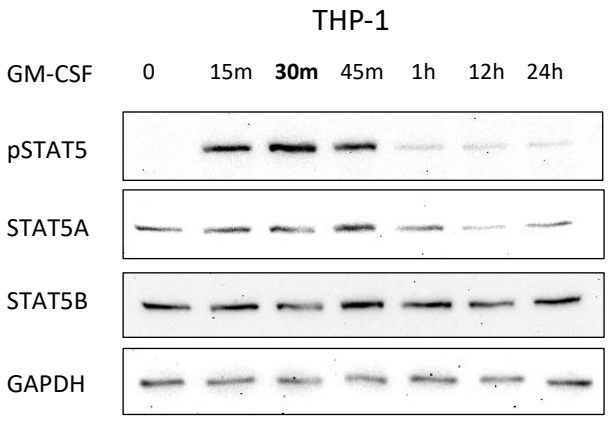

Figure 11. Kinetics of STAT5 phosphorylation with GM-CSF in THP-1 cells.

Immunoprecipitation of STAT5A or STAT5B

Immunoprecipitation experiments were performed as follows.

1. Proteins were extracted using a modified RIPA buffer recipe supplemented with protease inhibitors as indicated in Table 7:

Inhibitor	Final concentration
25x Complete cocktail of serine and cysteine proteases inhibitors	1x
Na_3VO_4, 100 mM	1 mM
NaF, 2M	5 mM
ß-glycerophosphate, 500 mM	5 mM

Table 7. Protease inhibitors mix added to RIPA buffer prior to the protein extraction

2. To wash the beads, 20 µl of the agarose protein A/G beads (Santa-Cruz, sc-2003) were re-suspended in 1 ml of RIPA buffer for each pull-down. Beads were spun down and 300 µl of RIPA buffer was added. The washed beads were conjugated with either 3 µg of IgG control Ab or 3 µg of Ab of interest (αSTAT5A (sc-1081) or αSTAT5B (sc-1656)) for 1 h at 4°C on the rotation wheel (6 rpm). Afterwards, beads were spun down for 1 minute with 3.500 rpm at 4°C and the supernatants were discarded.
3. The protein concentration in lysates was assessed with help of Bradford protein assay and volume of lysates corresponding to 1 mg of proteins was transferred to tubes with beads-antibodies conjugates. A small volume of lysates was saved as input sample (10% of input, frozen at -80°C). Pre-cleared beads with antibodies and lysates were incubated over-night at 4°C on the rotation wheel (6 rpm).
4. To wash the immunoprecipitated (IP) complexes, beads were centrifuged down for 1 minute at 3500 rpm and 4°C. Supernatants were removed and IP complexes were washed with 1ml of extraction buffer supplemented with protease and phosphatase inhibitors. This step was repeated 4 times.
5. Beads were centrifuged down and all the supernatant was removed with help of syringe and a needle. Both IP complexes and input controls were resuspended in 4 X sample buffer with 20% of β-mercaptoethanol and heated for 5 minutes at 95°C. The beads were centrifuged and equal volumes of the supernatants were loaded on the 10% SDS-PAGE gel. Afterwards, the western-blotting protocol described in the first chapter was used.

Immunofluorescence analysis

Immunofluorescence experiments were performed to analyze the localization of uSTAT5A/B and pSTAT5A/B in the cellular compartments. The cells were pre-induced with RPMI1640 medium containing 10 % of GM-CSF (supernatants derived from the 5637 cell line) for 30 minutes. Cells were counted and 0.15 x10^6 cells were transferred on coverslips pre-coated with 0.01 g/ml of Poly-L-Lysine (Sigma). After 5 minutes medium was carefully aspirated and cells were fixed using 4% Formaldehyde (Pierce™, Methanol-free) for 10 minutes at room temperature. The cover slips were washed once with 3 ml of PBS and permeabilized for 10 minutes using 0,1% of Triton-X (Sigma) in PBS. After performing two additional washing steps with PBS, cells were covered with 1% of BSA (Sigma) in PBS and blocked at 4°C.

Incubation with primary antibodies was performed using either a STAT5A antibody of rabbit origin (sc-1081) or a STAT5B antibody of mouse origin (sc-1656). Antibodies were diluted 1:200 in 1% BSA in PBS and 100 µl of the mix was pipetted on a BRAND® PARAFILM® M sealing film (Sigma). Cover slips with blocked cells was placed on the drop and incubated for 1 h at 37°C. Afterwards, the cover slips were transferred to a 6-well plate and washed 3 times with 3 ml of 0.1% Tween in PBS.

The secondary antibody mix was prepared using Hoechst 33342 (Invitrogen) for counter staining of the nucleus (diluted 1:1000), a secondary antibody (anti-rabbit) coupled with Alexa488 fluorophore (Invitrogen, A-11034) diluted 1:600 and a secondary antibody (anti-mouse) coupled with Alexa546 fluorophore (Invitrogen, A-11030) diluted 1:600. Again, 100 µl of the mix was pipetted onto PARAFILM and cover slips with cells incubated with primary antibodies were placed onto the drop. In addition, a negative control was prepared using cells that were not incubated with the primary antibodies, but only exposed to the secondary antibody mix allowing us to control unspecific staining originating from the secondary antibodies. Cover slips were incubated for 1 h at 37°C, washed 3 times with 3 ml of 0,1% Tween in PBS, mounted on the microscope slide using Fluoroshield (Sigma) and kept in the dark at 4°C until analysis. The IF samples were analyzed using a Zeiss microscope, with 63x immerse oil objective (Plan-Apochromat 63x/1.40 Oil DIC M27), digital zoom 4x, pinhole 100 µm.

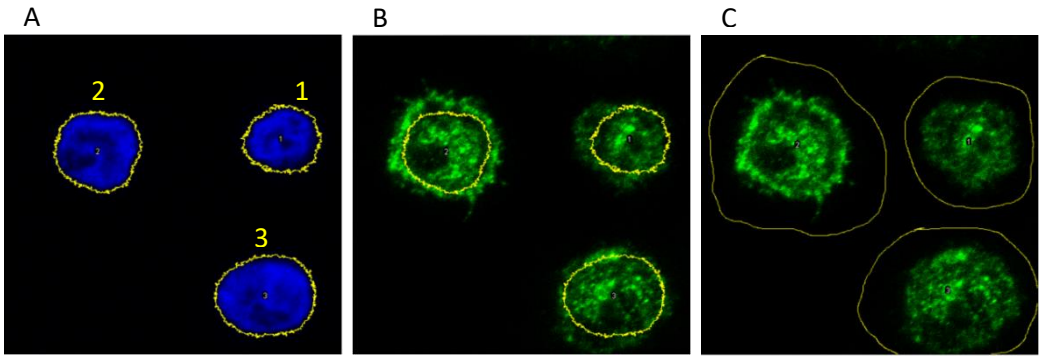

Figure 12. Strategy of fluorescence intensity measurement in nucleus and cytoplasm

As a negative control, stainings with secondary antibodies only and Hoechst 33342 were used to remove background derived from unspecific binding. All detection channels were set a way that no signal was observed in the negative controls (negative control staining presented in the Supplementary figure 3. All pictures were taken applying the scanning mode and only the stacks from the middle section of the cells were used for the further analysis. Above, an example in SKM-1 cells shows how the percentages of uSTAT5A inside and outside of the nucleus were calculated using FiJi software (ImageJ, version 1.49, NIH).

First a picture with signals recorded in the Hoechst channel was opened and the area of the nucleus was marked using the threshold function (Huang preset). Using the Analyze particles function objects with more square pixels than 20 were considered and added to the ROI manager including marking by the overlay outlines (Fig 12A). Afterwards, pictures recorded in the green and red channels were imported (example using uSTAT5A staining, Alexa488 – green channel) and the previously set area of the nucleus was overlaid (Fig 12B). Using ROI manager the raw intensity of uSTAT5A signal in the nucleus was measured (Table 8). To analyze the total signal in the cell, the whole area surrounding the cell was manually marked (Fig 12C) and measured using ROI manager (Table 8). Based on these values the percentage of uSTAT5A localization inside and outside of the nucleus was calculated and plotted.

Cells	uSTAT5A signal Raw intensity in the nucleus	uSTAT5A signal Raw intensity total signal	uSTAT5A Signal in the nucleus [%]	uSTAT5A Signal in the cytoplasm [%]
1	603673	1008114	59,9	40,1
2	1081407	2283362	47,4	52,6
3	1043910	1564137	66,7	33,3

Table 8. Example of raw intensity signal quantification and calculation of localization percentage.

Murine leukemia models.

Mouse strains

The mouse strain used as a bone marrow donor in our experiments was originally generated to monitor the role of *Stat5* gene expression in mammary epithelium during pregnancy [80]. Briefly, *Stat5$^{f/f}$* mice, in which the *Stat5a* and *Stat5b* gene loci are flanked with *loxP* sites, were crossed with C57BL/6J mice expressing the *Cre recombinase* gene under the control of the *Mx1* gene promoter. The promotor can be activated by intraperitoneal administration of the polyinosinic-polycytidylic acid (pIpC) [160]. The resulting mouse strain (*Stat5$^{f/f}$_Mx1-Cre*) was a source of hematopoietic stem and progenitor cells for primary transplantation experiments.

Genotyping

The tips of mice tails were cut and collected in eppendorf tubes. They were immediately treated with digestion buffer (100 mM Tris-HCl pH=8,5, 5 mM EDTA, 0,2% SDS, 200 mM NaCl) supplemented with 1 mg/mL Proteinase K (Qiagen) for 4 h at 57°C and light shaking. Afterwards, the DNA was precipitated with isopropanol for 1 h at -20°C. The resulting DNA pellet was cleaned by re-suspension in 70% EtOH, centrifugation and finally air-drying the pellet overnight. The DNA was re-suspended in 0.1 x TE buffer and used for the genotyping PCR with one of the following primers sets (sequences are listed in the Supplementary Figure 2:

- Stat5 wt – specific to the wild-type Stat5 gene (primers Stat5_HH_ 1 and 2)
- Stat5 floxed – amplifying the DNA containing flox-flanked Stat5 gene region (primers 3 and 4)
- Stat5 Mx-Cre – amplifying the DNA encoding Mx-Cre recombinase

The PCR reaction was not multiplexed and prepared in the way presented in the Table 9:

Reagent	Final concentration	Quantity for 25 µl of reaction mixture
Sterile deionized water	-	13.75 µl
10X Taq buffer	1x	2.5 µl
dNTP mix	0.2 mM of each	0.5 µl
Primer 1	2000 nM	0.5 µl
Primer 2	2000 nM	0.5 µl
Taq DNA Polymerase	5 U / 50 µl	0.25 µl
5X Q-Solution	1X	5 µl
Template DNA	10 pg to 1 µg	2 µl

Table 9. Composition of the PCR reaction for mouse genotyping

The amplification was performed under following conditions:

Stat5 wt - 65°C

Stat5 fl - 62°C

Mx1-Cre - 64°C

Cycling conditions:	time	
Initial Denaturation 96°C	5 min	
Denaturation 96°C	1 min	35 cycles
Primer Annealing XX°C	1 min	
Extending 72°C	1 min	
Final Extending 72°C	5 min	

Table 10. PCR run conditions.

An example of a genotyping result is presented in the Figure 13. All genotyped mice carry gene encoding Mx1-Cre recombinase (band at 380 bp). Only samples 3 and 4 have the region of *Stat5* genes flanked with a flox sequence ($Stat5^{fl/fl}$ – giving a band at 200 bp) – target for active Mx-Cre recombinase.

In line with that, samples 3 and 4 are negative for expression of un-flanked wild-type (WT) *Stat5* and samples 1 and 2 come from mice carrying the WT *Stat5* (bands at 450bp).

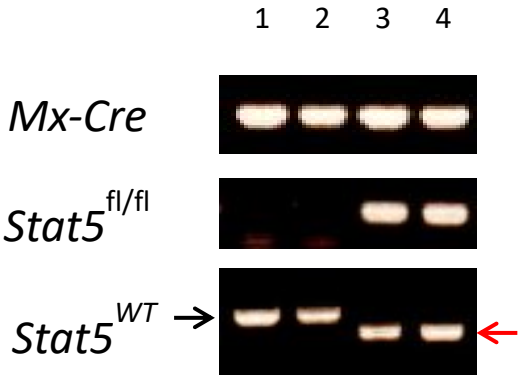

Figure 13. Example of mice genotyping. PCR reaction was performed to control for presence of genes encoding Mx1-Cre recombinase (380 bp), $Stat5^{fl/fl}$ (200 bp) or wild-type Stat5 (450 bp). Black arrow indicates specific product of wild-type Stat5 PCR, whereas unspecific product is indicated with a red arrow.

Bone Marrow Transplantation (BMT)

Production of viral supernatants

293FT cells were co-transfected with the MSCV_MLL-AF9_IRES-GFP (MA9) expression plasmid and the retroviral packaging plasmid Ecopack using TransIT LT-1 (Mirus). After 16 hours of transfection medium was exchanged with 4 ml DMEM media supplemented with 30% FBS and incubated for 24 h. The viral soups were analyzed for efficacy by a control transduction performed on BaF3 cell line and snap-frozen at -80°C for the experiment.

Extraction of bone marrow cells

Two days before BMT (day -2) C57BL/6J $Stat5^{fl/fl}$ or $Stat5^{fl/fl}$_Mx1-Cre mice between the age of 8-12 weeks were sacrificed. The bone marrow cells were obtained by flushing the femur and tibia bones with ice-cold PBS in sterile syringes. Cells of mice with the same genotype were pooled for further experiments. Collected Bone Marrow cells were re-suspended in Red Blood Cells lysis buffer (RBC buffer, Qiagen) for 5 min on ice. Afterwards, the cells were transferred on a sterile cell strainer to obtain a single cell suspension. The strainer was flushed one time with RBC buffer to collect all cells that were afterwards centrifuged for 5 minutes at 1500 rpm and re-suspended in sterile PBS.

Lineage depletion

Lineage depletion was performed with bulk bone marrow cells to enrich the population for immature hematopoietic stem and progenitor cells. With help of EasyPrep Separation magnetic kit (Stem Cell Technologies) non-hematopoietic stem cells and non-progenitor, lineage committed cells were targeted by antibodies recognizing the following markers: CD5, CD11b, CD19, CD45R/B220, Ly6G/C(Gr-1), TER119, 7-4; and were removed from the BM pool. A complete list of antibodies used in this process, including references can be found in supplementary table S1.

As next step, lineage-depleted cells were counted and seeded in 12-well suspension plates at a density of 2.,5 $\times 10^6$ cells per well in 2 ml DMEM medium supplemented with:

- 1% Penicillin- Streptomycin antibiotic solution (10.000 U/mL),
- 20% FBS
- IL-3 final concentration of 6 ng/mL (R&D systems, #403-ML)
- IL-6 final concentration of 1 ng/mL (PeproTech, #200-206)
- Stem Cell Factor (SCF) final concentration of 10 ng/mL (R&D Systems, #1832-01)

Cells were incubated over night at 37°C, 5% CO_2.

Transduction of hematopoietic progenitor cells

Normal hematopoietic stem and progenitor cells were transduced with MSCV-retroviruses expressing, MLL-AF9_IRES-GFP a potent leukemia driving fusion oncogene. One day before BMT (day -1) lineage-depleted cells were transduced with viral soups containing the retrovirus MA9. Briefly, 750 µl of the viral soup, 20 µl HEPES buffer and 4 µl Polybrene were added to each well containing lineage-depleted cells. The plates were centrifuged for 90 minutes at 2.000 rpm at 30°C, placed in the incubator for 4 h, and finally the medium was changed to fresh, fully supplemented DMEM media for overnight incubation. On the day of transplantation (day 0), a second transduction with the MA9 was performed and cells were cultured for additional 3 hours at 37°C.

Bone marrow transplantations

Primary transplantation

On day -1 healthy C57BL/6J recipient mice were irradiated with a lethal dosage (9 Gy) of gamma irradiation to suppress the immune system and avoid transplantation rejection. Transduced cells were collected, centrifuged and re-suspended in PBS for counting. At the same time one healthy C57BL/6J mouse was sacrificed to obtain bone marrow "helper cells" for the BMT. For one bone marrow transplantation 10^6 MA9-transduced cells were re-suspended in 300 µl of PBS and transplanted into a tail-vain of C57BL/6J irradiated, recipient mouse. Leukemia development was analyzed in two cohorts of recipient mice: Transplanted with the cells derived from C57BL6 $Stat5^{fl/fl}$ or transplanted with the cells obtained from the C57BL6 $Stat5^{fl/fl}$ xMx1-Cre mice.

Secondary transplantation and depletion of Stat5

To prepare the recipients for secondary transplantations the C57BL6/J wild-type mice were sub-lethally irradiated (4,75 Gy) one day prior to BMT. On the following day, leukemic bone marrow cells derived from MA9-postive C57BL6/J $Stat5^{fl/fl}$ or C57BL6/J $Stat5^{fl/fl}$_Mx1-Cre primary recipients were thawed and 10^6 cells were transplanted intravenously into irradiated secondary recipients. To allow proper engraftment of recipient cells, we waited 10 days before starting the induction of the Mx1-Cre recombinase. On days 10, 12 and 14 mice were injected intraperitoneally with 300 µl of pIpC.

Analyses of leukemic mice

After observing the first signs of disease (reduced motility, hunch-backed position, and ruffled coat) blood samples were taken and white blood cells counts (WBC) were analyzed. Sick mice with elevated WBC counts were culled, both the spleen and bone marrow cells were collected and frozen for further analysis. Remaining cells derived from the spleen were used for the protein extraction to control the levels of Stat5 expression.

FACS Analysis of leukemic mice bone marrow

To analyze the phenotypic changes of the bone marrow cells we performed FACS analyses. First, the cells were checked for the GFP positivity and only positive cells were used for the analysis. Bone marrow cells from both mice cohorts were stained with antibodies for GR-1 and CD11b (GR-1-PE: 108408, Biolegend; CD11b-APC: 101212, Biolegend)- known differentiation markers.

The Cancer Genome Atlas (TCGA)

Analysis of STAT5 mRNA expression was performed with help of the cBio Portal for Cancer Genomics [161] containing *The Cancer Genome Atlas* (TCGA) database with clinically annotated samples of adult de novo AML patients [37]. The samples were analyzed for mRNA expression of *STAT5A* and *STAT5B* in patients with *FLT3*^{WT} or mutant *FLT3*. Samples were grouped according to the FLT3 status: *FLT3*^{WT} group (119 patients), *FLT3*^{ITD} group (34 patients), and *FLT3*^{TKD} group (12 patients).

SILAC IP protocol

To perform quantitative proteomics, AML cells were exposed to non-radioactive, stable isotopes containing amino acids, which are incorporated into newly synthesized proteins during tissue culture. AML cells were either exposed to light SILAC-media containing normal Arginine and Leucine (composed of ^{12}C and ^{14}N isotopes – called 0/0), medium SILAC- media (composed of L-Arginine-$^{13}C_6$(Arg6) and L-Lysine-$^{2}H_4$(Lys4) – called 6/4), or heavy SILAC-media (composed of L-Arginine-$^{13}C_6{}^{15}N_4$ (Arg10) and L-Lysine-$^{13}C_6{}^{15}N_2$ (Lys8) – called 10/8). Successful incorporation of the isotope-labeled amino acids into newly synthesized proteins is achieved already after 5 doubling times. Here, AML cell lines were cultured using SILAC media (light -0/0, medium- 6/4 or heavy- 10/8) for two weeks. Protein lysates derived from all experimental conditions were extracted and immunoprecipitation with either a control IgG antibody (lysates derived from cells treated with the light 0/0 SILAC medium) or antibodies specific to STAT5A or STAT5B was performed. The immunoprecipitated target proteins, together with interacting partners were mixed in a 1:1 ratio with the immunoprecipitates derived from the control pull-down. Lysates within the mixture can be distinguished by Mass spectrometry analysis due to the incorporation of differently labeled amino acid in the proteome [162][163]. The detailed protocol used in this study is described below.

Protocol

The Immuno-precipitation was performed according to the following protocol:

1. Proteins were extracted from 100 x 10^6 cells using 1 ml modified RIPA buffer supplemented with protease inhibitors.
2. To wash the beads, 40 µl of the agarose protein A/G beads (Santa-Cruz, sc-2003) were re-suspended in 1 ml of RIPA buffer for each pull-down. Beads were spun down and 300 µl of RIPA buffer was added. The washed beads were conjugated with either 5 µg of IgG control Ab or 8 µg of Ab of interest (αSTAT5A (sc-1081) or αSTAT5B (sc-1656)) for 1 h at 4°C on the rotation wheel (6 rpm). Table 11 shows the strategy of pre-coating of beads with specific STAT5 targeting antibody or control antibody.

	0/0	6/4	10/8	Type of SILAC medium
	Vehicle control	Vehicle control	PKC412 treatment	treatment
Number of tubes prepared per condition	2 tubes: beads+ IgG control	1 tube: beads+ STAT5A ab 1 tube: beads+ STAT5B antibody	1 tube: beads+ STAT5A ab 1 tube: beads+ STAT5B antibody	MV4-11
	0/0		10/8	Type of SILAC medium
	2 tubes: beads+ IgG control		1 tube: beads+ STAT5A ab 1 tube: beads+ STAT5B antibody	THP-1
	2 tubes: beads+ IgG control		1 tube: beads+ STAT5A ab 1 tube: beads+ STAT5B antibody	SKM-1

Table 11. Design of the experiment. Table indicates SILAC media type used for each cell line and preparation of beads for the pull-downs.

Afterwards, beads were spun down for 1 minute with 3.500 rpm at 4°C and the supernatants were discarded

3. Between 3-4 mg of proteins were added per immunoprecipitation. A small volume of lysate was saved as input (10%) and the lysates were then transferred to eppendorf tubes with beads and antibodies complexes as listed below and indicated in the table X:
   - For SKM-1 and THP-1
   - the lysate extracted from cells cultivated with the light SILAC medium (0/0) were transferred to a tube with beads containing the IgG ctrl antibody
   - the lysate extracted from cells cultivated with the heavy SILAC medium (10/8) were transferred to a tube with beads containing the Ab of interest (αSTAT5A or αSTAT5B)

➢ MV4-11

- the lysate extracted from cells cultivated with the light SILAC medium (0/0) were transferred to a tube with beads containing the IgG ctrl antibody
- the lysate extracted from cells cultivated with the medium SILAC medium (6/4) were transferred to a tube with beads containing the Ab of interest (αSTAT5A or αSTAT5B)
- the lysate extracted from cells cultivated with the heavy SILAC medium (10/8) were transferred to a tube with beads containing the Ab of interest (αSTAT5A or αSTAT5B)

Tubes were incubated for over-night at 4°C on the rotation wheel.

4. The beads were centrifuged for 1 min/3.500 rpm/4°C. After removing the supernatant immune-complexes were washed with 1 ml of RIPA extraction buffer supplemented with protease and phosphatase inhibitors. This step was performed twice.
5. Beads were then centrifuged like in the previous step but washed with 0,5 ml of RIPA extraction buffer. Afterwards tubes with immunoprecipitates containing the antibodies against the protein of interest (STAT5A or STAT5B) were merged with the corresponding tubes containing the control IgG antibody. Solutions from corresponding eppendorf tubes were pooled together and the empty eppendorf tube was washed with 0,5 ml of extraction buffer using the same pipette tip and pooled again.
6. One more washing step was performed on the combined pull-down lysates.
7. Beads were spun down, the supernatant was removed completely, and 4X concentrated sample buffer supplemented with 1 mM DTT [1 M] was added. The sample was heated for 10 min at 70°C and left to cool- down at room temperature.
8. The alkylating agent chloracetamide(CAA) was added to obtain a final concentration of 5,5 mM and incubated for 30 min in the dark at RT.
9. Samples were kept frozen at -20°C.

Afterwards, the samples were analyzed in collaboration with the group of Dr Beli at the core facility of the Institute of Molecular Biology in Mainz (IMB). We also submitted snap-frozen pellets for the analysis of incorporation of the isotope labeled amino acids. Figure 14 shows the confirmation of the incorporation in THP-1 cells treated with either light or heavy SILAC media.

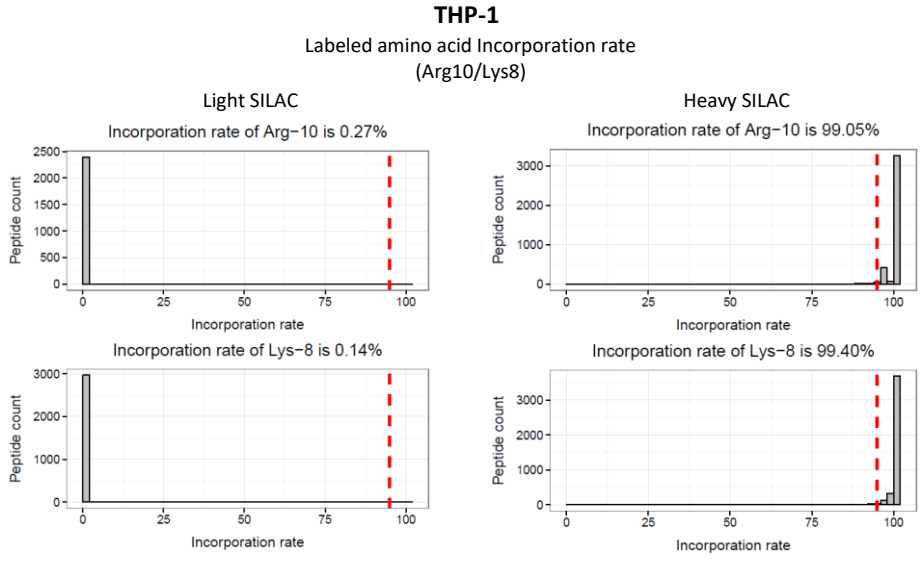

Figure 14. Confirmation of labeled amino acids incorporation in THP-1 cells.

As expected, the proteome of cells treated with the light SILAC medium is not enriched with heavy-labeled amino-acid forms. Contrary, the cells cultured with the Heavy SILAC medium incorporated the labeled forms of Arginine and Lysine into the proteome with a very high efficacy (>99%). Further handling of the samples including the in-gel digestion was performed by Jan Heidelberger (Beli laboratory) according to the protocol below:

1. Samples were run on a SDS-PAGE gel.
2. The gel was stained with Novex Colloidal blue stain kit (NuPAGE, Thermo Fischer Scientific) for 15 min - 1h and de-stained in water over-night
3. The desired bands were cut from the gel and sliced into small pieces (ca. 1×1 mm).
4. The gel pieces were covered with 1 ml of destaining solution (50% Ethanol, 50 mM ammonium bicarbonate in water, pH 8.0) and incubated in a thermo-mixer. This step was repeated 4-5 times for 15 min until gel slices are completely destained.
5. Gel pieces were dehydrated by adding 1 ml of absolute ethanol. The gel pieces were incubated for 2 x 10 min in a thermo-mixer.
6. After removing ethanol from gel pieces 50 µl of trypsin solution (25 µl trypsin (0.5 µg/µl) + 1 ml of 25 mM ammonium bicarbonate in water pH 8.0) were added and shook at room temperature (RT) for 30 min. Gel pieces were afterwards covered with 100 µl of 25 mM ammonium bicarbonate in water pH 8.0 and incubated overnight on 37 °C in an incubator.
7. The trypsin digestion was stopped by adding 30 µl of Peptide extraction buffer (30% acetonitrile, 3% trifluoroacetic acid) and incubated at room temperature for 20 minutes in a thermomixer (400-500 rpm).
8. The Gel pieces were covered with 100 µl of Peptide extraction buffer and incubated at RT for 20 min in a thermo-mixer.
9. The samples were spun down briefly, supernatants were removed and pooled with previous supernatants of the same tube.
10. The gel pieces were covered with Buffer B (80% acetonitrile, 0.5% acetic acid) and incubated at RT for 20 minutes in a thermo-mixer shaker (700 rpm).
11. Steps 9 was repeated
12. The gel pieces were covered with 100% Acetonitrile (ACN) and incubate at RT for 10 minutes in a thermo-mixer. Step 9 was repeated
13. The final volume of supernatant pools was reduced by performing SpeedVac (V-AQ, 45°C for 1 h) and proceeded with peptide desalting and filtering using stage tipping.

Processed lysates were than analyzed using quadruple Orbitrap mass spectrometer (Q Exactive Plus, 407 Thermo Scientific) equipped with a UHPLC system (EASY-nLC 1000, Thermo Scientific).

Results obtained from the Mass spectrometer were further analyzed using MaxQuant (version 1.5.2.8). Results were presented in form of ratio between signals coming from the peptides with incorporated heavy amino-acids and peptides with normal amino-acids (ratio between specific STAT5 proteins co-precipitation and control IgG immunoprecipitation) normalized to the normal amino-acids signals (IgG). As putative interacting partners we considered proteins with a normalized ratio score above 2. Some of the interactions were further validated by Co-IP.

Venny graphs presented in the result sections were prepared using an online tool developed by Stefan Jol (Jol, S.J. (2015) Make a Venn Diagram. https://www.stefanjol.nl/venny).

RNA-sequencing

To analyze gene expression changes upon uSTAT5 knock-down, THP-1 cell lines transduced with shSCR, shSTAT5A1 or shSTAT5B3 (THP-1) / were treated with 100 ng/ml doxycyclin for 3 days to induce shRNA expression. Cells were counted and 2×10^6cells were harvested for RNA extraction. The cell pellet was washed one time with ice-cold PBS, re-suspended in 1 ml of peqGOLD TriFast (Peqlab) and snap-frozen in liquid nitrogen. For each condition three biological replicates were prepared and submitted for sequencing. Samples were stored at -80°C until shipment (on dry-ice). The analysis was performed in collaboration with Dr. Lars Bullinger at the University Medical Center in Ulm.

RNA quality control

The RNA was extracted according to the manufacturers protocol and the quality of the RNA was assessed using Bioanalyzer Chip (Agilent RNA 6000 Nano Kit). All submitted sample obtained a RNA integrity number score (RIN) above 9 corresponding to high quality input. An example of the RNA quality control is presented in the Figure 15.

After quality controlling sequencing libraries were prepared using TruSeq RNA Kit v2 (polyA, non-stranded, Illumina) according to the manufacturers protocol.

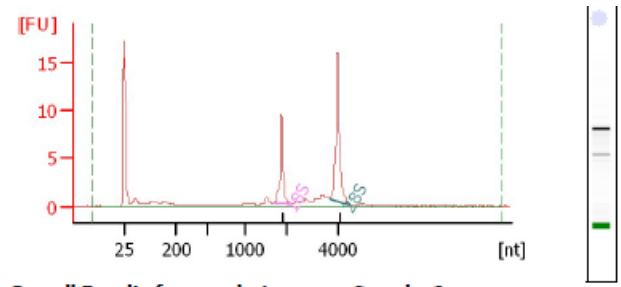

Overall Results for sample 1 : Sample 2

RNA Area:	54.5
RNA Concentration:	28 ng/µl
rRNA Ratio [28s / 18s]:	1.8
RNA Integrity Number (RIN):	9 (B.02.07)
Result Flagging Color:	
Result Flagging Label:	RIN:9

Fragment table for sample 1 : Sample 2

Name	Start Size [nt]	End Size [nt]	Area	% of total Area
18S	1,700	2,183	8.9	16.4
28S	3,658	4,475	16.0	29.3

Figure 15. RNA quality control - example

Sequencing and initial quality controls

The libraries were than sequenced using Illumina HiSeq 2500, on the same run (50 bp, SR= single read). Samples were distributed across the lanes to avoid the batch effect and four samples were sequenced on one lane, e.g. lane 1: THP1 shSCR #01-03 and THP1 shSTAT5A1 #01; lane 2: THP1 shSTAT5A1 #02-03 and THP1 shSTAT5B3 #01-02 etc.

The quality of sequencing was assessed by performing the quality controls of the resulting ".fastq" files. It was done using the R-studio software and library/packages named FastQC and Rqc. An insight on quality of sequencing is presented in the figure 16.

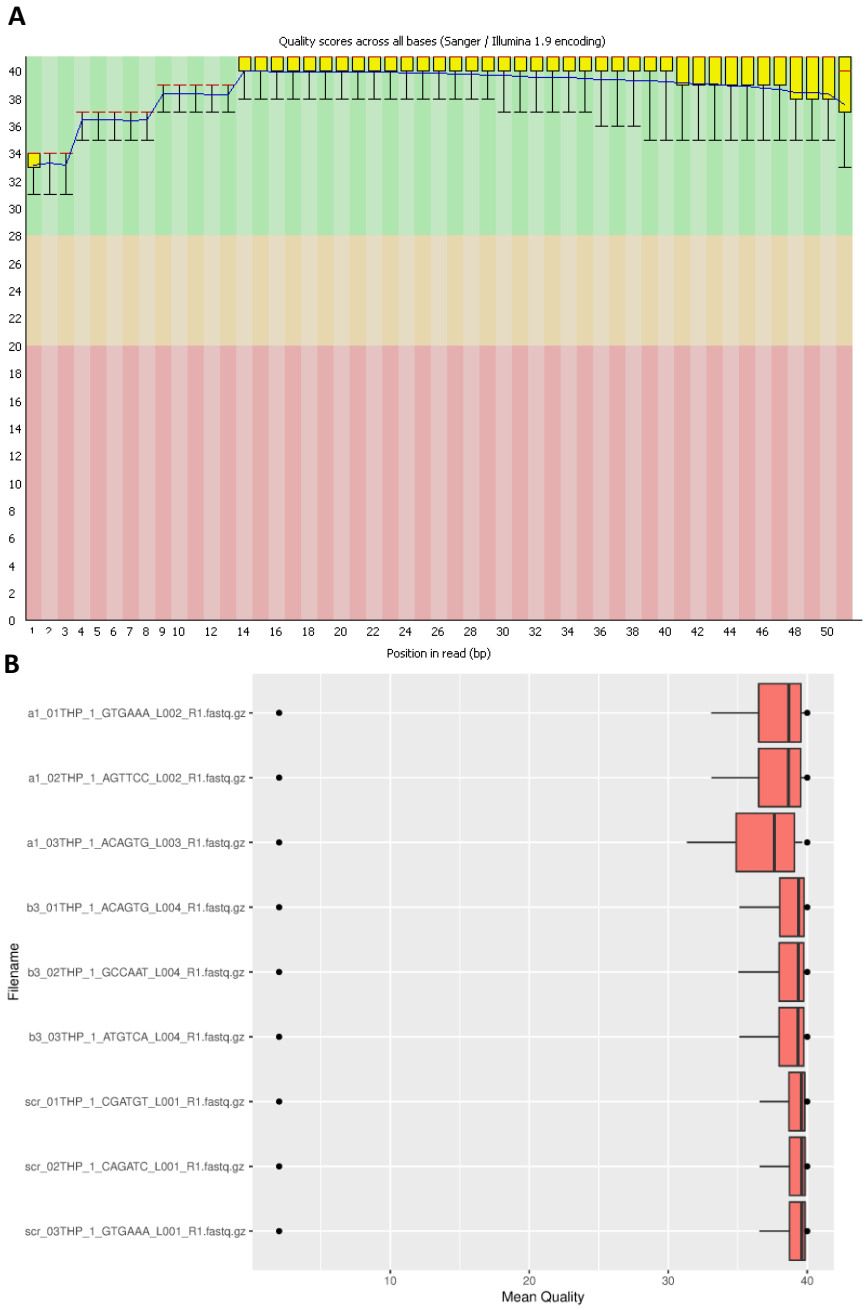

Figure 16. A. An overview of the range of quality values across all bases at each position in the FastQ file for THP-1 shSCR 1st replicate. Data obtained with FastQC package. Red line indicates median value, the yellow box represents the inter-quartile range (25-75%), the upper and lower whiskers represent the 10% and 90% points, and the blue line shows the mean quality. **B**. Comparison of samples shows an overview of per read mean quality distribution of all files as assessed using Rqc package.

Pre-processing of sequencing results

After assessing the sequencing quality, reads were aligned to the human genome. The alignment and quantification of gene counts was carried out using Spliced Transcripts Alignment to a Reference tool (STAR, release 2.4.2a) developed by Alexander Dobin [164]). Two genome indexes were submitted as references for the alignment: human genome from UCSC (ver. hg19 - ucsc.hg19_noAltHaps.fasta) and annotation file containing transcriptome from Gencode release 19 (GRCh37.p13, gencode.v19.chr_patch_hapl_scaff.annotation_UCSCcontigs_noAltHaps.gtf). The mapping of the RNA-seq reads to the genome was performed in "GeneCounts" quantification mode resulting in a SAM file with the alignment details as well as a quantification file (ReadsPerGene.out.tab table) containing number of counts per gene. Information related to our non-stranded libraries are saved in the first and the second column of the quantification table and corresponds to gene names and gene counts. The gene expression table was prepared by extracting these columns for each of the analyzed samples and fused into one file.

Differential gene expression analysis

The obtained gene count lists for each sequenced sample were used to create a gene expression table containing all samples and gene counts. The list was imported in the R-software and used to perform the differential gene expression analysis. The complete R-code used for this analysis with a brief description of each stage can be found in supplementary figure 4.

Principle Component Analysis and unsupervised hierarchical clustering.

To analyze distribution of sequenced samples we performed Principle Component Analysis including control cells (THP-1 shSCR), as well as uSTAT5 down-regulated cell lines (shSTAT5A1 and shSTAT5B3). The R-studio script is described in the supplementary figure 4.

Another tool used to analyze the separation of the sequenced samples was unsupervised hierarchical clustering. It was performed on the differentially expressed gene list normalized by cpm (counts-per-million) function and the script can be found in a supplementary figure 4.

Correlation across the replicates and conditions

To compare the correlation between the replicates for each condition, a "corr" function was used. For this purpose, we used a script, developed by Emil Karaulanov and Nastasja Krelm from the Bioinformatics core facility at IMB, Mainz. The script used to analyze the data is included in supplementary figure 4. Correlations between the replicates are presented in the Figure 17 and the correlations between conditions is shown in the Figure 18.

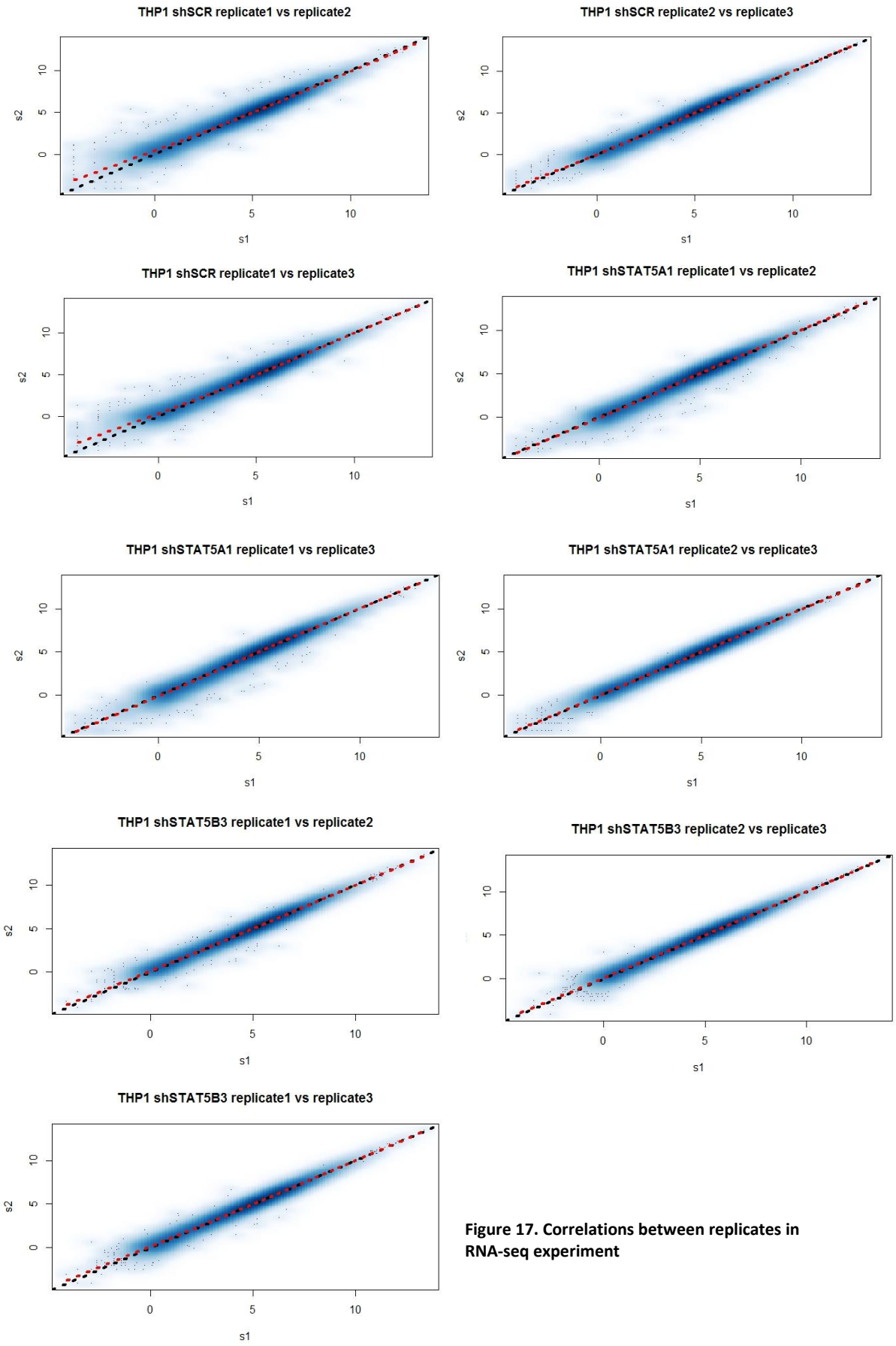

Figure 17. Correlations between replicates in RNA-seq experiment

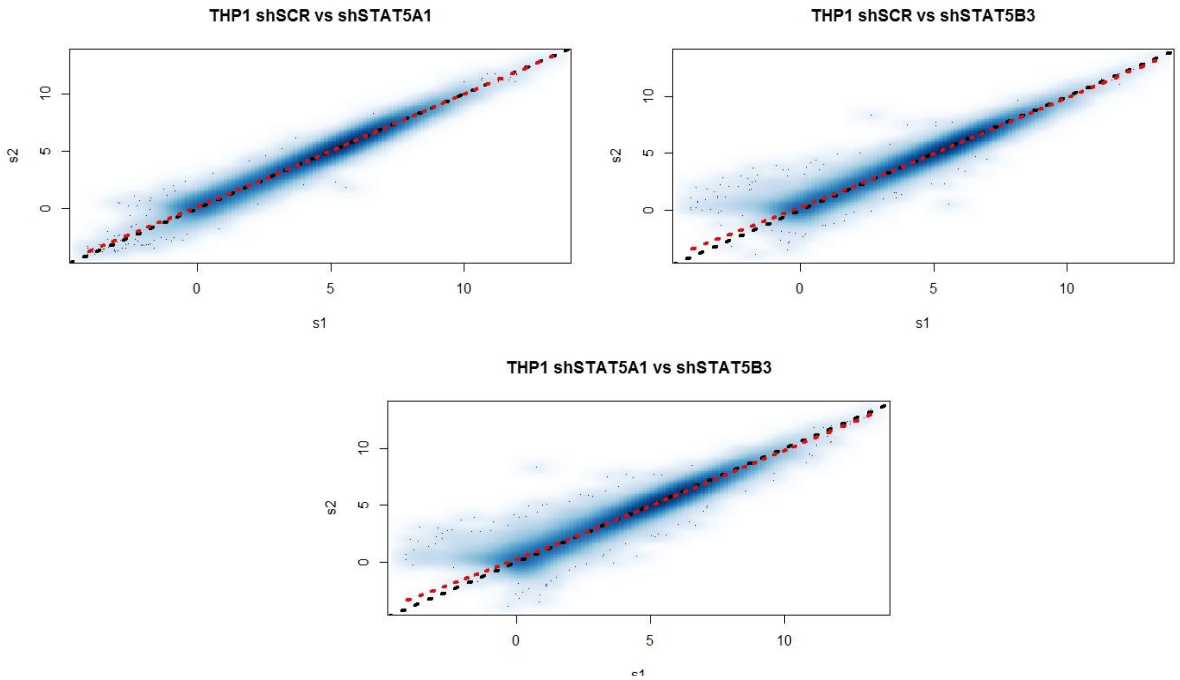

Figure 18. Correlation between conditions in RNA-seq experiment.

Differential gene expression between conditions

A list of the top-differentially expressed genes (DEG) was prepared to analyze the impact of uSTAT5A and uSTAT5B in transcriptional regulation. R-Studio script used to perform this analysis can be found in the supplementary figure 4.

Analysis of the gene expression changes after uSTAT5 down-regulation using the Gene Set Enrichment Analysis and Ingenuity Pathway Analysis

Gene Set Enrichment Analysis

The complete analysis of gene-expression profile can only be performed with help of tools that allow pathway analysis and shed light on biological processes involved in the observed phenotype. In contrast to classical approaches focusing on the discovery of single genes differently expressed between the samples, approaches described in this chapter aim at detecting even a subtle change in biological pathways and processes.

One of the tools used in this study was the "Gene Set Enrichment Analysis" (GSEA)method, a powerful analytical tool developed by the Broad Institute [165] [166]. Initially designed to analyze microarray data, it is also widely used by bioinformaticians to analyze data obtained from RNA-sequencing experiments. The power of the tool lies in the different approach of analysis. Existing methods (e.g. DAVID tool) are based on comparison of a novel experimentally defined list of genes with a curated list consisting of genes known to be important for a biological pathway with the aim to identify overlaps that are bigger than expected by random chance. In this case only genes that meet threshold of significance (genes that meet statistical threshold after differential gene expression analysis) are analyzed for a potential match with a reference list.

In contrast, GSEA method considers all genes in the experiment thereby preventing a loss of subtle changes in genes that could be below the Fold-change or significance thresholds. Furthermore, it takes fold change value into account. The fact that GSEA tool uses every datapoint detected in sequencing in its statistical algorithm will make a huge, positive impact on sensitivity compared to DAVID.

All genes that were mapped and scored with a gene count were included in the analysis. Samples upon knock-down of uSTAT5 were compared with shSCR controls. A fold change between the conditions was calculated and the list of genes was ranked by increasing log2Fold-change scores. The pre-ranked list was submitted to the Java-based GSEA software and the analysis was run with the following parameters:

- Enrichment statistic – classic
- Max. size of a gene set – 1000
- Min. size of a gene set – 15
- Normalization mode –meandiv
- Make detailed gene set report – true
- Seed for permutation – timestamp

Out of 17.786 gene sets available in the Molecular Signatures Database (MSigDB) we only analyzed curated once (as recommended by Broad Institute) and the Gene Ontology (GO) datasets.

For the discovery of drugs that could induce a similar phenotype as observed upon uSTAT5B down-regulation, we used an existing drug signatures database (DSigDB) [167]. It represents a collection of gene sets, which are derived from already available drug-induced gene-expression signatures [168]. Comparisons were performed by incorporation of DSigDB gene sets into GSEA and run against the gene expression profile upon uSTAT5 down-regulation. Among cell lines used to create the connectivity map was HL60. We filtered the results for this cell line and prepared the list of the most significant

comparisons for the genes up-regulated after the drug treatment (UP, compared to the genes enriched in the uSTAT5B knock-down cells) and the genes downregulated after the drug treatment (DOWN, compared to the genes enriched in the control shSCR cells). Only the compounds with both UP and DOWN signatures significantly enriched like our gene expression data were short-listed.

Ingenuity Pathway Analysis (IPA)

Ingenuity Pathway Analysis (IPA, Qiagen) is a powerful analysis and search tool to interpret data from genomics and proteomics experiments. In frames of this dissertation it was used to analyze the interactome of STAT5A and B proteins. In this case the list of interacting proteins from mass spectrometer analysis was imported and investigated for an enrichment of biological pathways. The software was also used to analyze changes of STAT5A and B interacting partners depending on phosphorylation status of the STAT5 proteins in MV4-11 cells.

Finally results of the gene expression analysis after down-regulation of uSTAT5A or B in THP-1 cells were imported to IPA as gene names with fold change in expression and this list was investigated for biological pathway enrichment and possible up-stream regulators that cause analogous changes in gene expression.

Treatment of THP-1 AML parental cell line using a combination of chemotherapeutics and STAT5 down-regulation.

Treatment of THP-1 cells was performed with or without doxycycline induction of shRNA expression in combination with AraC or ATRA. For this experiment cell lines transduced with shSCR, shSTAT5A1 or shSTAT5B3 were used. Both drugs were pre-diluted with PBS and cells were exposed to final concentrations of 100 nM ATRA and 500 nM of AraC for 6 days. To ensure that there is no effect of the vehicle, the same dilution of DMSO in PBS was added to the control cells. On day 6 of treatment cell cycle analysis and cell proliferation assays were performed.

AML cell lines were treated with Dihydroergotamine (DHE) a drug soluble in DMSO and hardly soluble in aqueous solutions. To reach working concentrations DHE was pre-diluted to 1000x final concentration in DMSO and pipetted directly into culture medium with 1:1000 dilution rate. As a vehicle control an equal volume of DMSO was added corresponding to final 0,1% of DMSO in medium.

Statistics

Unless otherwise specified, data are presented as mean ± standard deviation (SD). Comparisons between 2 groups were performed using the unpaired Student *t*-test. A *P* value of <.05 was considered significant. For animal studies, Kaplan-Meier survival analysis was performed, and survival was calculated using the log-rank test. Statistical computations were performed using GraphPad Prism software, version 5.0.

Results

Endogenous expression and localization of STAT5A and B in AML models.

The role of STAT5 proteins in normal hematopoiesis and leukemogenesis has been broadly investigated in cell line or murine models applying RNAi or genetic depletion strategies [83],[80] [84],[119],[124]. In most cases, potential differences between phosphorylated and un-phosphorylated STAT5 as well as between STAT5A and STAT5B members were not considered.
To explore the functional role of uSTAT5, we first screened patient samples and several AML cell lines for STAT5A and STAT5B expression as well as for activation levels. In addition, we investigated sub-cellular localization of both proteins using confocal microscopy.

Expression of STAT5 proteins in primary patient samples

To analyze the expression of STAT5 in primary AML patient samples, proteins were extracted from AML BM cells derived from patients treated at the Department of Hematology and Oncology of the University Medical Center of Mainz and analyzed by western-blotting. As part of the diagnostic procedure samples were investigated in hospital laboratories for presence of common mutations, percentage of leukemic blasts in biopsy and karyotype of patient. Results are combined in the table 12.

Patient number	BioBank number	Sex	Age at diagnosis	blast [%]	cytogenetics	FLT3 ITD	NPM1	FLT3 TKD
1	2656	female	77	78	46, XX[20]	0	1	0
2	6533	male	61	79	46, XY[20]	0	1	0
3	6555	male	79	76	46, XY[20]	0	1	0
4	8553	male	78	80	46, XY[20]	0	1	0
5	7730	female	63	87	46, XX, t(15,17)(q22;q12)[21]/46, XX	0	0	0
6	9128	male	19	81	46, XY[20]	0	0	-
7	4020	male	71	84	46, XY[20]	1	0	0
8	6646	female	70	90	46, XX[20]	1	0	0
9	8695	female	74	>90	46, XX[20]	1	0	0

Table 12. List of patient samples used in the study. Presence of mutation described with "1" for sample positive for mutation, or "0" for a negative sample.

The result of western blot analysis is presented in Figure 19 showing active, pSTAT5 in all 3 samples (7, 8, 9) derived from patients harboring a *FLT3*^{ITD} mutation. In these samples the levels of pSTAT5A and pSTAT5B protein expression are also high. In *FLT3*^{WT} samples, we also observed high protein expression of uSTAT5A and uSTAT5B (5 of 6 samples), but none of the samples had evidence of STAT5 phosphorylation. Interestingly, in *FLT3*^{ITD}-positive cells pSTAT5A and pSTAT5B proteins are expressed at a similar level, whereas in *FLT3*^{WT}-cells uSTAT5B expression levels are higher compared to uSTAT5A.

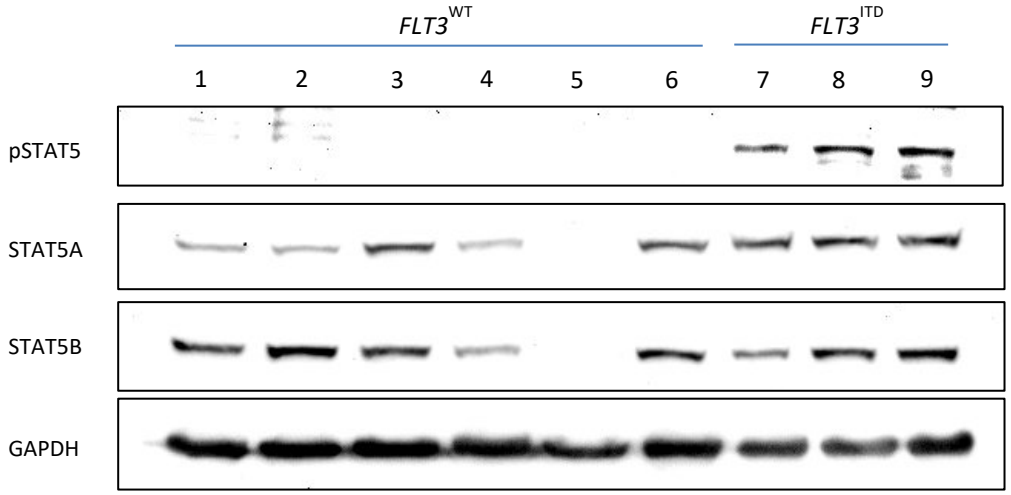

Figure 19. Endogenous levels of STAT5A and B protein expression in AML cell lines analyzed by western-blotting.

mRNA and protein levels of STAT5A and STAT5B differ among AML cell lines.

The *STAT5A* and *STAT5B* mRNA levels were compared in different AML cell lines selected for the study (Figure 20). At mRNA levels expression of both *STAT5* members is higher in *FLT3*^{WT}-cells (THP-1 and SKM-1) compared to cells harboring the *FLT3*^{ITD} mutation (MV4-11, MOLM-14).

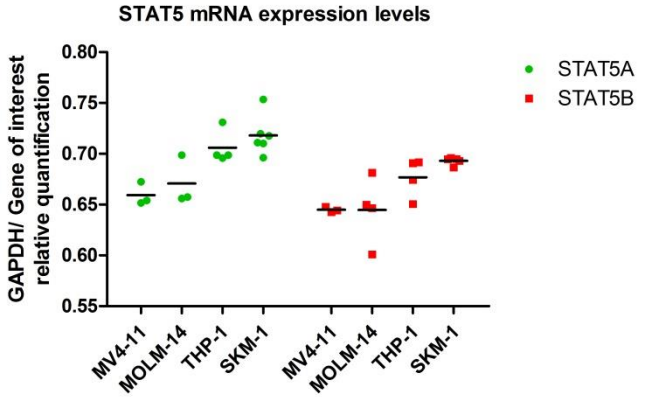

Figure 20. Endogenous levels of *STAT5A* and *B* mRNA expression in AML cell lines analyzed by qRT-PCR. Shown is the relative expression to *GAPDH*. N=4.

To verify whether the observed higher mRNA expression levels also influence the levels of STAT5 protein expression, proteins were extracted and analyzed by western blot. Results presented in Figure 21 show comparable levels of STAT5 protein expression in *FLT3*^{ITD}-positive and *FLT3*^{WT}-cell lines. Again, despite high endogenous expression levels of STAT5, no evidence of STAT5 phosphorylation was detected in *FLT3*^{WT} cell lines.

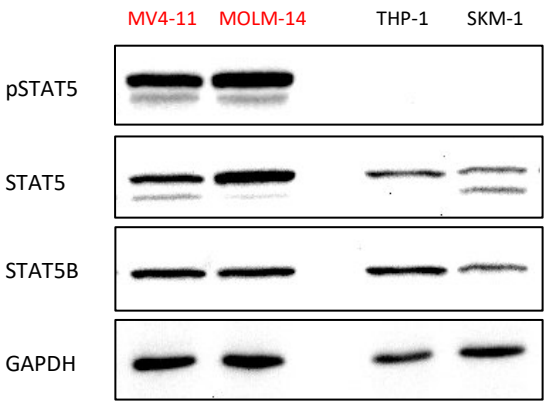

Figure 21. Endogenous STAT5A and B protein levels and STAT5 phosphorylation in different AML cell lines assessed by Western-blotting analysis.

Analysis of phosphorylation of STAT5A and STAT5B at Tyr694/Tyr699

Transcriptional activation of STAT5 proteins is known to be directly dependent on the phosphorylation of STAT5A at Tyr694 and STAT5B at Tyr699 residues. In the AML cell lines THP-1 and SKM-1 phosphorylation of STAT5 proteins was not detected in Western-blotting assays. To analyze, whether STAT5 can be phosphorylated upon growth factor stimulation, we treated the cells with GM-CSF, a known potent activator of STAT5 phosphorylation. Further, the possibility to induce STAT5 phosphorylation upon GM-CSF treatment will allow us to investigate STAT5A and STAT5B function prior and after induction. The kinetics of this activation was analyzed by immunoblotting and is presented in the Materials & Methods section (Fig. 11).

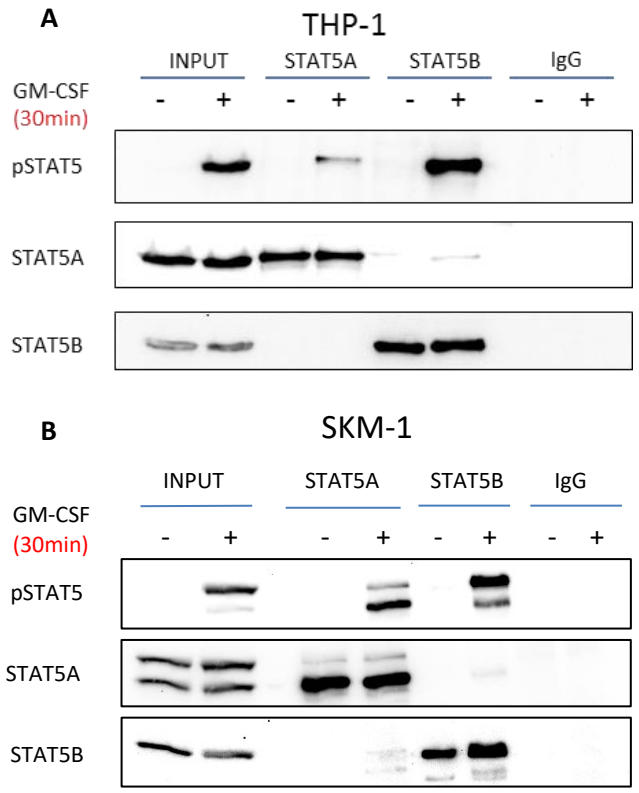

Figure 22. AML cell lines THP-1 (**A**) and SKM-1 (**B**) were treated with GM-CSF for 30 minutes. Immunoprecipitation followed by immunoblotting was performed using antibodies as indicated. 10% of lysates were used for input control and pull-down with IgG was used as a negative control.

To confirm that STAT5 proteins in *FLT3*^{WT} AML cell lines are indeed un-phosphorylated and not only due to a lack of sensitivity upon immunoblotting, we performed immunoprecipitation using specific anti-STAT5A or anti-STAT5B antibodies followed by immunoblotting. The cells were either untreated or stimulated with GM-CSF for 30 minutes prior to protein extraction. Results of the experiment are presented in the Figure 22. In untreated cells no signs of phosphorylation of STAT5A or STAT5B were observed, even after immunoprecipitation. Of note, GM-CSF activation affected both STAT5 members, but STAT5B became substantially more phosphorylated compared to STAT5A.

Cellular localization of STAT5 proteins – Immunofluorescence analyses.

The canonical pathway of STAT5 protein activation states, that uSTAT5 is located in the cytoplasm and upon activation translocates into the nucleus. Based on this assumption, in cells with uSTAT5A or uSTAT5B both proteins are expected to reside in the cytoplasm. To verify this hypothesis, THP-1 and SKM-1 cells, untreated or stimulated with GM-CSF for 30 minutes, were fixed with paraformaldehyde, stained with specific anti-STAT5A or anti-STAT5B antibodies and analyzed with the confocal microscope. The representative pictures are shown in the Figure 23.

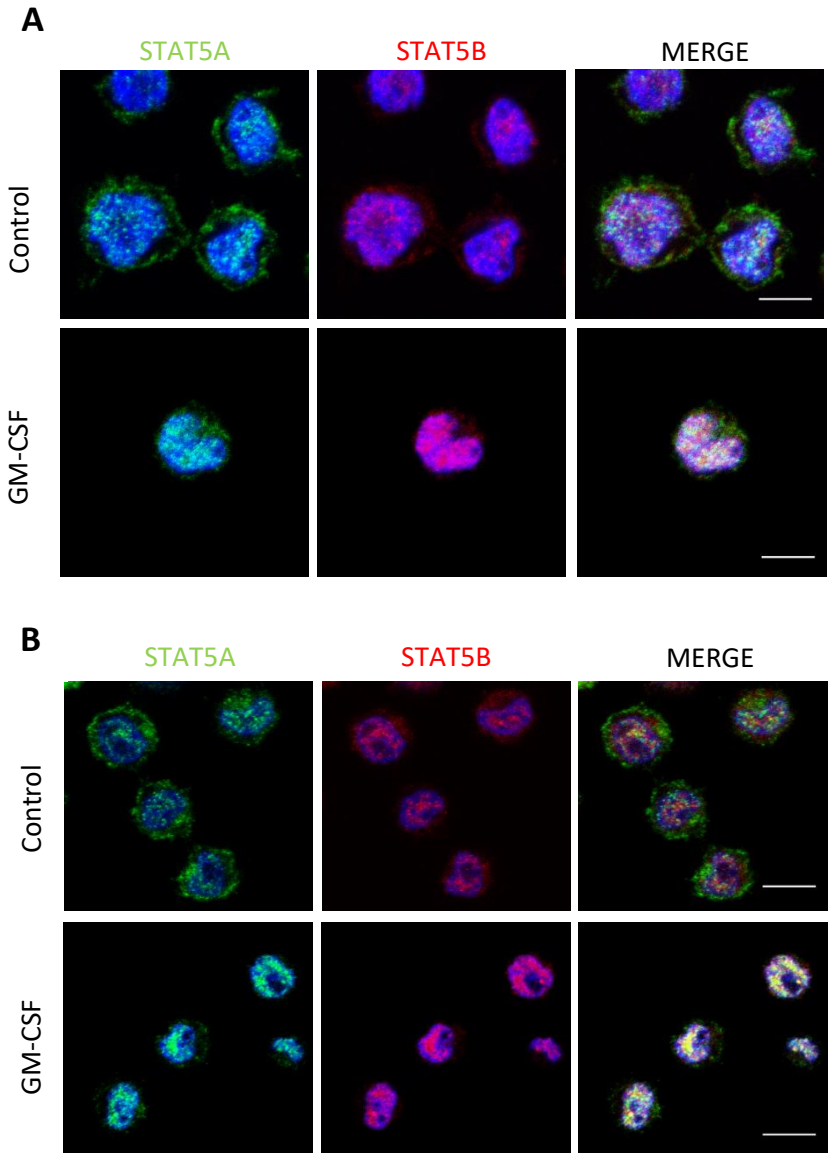

Figure 23. Immunofluorescence analysis of STAT5A (green) and STAT5B (red) localization in THP-1 (**A**) or SKM-1 (**B**) cells. Cells were either stimulated with GM-CSF for 30 minutes or un-stimulated. DAPI was used for counter-staining of the nucleus. Scale bar corresponds to 10 µm.

As expected, GM-CSF treatment results in a shift into the nucleus of pSTAT5A and pSTAT5B. In addition, merged figures indicate the formation of heterodimers in the nucleus and that pSTAT5A and pSTAT5B bind to common target genes. Surprisingly, in addition to cytoplasmic localization uSTAT5 proteins could also be detected in the nucleus (Figure 23). Quantification of the signal in each cellular compartment demonstrated an almost equal distribution of uSTAT5A between both compartments whereas uSTAT5B was primarily localized in the nucleus (Figure 24). Upon GM-CSF treatment translocation into the nucleus was increased for both pSTAT5 proteins.

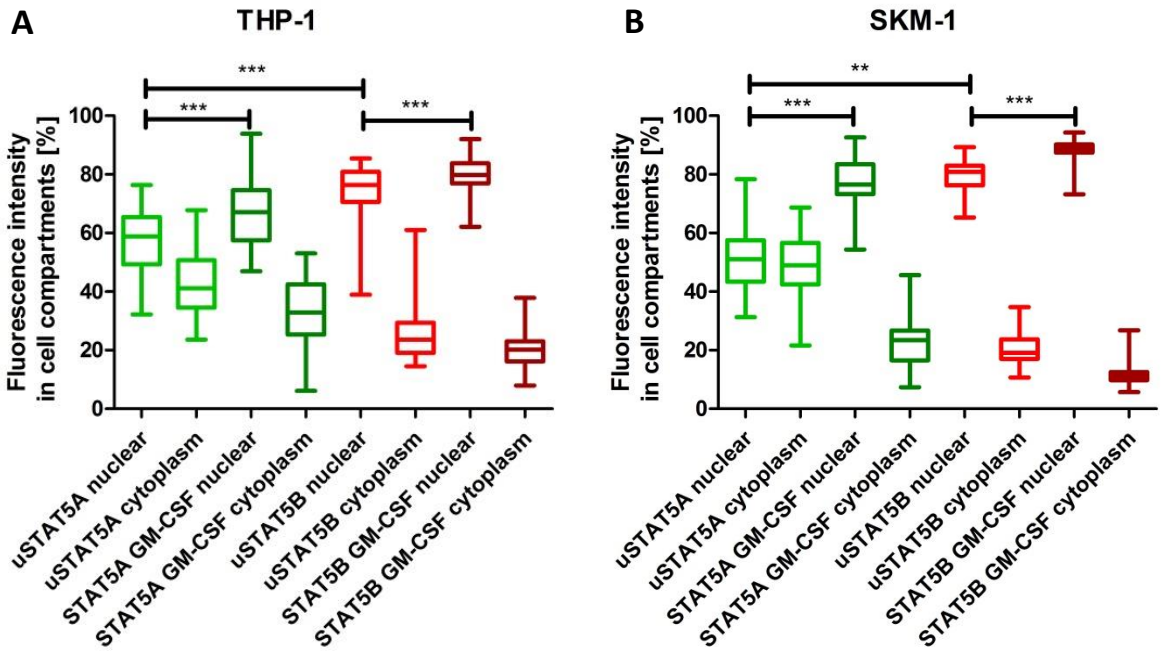

Figure 24. Quantification of STAT5A and STAT5B localization in control and GM-CSF treated THP-1 (**A**) or SKM-1 cells (**B**). For each condition, 50 cells were analyzed. The box and whisker graph shows 25th-75th percentiles of data by box extension. Whiskers indicate minimum and the maximum value for each condition. **:p<0.01; ***:p<0.001 (student t-test).

Functional analyses of uSTAT5 in AML cell lines

shRNA-mediated knock-down of STAT5A and STAT5B

To analyze the role of un-phosphorylated STAT5 in AML cell lines we took advantage of an inducible short-hairpin RNA-mediated knock-down. Using lentiviral transduction, constructs with control shRNA (shSCR) or shRNA targeting STAT5 transcripts were introduced into THP-1, SKM-1, MV4-11 and MOLM-14 AML cell lines.

Validation of knock-down efficacy

To induce the expression of shRNAs, AML cell lines were cultured in the presence of doxycycline at a concentration of 100 ng/ml for 3 days. Changes in STAT5A and STAT5B mRNA expression levels were evaluated by qRT-PCR (Figure 25) and at protein levels by immunoblotting (Figure 26).

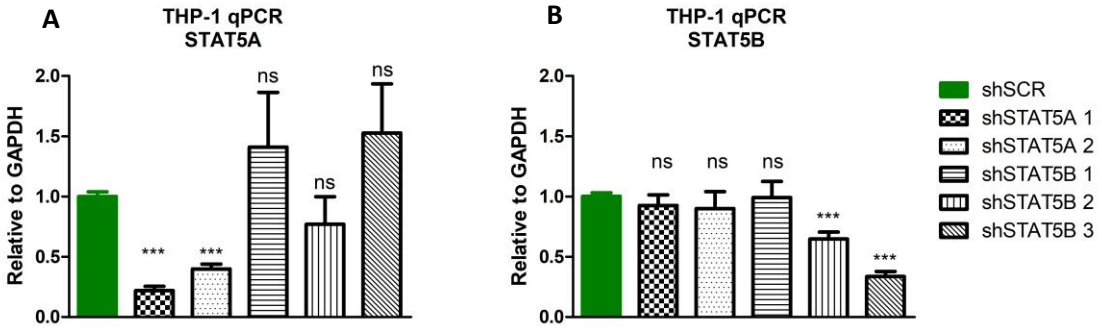

Figure 25. Analysis of the efficacy of STAT5 down-regulation. The mRNA levels of STAT5A (**A**) and STAT5B (**B**) were measured by qRT-PCR in the cell lines transduced with shRNA targeting STAT5A (2 different clones), STAT5B (3 different clones) or an unspecific, non-targeting control (shSCR, green). Results are presented as a fold-change in relation to shSCR control. ns=not significant; **:p<0.01; ***:p<0.001 (student t-test).

To suppress STAT5A expression, two different shRNA clones (STAT5A 1 and 2) were used. Both clones significantly down-regulate STAT5A expression with almost complete suppression upon induction of clone 1. No effects were observed on STAT5B expression levels indicating highly specific targeting (Figure 25). To knock-down STAT5B, three different clones were used (STAT5B 1, 2, 3). Only clones 2 and 3 caused a significant knockdown at mRNA levels without affecting STAT5A levels. Similar results were observed at protein expression levels (Figure 26). The best effects were observed for STAT5A clone 1 and STAT5B clone 3.

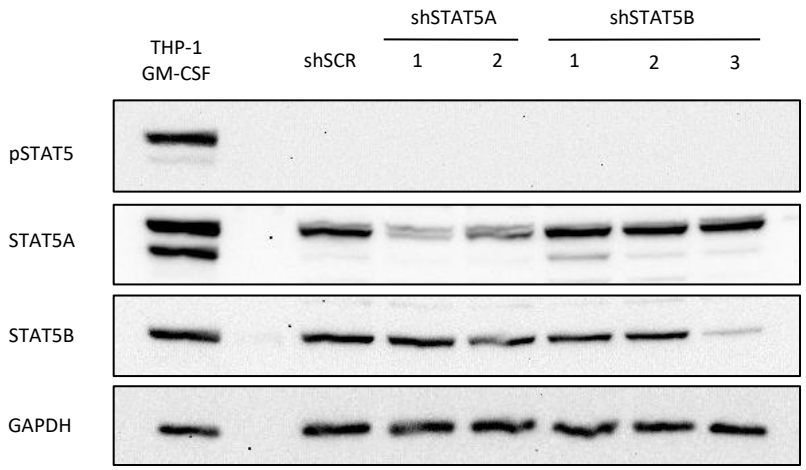

Figure 26. Analysis of knock-down efficacy of STAT5 protein expression levels in THP-1 cells. Protein levels of STAT5A and STAT5B were measured by western-blot analysis in cell lines transduced with shRNAs specifically targeting STAT5A, STAT5B or an unspecific shSCR control. Expression of GAPDH was used to control equal loading.

Similar effects were observed in other AML cell lines both on mRNA levels (as shown for SKM-1, MV4-11 and MOLM-14 in Supplementary Figure S6) and on protein levels (presented for SKM-1 and MV4-11 in Supplementary Figure S7).

Production of stable cell lines with an opportunity for inducible knock-down induction gives a lot of flexibility in terms of planning of experiments. However, to make sure the tet system is inducible only upon doxycycline supplementation and there is no knock-down of shRNA targeted transcripts due to promotor leakage a western-blot analysis of cell lines with and without doxycycline induction were performed for THP-1 derived cells (Fig 27).

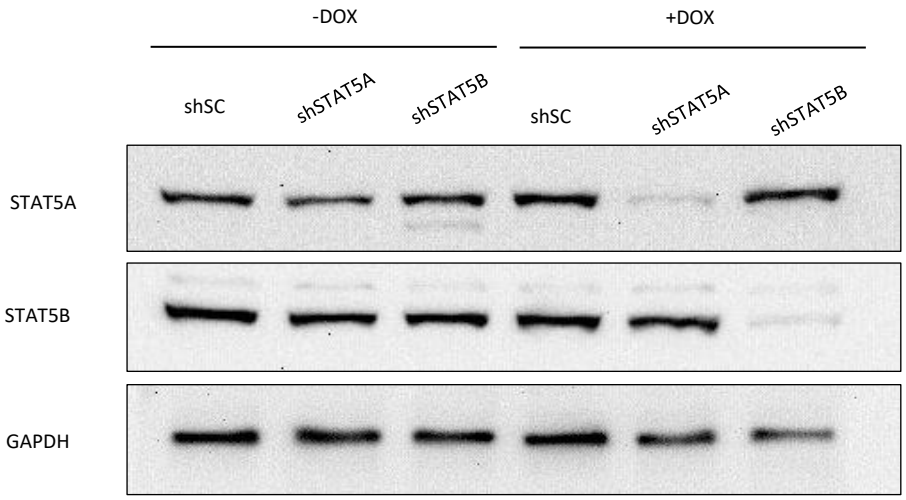

Figure 27. Analysis of inducible knock-down system in THP-1 derived cells with or without doxycycline induction. Protein levels of STAT5A and STAT5B were measured by western-blot analysis in cell lines transduced with shRNAs specifically targeting STAT5A, STAT5B or an unspecific shSCR control. Expression of GAPDH was used to control equal loading.

Protein levels of STAT5A and STAT5B remain high when cells are not exposed to doxycycline and upon addition of doxycycline to the medium shRNAs expression is switched on resulting in strong down-regulation of STAT5 proteins.

Proliferation of AML cell lines is affected upon STAT5 down-regulation.

To analyze the impact of STAT5 down-regulation on proliferation, genetically modified AML cell lines were treated with doxycycline for 3 days. An equal number of cells was transferred into a new flask and the number of viable cells was analyzed by the trypan-blue exclusion assay for five additional days. As shown in Figure 28, knockdown of STAT5A or STAT5B caused a significant reduction in proliferation compared to shSCR-control cells. In THP-1 and SKM-1 cells, both cell lines expressing uSTAT5 proteins, cell growth was almost completely abolished upon uSTAT5B knock-down and strongly reduced upon uSTAT5A knock-down (Figure 28A). In FLT3-mutant cells, pSTAT5A knock-down was only moderate, whereas pSTAT5B knock-down strongly inhibited cell proliferation in MV4-11 cells but not in MOLM-14 cells (Figure 28B).

The results were confirmed in an independent MTT assay (Supplementary Figure S8).

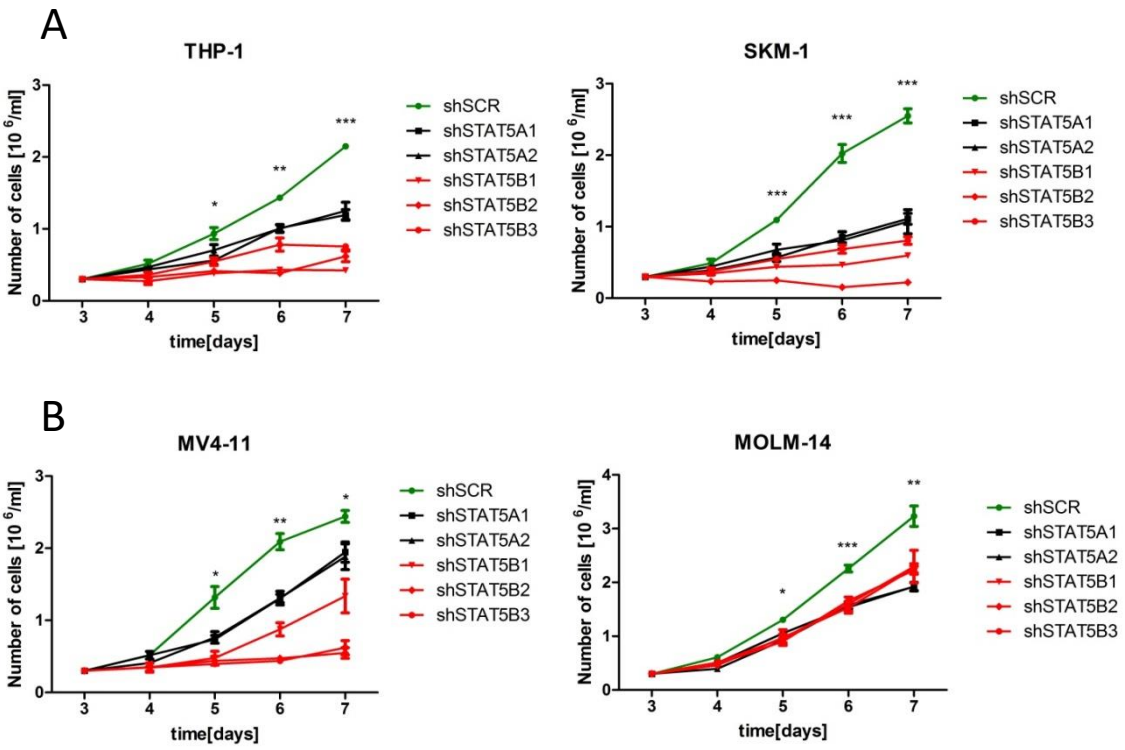

Figure 28. Cell growth of the *FLT3*^{WT} AML cell lines (panel A) and *FLT3*^{ITD}-positive cells (panel B) upon down-regulation of STAT5 proteins. Cells were pretreated with doxycycline for 3 days. Equal numbers of cells were plated into new flasks and cell number was evaluated daily for five additional days.*:p<0.05 ; **:p<0.01; ***:p<0.001 (student t-test).

STAT5 down-regulation causes cell cycle arrest and increased apoptosis

To analyze the impact of STAT5 on cell cycle progression propidium iodide DNA staining followed by FACS analysis were performed on day 6 after doxycycline induction (day 4 for SKM-1 cells due to a substantial decrease of viable cells upon knock-down). Results are presented in Figure 28.

Compared to shSCR control cells, conditional knock-down of uSTAT5A resulted in a slight increase of the subG1 fraction in SKM-1 and THP-1 cells, indicating apoptotic cell death. In FLT3-mutant cell lines, knock-down of pSTAT5A causes a minor, but still significant increase in the G1 phase of the cell cycle.

In line with our proliferation assays, uSTAT5B suppression strongly induced a G1 cell cycle arrest and apoptotic cell death in THP-1 and SKM-1 cells. Similar effects were observed in MV4-11 cells. In MOLM-14 cells down-regulation of pSTAT5B expression only caused a G1 cell cycle arrest without induction of apoptosis (Figure 29).

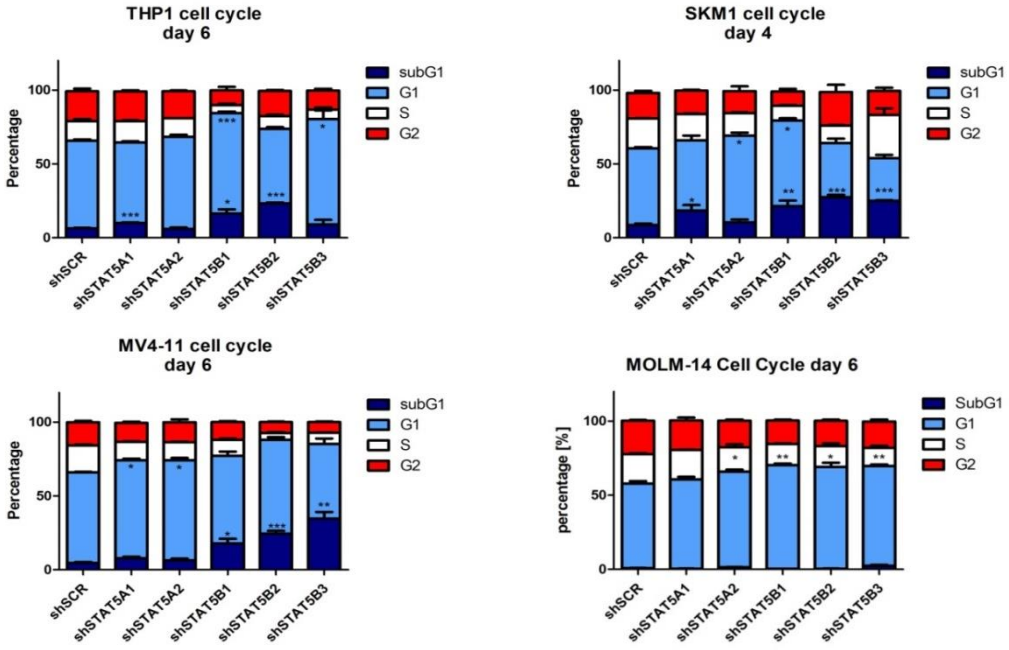

Figure 29. Impact of STAT5A and STAT5B down-regulation on the cell cycle progression in different AML cell lines. Cells were treated with doxycycline for up to 6 days and cell cycle analysis was performed. Shown is the percentage of cells per cell cycle phase. Statistical analysis was performed to compare SubG1 or G1 phase of the cell cycle in control cells with STAT5 knock-down cells. .*:p<0.05 ; **:p<0.01; ***:p<0.001 (student t-test).

Loss of STAT5 results in induction of differentiation

The proliferation and cell cycle analyses demonstrated a significant role of STAT5 in maintaining cellular fitness. The phenotype observed after down-regulation of STAT5 and in particular STAT5B, namely inhibition of cell growth, a G1 cell cycle arrest and apoptotic cell death was accompanied with remarkable morphologic changes as revealed by light microscopy (data not shown). To explore, whether STAT5 knock-down induces differentiation, we investigated the expression of different differentiation markers by FACS analysis. CD11b (Intergrin alpha M encoded by the *ITGAM* gene) is an integrin present on the surface of myeloid lineage cells and represents an established marker to track differentiation of these cells [169]. Another marker is CD117 (cKIT receptor tyrosine kinase encoded by the *KIT* gene), highly expressed on hematopoietic stem and progenitor cells, as well as leukemic blasts [170].

Analysis of CD11b upon STAT5B down-regulation showed an increased expression in all analyzed AML cell lines (Figure 30A). Down-regulation of uSTAT5A resulted in a significant increase of CD11b expression only in the cell lines with steady-state uSTAT5. In contrast, expression of cKIT was down-regulated upon STAT5B knock-down in MV4-11 and THP-1 cells only and STAT5A knock-down did not influence the expression of cKIT (Figure 30B).

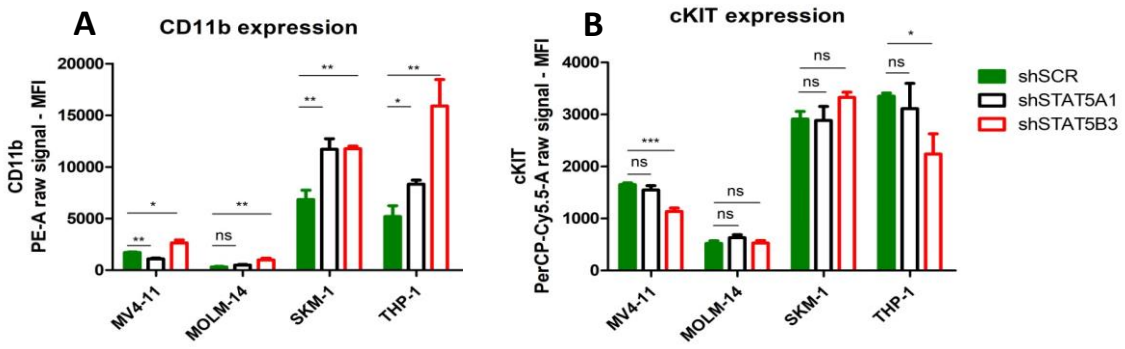

Figure 30. Impact of STAT5A and STAT5B down-regulation on differentiation markers of AML cell lines. Cells were treated with doxycycline for 3 days and expression of CD11b (**A**) and c-KIT (**B**) was analyzed by FACS analysis. Shown are combined data representing 3 replicates (n=3). MFI stands for Median Fluorescence Intensity. ns= non-significant; *:p<0.05 ; **:p<0.01; ***:p<0.001 (student t-test).

Down-regulation of STAT5B causes changes in morphology of AML cells

To provide further evidence for induction of differentiation upon STAT5B knock-down, we performed May-Grünwald-Giemsa stainings (Figure 31).

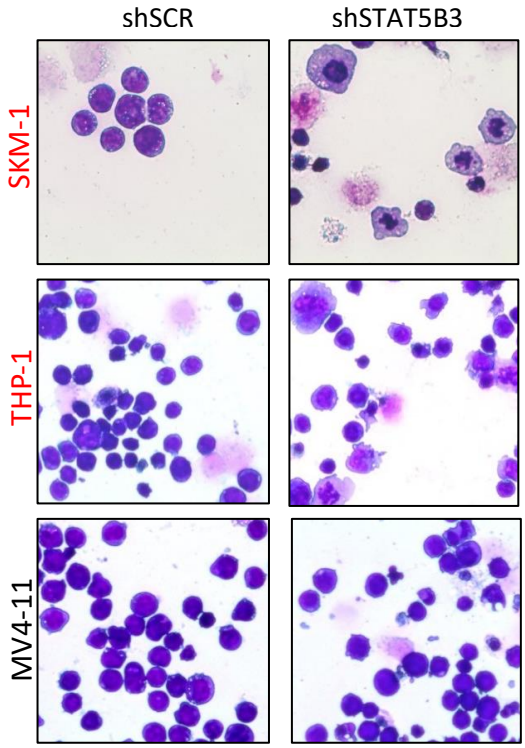

Figure 31. May-Grünwald-Giemsa stainings of the AML cell lines upon STAT5B down-regulation. Stainings were performed on the day 7 of doxycycline induction. Scale bar corresponds to 10 µm.

In line with the observed changes in CD11b and cKIT expression, knock-down of uSTAT5B shifted cells into a more mature phenotype compared to shSCR control cells as indicated by larger cell sizes, an increased cytoplasmic:nucleus ratio, kidney-shaped nuclei or vacuoles in the cytoplasm. In contrast only minor effects were observed in MV4-11 cells, which express pSTAT5.

In vivo experiments: Effect of *Stat5* on malignant transformation and leukemogenesis

Genetic depletion of *Stat5* causes enforced differentiation in a MLL-AF9 bone marrow transplantation model

To assess the effect of Stat5 on malignant transformation and leukemogenesis we took advantage of a transgenic mouse model, in which both *Stat5*-members can be depleted upon treatment with pIpC. As described in the Material & Method section, *Stat5*$^{fl/fl}$*_Mx1-Cre* or *Stat5*$^{fl/fl}$ bone marrow cells were transduced with retroviruses expressing MA9 and transplanted into primary C57BL/6J recipient mice.

The scheme of the in vivo experiment is presented in the Figure 32. The aim of the first BMT was to obtain high numbers of fully transformed AML cells for further experiments, therefore no pIpC-injections were performed.

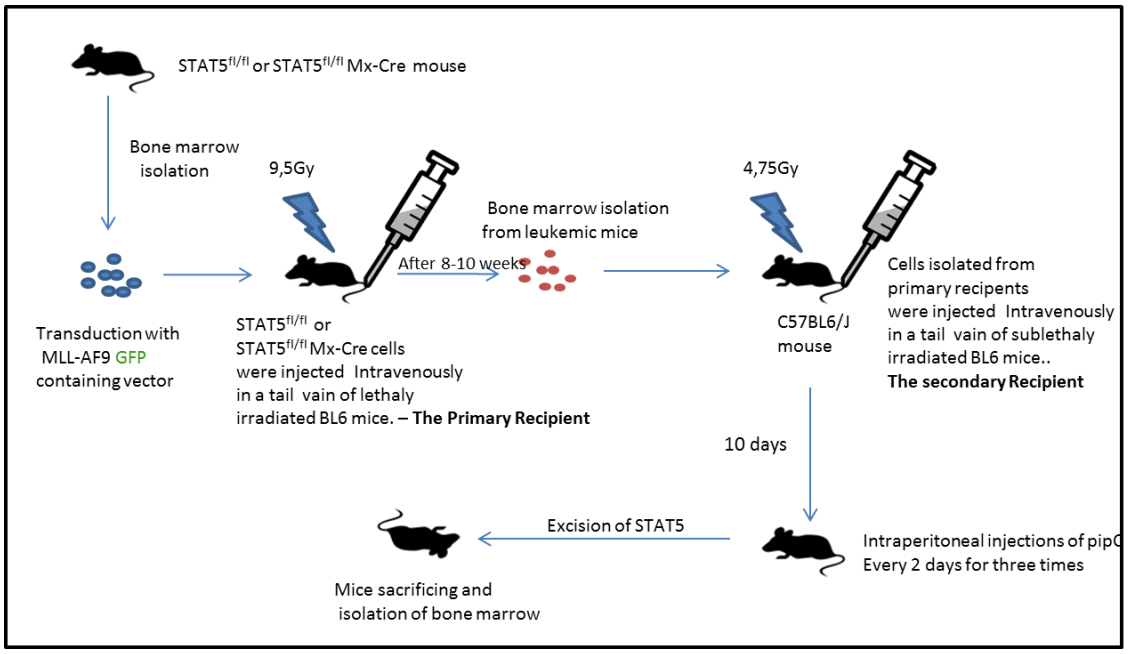

Figure 32. In vivo experiment scheme

At signs of disease, mice blood count and morphology were checked, the leukemic mice were sacrificed and the bone marrows were frozen. As shown in figure 33 *Stat5*$^{fl/fl}$*_Mx1-Cre*-MA9 and *Stat5*$^{fl/fl}$-MA9 recipients died after a median disease latency of 77,5 and 61 days, respectively. Both groups developed acute myeloid leukemia as revealed by FACS analysis and cytology (data not shown). Although pIpC was not injected in this experiment, we speculate that in some cells spontaneous Stat5 excision occurred, which likely caused the prolonged disease latency.

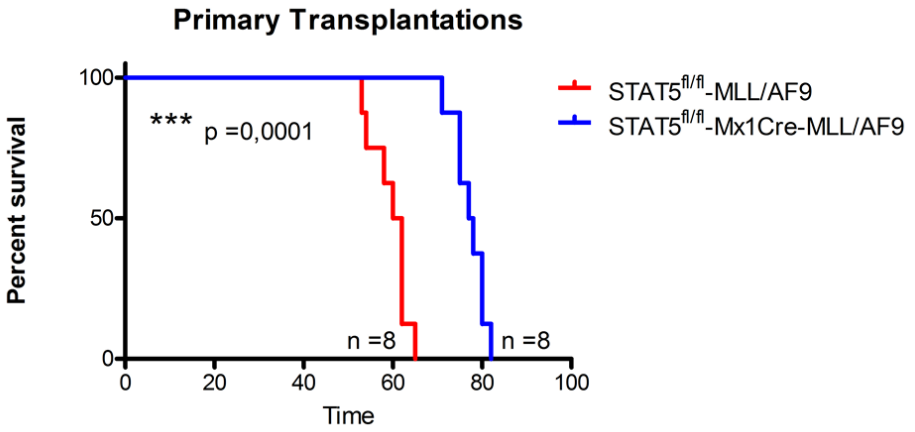

Figure 33. Kaplan-Meier plot showing the results of the primary transplantation round. Each group consists of 8 recipient mice**.** p=0.0001 (Log-rank (Mantel-Cox) Test).

To explore, whether excision of Stat5 can prevent leukemia development, we performed a secondary BMT experiment. The secondary transplantation was performed in two independent experiments presented here together. This time, to induce Stat5 depletion, pIpC was injected 3 times – on day 10, 12 and 14. Median survival of the *Stat5$^{fl/fl}$* control was 26 days similar to reports of many other groups (Figure 34). Surprisingly, depletion of Stat5-resulted in significantly reduced survival and mice died around day 15.

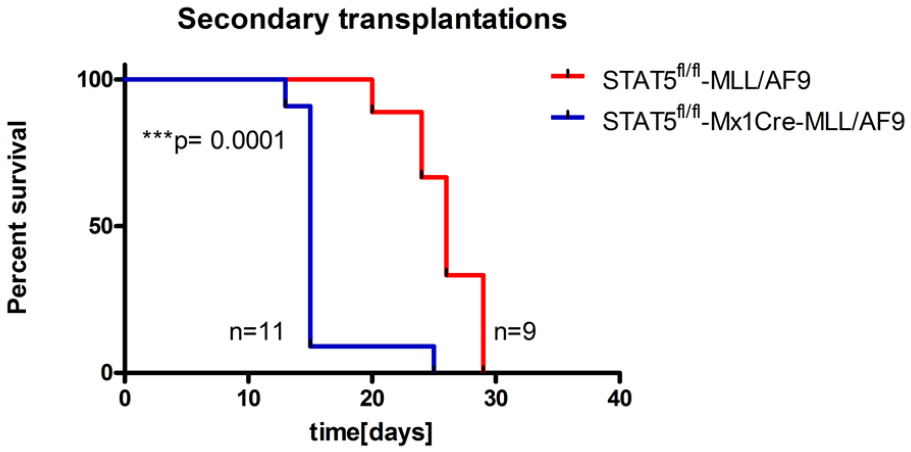

Figure 34. Kaplan-Meier plot showing the results of the secondary transplantation round. Control group consists of 9 recipient mice, whereas cohort of mice investigated for Stat5 excision consists of 11 animals. p=0.0001 (Log-rank (Mantel-Cox) Test).

To confirm that *Stat5* depletion was efficient, we examined the levels of STAT5 protein expression in blasts derived from spleens of 3 mice of each experimental group. As shown in figure 35, Stat5 depletion was nearly complete in 3 animals, whereas Stat5 was highly expressed in control mice.

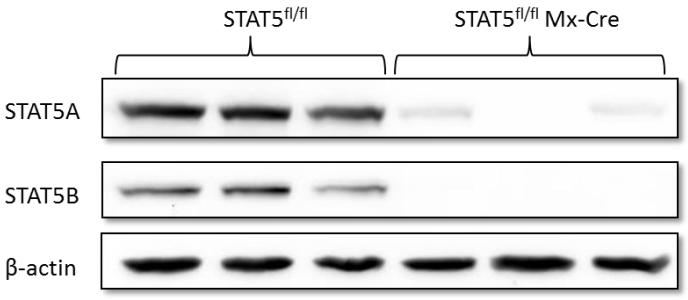

Figure 35. Analysis of the STAT5 proteins expression after excision of the *Stat5* genes loci in the secondary recipients.

To gain insight into the cause of death briefly after pIpC injections, we took blood samples derived from day 15 in the experimental group (*Stat5$^{fl/fl}$_Mx1-Cre*-MA9) as well as the control group, which appeared to be healthy at this time point. The results of the blood counts are presented in the Figure 36. On day 15 the control group showed normal white blood cell counts (WBC) in the peripheral blood. In contrast, *Stat5$^{fl/fl}$_Mx1-Cre*-MA9-transplanted mice had extremely high WBCs at this time point, which were still higher compared to the control group at leukemia onset (day 26).

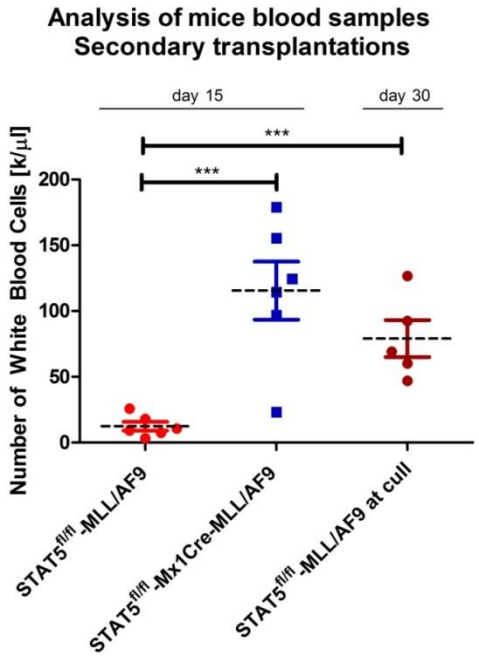

Figure 36. Analysis of the white blood cells counts in the peripheral blood taken from the secondary recipient mice at the indicated time points. ***:p<0.001 (student t-test).

We next analyzed the phenotype of leukemic blasts derived from the experimental and the control group by flow cytometry. As shown in Figure 37, in both groups bone marrow cells were highly enriched for GFP positive cells (between 80-90%) indicating expression of the oncogenic fusion gene MLL-AF9. The gated GFP-positive population was then investigated for the expression of CD11b and Gr-1, both markers of differentiated hematopoietic cells. Surprisingly, the *Stat5*$^{fl/fl}$*_Mx1-Cre*-MA9-group, depleted of *Stat5,* showed a strong increase in the double-positive cells compared to the control group suggesting a more mature, differentiated phenotype. We speculate, that the observed high WBCs upon *Stat5*-depletion was caused by a so-called differentiation syndrome, which is also observed in acute promyelocytic leukemia (APL) upon ATRA treatment in human disease and occurs in 25% of treated patients [171].

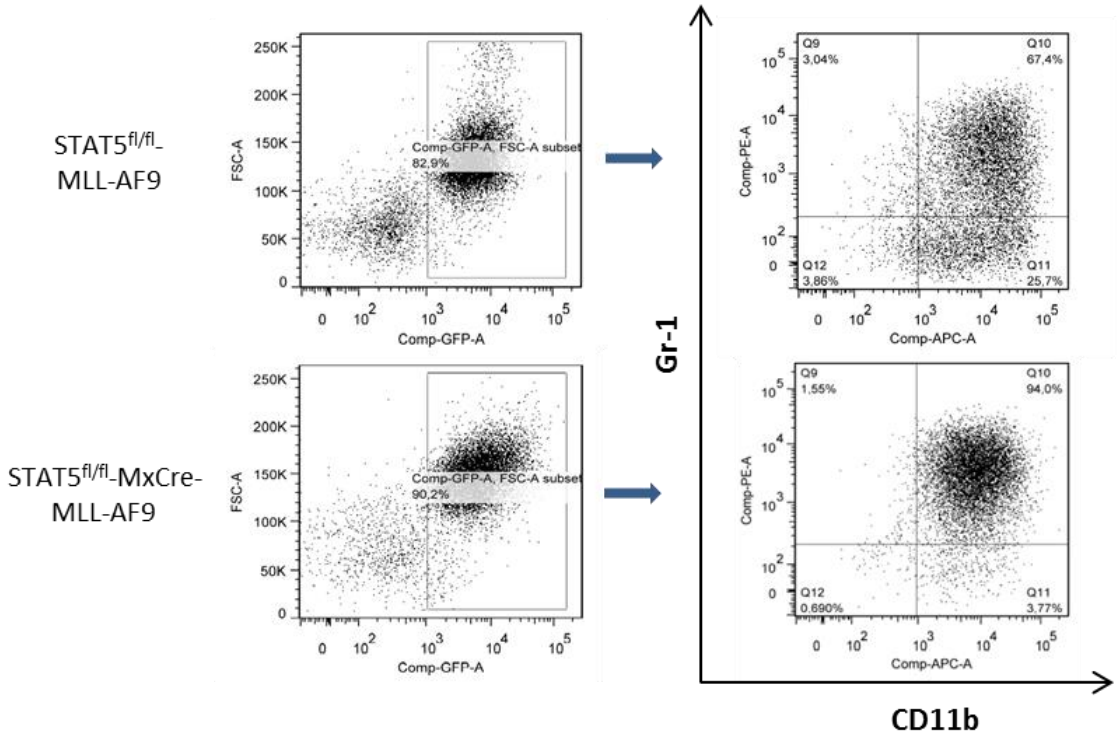

Figure 37. Phenotyping of the bone marrow derived cells after secondary transplantation. First, population of bone marrow cells was examined for GFP positivity to analyze only the MA9 transduced cells. Afterwards the selected population was investigated for expression of CD11b and Gr-1.

Members of Stat family of transcription factors are important in maintenance of AML cell lines

Recently Wang and colleagues generated a gene-importance dataset across 13 human AML cell lines using a genome-wide CRISPR-based screens [172]. For each gene 10 single-guide RNA (sgRNA) sequences were designed. The resulting sgRNA library was introduced into the cells via lentiviral transduction. Effects of sgRNA and CRISPR Cas9-mediated gene excision on proliferation of AML parental cell line was analyzed shortly after sgRNA-library transduction and after 14 days, resulting in log2 of fold change score for the abundance of each sgRNA. We took advantage of this publicly available data-set to explore the role of each STAT family member in AML cell lines (Figure 38).

The results indicate only minor impact of STAT1-4 on AML cell line maintenance. In contrast, a strong

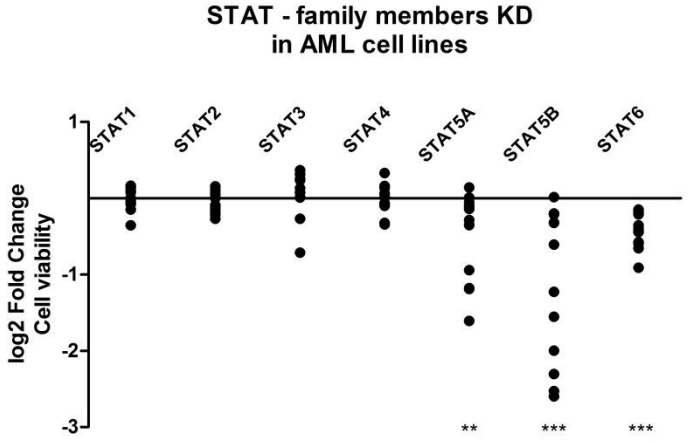

Figure 38. Effects of down-regulation of STAT family members on viability of AML cell lines. Significant influence of STAT5A, STAT5B and STAT6 down-regulation as compared to STAT1. **:p<0.01; ***:p<0.001 (student t-test).

and significant decrease in sgRNA abundance was observed for STAT5A, STAT5B and STAT6 specific sgRNAs. Interestingly, more cell lines were affected upon STAT5B depletion compared to STAT5A. This fact should not be surprising in terms of cell lines harboring *FLT3*^{ITD} mutation. In this background a constitutively active tyrosine kinase activates a variety of downstream signaling pathways including the JAK2-STAT5 pathway. Disruption of this pathway leads to decreased proliferation of *FLT3*^{ITD} AML cell lines. Interestingly STAT5 knock-down also decreased viability in the majority of *FLT3*^{WT} cell lines (exception of NB4, OCI-AML2, and THP-1 for STAT5A targeting and OCI-AML2 for STAT5B targeting) supporting our hypothesis that uSTAT5 maintains survival of AML cells.

Expression of STAT5 mRNA in *FLT3*^{mutant} and *FLT3*^{WT} patient samples – TCGA database.

Within a *FLT3*^{ITD}-background pSTAT5 proteins have been shown to act as important transducers of signaling promoting survival and proliferation of leukemic blasts [124]. The role of uSTAT5 proteins in a *FLT3*^{WT} background is poorly understood so far. We therefore analyzed the expression levels of STAT5A and STAT5B in the context of the FLT3 mutation status: uSTAT5 mRNA steady state levels could be i) increased to act as an inducer of early immediate genes; ii) downregulated because they have no immediate function; or iii) expressed due to yet unknown functions.

To address this question, we analyzed *The Cancer Genome Atlas* (TCGA) database containing clinically annotated samples of adult de novo AML patients [37]. Samples were grouped according to the FLT3 status: *FLT3*^{WT} group (119 patients), *FLT3*^{ITD} group (34 patients), and *FLT3*^{TKD} group (12 patients). Expression of *STAT5* mRNA is presented in the Figure 39.

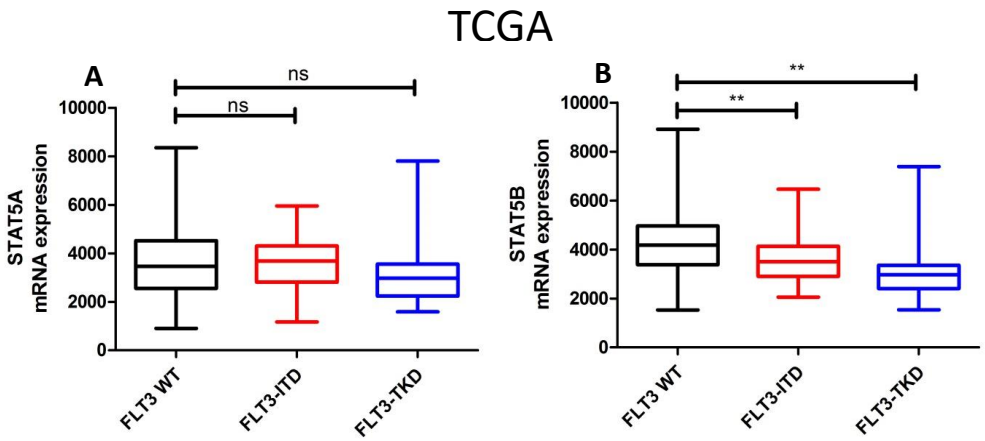

Figure 39. Expression of *STAT5A* (A) and *STAT5B* (B) mRNA depending on the FLT3 mutation status in the AML patient cohort from TCGA. The box and whisker graph shows 25th-75th percentiles of data by box extension. Whiskers indicate minimum and the maximum value for each group of patients. ns=non-significant;**:p<0.01 (student t-test).

Whereas the FLT3 mutation status did not affect levels of STAT5A mRNA expression, significantly Higher levels of STAT5B mRNA expression were observed in AML patients with a *FLT3*^{WT} status compared to patients carrying *FLT3*^{ITD} or *FLT3*^{TKD} mutations.

Identification of novel STAT5-protein interaction by mass spectrometry-based quantitative proteomics

To gain insight in the biological role of uSTAT5A/B and pSTAT5A/B proteins in AML cells, we investigated their interaction partners by performing mass spectrometry-based quantitative proteomics in combination with a “Stable Isotope Labeling by Amino acids in Cell culture (SILAC)” approach. We performed IP experiments using specific anti-STAT5A and anti-STAT5B antibodies with lysates derived from cell lines with steady-state uSTAT5 (THP-1 and SKM-1) or pSTAT5 (MV4-11). In addition, to identify difference between phosphorylated and un-phosphorylated STAT5 states, MV4-11 cells were treated with PKC412, a potent FLT3-inhibitor, which causes almost complete de-phosphorylation of FLT3 and its downstream mediator STAT5. A protein was only considered as a STAT5-interaction partner, if the enrichment score was > 2 compared to unspecific IgG controls.

Interacting partners of uSTAT5A

Mass spectrometry upon uSTAT5A pull-down identified 171 putative interacting proteins in THP-1 lysates and 266 putative interacting proteins in SKM-1 lysates. Of all identified proteins, 115 binding partners were shared between both cell lines (Figure 40A, a detailed list is shown in supplementary Table S1). Proteins with the highest enrichment score relative to IgG control are presented in figure 40B. STAT5A (indicated with a green dot) was among the proteins with the highest enrichment score, confirming good efficacy of the IP.

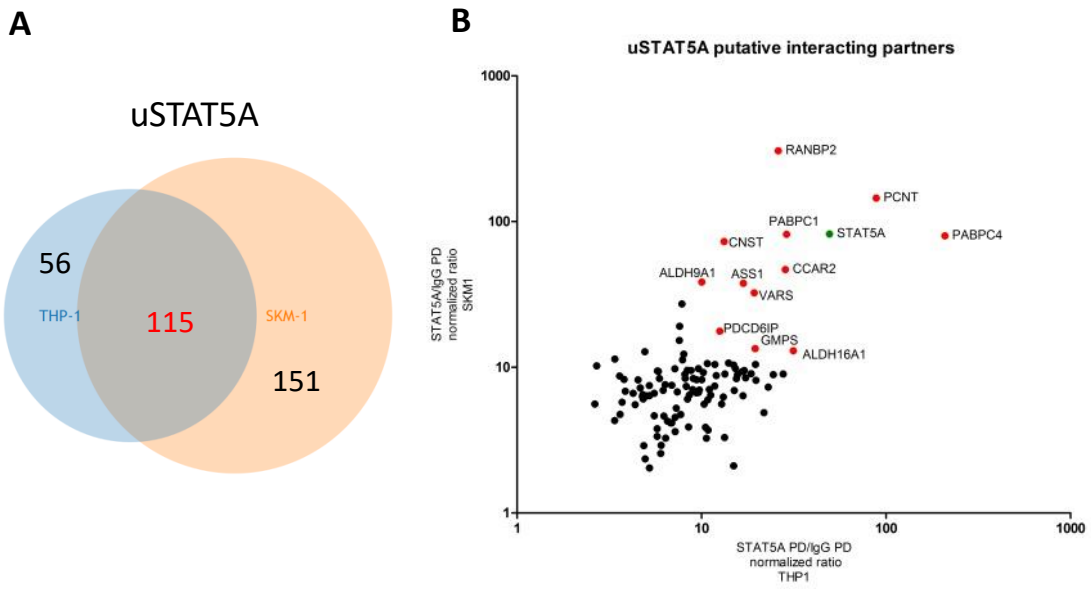

Figure 40. Interacting partners of uSTAT5A protein in two AML cell lines. **A)** Venn-diagram showing individual and shared interacting proteins for each cell line. **B)** Shared interacting proteins plotted relative to the ratio of anti-STAT5:anti-IgG pull-down.

To explore potential biological pathways or processes in which uSTAT5A and its interacting partners might be involved shared proteins were analyzed using the Ingenuity Pathway Analysis tool (IPA, Qiagen). In figure 41 the top-5 pathways and processes regulated by the identified protein-protein interactions are listed.

Name	p-value
EIF2 Signaling	3,38E-14
Regulation of eIF4 and p70S6K Signaling	3,46E-11
tRNA Charging	3,71E-11
mTOR Signaling	8,56E-08
Cell Cycle Control of Chromosomal Replication	9,72E-08

Figure 41. Pathways and processes signatures enriched for the interactome of uSTAT5A.

Pathway analysis using IPA revealed interaction of uSTAT5A with proteins involved in maintenance of translation related processes like EIF2 signaling and regulation of eIF4 and p70S6K signaling (interaction with EIF2S1, EIF3C and PABPC1) and tRNA charging (interaction with various t-RNA synthetases). In addition, top 5 pathways, in which uSTAT5A interacting proteins are involved, included mTOR signaling (similar interacting partners like for EIF2 signaling) and cell cycle control (Interaction with MCM family members 2-7).

Single putative interactions with the strongest enrichment scores and their functions are described below:

Cell Cycle and Apoptosis Regulator 2 (**CCAR2**, also known as Deleted in breast cancer-1 (**DBC-1**)) is one of the genes cloned from human chromosome region 8p21, a region homozygously deleted in breast cancers by [173]. CCAR2 was reported to exhibit pro-apoptotic functions in TNF-α mediated apoptosis [174], but on the other hand, through competition with MDM2 binding, it can bind to and stabilize p53 and functions as a tumor suppressor [175]. Other reports supporting the pro-apoptotic function of DBC1 demonstrated the direct interaction with SIRT1 thereby inhibiting SIRT1-mediated de-acetylation of p53 [176],[177].

Poly(A) Binding Protein Cytoplasmic 1 (**PABPC1**) interacts with the poly(A) tails at the 3-prime end of mRNA and mediates the formation of the mRNA loop promoting the start of translation [178]. It can also play a role in nonsense-mediated mRNA decay [179]. Recently, it has also been reported that it can translocate into the nucleus and bind pre-mRNA poly(A)tails of the transcripts [180] thereby stabilizing newly synthesized mRNA and mediating the nuclear export. The PABPC4 is a member of the same family and it is described to interact with the poly(A) tails of mRNA in analogical manner, however, it was also reported to be crucial in the final stages of erythroid differentiation[181] and its expression increases by 5-fold in activated T-cells [182]. How uSTAT5A-binding contributes to these different functions is unknown.

Pericentrin (**PCNT**) through its anchoring function in the centrosomes has been linked to regulation of different stages of cell-cycle progression. Tibelius and colleagues showed that PCNT is required for Checkpoint Kinase 1 (CHK1) recruitment to centromeres regulating the G2-M phase transition[183]. Lack of PCNT leads to premature entry in mitosis. Loss-of-function mutations in the *PCNT* gene result in primordial dwarfism in humans due to disorganization of the mitotic spindle and mis-segregation of chromosomes [184].

Different members of the minichromosome maintenance protein complex (**MCM**) have been identified as uSTAT5 interactors in pull-down experiments. The MCM complex consists of 6 members that form a ring-shaped complex and mediate replication fork formation but thanks to helicase activity they also contribute to the elongation step [185]. Evolutionary conserved in all eukaryotes, MCM-ring recruitment to chromatin is a pre-requisite for polymerase binding and it is crucial for proper replication of DNA and progression of the cell cycle. It is of high interest if down-regulation of uSTAT5 would affect the levels and function of MCM proteins and thereby causing the observed cell cycle arrest. A summary of MCM interactions with uSTAT5A or B in all tested cell lines can be found in supplementary Table S5. In all analyzed cell lines uSTAT5A binds to MCM2-7 family members and these interactions are not present for pSTAT5A (with exception of MCM7).

RAN Binding Protein 2 (**RANBP2**, also known as NUP358) is a protein that localizes to the nuclear pore complex and is a major component of the filaments that emanate into the cytoplasm. It has been reported to play a role in nuclear import, by mediating importin-based transport [186], transportin dependent nuclear import [187], as well as regulating a CRM-1 mediated nuclear export [188]. In addition, in complex with RanGAP1 the protein is crucial for stable interaction between kinetochore and microtubules and its depletion leads to accumulation of mitotic cells with multipolar spindles and unaligned chromosomes [189].

Interacting partners of uSTAT5B

Mass spectrometry upon uSTAT5B pull-down identified 31 putative interacting proteins in THP-1 lysates and 21 putative interacting proteins in SKM-1 lysates. 11 protein binding partners were detected in both cell lines (Figure 42A, detailed list in a supplementary Table S2). Proteins with the highest enrichment score relative to IgG control are presented in figure 42B. uSTAT5B (indicated with a green dot) was among the proteins with the highest enrichment score, confirming good efficacy of the IP. Comparison of the enrichment score over IgG control between uSTAT5A and uSTAT5B pull-down demonstrated that the pull-down efficacy is similar in both experiments. Interestingly, the number of putative interacting partners is strikingly lower upon uSTAT5B pull-down. It may be that uSTAT5A is involved in a variety of biological processes via protein-protein interactions while uSTAT5B seems to play a different role. Due to low number of identified interacting partners no pathway analysis was performed.

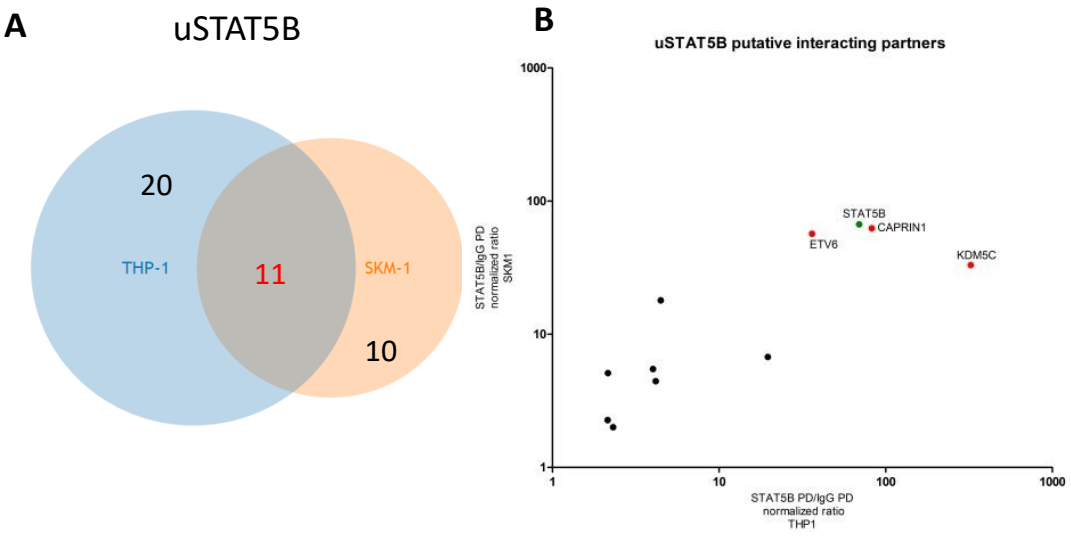

Figure 42. Interacting partners of uSTAT5B in two THP-1 and SKM1 cells. **A)** Venn-diagram showing individual and shared the interacting proteins for each cell line. **B)** Shared interacting proteins plotted relative to the ratio of anti-STAT5: anti-IgG pull-down.

The most interesting interacting partners and their functions will be briefly described in this chapter. Lysine Demethylase 5C (**KDM5C**, also known as JARID1C or SMCX) is a protein belonging to JARID1 subfamily of JARID DNA-binding proteins [190]. The family consists of 3 other members: KDM5A

(JARID1A), and KDM5B (JARID1B), KDM5D (JARID1D) [191]. KDM5 proteins are able to demethylate H3K4 tri- and di-methylation marks linked to an active euchromatin state [192]. Mutations within *KDM5C* gene were reported to cause a X-linked mental retardation syndrome and therefore it is thought to play an important role in human brain function [193]. In line, KDM5C was recently reported to be linked to Huntington disease [194].

In the early stages of replication enzymatic activity of KDM5C is required to remove the active H3K4me3-mark from active promotors in order to allow binding of PCNA and the formation of a replication pre-initiation complex [195]. Another report has linked KDM5C to inhibition of transcriptional activity by de-methylation of active promoters upon DNA-damage. KDM5C is SUMOlyated by SUMO-2, which leads to its higher occupancy at chromatin [196].

Studies conducted in embryonic stem cells indicate that KDM5C binding to promotor regions can be targeted by a direct protein-protein interaction with gene specific transcription factors e.g. c-MYC. The activity of KDM5C also depends on the type of regulatory elements within the genome it binds to and the H3K4 methylation status. Thus, at promotor sites KDM5C has a repressive role. On the other hand, at enhancer regions rich in H3K4 mono-methylation KDM5C removes spurious H3K4 di- or trimethylation marks thereby preventing binding of transcription factors and complexes at wrong regions. This way the protein is supporting enhancer functions [197].

Another putative interacting partner of uSTAT5B is ETS variant 6 (**ETV6** also known as TEL1 (Translocating E26 transforming-specific leukemia1)), a member of the ETS (E26 transforming specific) family of transcriptional regulators.

ETV6 has been shown to play an important role in both embryonic and hematopoietic development. Depletion of Etv6 in mice led to embryonic lethality at day 10.5-11.5 of development due to mesenchymal and neural cell apoptosis and defective angiogenesis in the yolk sac [198], whereas primary hematopoiesis was unaffected at this stage. In line it has been reported that ETV6 is not required for the differentiation of blood lineages in adult mice but is essential for establishing hematopoiesis within the bone marrow of mice. A possible mechanism involves its functions in transducing signals from the BM microenvironment in HSCs or progenitor cells [199]. These findings make ETV6 an important player contributing to maintenance and survival of HSCs. Also, in the context of malignant hematopoiesis ETV6 remains an interesting player. It has been found to be involved in 48 chromosomal translocations with more than 30 different fusion partners (reviewed by Braekeleer et.al [200]). In most cases ETV6 drives leukemogenesis via i) fusion with a partner that possess kinase activity resulting in constitutive activation upon fusion; ii) fusion with a transcription factor causing reprogramming of target genes of the fusion partner; or iii) loss of function of the fusion partner.

Interaction partners of phosphorylated and un-phosphorylated STAT5 in MV4-11 cells

For experiments performed with MV4-11 cells we included third, medium type of SILAC medium and pre-treated the cells cultured with the heavy medium with 100 nM of PKC412 for 4 h prior to protein extraction in order to detect differences in binding partners between uSTAT5 and pSTAT5 using the same cell line. The level of STAT5 phosphorylation was evaluated by immunoblotting (Figure 43).

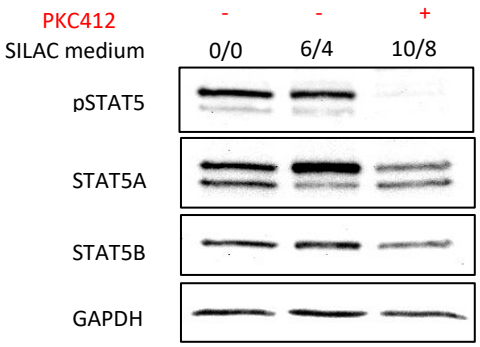

Figure 43. Confirmation of the PKC412 treatment of MV4-11 AML cell line.

Mass spectrometry upon STAT5A pull-down identified 9 proteins which exclusively interact with pSTAT5A and 19 proteins interacting with uSTAT5A only. 53 proteins could be detected in both conditions (Figure 44A, detailed list can be found in supplementary table S3)) .

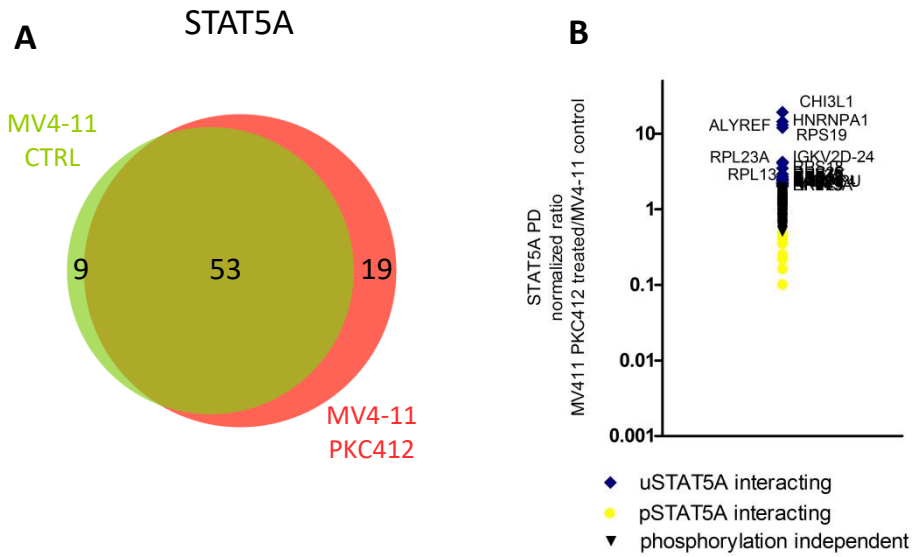

Figure 44. Interacting partners of phosphorylated and un-phosphorylated STAT5A protein in MV4-11 cells. **A.** MV4;11 cells were treated with PKC412 (100 nM, red) or vehicle control (light green) for 4 hours. The Venn-diagram shows the number of interactions and the overlap between control and PKC412 treated cells (dark green). **B.** 53 proteins interacting with STAT5A in both un-phosphorylated state after PKC412 treatment (blue) and in the phosphorylated state (yellow) were ranked according to enrichment of interaction strength upon PKC412 treatment. Interacting partner was assigned to the corresponding group after reaching fold change >2 (uSTAT5A interacting) or <0,5 (pSTAT5A interacting) of STAT5A binding enrichment after PKC412 compared to vehicle control.

Since a SILAC-based mass-spectrometry approach was performed, we were able to gradually quantify the interaction according to the phosphorylation state of STAT5A (Figure 44B). To explore potential biological pathways or processes in which uSTAT5A and its interacting partners might be involved, IPA was performed. In figure 45 the pathways and processes regulated by the identified protein interactors of uSTAT5A (red bars) or pSTAT5 (green bars) are listed. As mentioned earlier, “EIF2 Signaling”, “Regulation of eIF4 and p70S6K Signaling” and “mTOR Signaling” were the top hits in SKM-1 and THP-1 cells indicating an important role of uSTAT5A in the regulation of translation. In PKC412 treated MV4-11 cells, which induces uSTAT5A we were able to identify

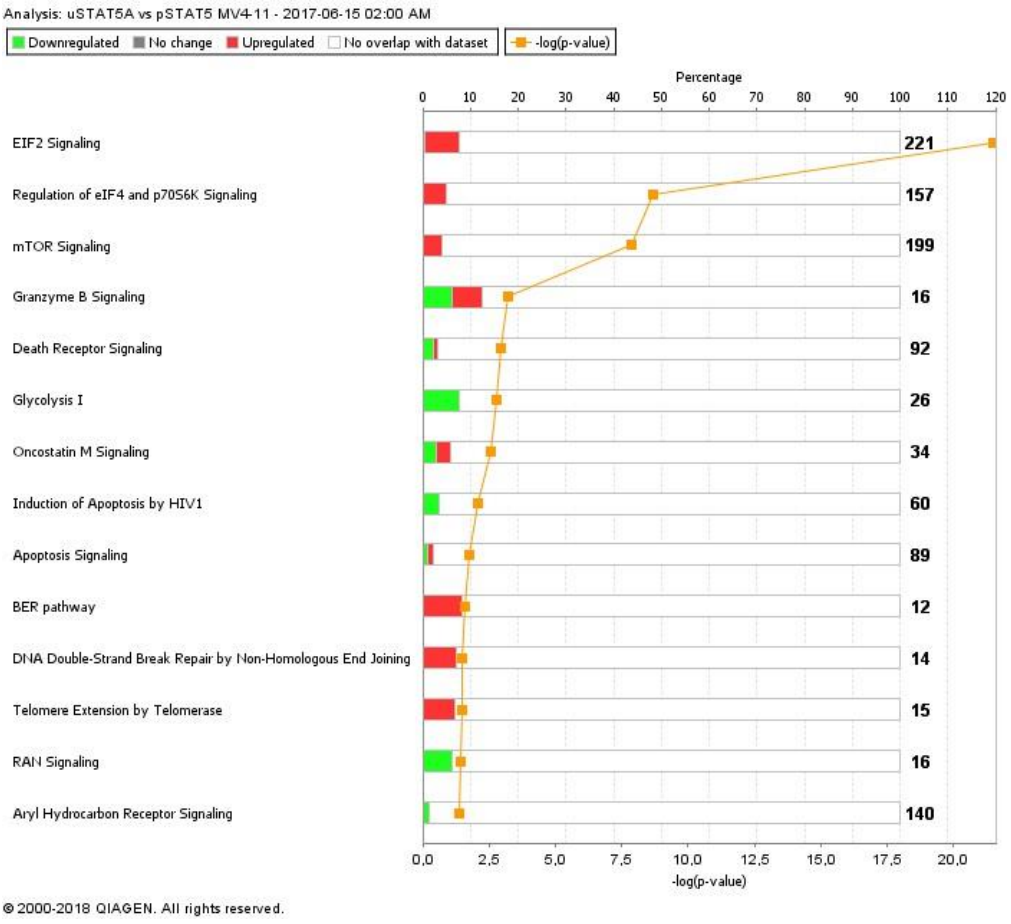

Figure 45. Pathways including proteins enriched for the interactome of uSTAT5A and pSTAT5A in MV4-11 cells. Bold numbers indicate total number of proteins in a pathway. Top X-axis shows percentage of proteins from a pathway that overlap with the input list. The bottom x-axis corresponds to significance of finding. Overlap of STAT5A interacting proteins with the pathway is represented by red bars (interactors of uSTAT5A) or green bars (interactors of pSTAT5A).

HNRNPA1, RPS19, RPL23A, and RPL13 as interacting partner proteins, all of them involved in EIF2, eIF4 and p70S6K signaling pathways contributing to translation (Figure 45). In contrast, Enolase 1 (ENO1) and 6-phosphofructokinase (PFKL) were discovered as pSTAT5A interactors and both are important enzymes in Glycolysis.

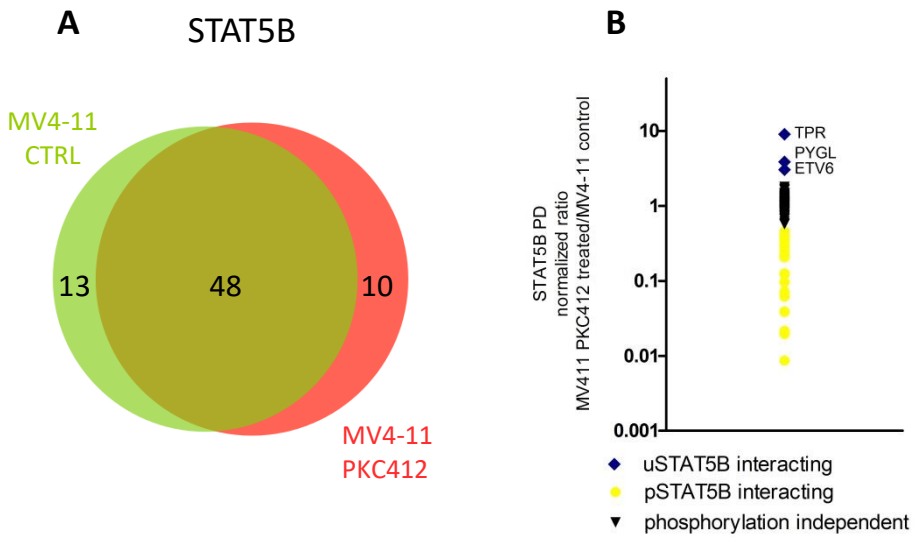

Figure 46. Interacting partners of phosphorylated and un-phosphorylated STAT5B protein in MV4-11 cells. **A.** MV4;11 cells were treated with PKC412 (100 nM, red) or vehicle control (light green) for 4 hours. The Venn-diagram shows the number of interactions and the overlap between control and PKC412 treated cells (dark green) **B.** 48 proteins interacting with STAT5A in both un-phosphorylated state after PKC412 treatment (blue) and in the phosphorylated state (yellow) were ranked according to enrichment of interaction strength upon PKC412 treatment. Interacting partner was assigned to the corresponding group after reaching fold change >2 (uSTAT5B interacting) or <0,5 (pSTAT5B interacting) of STAT5B binding enrichment after PKC412 compared to vehicle control.

The same type of analysis was performed to identify STAT5B interacting proteins. Again, MV4-11 cells were treated with PKC412 or vehicle control. In contrast to SKM-1 and THP-1 cells, no differences in the number of identified proteins were detected upon pull-down of STAT5A or STAT5B. This might be due to the fact, that de-phosphorylation was not complete, although no signals were detected in western-blot analysis (Fig.43). Applying mass spectrometry we identified 13 proteins exclusively interacting with pSTAT5B and 10 proteins with uSTAT5B. 48 proteins could be detected in both conditions (Figure 46A, detailed list in Supplementary Table 4).

Again, we quantitatively analyzed the enrichment of STAT5B-bound proteins in dependence of the phosphorylation state (Figure 46B). Interestingly, among proteins bound to uSTAT5B ETV6 was found to be highly enriched. Limited binding of STAT5B and ETV6 was already present in untreated control cells and was enhanced upon PKC412 treatment (Figure 46B). This finding could indicate that in the background of constitutively active FLT3, STAT5B phosphorylation is not complete. To explore potential biological pathways or processes in which uSTAT5B and its interacting partners might be involved IPA was performed. In Figure 47 the top pathways and processes regulated by the identified protein-protein interactions are listed. (Figure 47).

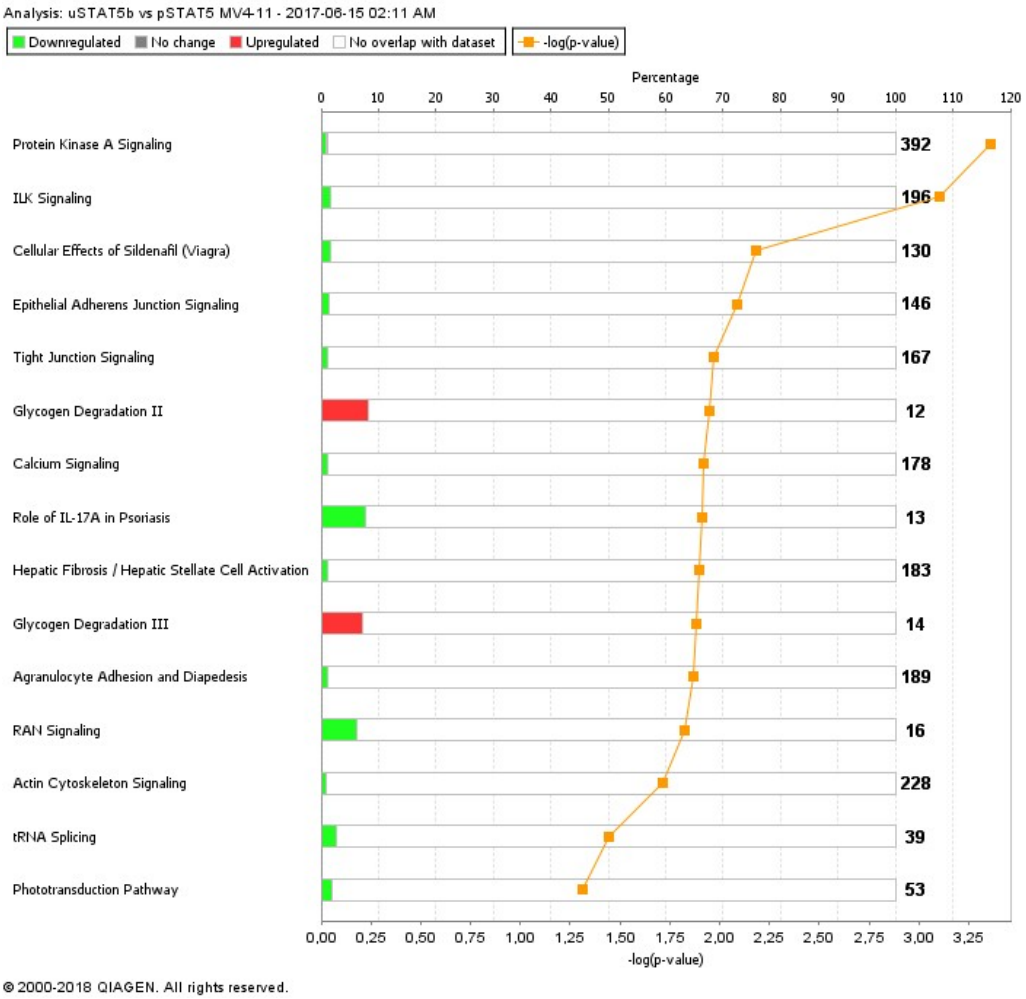

Figure 47. Pathways including proteins enriched for the interactome of uSTAT5B and pSTAT5B in MV4-11 cells. Bold numbers indicate total number of proteins in a pathway. Top X-axis shows percentage of proteins from a pathway that overlap with the input list. The bottom x-axis corresponds to significance of finding. Overlap of STAT5B interacting proteins with the pathway is represented by red bars (interactors of uSTAT5B) or green bars (interactors of pSTAT5B).

Among the proteins binding stronger with pSTAT5B are Myosin light chain 1 (MYL1), Phosphodiesterase 6H (PDE6H), and Histone variant 3 (H3F3A) all linked to protein kinase A pathway. Among other proteins in protein kinase A pathway we also discovered Glycogen Phosphorylase L (PYGL), but it strongly interacts with uSTAT5B. This enzyme is mediating a conversion of glycogen to glucose and is also found in the glycogen degradation pathways II and III in the IPA analysis.

Next to proteins that interact with STAT5A/B in a phosphorylation-dependent manner we produced a lists of protein interactors that bind independently from tyrosine phosphorylation status. These lists of STAT5A (53 proteins) and STAT5B (48 proteins) interactors were analyzed for pathway enrichment with help of IPA. Results of these analyses are presented in Figure 48.

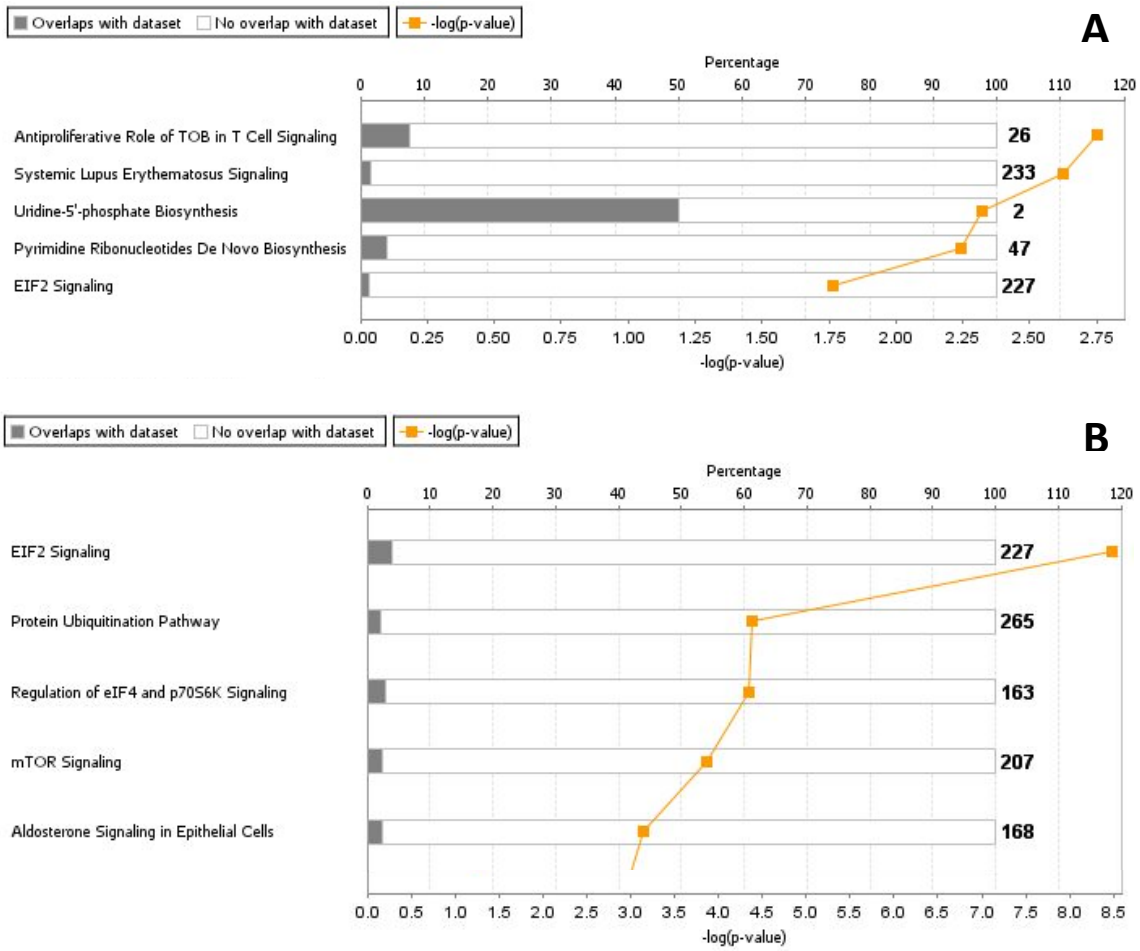

Figure 48. IPA analysis of pathway enrichment for STAT5A (panel A) or STAT5B (panel B) phosphorylation independent protein interactors.

Analysis showed enrichment of members of the EIF2 pathway indicating common function of pSTAT5A and pSTAT5B in MV4-11 cells. Surprisingly this is the only common function based on identified interacting partners. To evaluate the differences between STAT5A and STAT5B interacting partners in MV4-11 cells in control conditions and after treatment with PKC412 we analyzed interactors in Venn diagram presented as supplementary figure S9. It confirms that overlap between pSTAT5A/uSTAT5A and pSTAT5B/uSTAT5B interacting proteins is minor. These results point out at distinct biological functions of the two proteins in un-phosphorylated and phosphorylation states.

Comparison of uSTAT5A and uSTAT5B interacting partners

In order to investigate interactome differences between uSTAT5A and uSTAT5B we compared the lists of uSTAT5A/B interactors common in THP-1 and SKM-1. Results presented in Figure 49 show very minor overlap between the two groups indicating different interactors of uSTAT5A and uSTAT5B and suggesting distinct biological functions of these interactions. The interactors common for both uSTAT5

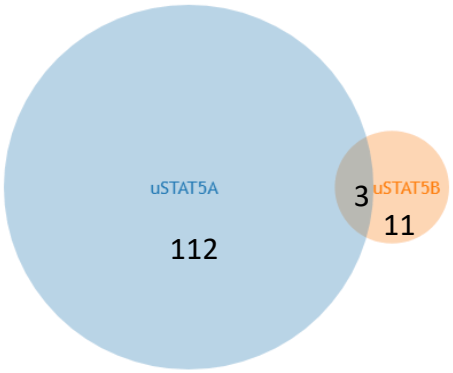

Figure 49. Comparison of interactors of uSTAT5A and uSTAT5B.

are TRIM21 and 28, and WDR1. We also analyzed the list of interactors of uSTAT5A/B and compared them to results derived from MV4-11 cells. This way we compared if uSTAT5 interactors from cell lines with endogenous uSTAT5 (THP-1 and SKM-1) are still immune-precipitated with pSTAT5 in MV4-11 cells. Results of these comparisons are presented in supplementary figures S10 and S11. This way we were able to demonstrate that the majority of uSTAT5A interactors from THP-1 and SKM-1 are not present among pSTAT5 interacting proteins in MV4-11 cells, but interestingly, this list was only modestly overlapping with proteins pulled-down with uSTAT5A after PKC412 treatment in MV4-11. This could be explained by residual phosphorylation levels after PKC412 treatments. Thanks to SILAC approach we could also directly compare the treatment conditions in MV4-11, showing that several of the proteins commonly interacting in control and after PKC412 induced de-phosphorylation show enrichment towards uSTAT5A binding. In terms of uSTAT5B interacting partners we could observe an analogical situation.

This serves as another proof for a strikingly different biological role of STAT5 proteins in its unphosphorylated form, in this case based on protein interacting partners. Impact of these interactions on biology of AML cells remains to be investigated.

Validation of the interacting partners by immunoprecipitation and western-blotting analysis.

To confirm some of the identified protein-protein interactions upon pull-down and mass spectrometry, immunoprecipitation of STAT5A or STAT5B was performed and potential binding partners were analyzed by immunoblotting. Further, to compare the interactions according to the level of STAT5 phosphorylation THP-1 cells were stimulated with GM-CSF or vehicle control prior to the protein extraction.

Results shown in Figure 43 confirm the physical interactions between STAT5A and DBC1, and between STAT5B and ETV6. Furthermore, the interaction with ETV6 is dependent on the phosphorylation status of STAT5B. Induction of STAT5B phosphorylation upon GM-CSF stimulation caused substantial loss of ETV6 binding. This confirms our observations of the SILAC IP experiments. DBC1 was only bound by STAT5A and was slightly decreased upon STAT5A phosphorylation. To rule out the possibility that the confirmed interactions are only cell line specific, similar experiment were performed using MV4-11. In this cell line the un-phosphorylated state was achieved with PKC412 pre-treatment prior to protein extraction. The results presented in the Figure 50 show the interactions of STAT5A and STAT5B with their binding partners. Again, STAT5B-ETV6 binding was highly dependent on the STAT5B phosphorylation. Whereas only minor ETV6 binding was observed in untreated control cells, PKC412-mediated STAT5B de-phosphorylation strongly enhanced the interaction of uSTAT5B and ETV6 (Figure 51). In conclusion, the pattern observed in the THP-1 cells is also true for MV4-11cells: ETV6 binds to STAT5B in a phosphorylation-dependent manner.

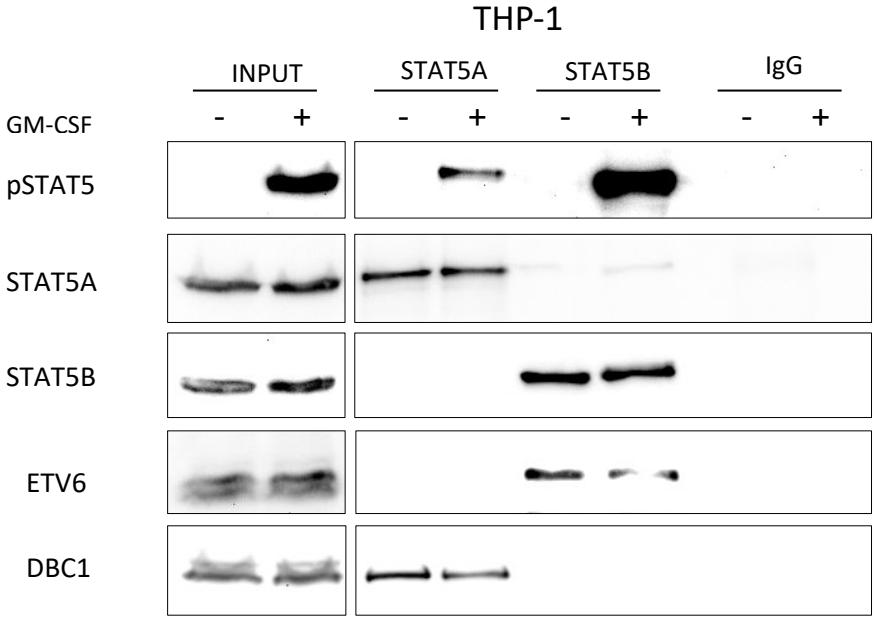

Figure 50. Co-immunoprecipitation experiments confirm the interaction of STAT5A and STAT5B with DBC1 and ETV6, respectively. THP-1 cells were stimulated with GM-CSF for 30 minutes followed by protein extraction and immunoprecipitation performed as indicated.

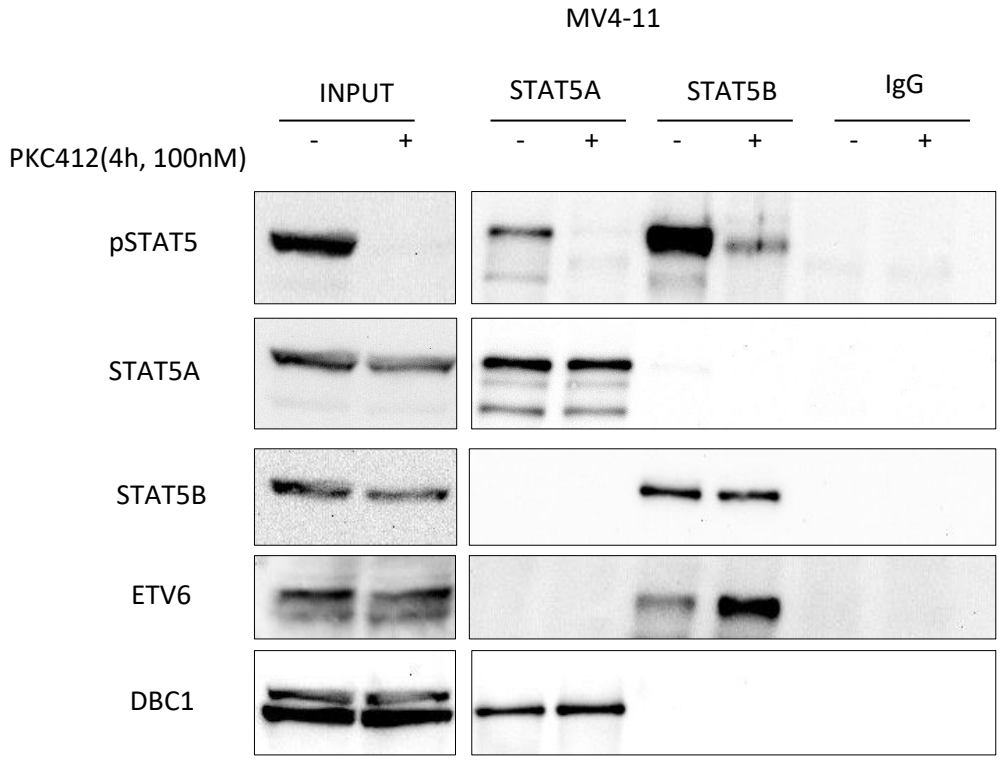

Figure 51. Co-immunoprecipitation experiments confirm the interaction of STAT5A and STAT5B with DBC1 and ETV6, respectively. MV4;11 cells were with 100 nM PKC412 or vehicle control for 4 hours followed by protein extraction and immunoprecipitation performed as indicated.

RNA-seq

To gain insight in the transcriptional profile upon STAT5A and STAT5B knockdown and whether this profile corresponds to the observed phenotype, e.g. enhanced differentiation upon STAT5B knockdown, we performed RNA-sequencing (RNA-seq) analysis in THP-1 cells expressing uSTAT5 with and without STAT5A or STAT5B knockdown. We first generated PCA plots and performed an unsupervised hierarchical clustering to visualize the distribution of the samples and dispersion between them (Figure 52).

First, it is striking that the down-regulation of uSTAT5B (green labels) causes an increased change in gene expression compared to other groups. The replicates for the uSTAT5B knock-down data set also seem to be clustering together, which indicates the good correlation between the replicates. Another interesting observation is that the control samples (red labels) and uSTAT5A (blue labels) knock-down samples tend to cluster together showing that targeting uSTAT5A has a minor impact on gene expression compared to uSTAT5B down-regulation.

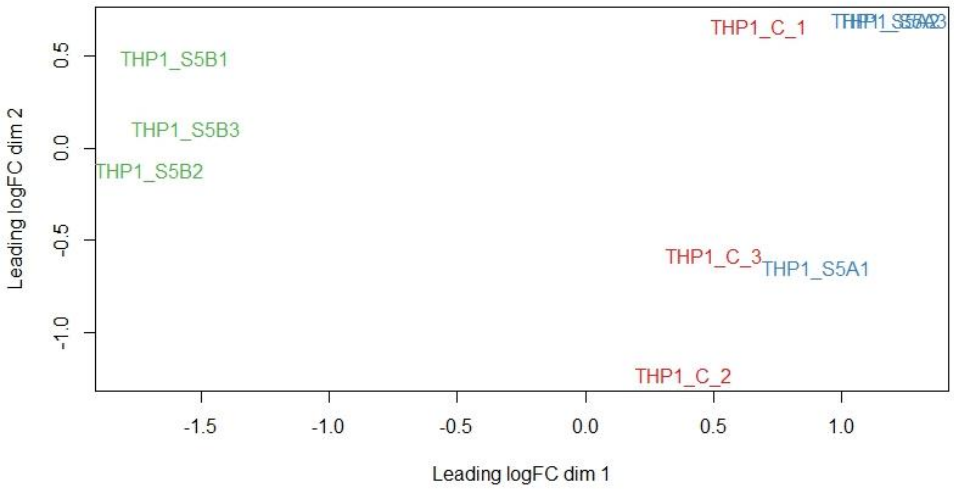

Figure 52. PCA plot for THP-1 RNA-seq samples.

The resulting plot (Figure 53) confirms the observations of the PCA. The data obtained from sequencing of samples after STAT5B knock-down cluster differently than the rest of the samples. One of the replicates within the STAT5A knock-down group clustered together with the control samples. This was also observed in the PCA.

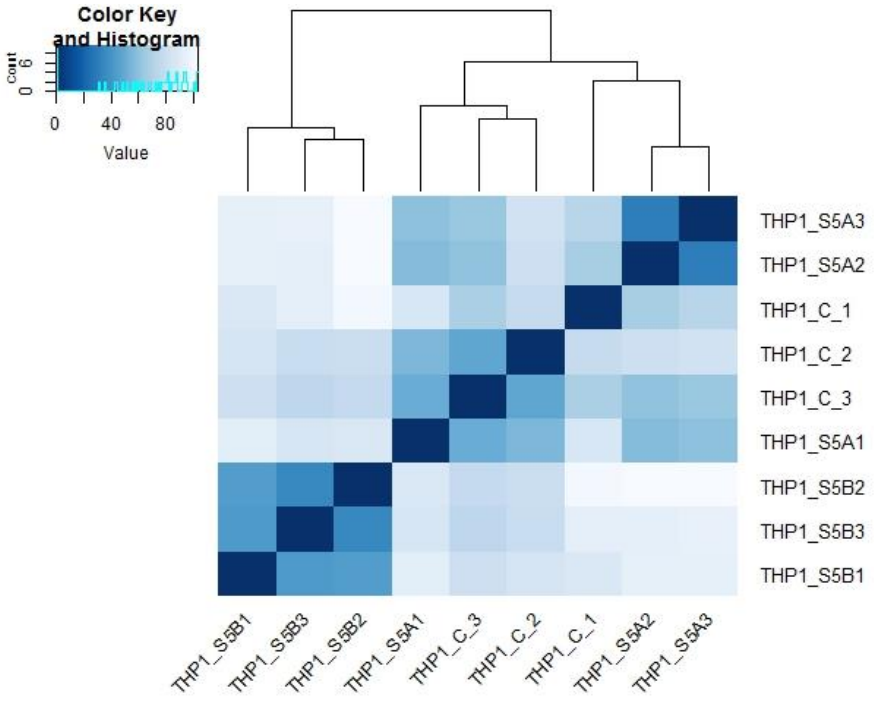

Figure 53. Unsupervised hierarchical clustering of samples from RNA-seq experiment for THP-1 cells.

A

Top downregulated genes
TERF2IP
SERINC3
MMP2
ATP10A
ANKRD52
TNFRSF21
ADD1
COL27A1
PSMA5
HK1
LRPAP1
VAT1L
TMEM119
FBXO28
AASDHPPT
GIMAP8
PCDHB2
CHST13
CYSLTR1
MFN1
CUL4A
STK38
ST14
CRTAP
DUSP27

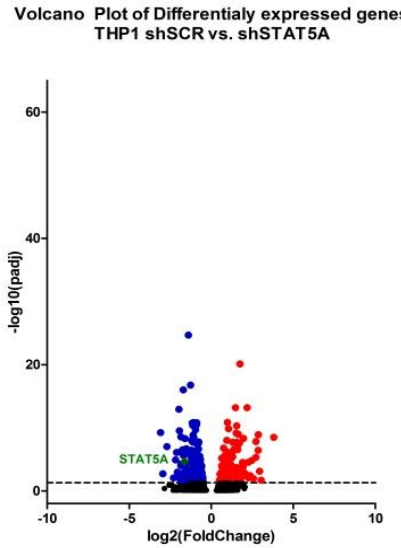

Top upregulated genes
SEMG1
HSH2D
IGSF1
ITGA4
PCOLCE2
MS4A7
SEMA3A
EEF1A1P6
RXFP2
PTMAP3
MAK
CERKL
CIB3
EEF1A1P4
NAV3
WNT7B
RGCC
ARPC3
CMAHP
S1PR3
BCAS4
USP31
IL1RAP
SESN1
MOXD1

B

Top downregulated genes
AKR1C3
SFT2D1
PTPRN2
FOXP4
COPG1
CHST12
SMIM13
ABCA2
MEF2D
STAT5B
CLSTN2
AKR1C2
EVA1B
ARPC1A
SEPT5
IFIT2
CTSG
DDA1
EXOC2
RBBP8
IGSF1
RRAGA
ROS1
KIF17
TCF23

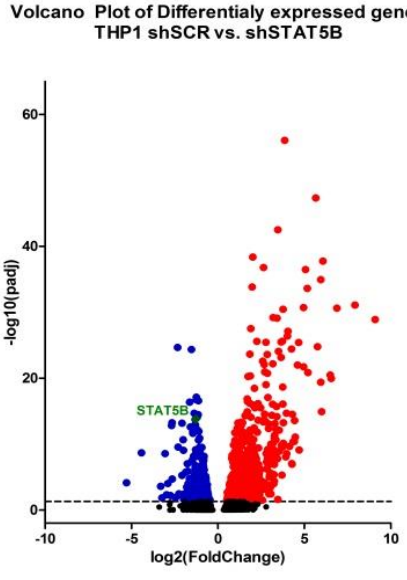

Top upregulated genes
PTK2
MFNG
CYBB
PLXDC2
EPHX2
VCAN
MAGED1
ZNF43
ITGAM
AOC1
ZNF662
DLX3
PCDHGB4
LILRB2
OLFML3
ABCA6
RTN1
HLA-DRB1
PI15
CXORF57
SIGLEC12
CD4
CD86
SIRPB2

Figure 54. Volcano plots showing changes in gene expression in THP-1 cells upon **A)** STAT5A or **B)** STAT5B knock-down.

To investigate changes in gene expression upon down-regulation of uSTAT5A or uSTAT5B the differential gene analysis (DGE) was performed for each condition separately. The adjusted p-value (p_{adj}) was calculated for each gene. For further analysis only genes meeting the cut-off of $p_{adj}<0.05$ were considered (with exception of GSEA). Reduction of uSTAT5A levels resulted in downregulation of 252 and upregulation of 188 genes. In case of uSTAT5B depletion, 356 genes were downregulated and an surprisingly high number of 593 genes were upregulated (Figure 54 and 55).

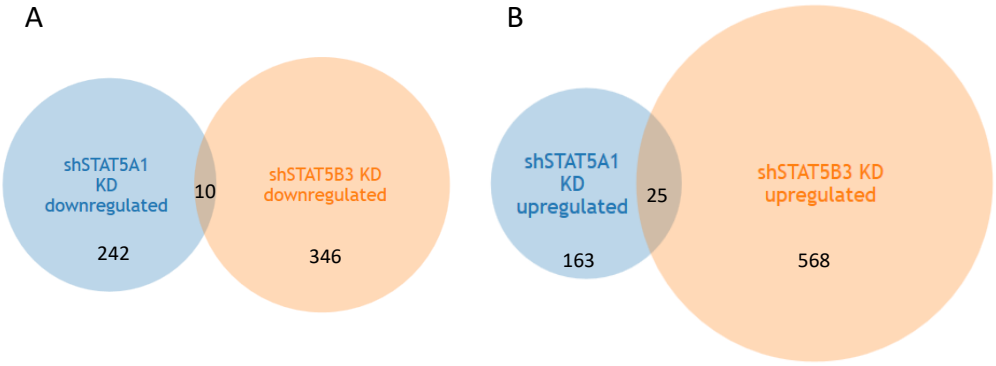

Figure 55. Comparison of **A)** down- or **B)** up-regulated genes upon uSTAT5A and uSTAT5B knock-down.

To address the question whether the expression of a common set of genes was differentially expressed, gene lists of up- or downregulated genes upon knock-down of uSTAT5A or uSTAT5B were compared (Figure 55). Among differentially regulated genes, only 10 genes were down-regulated and 25 up-regulated upon uSTAT5A as well as uSTAT5B knock-down. These data suggest that uSTAT5A and uSTAT5B have different biological functions in AML cells.

We next analyzed the lists of differentially expressed genes to identify well-established STAT5 target genes. Figure 56 shows the fold change of gene expression for STAT5 itself and selected STAT5-target genes. Down-regulation of uSTAT5A and uSTAT5B was highly specific with similar efficacy. Upon knock-down of uSTAT5A, we observed a decent, but not significant up-regulation of uSTAT5B suggesting the presence of a compensatory mechanism. Interestingly, STAT6, another member of the STAT family, was up-regulated after uSTAT5B knock-down.

Among down-regulated genes we were able to find a small number of known STAT5 target genes, which turned out to be regulated by both uSTAT5A and uSTAT5B in THP-1 cells (e.g. OSM, BCL11A and data not shown). In contrast, expression of BCL-2 and GP9 was preferentially regulated by uSTAT5B whereas BCL9L emerges as uSTAT5A target gene.

This first preliminary analysis confirmed the efficacy and specificity of our knock-down approach and again provided evidence for different functions of uSTAT5A and uSTAT5B, even in the regulation of already established STAT5 target genes.

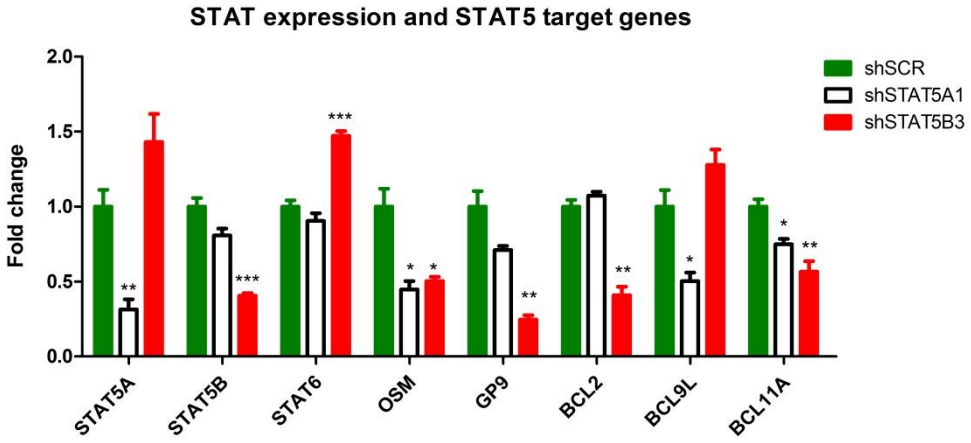

Figure 56. Expression of STAT5 and its target genes. Graph shows changes in expression of known STAT5 target genes upon down-regulation of uSTAT5A (white bars), down-regulation of uSTAT5B (red bars) compared to control (green bars).*:p<0.05; **:p<0.01; ***:p<0.001 (student t-test).

Gene Set Enrichment Analysis

To obtain a systematic overview of STAT5-regulated biological processes, we analyzed the list of differentially expressed genes by Gene Set Enrichment Analysis (GSEA). We compared THP-1 shSCR condition to THP-1 shSTAT5A or shSTAT5B. Gene sets enriched with an FDR of q <0.05 were considered as significant. The top 5 enriched gene sets for each of the knock-down experiment, were plotted and are presented in Figure 57.

In case of differentially expressed genes after knock-down of uSTAT5A significant enrichment scores were only observed for genes highly expressed in control cells, but down-regulated after uSTAT5A knock-down. In the KEGG curated database the top enriched gene set is RIBOSOME, which consists of genes encoding proteins for small and large ribosomal subunits. Another affected gene set is composed of members of the Arachidonic acid metabolism pathway, followed by genes playing roles in prion disease and depression. Genes involved in JAK-STAT signaling are also among gene sets de-regulated upon uSTAT5A knock-down.

Differentially expressed genes after uSTAT5A knock-down were also compared to another curated database – REACTOME. As expected and in line with the results of the KEGG database, the sets of genes active in control cells and lost upon uSTAT5A knock-down are linked to translation. Strong loss of genes encoding ribosomal subunits will likely impact protein synthesis. Among other gene sets we have identified NONSENSE_MEDIATED_DECAY_ENHANCED_BY_THE_EXON_JUNCTION_COMPLEX, containing genes playing a role in degradation of mRNA harboring premature termination codons.

For uSTAT5B knock-down results GSEA helped to identify gene sets that were either up-regulated or suppressed upon STAT5B knockdown (Figure 57B). We run the analysis with the KEGG curated database and among top hits was a gene set enriched for genes important for DNA replication (affected CDT1 and MCM7 expression). Further, RNA metabolism, represented by enrichment of gene sets important for RNA transcription and spliceosome functions, was also affected after uSTAT5B knock-down.

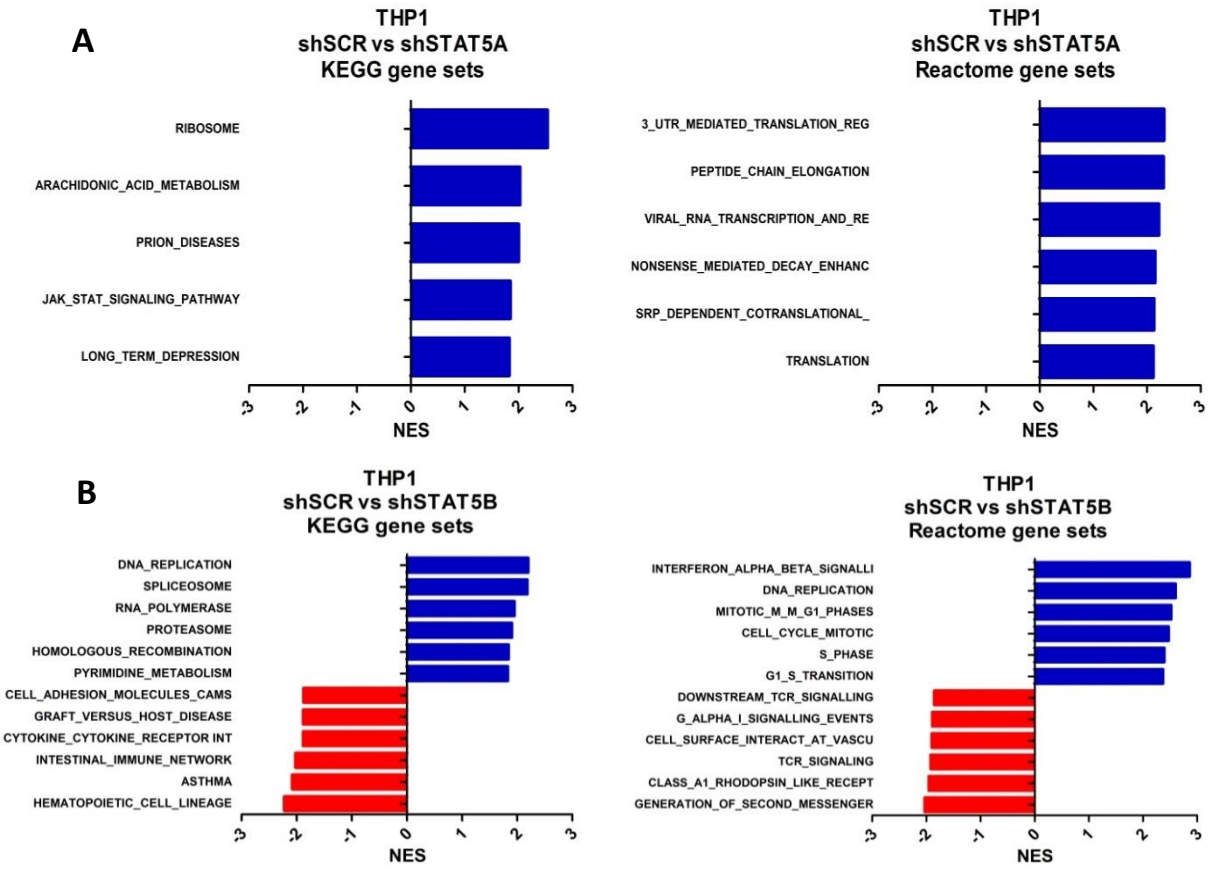

Figure 57. Gene Set Enrichment Analysis sheds light on biological processes upon uSTAT5 knock-down. List of differentially expressed genes after uSTAT5A knock-down (A) or uSTAT5B knock-down (B) was analyzed for pathway enrichment using KEGG and Reactome gene sets. Pathways deactivated upon knock-down are depicted in blue and the activated pathways are presented in red.

Another key regulator of cellular homeostasis, the proteasome, also seems to be regulated by uSTAT5B (genes encoding for members of the 26S subunit are down-regulated). Finally, homologous recombination seems to be altered after uSTAT5B down-regulation. This is a pathway commonly used in repair of DNA double-strand breaks and one of the major components RAD51C is down-regulated after uSTAT5B knock-down. In line, gene sets identified in the Reactome data base, which were enriched in control cells (THP-1 shSCR) but lost upon knock-down also contained DNA replication genes and sets involved in cell cycle progression. This DNA replication-based dysregulation explains the observed cell-cycle arrest in AML cell lines after uSTAT5B knock-down. In addition, the Interferon alpha/beta signaling pathway was found to be lost upon uSTAT5B knock-down in the Reactome gene sets.

We also observed enrichment of gene sets, for genes up-regulated upon uSTAT5B knock-down. Using the KEGG curated database, the highest enrichment score included genes involved in hematopoietic cell lineage regulation. These genes are primarily expressed in committed lineage-positive differentiating cells. Other significantly enriched gene sets, such as asthma, intestinal immune network or graft versus host disease were comprised of members of the human leukocyte antigen (HLA) family, present on antigen-presenting cells (APC) like monocytes. Changes in HLA gene expression after uSTAT5B down-regulation are presented in the Figure 58.

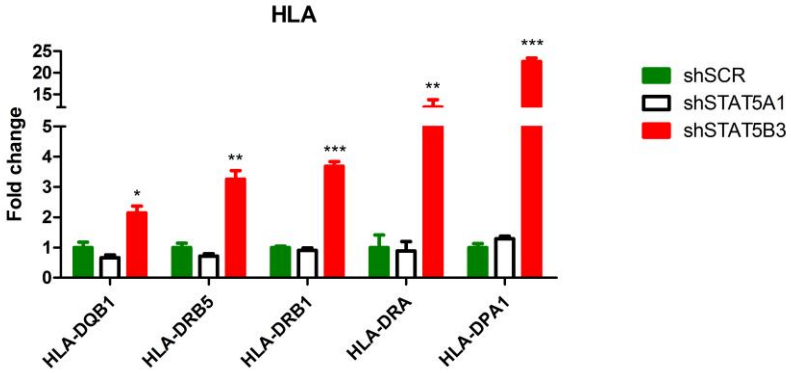

Figure 58. HLA genes expression is highly increased after STAT5B down-regulation. Graph shows changes in expression of HLA genes upon down-regulation of uSTAT5A (white bars), down-regulation of uSTAT5B (red bars) compared to control (green bars). *:p<0.05; **:p<0.01; ***:p<0.001 (student t-test).

In line with the observation of induction of differentiation upon uSTAT5B knockdown, the enriched gene set "cytokine-cytokine receptor interaction" contained several markers expressed on mature hematopoietic cells, like interleukins and chemokine receptors (increased expression of IL21 receptor, IL7 receptor, Interleukin 16, Chemokine receptors CCR1 and 2, and CXCR4). Finally, the enriched gene set named "cell adhesion molecules (CAMs)" contained genes encoding proteins important for monocytes to migrate across endothelia. We also analyzed what gene sets from the Reactome curated database were enriched in uSTAT5B depleted cells. Several gene set were very similar to the KEGG database such as HLA family, adhesion molecules and cytokine receptors confirming the overexpression of genes and markers typical for differentiated cells upon uSTAT5B knock-down in THP-1 cells. Further, gene expression profile upon knock-down of uSTAT5B correlated with the genes expressed on mature hematopoietic cells, but not hematopoietic stem cells [201] (Figure 59).

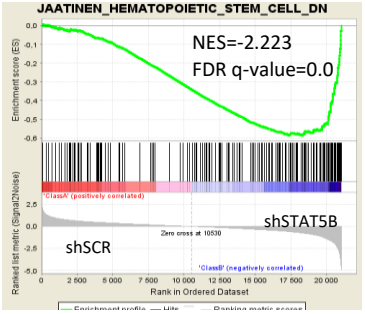

Figure 59. Genes up-regulated after STAT5B knock-down compose set of genes down-regulated in HSC.

Ingenuity Pathway analysis confirms differentiation of THP-1 cells upon uSTAT5 down-regulation.

The analysis of gene expression changes upon STAT5 knock-down was also performed with the Ingenuity Pathway Analysis (IPA) tool (methods section). Canonical pathways altered after uSTAT5 down-regulation are presented in Figure 60 for uSTAT5A (top panel) and uSTAT5B knock-down (bottom panel).

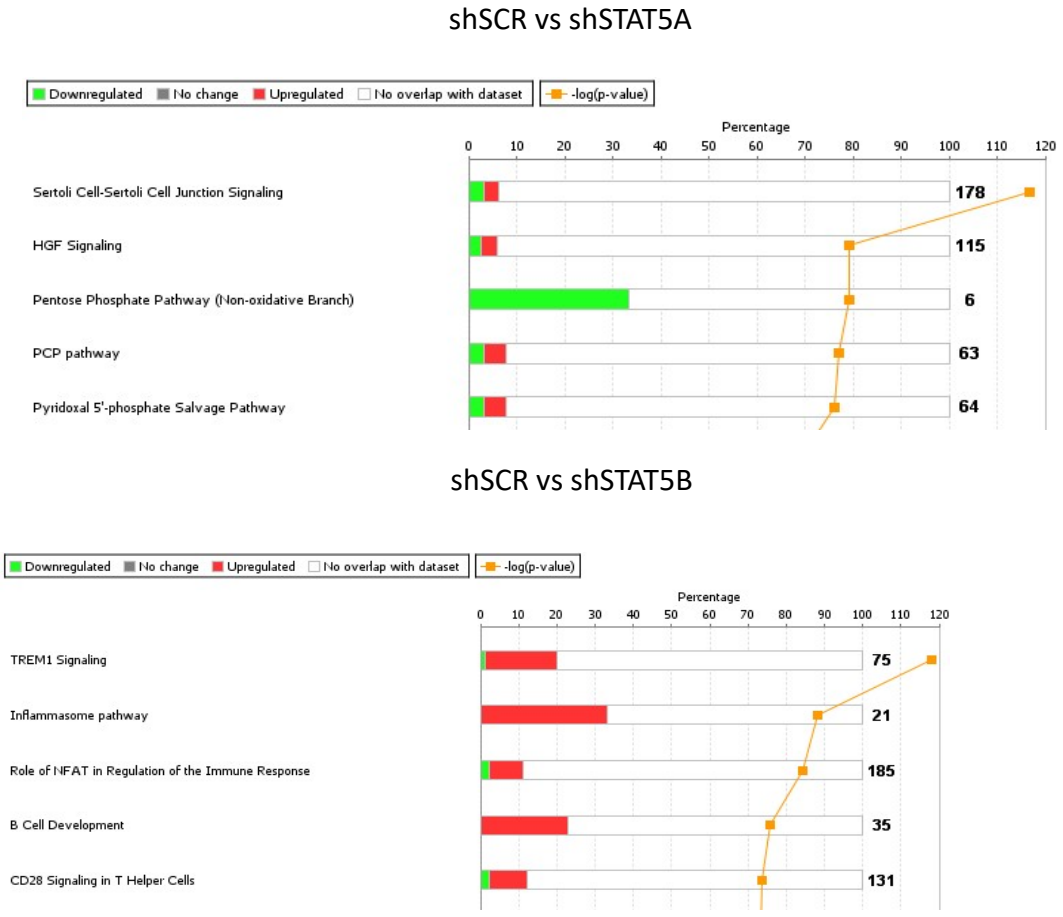

Figure 60. Ingenuity Pathway Analysis of gene expression changes after STAT5 down-regulation. Bold numbers indicate total number of genes in a pathway. Top X-axis shows percentage of genes from a pathway that overlap with the input list. The bottom x-axis corresponds to significance of finding. Overlap of the genes deregulated upon uSTAT5A (top) or uSTAT5B (bottom) knock-down with the pathway is represented by red bars (upregulated genes after KD) or green bars (down-regulated genes after KD).

Results for uSTAT5A down-regulation were not very conclusive. Although some of the genes belonged to the same pathways, these genes were either up- or down-regulated. The most obvious change was observed within the pentose phosphate pathway, where all genes were down-regulated. In the non-oxidative branch of the pathway the side products from the oxidative part are metabolized to five-carbon sugars used later for nucleotide synthesis.

Upon uSTAT5B down-regulation, the TREM-1 signaling pathway was strongly induced. This pathway is active in mature myeloid cells including neutrophils, monocytes and macrophages. To validate its activation, we screened for members of this pathway in the gene expression data and found strong induction of expression of TLR family members (Figure 61). Also members of other pathways were

strongly up-regulated upon uSTAT5B knock-down. Under physiological conditions, all of them are highly expressed in mature hematopoietic cells.

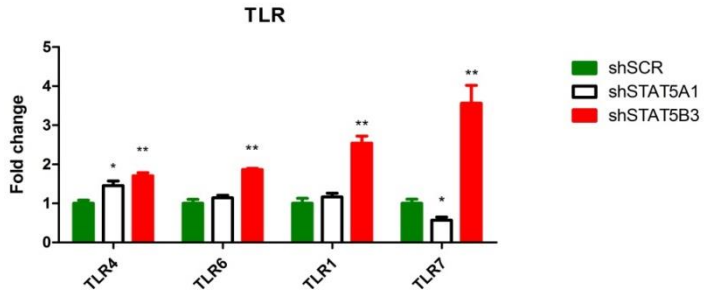

Figure 61. Increased expression of members of the TREM-1 pathway after uSTAT5B down-regulation in THP-1 cells (red bars), upon down-regulation of uSTAT5A (white bars) compared to control (green bars). *:p<0.05; **:p<0.01 (student t-test).

Increase of the cluster of differentiation markers expression upon STAT5B down-regulation

Among genes differentially expressed after down-regulation of uSTAT5B, we observed a significant increase in many cluster of differentiation (CD) marker. Most of these CD molecules are typically expressed on mature differentiated cells of the hematopoietic system. These changes are presented in the Figure 62.

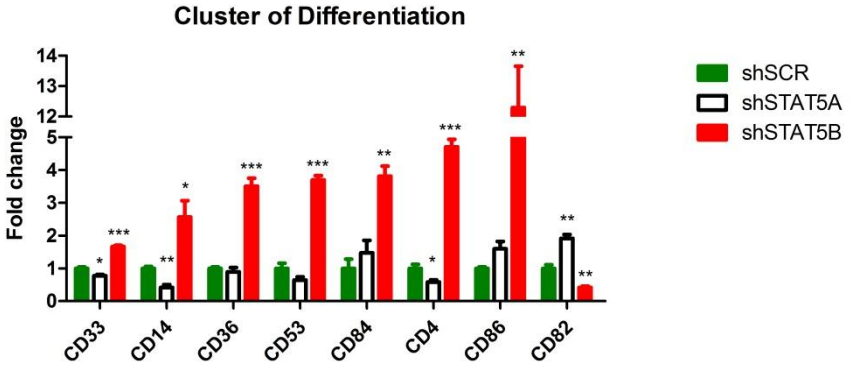

Figure 62. Graph shows changes in expression of Cluster of differentiation markers normally present on mature hematopoietic cells upon down-regulation of uSTAT5A (white bars), down-regulation of uSTAT5B (red bars) compared to control (green bars). *:p<0.05; **:p<0.01; ***:p<0.001 (student t-test).

STAT5-dependent expression of important epigenetic regulators

So far, we have demonstrated, that down-regulation of uSTAT5B in the THP-1 cells induces hematopoietic differentiation. Activation of the TREM-1 pathway, alterations in cell cycle progression and expression of e.g. CD11b are hallmarks of these findings, but it remains elusive how does uSTAT5B influence these processes. Upon uSTAT5B down-regulation we observed strong induction of genes, which were completely turned off in uSTAT5B expressing cells. Further analysis of Gene Ontology database using GSEA software indicated the loss of heterochromatin signatures after down-regulation of uSTAT5B (Figure 63). These findings indicate that activation of gene expression could be regulated by epigenetic-based mechanisms.

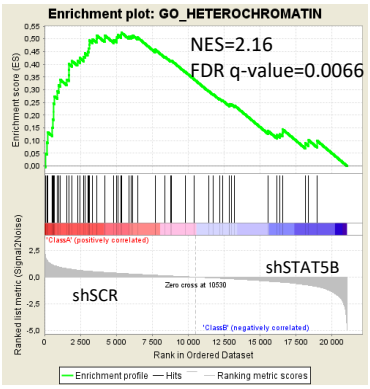

Figure 63. Heterochromatin signature lost upon down-regulation of STAT5B.

To prove this hypothesis, the list of differentially expressed genes was investigated for genes with known functions in maintaining the epigenetic landscape. We were able to identify a number of genes encoding either epigenetic writers/erasers, direct regulators of DNA methylation or proteins that influence compaction of the DNA strand. Most of them turned out to be regulated by uSTAT5B, however few may be target genes of uSTAT5A. Fold changes in expression is presented in Figure 64. Interestingly, some were pulled-down in our co-IP experiments (e.g. KDM5C).

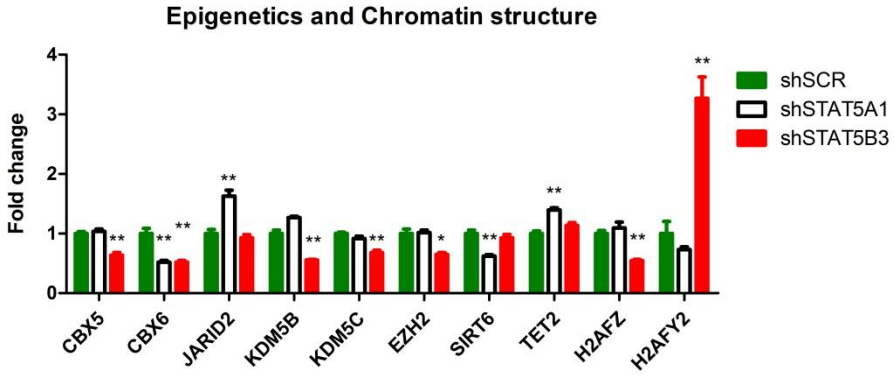

Figure 64. Expression of epigenetic state modifiers after STAT5 down-regulation. Graph presents changes in expression of major epigenetic players upon down-regulation of uSTAT5A (white bars), down-regulation of uSTAT5B (red bars) compared to control (green bars). *:p<0.05; **:p<0.01 (student t-test).

Treatment of THP-1 AML parental cell line using a combination of chemotherapeutics and STAT5 down-regulation.

Down-regulation of uSTAT5B in AML cell lines was followed by induction of differentiation. To further analyze this phenomenon, we decided to combine STAT5 knock-down with standard chemotherapeutics used in treatment of AML patients. THP-1 cell lines transduced with shSCR or shRNA directed against STAT5A or STAT5B were treated with ATRA or AraC for 6 days followed by analysis of cellular proliferation (Figure 65). Treatment with ATRA or AraC significantly reduced cell proliferation, but induction of shSCR expression via doxycycline treatment had no further effect on cell growth.

Contrary, knock-down of uSTAT5A led to significant decrease in cell number compared to the drug treatments alone, for both AraC and ATRA. Similar results were observed upon uSTAT5B down-regulation; however, these changes were not significant.

In addition, cell cycle analysis was performed on day 6 (Figure 57A). ATRA treatment induced a slight increase in the subG1 apoptotic cell population and a G1 arrest in control cells whereas AraC treatments caused an increase in S phase and apoptosis. Additional knockdown of uSTAT5A or uSTAT5B led to a significant increase in apoptosis, which was most prominent upon uSTAT5A knock-down in combination with AraC (Figure 66) Almost 80% of cells were dead after 6 days of treatment

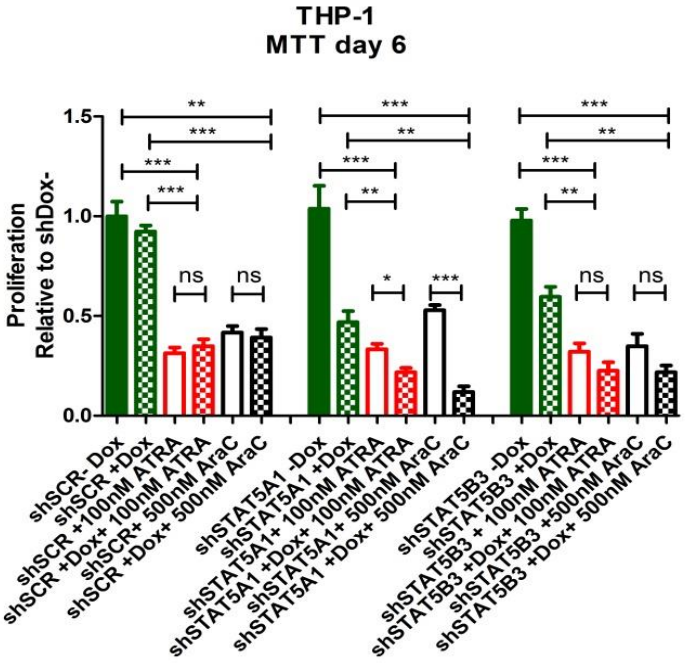

Figure 65. Combination of STAT5 down-regulation and chemotherapeutic treatments with ATRA or AraC. THP-1 control (shSCR), STAT5 down-regulated (shSTAT5A1) or STAT5B down-regulated (shSTAT5B3) cells were treated for 6 days with 100nM ATRA or 500nM AraC without and with doxycycline induction of knock-down (check pattern). Proliferation of cells was than assessed by MTT. ns= non-significant; **:p<0.01; ***:p<0.001 (student t-test).

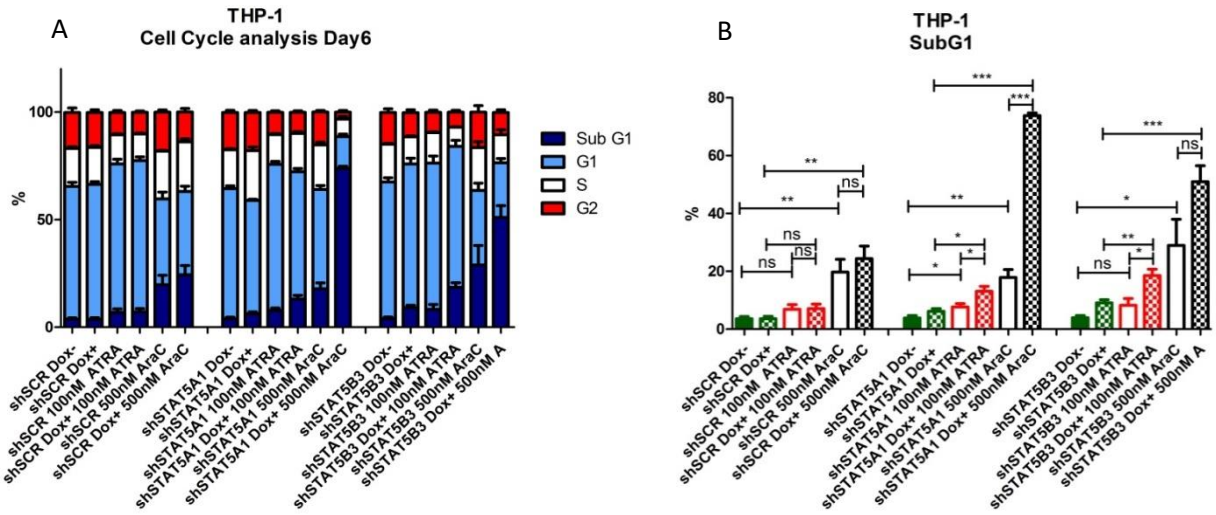

Figure 66. Cell cycle analysis after combinational treatment of ATRA or AraC with STAT5 down-regulation. THP-1 control (shSCR), STAT5 down-regulated (shSTAT5A1) or STAT5B down-regulated (shSTAT5B3) cells were treated for 6 days with 100nM ATRA or 500nM AraC without and with doxycycline induction of knock-down (check pattern). Progression of the cell cycle was than assessed by PI staining and SubG1 populations were compared. ns= non-significant; *:p<0.05; **:p<0.01; ***:p<0.001 (student t-test).

Strong reduction of cell number and drastic increase in apoptotic cell population after combining chemotherapeutics with knock-down of STAT5 proteins is a novel finding. It would be of interest to find a compound to target cells in a similar manner as upon STAT5 knock-down. The next chapter summarizes experiments where we treat THP-1 cells with a novel drug.

Discovery of drugs with anti-leukemic potential using a Drug Signatures Database with a GSEA-based approach

The established RNA-expression profile upon uSTAT5B knock-down enabled us to search for drugs, which may induce changes similar way. For this purpose, we took advantage of the Drug Signature Database, a publicly available database of transcriptional expression profiles obtained upon various drug treatments and compared our gene-expression data to compounds in this database using GSEA). Among the drugs with the highest normalized enrichment score (NES) scores was Dihydroergotamine (DHE). The results of the enrichment analysis of DHE-mediated gene-expression changes and gene-expression data obtained from RNA-seq analysis after uSTAT5B knock-down in THP-1 cells are presented in the Figure 67.

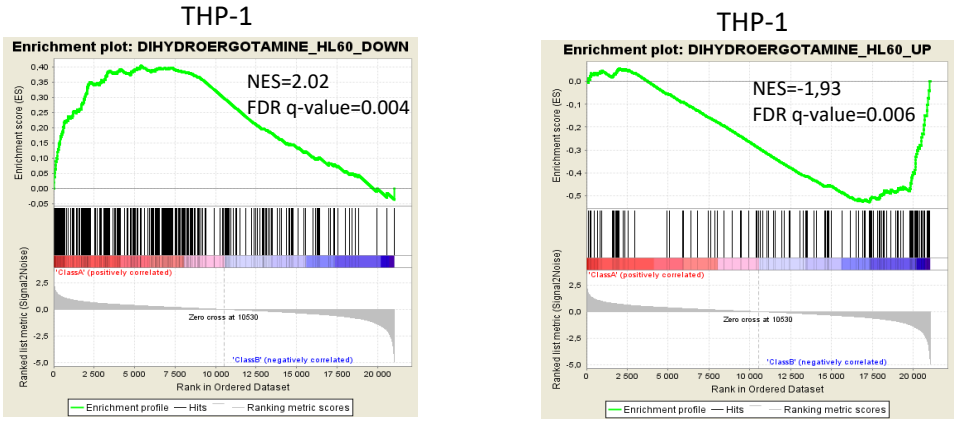

Figure 67. GSEA using drug signatures database reveals Dihydroergotamine as a potential drug that mimics uSTAT5B down-regulation.

DHE is an FDA-approved drug for the treatment of acute migraine. It binds with high affinity to 5-HT1Da and 5-HT1Db receptors and acts as an agonist. Two possible mechanisms of migraine treatment with DHE were proposed: i) vasoconstriction; and ii) inhibition of inflammation by regulation of pro-inflammatory peptide release in the nerve endings [202]. There are no reports or data indicating a possible role of DHE in the treatment of AML.

Dihydroergotamine as a novel drug in treatment of Acute Myeloid Leukemia

The AML cell lines THP-1, SKM-1 and MV4-11 were exposed to DHE alone or in combination with chemotherapeutics to explore a potential role of DHE in AML therapy. On day 6 cell proliferation of control and treated cells was analyzed using a MTT assay. The results of this experiment are presented in the figure 68.

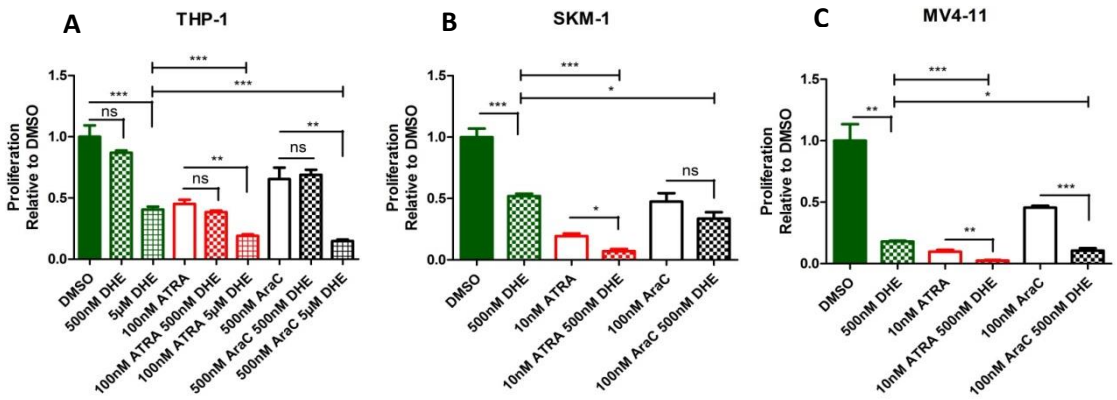

Figure 68. DHE treatments of AML parental cell lines – MTT. THP-1 (**A**), SKM-1 (**B**) and MV4-11 (**C**) cells were treated for 6 days with 10/100nM ATRA or 100/500nM AraC alone or in combination with 500nM-5uM DHE. Proliferation of cells was than assessed by MTT. ns= non-significant; *:p<0.05; **:p<0.01; ***:p<0.001 (student t-test).

In all three cell lines the treatments with DHE decreased the cell number to levels comparable with ATRA or AraC treatment. In case of SKM-1 and MV4-11 cells nanomolar concentrations caused a decrease in cell number by 50% or more. For THP-1 cells higher concentrations were required. Importantly the combination of ATRA and DHE treatment showed additive effects for all 3 cell lines resulting in a further decrease of cell growth. Additive effects could also be observed for the combination treatments of DHE and AraC for THP-1 and MV4-11 cells but for SKM-1 cells.

At the same time-points cell cycle analysis was performed. The results are shown in the figure 69.

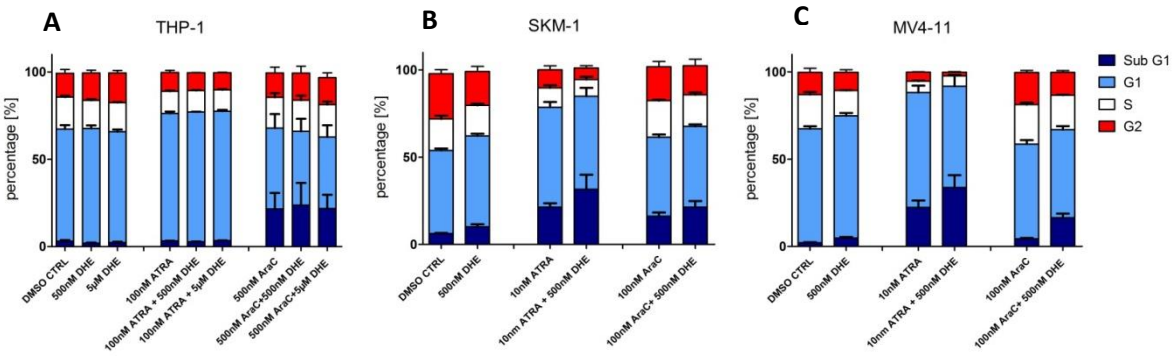

Figure 69. Cell cycle analysis of the AML cell lines treated with DHE. THP-1 (**A**), SKM-1 (**B**) and MV4-11 (**C**) cells were treated for 6 days with 10/100nM ATRA or 100/500nM AraC alone or in combination with 500nM-5uM DHE. Cell cycle progression of the cells was than assessed by PI staining.

At concentrations used in the previous experiment no additional DHE-effects were seen in combination therapies with ATRA or AraC. For SKM-1 and MV4-11 cells DHE treatment caused a slight increase of apoptosis. To further evaluate the impact of DHE treatment on THP-1 cells, analysis for expression of a cluster of differentiation markers was performed. We were able to show that CD14 and CD33, two markers with increased expression levels after uSTAT5B down-regulation were also up-regulated upon DHE treatment (Fig. 70). Additional treatment with ATRA further increased the expression of CD33. These findings may explain the discrepancy between significant inhibition of proliferation (Figure 68) but no evidence of apoptotic cell death (Figure 69).

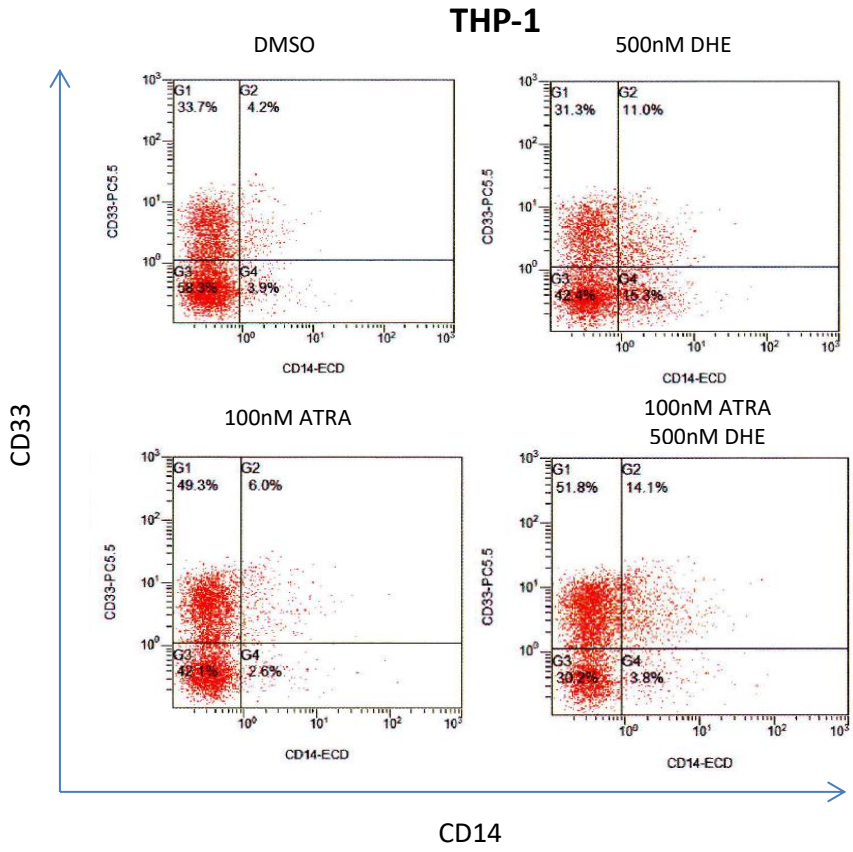

Figure 70. FACS analysis of CD33 and CD14 expression after DHE and ATRA treatments

Role of ETV-6 in AML cell lines

Protein expression of ETV6 depends on uSTAT5B levels

Among novel uSTAT5B interacting proteins ETV6 was pulled down in all 3 AML parental cell lines and this interaction was shown to be dependent on STAT5B phosphorylation. Analysis of the gene expression changes in THP-1 cells upon uSTAT5 down-regulation did not show any significant changes in *ETV6* mRNA expression.

To analyze possible changes on protein levels, down-regulation of uSTAT5A or uSTAT5B was induced in THP-1 and SKM-1 cells and Western blot analysis was performed (Figure 71).

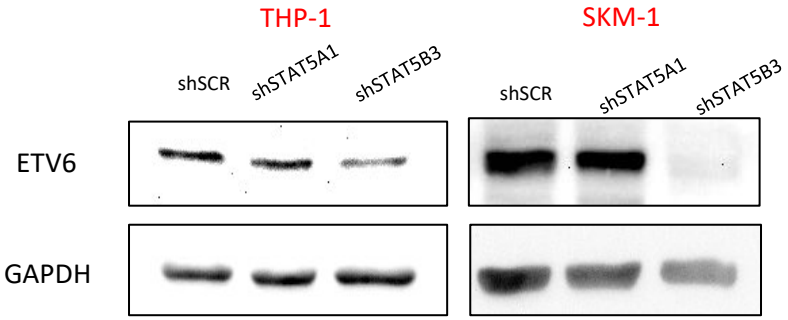

Figure 71. Analysis of ETV6 protein expression levels in THP-1 and SKM-1 cells. Protein levels of ETV6 were measured by western-blot analysis in cell lines transduced with shRNAs specifically targeting uSTAT5A, uSTAT5B, or an unspecific shSCR control. Expression of GAPDH was used to control equal loading.

In THP-1 and SKM-1 cell lines down-regulation of uSTAT5B, but not uSTAT5A led to a decrease in ETV6 levels. Despite no influence of STAT5B level on *ETV6* RNA expression was observed, protein levels of ETV6 seem to be dependent on the presence of STAT5B in THP-1 and SKM-1.

Down-regulation of ETV6 in AML cell lines

To analyze the role of ETV6 in AML cells a conditional shRNA-mediated knock-down was performed in THP-1 and MV4-11 cells. The efficacy of down-regulation using three different shRNA sequences was analyzed in THP-1 cells and is presented in the Figure 72.

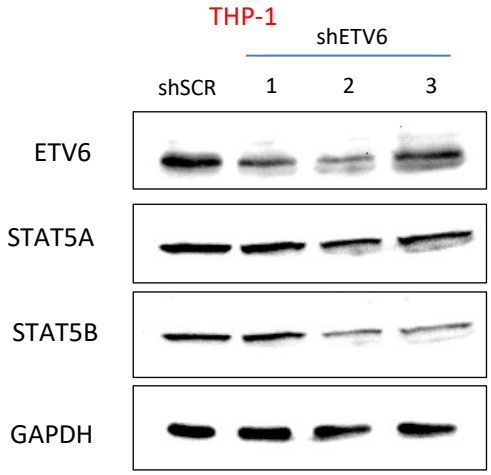

Figure 72. Analysis of knock-down efficacy of ETV6 protein expression levels in THP-1 cells. Protein levels of ETV6, STAT5A, and STAT5B were measured by western-blot analysis in cell lines transduced with shRNAs specifically targeting ETV6 or an unspecific shSCR control. Expression of GAPDH was used to control equal loading.

As observed in Western blot, all shRNAs showed downregulation of ETV6 protein levels with the strongest efficacy in clone 2. Interestingly, knock-down of ETV6 using this clone resulted in decreased expression of uSTAT5B and to smaller extend uSTAT5A. To gain better understanding on cross-talk between ETV6 and STAT5B we used newly established cell lines to perform functional experiments in THP-1 and MV4-11 cells.

Functional analysis of ETV6 knock-down

After establishing new shETV6 conditional knock-down cells, we investigated the functional consequences of ETV6 down-regulation. Upon knock-down of uSTAT5B AML cell lines had shifted towards a more mature and differentiated phenotype, characterized by elevated levels of CD11b expression. Interestingly, down-regulation of ETV6 also caused an increase of CD11b expression in THP-1 AML cells (Figure 73A).

The same experiment was performed in MV4-11 cells. Surprisingly, knockdown showed an opposite effect with down-regulation of CD11b, which expression is already weakly expressed at baseline in these cells (Figure 73B). Other markers might be more relevant in MV4-11cells.

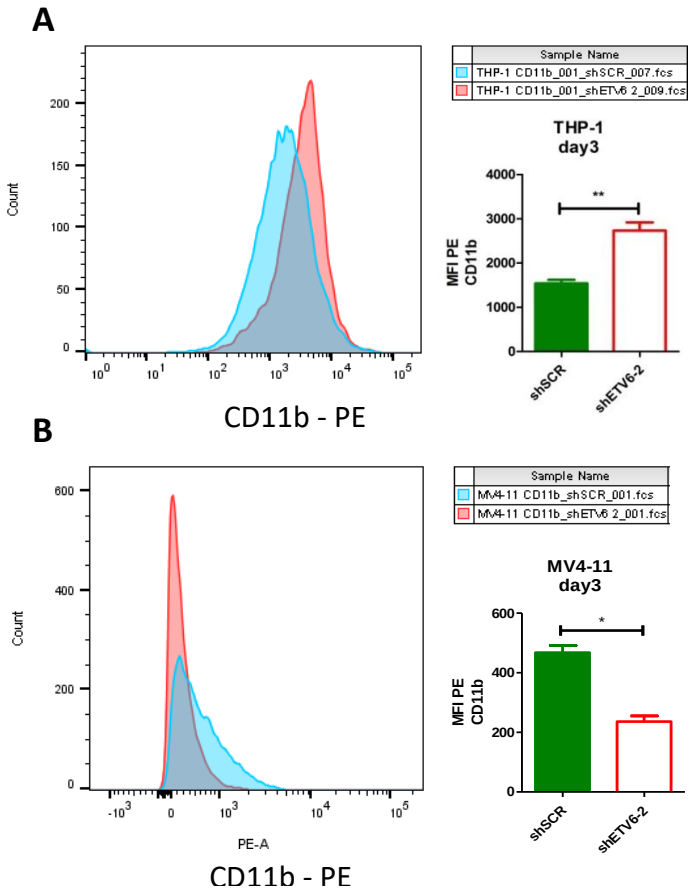

Figure 73. Impact of ETV6 down-regulation on differentiation of AML cell lines. Cells were treated with doxycycline for 3 days and expression of CD11b in THP-1 (**A**) and MV4-11 cells (**B**) was analyzed by FACS analysis. Shown are representative FACS histograms and combined data representing 3 replicates (n=3). MFI stands for Median Fluorescence Intensity. *:p<0.05 ; **:p<0.01 (student t-test).

The finding that ETV6 and STAT5B are interacting partners and expression of both causes a block in differentiation in AML cells is a new non-canonical function for both proteins. To further investigate

whether other features of STAT5B knock-down also depend on ETV6, the proliferation of cells after ETV6 down-regulation was evaluated via MTT assay (Figure 74).

Proliferation of THP-1 or MV4-11 is not dependent on ETV6 expression as assessed by MTT assay.

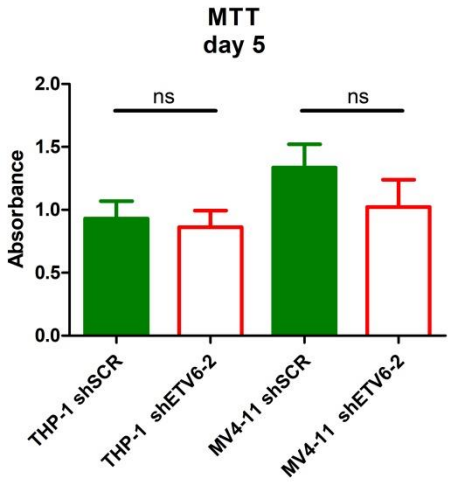

Figure 74. Cellular metabolic activity and proliferation upon ETV6 knock-down assessed by MTT assay

Combined analysis of transcriptomic and proteomic data

A comparison of RNA-seq and SILAC IP

Identification of new putative interacting partners of STAT5 in AML parental cell lines resulted in the identification of proteins involved in epigenetic regulation, mRNA processing and other crucial processes governing cell stability. To further analyze the role of the novel discovered interactors, we compared the proteomics data with the THP-1 gene expression profiles obtained after down-regulation of uSTAT5A and uSTAT5B.

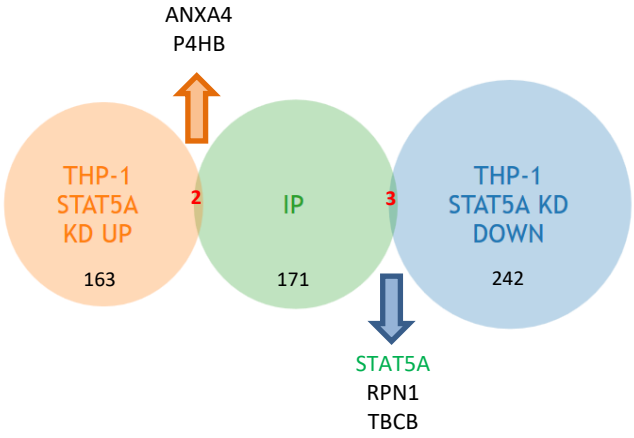

Figure 75. Comparison of gene expression data obtained upon uSTAT5A down-regulation (orange for up-regulated genes, blue for down-regulated genes) with the list of uSTAT5A interacting proteins (green).

First, the lists of putative uSTAT5A interactors and differentially expressed genes upon uSTAT5A down-regulation in THP-1 cells were compared for potentially shared genes and corresponding proteins (Figure 75). The common list consisted of 4 proteins, which were identified as interacting partners of uSTAT5A and where gene expression was affected upon uSTAT5A knock-down. Two of them, ANXA4 and P4HB, are up-regulated after STAT5A knock-down.

Annexin A4 (ANXA4) is a protein involved in membrane trafficking, cell growth and apoptosis. Increase of expression observed upon uSTAT5A KD may be one of the reasons for the increase of SubG1 population of cells after uSTAT5A knock-down corresponding to an increasing number of early apoptotic cells.

Prolyl 4-Hydroxylase Subunit Beta (P4HB) is a multifunctional protein that catalyzes the formation and rearrangement of disulfide bonds and acts as proteins chaperone in endoplasmic reticulum [203].

Two other interactors of uSTAT5A, for which gene expression levels were down-regulated after uSTAT5A knock-down are RPN1 and TBCB.

Ribophorin I (RPN1) is a protein associated with the proteasome and coordinates processing factors mediating degradation of poly-ubiquitinated substrates [204], [205].

Tubulin Folding Cofactor B (TBCB) mediates proper tubulin folding [206],[207] as well as dissociation [208].

Analogical analysis was performed for uSTAT5B (Figure 76). In this case, a common list consists of 3 proteins which were identified as interacting partners of uSTAT5B and where gene expression was affected upon uSTAT5B knock-down.

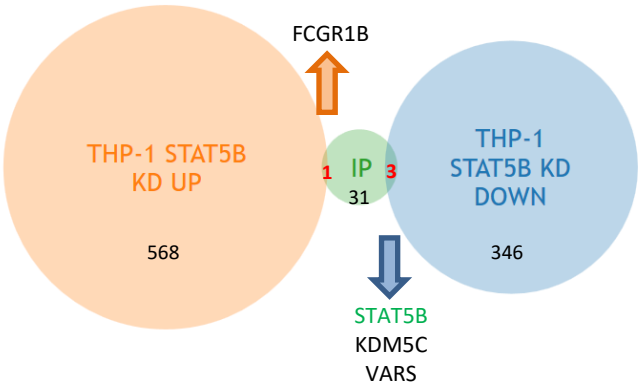

Figure 76. Comparison of gene expression data obtained upon STAT5B down-regulation (orange for up-regulated genes, blue for down-regulated genes) with the list of uSTAT5B interacting proteins (green).

One of them, FCGR1B interacts with uSTAT5B and expression of its coding gene is up-regulated upon uSTAT5B down-regulation.

Fc Gamma Receptor Ib (FCGR1B) encodes CD64, protein commonly expressed on monocytes and macrophages [209],[210]. The upregulation of expression is in line with the more differentiated phenotype of THP-1 cells upon uSTAT5B knock-down, but why CD64 interacts with STAT5B remains unclear.

Expression of two other genes encoding uSTAT5B interacting partner proteins was reduced after uSTAT5B knock-down: KDM5C and VARS. Interestingly, KDM5C was among the top uSTAT5B interacting partner proteins in both SKM-1 and THP-1 cell lines and its role in maintaining the epigenetic landscape of cells has already been described in the SILAC IP chapter of this thesis.

Valyl-TRNA Synthetase (VARS) is an enzyme that catalyzes amino-acetylation of tRNA with Valyl a pre-requisite to perform translation of proteins. The role of this enzyme in charging of tRNA with amino-acids makes it crucial for initiation of translation and elongation of peptides [211]

This cross-analysis of proteomics and genomics data is another confirmation of the novel roles of uSTAT5 proteins. Gene expression data show significant loss of enrichment for heterochromatin formation and regulation (GSEA) upon uSTAT5B knock-down. A possible mechanism of regulation could involve the interaction of uSTAT5B and KDM5C discovered by SILAC IP in three AML parental cell lines. Upon down-regulation of uSTAT5B expression of the gene encoding VARS is reduced. The mechanisms by which expression of VARS is regulated remains unknown, but as a protein it also interacts with uSTAT5A in AML cell lines, which indicates that both STAT5 proteins are novel players in the regulation of translation (process altered in GSEA, see RNA-seq. results section).

Comparison of gene expression data upon STAT5 down-regulation and recent CRISPR mediated screens for genes essential for AML maintenance

Recently, Wang and colleagues using genome-wide CRISPR-based screens, were able to generate a gene importance dataset across 13 human AML cell lines [172]. This study was already analyzed for STAT family members essential in AML cell lines in the previous chapters of the result section.

We took advantage of this study and compared the list of genes targeted by Wang et. al. with our lists

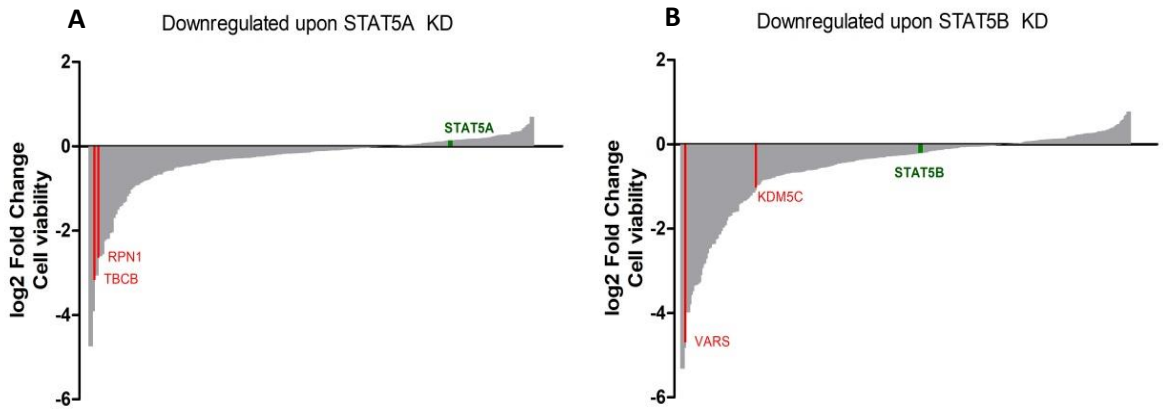

Figure 77. Waterfall plots illustrating genes essential for THP-1 AML cells. Genes down-regulated upon knock-down of uSTAT5A (**A**) or uSTAT5B (**B**) listed by their impact on THP-1 viability as assessed by CRISPR-mediated screen performed by Wang et. al.

of differentially expressed genes (adjusted p-value <0,05) after uSTAT5A or uSTAT5B knock-down.

Figure 77A shows waterfall-plots for the results after uSTAT5A down-regulation. Of 242 genes, that showed a decrease in gene expression, 234 were targeted in the Wang study. Interestingly, uSTAT5A targeting in THP-1 cells showed only minor effects on viability in this cell line. On the other hand, for many of the genes, for which we observed down-regulation after uSTAT5A knock-down, the log2 fold change was negative, which indicates the expression of this genes is required for THP-1 cells survival. Among genes with the highest negative fold change are TBCB and RPN1, also discovered as new interacting partners of uSTAT5A and that are also down-regulated upon uSTAT5A knock-down.

Panel B of Figure 77 shows analogical data for genes that were down-regulated upon uSTAT5B knock-down. Of 346 genes that showed a decrease in gene expression, 329 were targeted in Wang study. Here, according to Wang et al. targeting of uSTAT5B impacts on survival of THP-1 cells in a negative manner. Interestingly, among genes with strong influence on cells survival is VARS, a novel uSTAT5B protein interacting partner. Worth mentioning is also KDM5C, another protein in the uSTAT5B interactome, comprising a strong negative impact on proliferation. Generally, genes down-regulated together with uSTAT5B have stronger impact on survival of THP-1 AML parental cell line compared to genes affected by uSTAT5A knock-down.

Epigenetic modifiers affected by uSTAT5B knock-down

uSTAT5B down-regulation was strongly associate with a significant loss of a heterochromatin maintenance gene signature (as shown with GSEA). In line with this, analysis of genes regulated upon uSTAT5B knock-down revealed many key epigenetic regulators. Among them, we observed genes encoding stabilizers of heterochromatin (CBX5), histone marks writers (EZH2) as well as erasers (KDM5B and C), all these changes promoted the formation of euchromatin regions. To explore if these observations are specific to THP-1 cells or are more global, we took advantage of TCGA data sets of AML patients [37] to analyze correlations between mRNA expression of STAT5B and CBX5, KDM5B, KDM5C and EZH2. In addition, the patient samples were divided into subgroups based on their *FLT3* mutation status: *FLT3*^{WT}, *FLT3*^{ITD} and *FLT3*^{TKD}.

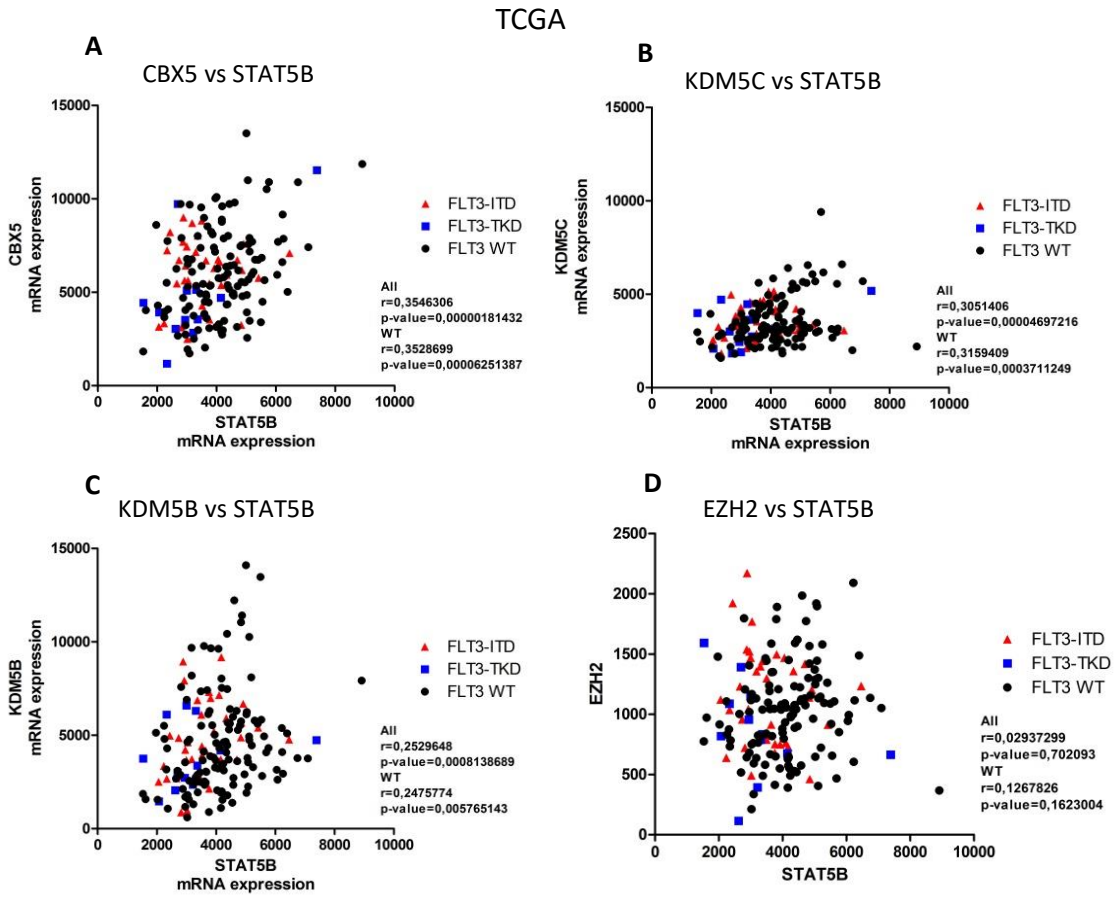

Figure 78. Correlations between STAT5B mRNA expression and selected epigenetic modifiers in TCGA patient's database. Patients were grouped according to FLT3 mutation status to *FLT3*^{WT} (black dots), *FLT3*^{ITD} (red triangles), and *FLT3*^{TKD} (blue squares). Expression of STAT5B mRNA was plotted against the expression of CBX5 (**A**), KDM5C (**B**), KDM5B (**C**), and EZH2 (**D**). r- pearson correlations for subtypes of samples.

Correlations between STAT5B mRNA expression and different epigenetic modifiers is shown in Figure 78. The significant and positive pearson correlation was achieved for comparisons of STAT5B and CBX5, STAT5B and KDM5B, STAT5B and KDM5C mRNA levels but was not significant for EZH2. Interestingly, slightly higher correlation between STAT5B and KDM5C mRNA expression was observed in FLT3^{WT} patients (uSTAT5) compared to all samples and compared to FLT3^{MUT} patients (pSTAT5, pearson correlation 0,29, not shown in the graph).

With KDM5C and CBX5 emerging as uSTAT5B targets and/or interacting partners involved in maintenance of epigenetic landscape, we decided to compare their mRNA expression levels in cells at different stages of normal myeloid differentiation and in AML blasts taking advantage of the Bloodspot database combining micro-array data from both healthy individuals and AML patients (bloodspot.eu [212].

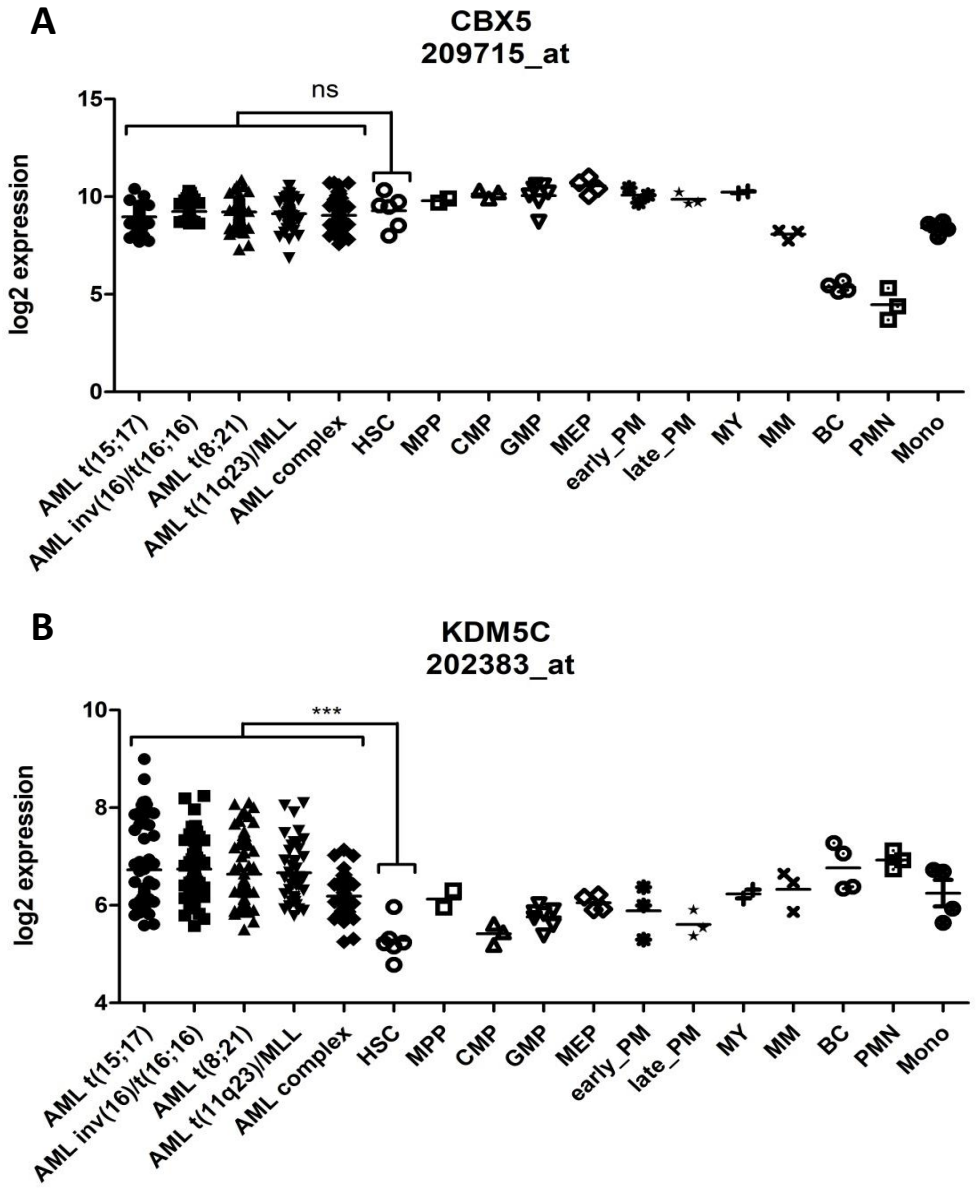

Figure 79. Expression levels of CBX5 (**A**) and KDM5C (**B**) in different subtypes of AML compared to healthy cells of the blood system. HSC – Hematopoietic Stem Cell, MPP – Multipotential progenitor, CMP – common myeloid progenitor, GMP- granulocyte/monocyte progenitor, MEP – Megakaryocyte/Erythroid Progenitor, PM- Promyelocyte, MY-Myelocyte, MM-Metamyelocyte, BC-Band Cell, PMN- polymorphonuclear cells, Mono- Monocytes.

As shown in the Figure 79A, levels of CBX5 expression do not differ between AML blast and healthy HSCs derived from patients. The expression levels remain stable in progenitor cells, but slight decrease in differentiated cells like monocytes and especially late cells of the myeloid lineage (MM, BC, PMN).

On the other hand, figure 79B presents expression levels of KDM5C and a stronger induction of its mRNA in various AML types compared to healthy HSCs. This would imply a possible option for therapeutic intervention with KDM5C inhibitors in AML cells, possibly without affecting healthy HSC cells, which express lower levels of the enzyme. In case of healthy hematopoietic cells, KDM5C expression is increasing with a more differentiated phenotype of hematopoietic cells.

Discussion

Expression of STAT5, phosphorylation status and role in AML models

The relevance of STAT5 signaling has been demonstrated in many types of human cancer ([110],[111], [112]). Specifically, hematological malignancies rely on STAT5 promoted proliferation and self-renewal activity [68],[121],[124]. In AML, upstream FLT3-ITD mutations cause constitutive phosphorylation of STAT5 proteins. Interestingly, this mutation is present in approximately 25% of AML patients, indicating relevance of phosphorylated STAT5 in AML. Within this project we investigated the role of uSTAT5 in $FLT3^{WT}$ AML and whether its expression is required for maintenance of AML cells. We also explored the function of two almost identical STAT5 members, STAT5A and STAT5B.

To analyze the level of phosphorylation and expression of STAT5A and STAT5B in AML models, we initially analyzed AML patient samples. As expected, we could demonstrate phosphorylation of STAT5 at Tyrosine residue 694/699 in all FLT3-ITD mutated patient samples and total levels of STAT5A and B were high. Comparing this group to $FLT3^{WT}$ samples we did not observe any decrease in total STAT5B protein expression and only a minor reduction in STAT5A expression in some samples. Most importantly, the $FLT3^{WT}$ group did not show any obvious phosphorylation of STAT5 proteins as assessed by Western-blotting.

To explore, whether this can also be observed in AML cell line models, we investigated 2 cell lines with $FLT3^{WT}$- expression – THP-1 and SKM-1 - and compared these cells with two cell lines harboring a FLT3-ITD mutation – MV4-11 and MOLM-14. Also, in this case we could not detect any phosphorylation of STAT5 in $FLT3^{WT}$ cell lines, whereas expression levels STAT5A and STAT5B were almost identical in both groups (slightly weaker expression of STAT5A in FLT3-ITD background).

We further observed that transcriptional levels of STAT5A and STAT5B in the same cell lines were higher in cells with uSTAT5 as compared to FLT3-ITD cells. Analyzing gene expression data derived from a TCGA collection of AML patient samples, STAT5B mRNA expression was significantly higher in $FLT3^{WT}$ patients compared to FLT3 mutated samples, which usually express pSTAT5.

To verify whether STAT5A and STAT5B in THP-1 and SKM-1 cells are indeed un-phosphorylated, we performed pull-down experiments for STAT5A and STAT5B and investigated the presence of tyrosine phosphorylation. As a positive control we pre-treated the same cell lines with GM-CSF to induce phosphorylation of STAT5 in this cell lines. Even after enriching STAT5A or STAT5B proteins by pull-downs, there was no trace of pSTAT5 signal, which could be strongly induced upon treatment of cells with GM-CSF. Additionally, treatment with GM-CSF resulted in stronger phosphorylation of STAT5B as compared to STAT5A.

Using two $FLT3^{WT}$ cell lines THP-1 and SKM-1 as a model, we performed analysis of STAT5A and STAT5B subcellular localization with help of confocal microscopy. In a control state uSTAT5A protein was found in both cytoplasmic and nuclear compartments with comparable signal intensities. Interestingly, for both cell lines uSTAT5B was more localized in the nucleus compared to uSTAT5A. The same experiment was performed in parallel with cells pre-treated with GM-CSF. This treatment resulted in a strong shift of STAT5A and the remaining STAT5B into the nuclear compartment.

These findings demonstrate high expression levels of uSTAT5A and uSTAT5B in AML. While most studies focus on models where constitutively active STAT5 promotes leukemogenesis, we can show that uSTAT5 is also highly expressed. Protein expression of STAT5A is higher in FLT3-ITD models where it was reported to be constitutively activated and induce expression of target genes in a transcription factor like manner, in FLT3-WT cells lower levels of STAT5A were observed, where it has no major function reported so far. Contrary, STAT5B protein and mRNA levels are comparable in FLT3-WT and FLT3-ITD cell lines indicating a possible role of STAT5B in both models. On top of that, our experiments provide proof that both uSTAT5A and uSTAT5B are localized both in cytoplasm and the nucleus of AML cells. In a previous report the presence of uSTAT in the nucleus has been shown and was thought to act as a part of a steady-state regulatory system, that can propagate signal and reach its target genes in a faster manner upon stimuli [104]. In this case, the levels of STAT5A and STAT5B should be similar, and localization of both proteins should remain stable. It has also been shown that in FLT3-ITD models pSTAT5A is more crucial for leukemic cells than pSTAT5B [95], which could suggest stronger accumulation of uSTAT5A in the nucleus ready to respond to a stimulus. In fact, we observe the opposite which lead to a hypothesis that uSTAT5 proteins may have additional functions than a steady-state signal transducer. They could be a part of a novel, not described up to date non-canonical pathway.

To validate this hypothesis, we decided to evaluate the role of uSTAT5A and uSTAT5B in AML by performing the knockdown experiments in $FLT3^{WT}$ and FLT3-ITD cells. Short-hairpin RNA sequences were cloned into plasmid, expression was regulated by doxycycline induction. The constructs were transduced into pSTAT5 cell lines (harboring FLT3-ITD mutation) or uSTAT5 cells (wild type FLT3 cells). As, expected down-regulation of pSTAT5 in MV4-11 and MOLM-14 FLT3-ITD cell lines, which rely on STAT5 signaling, lead to significantly slower proliferation and decreased metabolic activity as assessed by MTT. It has been demonstrated that pSTAT5 induces proliferation in FLT3-ITD cells [124], but the effects upon down-regulation were minor. Interestingly, down-regulation of uSTAT5A and especially uSTAT5B in THP-1 and SKM-1 cells resulted in much stronger inhibition of proliferation compared to FLT3-ITD cells.

Analysis of the cell cycle profile after STAT5A and STAT5B knockdown showed de-regulated cell cycle progression in all investigated cell lines. Modest effects were observed in MOLM-14 cells where knock-down of pSTAT5 resulted in a minor arrest in G1 phase of the cell cycle. In MV4-11 cells down-regulation of STAT5B induced apoptotic cell death whereas down-regulation of STAT5A resulted in a G1 arrest. Interestingly, down-regulating of either uSTAT5A or uSTAT5B in $FLT3^{WT}$ cells caused an increase of the subG1 population. Interestingly the phenotype we observe after down-regulation of STAT5 and especially STAT5B in AML cell lines closely resembled the effects of terminal differentiation caused by ATRA treatment in myeloid leukemia cell lines (Dimberg A, Blood 2002; Altucci L, Nat Medicine 2001).

To verify whether stalled cell cycle progression is linked to differentiation, flow cytometry experiments were performed to follow-up markers present on mature myeloid cells – CD11b and markers normally found on the un-differentiated progenitor cells or leukemic cells like cKIT. Interestingly down-regulation of STAT5B resulted in strong induction of CD11b expression in all cell lines with a strongest increase observed in uSTAT5 cells. Expression of cKIT was down-regulated upon STAT5B knock-down

only in THP-1 and MV4-11 cells. Increase of CD11b expression was also observed in THP-1 and SKM-1 upon STAT5A knock-down, but not as prominent as observed upon STAT5B knockdown cells.

To verify whether these changes lead to definite differentiation of the cells, morphology of control cell lines and STAT5A or STAT5B knock-down cells were compared by performing May-Grunwald-Giemsa staining. Both uSTAT5 cell lines THP-1 and SKM-1 showed a strong change in phenotype towards more mature hematopoietic cells upon uSTAT5B knock-down, whereas no significant changes were visible in MV4-11.

To confirm that the observed impact of STAT5 expression on AML cells survival, proliferation and maintenance of the differentiation block is not just an effect limited to in vitro culture of cells, we decided to validate our observations in vivo. Induction of Stat5 excision in mice was performed during the secondary transplantation. Confusingly, mice of the $Stat5^{fl/fl}$_Mx1Cre cohort died rapidly after induction of Stat5 knock-down in secondary recipients, and much earlier than the control group. It was accompanied by a very high WBC counts in blood, higher than in the control group at the time of cull. Flow cytometry analysis of bone marrow cells indicated similar levels of leukemic cells (GFP positive) in the BM of both cohorts, but at the same time the phenotype of BM cells collected from both groups was different. Leukemic cells from $Stat5^{fl/fl}$_Mx1Cre mice showed a more mature, differentiated phenotype as assessed by higher expression of CD11b and Gr-1 compared to the control group. The possible explanation of this observation could be a differentiation syndrome, also known as ATRA-syndrome observed in acute promyelocytic leukemia (APL) patients [213]. According to this report, 26% of APL patients treated with ATRA showed symptoms of this syndrome, namely fever and respiratory distress already after 2 days of treatment. Three deaths per nine patients with ATRA syndrome occurred and in six out of nine patients' clinicians observed WBC rising to a level of at least 20×10^9 cells/L. Another group suggested that the strong expansion of WBCs could be in part explained by secretion of specific hematopoietic growth factors (IL-1 beta, IL-8 and G-CSF) by the APL cells in response to ATRA [214]. Treatment of ATRA has been reported to cause a prompt differentiation of leukemic blasts. Similarity of the symptoms between our in vivo Stat5 depletion experiments and the ATRA-syndrome is striking. We believe that depletion of Stat5 in mice could have very similar outcome as to ATRA treatment in some patients. Indeed, gene expression data obtained from THP-1 cells show that STAT5 knock-down, and especially STAT5B knockdown, leads to a strong shift towards a mature, differentiated phenotype. Additionally, increased expression of various cytokines and receptors present on mature hematopoietic cells has been observed, which is likely to be missed in vitro, but may lead to an out-burst of differentiated cells in-vivo.

In fact, analysis of gene expression data upon uSTAT5B knock-down indicated that similar changes could be caused by ATRA treatment (tretinoin), as revealed by IPA (Supplementary Figure S12). Severe ATRA-syndromes can be controlled today by adding chemotherapy to ATRA treatment or the administration of corticosteroids upon increase of WBC count [215]. It would be interesting to check whether this also extends the survival in $Stat5^{fl/fl}$_MX1Cre cohort in secondary recipients upon Stat5 excision.

Identification of uSTAT5-regulated gene-expression profiles and novel interacting partners

Our results suggest an emerging role of uSTAT5 in the maintenance of a differentiation block in AML models. To confirm this hypothesis and obtain insights into the mechanism that regulates this process we performed RNA-seq of THP-1 cells after uSTAT5 KD. In addition, we analyzed the interactome of uSTAT5A/B and pSTAT5A/B in THP-1, SKM-1, and MV4-11 cells.

Conditional knock-down of uSTAT5B in THP-1 cells resulted in stronger changes of gene expression compared to uSTAT5A KD. In fact, scrambled controls and uSTAT5A KD showed a similar gene expression program as concluded from PCA plots and unsupervised hierarchical clustering.

uSTAT5B knock-down showed 4-times more genes to be up-regulated compared to uSTAT5A (Volcano plots and Venn diagrams), but similar numbers of down-regulated genes. Interestingly, there was not a big overlap between genes up- or down-regulated by uSTAT5A and uSTAT5B pointing out rather different functions of these proteins than a functional redundancy. Otherwise, we could still observe several known pSTAT5 target genes to be down-regulated in both conditions (OSM, GP9, BCL11A).

GSEA performed on gene-expression profiles obtained after STAT5A knock-down demonstrated reduced activity of translation and peptide elongation processes. Specific analysis of individual genes, after STAT5A knockdown identified Ribophorin 1 (RPN1), Eukaryotic translation initiation factor 3 (EiF3) and Eukaryotic translation elongation factor 2 (EEF2) together with the family of ribosomal protein coding genes to be suppressed.

EIF3 is a translation initiating factor, which also exhibits regulatory functions during protein chain elongation [216]. EIF3 protein subunit levels were found to be elevated in different types of cancer e.g. lung [217], breast [218], or cervical cancer [219]. In addition, overexpression of these subunits in NIH3T3 cells leads to the development of a malignant phenotype, specifically increased proliferation, viability and resistance to apoptosis [220]. Very recently, another group indicated that down-regulation of one of the subunits of EIF3 resulted in an inhibition of proliferation in an AML model. Furthermore, U937 cells deprived of EIF3 showed a cell cycle arrest at S/G2 and increased apoptosis [221].

Interestingly, IPA analysis of proteins detected as uSTAT5A interactors showed strong enrichment for pathways related to translation initiation (EIF2 signaling and regulation of eIF4 and p70S6K signaling, tRNA charging). In addition, RPN1 has been shown to exclusively interact with pSTAT5A whereas RPL and RPS, both are involved in the formation of ribosomal subunits, have been pulled down only with uSTAT5A. These findings support our data obtained in gene expression studies and indicate an important role of STAT5A in the regulation of translation as a novel function.

Another novel putative interactor of STAT5A is DBC1. This interaction was further confirmed by Co-IP experiments showing equal binding independent of the STAT5A phosphorylation status. We had recently investigated the role of SIRT1 in AML models [222]. We were able to show that targeting of FLT3 in AML cell lines leads to phosphorylation of DBC1, enhanced binding of DBC1 to SIRT1 followed by an increase of p53 acetylation. The DBC1-mediated inhibition of the enzymatic activity of SIRT1 results in reactivation of the p53 pathway and can help to eradicate leukemia propagating cells. It would be interesting to explore the role of the direct interaction between STAT5A and DBC1, which

here was observed in a $FLT3^{WT}$ background, and whether this interaction affects the DBC1-SIRT1-p53 axis.

IPA analysis of uSTAT5A interacting partners revealed proteins enriched in cell cycle control containing all members of MCM family. Transcriptional levels of MCM family members remained stable upon STAT5A down-regulation, but moderate reduction of mRNA expression of MCM5 and 7 was observed after down-regulation of STAT5B.

Members of the MCM family have also been linked to regulation of transcription. For example, upon IFN-gamma-mediated activation, STAT1 interacts with the MCM5/3 complex and regulates the expression of IFN-gamma response genes [223]. Several members of the MCM family were co-immunoprecipitated with inactive, uSTAT5A or STAT5B in THP-1 and SKM-1 cells. Whether this interaction is further enforced upon activation of STAT5 signaling needs to be investigated. Result in MV4-11 cells showed that MCM7 interacts with both, uSTAT5A and pSTAT5A, but stronger interaction is observed with phosphorylated STAT5A.

Down-regulation of uSTAT5B was accompanied by strong phenotypic changes of AML cells indicating differentiation of the cells. Indeed, analysis of the gene expression data using GSEA revealed upregulation of gene sets highly expressed in hematopoietic lineage committed cells, as well as adhesion molecules present on the surface of differentiated cells of the myeloid lineage [224].

On the other hand, many pathways active in control THP-1 cells were dysregulated upon STAT5B knock-down. Among enriched gene-sets we identified differential regulation of DNA replication, but also cell cycle related processes like progression from G1-S phase.

Analysis of genes dysregulated in the mentioned gene-sets identified several members of the replication initiation complex to be differentially expressed upon STAT5B down-regulation, e.g. Chromatin Licensing and DNA Replication Factor 1 (CDT1), replication factor 1 (RFC1), MCM5 and MCM7 as down-regulated genes. Several reports have shown that formation of the replication initiation complex is mediated by Cdc6 and Cdt1 which interact with the MCM complex and load it on DNA [225],[226].

Furthermore, MCM family members, essential elements of the replication initiation complex, were shown to interact with both STAT5A and STAT5B in SILAC IP experiment. Among STAT5B MCM-interacting proteins, we did not observe an overlap in THP1 and SKM-1 cells. Interestingly, the uSTAT5B interactor list in THP-1 contained MCM5, MCM6, and MCM7 whereas in SKM-1 we could detect MCM3 and MCM4. It was proven that depletion or mutation of one of the complex members can influence proper function of the whole complex [227] and MCM4, 6, and 7 are linked to helicase activity of the complex and initiate DNA replication [228]. Additionally, SILAC IP experiments performed in MV4-11 cells revealed that MCM3 is exclusively interacting with uSTAT5B and not with pSTAT5B, indicating another novel, non-canonical role of uSTAT5B in the regulation of replication initiation.

In addition, STAT5B KD caused an increase in transcript levels of CDKN1B encoding p27, a cyclin-dependent kinase inhibitor controlling entry from G1 to S phase of the cell cycle. It has been shown to accumulate during oligodendrocyte differentiation and was associated with arrested cell division, however, overexpression of p27 alone was not enough to induce terminal differentiation [229]. Global depletion of p27 deletion in transgenic mice caused an increase in size by 1/3 compared to control

animals, and affected all organs [230]. It would be interesting to verify whether the observed modest up-regulation of p27 mRNA levels is followed by a strong increase in p27 protein levels, which has been observed in ATRA induced differentiation of acute myeloid cells [231].

In SILAC based STAT5 pulldown experiments followed by mass spectrometry we have identified KDM5C as a novel STAT5B interactor in all analyzed AML cell lines. Furthermore, induction of *STAT5B* down-regulation caused reduced expression levels of KDM5C transcripts (RNA-seq). KDM5C has been shown to alter the epigenetic landscape of cells and is an established epigenetic modifier (reviewed by [232]. While investigating X-linked mental retardation (XLMR) families, KDM5C was discovered to be mutated in approximately 3% of patients with missense mutations located in an evolutionary conserved amino acid region [193]. Further, investigations by Iwase et al. described KDM5C as a H3K4 trimethyl-histone demethylase, catalyzing demethylation of H3K4me3 to H3K4me1, but not influencing methylation of other lysine residues (H3K9, -27, -36). Mutations of KDM5C described in XLMR led to disturbed demethylase activity. The impact of KDM5C in XLMR was confirmed using an RNAi approach: down-regulation of KDM5C led to impaired neuronal development in zebrafish and mammals [192]. As a member of the histone de-methylase family, KDM5C can primarily remove methylation groups present on lysine 4 of histone 3 commonly located in promotor regions, thereby causing repression of gene expression. Interestingly, further studies performed by Jensen and colleagues revealed several genes to be up-regulated in XLMR patients harboring a KDM5C mutation compared to healthy individuals. Among up-regulated genes, SLAMF6 (important role in lymphocytic differentiation) and EMILIN2 (extracellular matrix component) have also elevated expression levels in our RNA-seq data upon STAT5B KD.

In a recent study in an ESC-model it was shown that lysine-specific demethylase 1 (LSD1 or KDM1A) plays a major role in differentiation by inactivating (histone de-methylation) enhancer regions, which are essential for the complete shutdown of the ESC gene expression program followed by induction of differentiation [233]. Interestingly, another study linked LSD1 to a STAT5-dependent transcriptional program for both canonical and non-canonical regulated genes [98]. Inhibition and down-regulation of LSD1 was also shown to cause differentiation of monocytic leukemic cells and suppress proliferation [234]. Inactivating mutations in KDM5C have been reported in renal carcinoma [235] resulting in de-repression of gene expression.

Rondinelli and colleagues discovered a novel role of KDM5C in restoring heterochromatin signatures on DNA after replication by interaction with the H3K9me3 writer SUV39H1, as well as with the heterochromatin stabilizing and maintaining protein HP1α [195]. Loss of KDM5C in a model of renal carcinoma led to genomic instability. These findings indicate a strong cross-talk between H3K4me3 and H3K9me3 histone marks and its regulation of gene expression. Further, direct interaction of PCNA and KDM5C seems to be a pre-requisite of KDM5C-chromatin binding [236]. Additionally, KDM5C was recently listed among novel proteins identified by means of mass spectrometry to be recruited to chromatin during DNA replication [237]. KDM5C is involved in early origin firing of replication and required for PCNA binding to chromatin [195]. Upon down-regulation of KDM5C cells cannot progress into S phase of the cell cycle. This could be another reason for the observed phenotype AML cells upon down-regulation of uSTAT5B. Interestingly, among proteins recruited to chromatin during DNA replication, Alabert and colleagues have identified STAT5, but without distinguishing between STAT5A and STAT5B.

The observation that KDM5C is involved in suppression of transcription by removing H3K4me3-marks at promotor regions has been confirmed by Outchkourov and colleagues. Additionally, by investigating genome-wide binding of KDM5C in mouse ESCs, they identified several KDM5C-bound enhancer elements, removing spurious H3K4me3/2 modifications, which could cause unwanted binding of transcription factor complexes in this area [197]. This way KDM5C was shown to promote enhancer function in ESC cells.

Potential consequences of its interaction with STAT5B could be investigated in ChIP-seq. experiments. For example, loss of KDM5C upon STAT5B knock-down could result in increased H3K4me3-marks at promoters of genes involved in differentiation resulting in up-regulation of gene-sets linked to mature hematopoietic cells as observed in our RNA-sequencing data.

Additional analysis of STAT5B and KDM5C binding across the genome could also be addressed in ChIP-seq experiments and could provide insight into following questions: i) Does STAT5B regulate the expression of KDM5C in AML; ii) Are there any common promoter regions in AML blasts bound by both STAT5B and KDM5C; and iii) Is KDM5C located at promoters of differentiation genes in AML blasts to repress their expression via removal of the H3K4me3 marks? If any of these assumptions is correct, we could confirm that down-regulation of STAT5B disrupts the STAT5B-KDM5C complex, resulting in decreased expression level of KDM5C and writing of H3K4me3 mark at the promotors of differentiation genes followed by differentiation of the cells. Whether this mechanism of epigenetic repression is true only for uSTAT5B or also pSTAT5B needs to be investigated.

In all AML cell lines investigated for novel interactors of STAT5B we discovered high enrichment for ETV6. Comparison of STAT5B interactors in MV4-11 cell line before and after treatment with PKC412 (analysis of pSTAT5 vs uSTAT5) revealed that ETV6 preferentially binds to uSTAT5B, which was confirmed via IP experiments in THP-1, SKM-1 and MV4-11 cell lines.

ETV6 has been described to play crucial roles in hematopoiesis and vascular development. It was described among other 3 genes (Gata2, Gfi1b, and cFos) necessary to mediate endothelial-to-hematopoietic transition in mice fibroblasts [238]. Depletion of *Etv6* in mice leads to embryonic lethality at day 10.5-11.5 due to defective yolk sac angiogenesis, but also in adults Etv6 is crucial for establishing hematopoiesis within the BM [198], [199]. Recent work in zebrafish also highlights the role of ETV6 in primitive hematopoiesis as a major regulator of hematopoietic progenitors[239]. The role of *Etv6* in definitive hematopoiesis has also been described and conditional depletion of *Etv6* led to the loss of BM HSCs [240]. Overexpression of Etv6 in cell lines and mouse models resulted in stronger differentiation into the erythroid lineage [241], [242] and vice versa suppression of ETV6 expression in zebrafish embryos caused impaired erythroid differentiation and anemia [239]. Similarly, reduction of *Etv6* levels in mice and zebrafish affected the pool of neutrophils indicating a role of *Etv6* in the myeloid lineage [239], [240].

The *ETV6* gene is known for its involvement in chromosomal translocations linked to hematological malignancies. It has been reported to participate in over 50 translocations with 30 different partner genes including tyrosine kinases (leading to constitutive activation), transcription factors (switch from transcriptional activator to a repressor and vice versa) and others [200].

ETV6 has been shown to directly interact with proteins that recruit histone deacetylases (HDAC) and mediate transcriptional repression [243]. Another way to promote transcriptional repression has been

described through a HDAC-independent mechanism via direct interaction with L3MBTL1, a member of Polycomb group of chromatin-associated proteins [244], or its co-repressor histone acetyltransferase TIP60 via direct protein-protein interaction [245].

ETV6 is known to regulate expression of genes via the ETS-motif within promoter regions, but surprisingly only a small number of genes have been identified as ETV6 targets. Among validated targets are the megakaryocyte-specific GPIIb and GPIbα genes, which are repressed by ETV6 in K562 cell line [246]. Another report showed that in Ras-transformed NIH3T3 cells ETV6 repressed the expression of endogenous matrix metalloproteinase stromelysin-1 and induced cellular growth inhibition [247]. In the same cellular model, ETV6 has been shown to repress expression of BCL-Xl affecting cell survival through regulation of apoptotic pathways [248]. In an overexpression model in 32D mouse myeloid cells, ETV6 was also reported to act as a tumor suppressor through augmenting the p53 pathway and authors observed a G1 arrest of the cell cycle [249]. Further efforts to establish a list of genes affected by ETV6 were made using an ETV6 overexpression model in HeLa cells. Microarray based experiments identified 87 genes, including 62 downregulated and 25 upregulated upon ETV6 overexpression [250]. In line with previous reports on ETV6 function, the identified repressed genes were members of pathways related to adhesion, cell proliferation, apoptosis and angiogenesis supporting the role of ETV6 as a tumor suppressor. Furthermore, overexpression of ETV6 caused a G1 arrest followed by reduced cell growth, blocked Ras-mediated cell growth in soft-agar assays, and reduced tumor formation in nude mice [251].

In a recent paper, ETV6 has been described as a novel regulator of ERG expression in AML, T-ALL cells as well as in normal HSPCs. Unnikrishnan and colleagues, applying reverseChIP followed by mass spectrometry analysis, identified proteins bound to the enhancer of *ERG* and identified ETV6 among other known regulators of ERG expression, which was described as 'transcription factor heptad' [252]. Moreover, in HSPCs binding of ETV6 was also found in other enhancer regions within the transcription factor heptad and down-regulation of ETV6 led to decreased expression of GATA2 and TAL1. In addition, prolonged down-regulation of ETV6 resulted in decreased expression of almost all TF heptad member (ERG, (FLI1, GATA2, TAL1, LYL1 and LMO2). As a next step, using AML patient gene expression data, the authors showed a correlation of expression of ETV6 and the majority of heptad TF. Further analysis of this dataset showed that high expression of ETV6 and TF heptad members significantly correlates with a poor prognosis. These data indicate, that ETV6 is part of a master complex and likely involved in the transcriptional regulation of processes such as differentiation and self-renewal.

No significant changes in ETV6 transcript expression were observed upon STAT5 down-regulation. ChIP-seq analyses of STAT5B and ETV6 binding genome-wide could shed light on the repressive role as a complex and possible re-distribution of ETV6 after STAT5 depletion. It is possible that ETV6 alone can induce repressive functions, while ETV6-STAT5B interaction promotes a transcriptional program supporting leukemic blast survival. This functional switch of ETV6 would be supported by increased expression of defined genes known to be targets of ETV6-mediated repression after STAT5B knock-down (eg. BCL-XL). On the other hand, degradation of ETV6 at protein levels has been observed in THP-1 and SKM-1 cell lines after STAT5B depletion. Additionally, down-regulation of ETV6 levels in THP-1 cells led to a minor, but significant induction of CD11b expression, which would suggest that both ETV6 and STAT5B are necessary to maintain the block in differentiation of leukemic blasts. However, the down-regulation of ETV6 did not influence proliferation of THP-1 cells. As a next step, it would be interesting to evaluate consequences of a double KD of ETV6 and STAT5B on leukemic cells.

The finding that STAT5B interacts with ETV6 and KDM5C indicates a novel mechanism involved in the regulation of transcriptional programs in AML blasts. Additionally, our data demonstrate that the ETV6-STAT5B interaction is stronger for unphosphorylated STAT5B. These results suggest different STAT5B and STAT5A gene targets in AML cell lines, which is further complicated by the status of STAT5 phosphorylation. Recently, Park and colleagues presented a study shedding light on the repressive role of uStat5a in the maintenance of a progenitor state of a Hpc7 mouse HSPCs cell model. Upon TPO induction and phosphorylation of Stat5, previously uStat5 was re-distributed to completely different loci in the genome. In this work the authors do not distinguish between Stat5a and Stat5b, which would be extremely interesting considering our findings. There is a high interest in establishing the binding profiles of both STAT5A and STAT5B in human models as they could play redundant roles and potentially influence the aggressive phenotype of different malignancies (AML, prostate cancer). Additionally, our drug treatment data suggest an additive effect in drugging AML cell lines with ATRA or AraC along with STAT5 KD. Treatment with DHE, presented here for the first time in AML cells, showed potential benefit of a drug so far only used to treat migraine to slow down proliferation and increase expression of cell line specific cluster of differentiation family members in THP-1, SKM-1 and MV4-11 cell lines. Summary of uSTAT5 functions discovered or pSTAT5 functions re-confirmed in this study is presented in table 13.

Function	uSTAT5A	uSTAT5B	pSTAT5A	pSTAT5B
Proliferation benefit	+	+	+	+
Block of Differentiation	-	Gene expression of mature myeloid cells markers overexpressed upon uSTAT5B KD (e.g. ↑ *ITGAM, CD4, IL21R, HLA-DRB1*)	-	-
Translation	↓*RPN1, EIF3* and *EEF2* upon uSTAT5A KD - Protein interacting partners (RPN1, EIF3, RPL, RPS proteins) also essential for translation	-	RPN1 protein interaction	-
Replication and Cell Cycle progression	Interacts with MCM2-7 proteins	- Interacts with MCM5-7 proteins - Replication and CC progression blocked upon uSTAT5B KD, ↓*CDT1, RFC1.*	Interacts with MCM7 protein	-
Epigenetic modifiers	↓*SIRT6* ↑*TET2, JARID2*	↓*CBX5-6, KDM5B-C, EZH2*	-	-
Regulation of transcription program	-	- Interaction with ETV6 and KDM5C proteins - repressing expression of differentiation genes by the complex?	-	-

Table 13. Summary of findings on uSTAT5A/B and pSTAT5A/B in leukemic cell lines.

Investigation of the role of uSTAT5 in AML cells led to the discovery of distinct functions of uSTAT5A and uSTAT5B. Firstly, gene expression profiles upon knock-down of uSTAT5A or uSTAT5B showed minor overlap of regulated genes. Secondly, interacting protein partners of uSTAT5A and uSTAT5B were also different and we could demonstrate differences between pSTAT5 and uSTAT5 by adding data from MV4-11 cells. In addition, novel protein interactions supported changes in gene expression and a unique role of uSTAT5A in regulation of translation and involvement of uSTAT5A/B in replication and cell cycle progression. Finally, based on our results uSTAT5B emerges as a regulator of differentiation arrest in AML cells and preliminary results suggest involvement of ETV6 and KDM5C, two novel uSTAT5B interacting proteins in this process.

A complete understanding of the uSTAT5/pSTAT5-mediated regulatory programs and comprehensive characterization of its underlying mechanisms, could help to discover more precise targets for future drug interventions in AML and other malignancies.

Supplementary figures

Supplementary Figure 1. Authentication of the AML parental cell lines

DNA extracted from AML cell lines was send for validation to Multiplexion (Ludwigshafen). The identity of each cell line was confirmed with the database standards. Results are presented below:

Information from Customer				Results			Summary			
Sample ID	Sample Name	Cell line name	If other: exact name	DNA quality	Best Hit with DataBase	Identity (%)	Present in Database?	Cross-Contamination?	Identity confirmed?	Genotype Code
3213	#1-THP1	THP-1		ok	THP-1	100	yes	no	confirmed	ATATTTTTTTATAAWTAAAAAAATTTAA ATAAAAAAAAAATTAAAAAT
3214	#2-NB4	NB-4		ok	NB-4	100	yes	no	confirmed	TTTTATAAATAATTAATTAAAATTTTATA TAATTAAAATTAATTTTTT
3215	#3-U937	U-937		ok	U-937	100	yes	no	confirmed	TTTTATAAAAAAAAAAAATTATATATAA ATWTTTATATTTAATTAAAA
3216	#4-MOLM14	MOLM-14		ok	MOLM-14	100	yes	no	confirmed	ATTTATATTTTTATWTATATAAATTTAA WTAAATAAAAAATTAWATTT
3217	#5-HL60	HL-60		ok	HL-60	100	yes	no	confirmed	ATATAAAAATAANNATATTTAATTTTATA TAAATWTTTTTAAATATAT
3218	#6-SKM1	SKM-1		ok	SKM-1	100	yes	no	confirmed	ATTTATATTTATTTTTAAATAATTTTATAA AAAWAAAAAATTATAAAA
3219	#7-OCIAML3	OCI-AML3		ok	OCI-AML3	100	yes	no	confirmed	ATTTAAAAATTTAAAAATTTAAATTTAAA TAAATATATAATTTTATAA
3220	#8-NOMO1	NOMO-1		ok	NOMO-1	100	yes	no	confirmed	WTATTTTTTTAATTAAATATAATTTTAAA AAAAWAAAWAATTTTATAA

Supplementary Figure 2. Sequences of oligonucleotide primers for RT-qPCR and PCR.

RT-qPCR

Target gene	Forward Primer	Reverse primer
STAT5A	CAGTGGTTTGACGGGGTGAT	GTCGTGGGCCTGTTGCTTAT
STAT5B	CAGAACACGTATGACCGCTG	CTGGAGAGCTACCATTGTTGG
GAPDH	GCTCTCTGCTCCTCCTGTTC	ACGACCAAATCCGTTGACTC

PCR

Target	Primer sequence
CS1276_Stat5_HH_1	GAA AGC ATG AAA GGG TTG GAG
CS1277_Stat5_HH_2	AGC AGC AAC CAG AGG ACT AC
CS1278_Stat5_HH_3	CCC ATT ATC ACC TTC TTT ACA G
CS1308_Stat5_HH_4	TAC CCG CTT CCA TTG CTC AG
Mx1_Cre#1_S	ACGACCGGCAAACGGACAGAAGCA
Mx1_Cre#1_AS	TCCCAACCTCAGTACCAAGCCAAG

Supplementary table S1. List of antibodies used in the project

Target	producer	Catalogue number	host organism	isotype	Experiment in thesis	Fluorophore/Tag	Additional info
ACTB	Sigma-Aldrich	A5441	Mouse	IgG1	WB	-	
CD11b	Biolegend	101212	Rat	IgG2b, κ	FACS	APC	anti mouse, human
CD11b	Biolegend	101208	Rat	IgG2b, κ	FACS	PE	
CD11b	eBioscience	13-0112	Rat	IgG2b, κ	in vivo (lineage depletion)	Biotin	anti-mouse
CD19	eBioscience	13-0193	Rat	IgG2a, κ	in vivo (lineage depletion)	Biotin	anti-mouse
CD45R/B220	eBioscience	13-0452	Rat	IgG2a, κ	in vivo (lineage depletion)	Biotin	anti-mouse
CD5	eBioscience	13-0051	Rat	IgG2a, κ	in vivo (lineage depletion)	Biotin	anti-mouse
cKIT	Biolegend	105824	Rat	IgG2b, κ	FACS	PerCP/Cy5.5	
DBC1	Bethyl	A300-432A	RAbbit	Polyclonal	WB	-	
ETV6	Santa Cruz	sc-166835	Mouse	IgG1	WB	-	
GAPDH	Cell Signaling	cs-2118	Rabbit	IgG1	WB	-	
GR-1	Biolegend	108408	Rat	IgG2b, κ	FACS	PE	anti-mouse
IgG	Biolegend	400114	Mouse	IgG1	FACS	PE	
IgG	Santa Cruz	sc-3877	Mouse	IgG1	SILAC-IP	-	
IgG	Merck	12-370	Rabbit	Polyclonal	IP	-	
Ly6G/C (GR-1)	eBioscience	13-5931	Rat	IgG2b, κ	in vivo (lineage depletion)	Biotin	anti-mouse
pSTAT5	Millipore	05-495	Mouse	IgG	WB	-	
STAT5A	Santa Cruz	sc-136081	Mouse	IgG1	SILAC-IP	-	
STAT5A	Santa Cruz	sc-1081	rabbit	Polyclonal	IF, IP, WB	-	
STAT5B	Santa Cruz	sc-1656	mouse	IgG1	IF, IP, WB, SILAC-IP	-	
TER119	eBioscience	13-5921	Rat	IgG2b, κ	in vivo (lineage depletion)	Biotin	anti mouse

Supplementary Figure 3. List of short-hairpin RNA used in the study including the target sequences and evaluation of possible off-target binding

1. TRCN…19304 described as shSTAT5A1

   Target sequence : GCTCTGAATTAGTCCTTGCTT

Show All entries | Show/hide columns (2 hidden) | Filter

Subject name	Gene hit	Subject start	Subject end	Subject ori	Genomic Location	Orientation	Query start	Query end	Length	Score
ENST00000588868.5	STAT5A	3028	3048	Forward	17:42311339-42311359 [Sequence]	Forward	1	21	21 [Sequence]	42.1
ENST00000345506.8	STAT5A	3697	3717	Forward	17:42311339-42311359 [Sequence]	Forward	1	21	21 [Sequence]	42.1
ENST00000621274.3	RAD17	2433	2446	Reverse	CHR_HSCHR5_2_CTG1_1:69414825-69414838 [Sequence]	Forward	4	17	14 [Sequence]	28.2

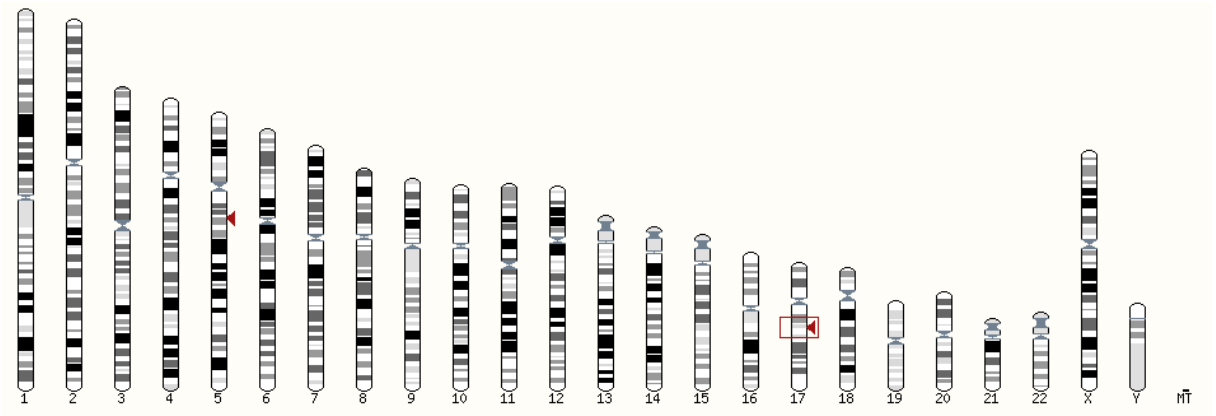

2. TRCN000019305 described as shSTAT5A2

   Target sequence : GCGCTTTAGTGACTCAGAAAT

Show All entries | Show/hide columns (2 hidden) | Filter

Subject name	Gene hit	Subject start	Subject end	Subject ori	Genomic Location	Orientation	Query start	Query end	Length	Score	E-val	%ID
ENST00000587646.1	STAT5A	449	469	Forward	17:42307668-42307688 [Sequence]	Forward	1	21	21 [Sequence]	42.1	4e-04	100.00 [Alignment]
ENST00000591556.1	STAT5A	503	523	Forward	17:42307668-42307688 [Sequence]	Forward	1	21	21 [Sequence]	42.1	4e-04	100.00 [Alignment]
ENST00000468096.5	STAT5A	505	525	Forward	17:42307668-42307688 [Sequence]	Forward	1	21	21 [Sequence]	42.1	4e-04	100.00 [Alignment]
ENST00000588868.5	STAT5A	1824	1844	Forward	17:42307668-42307688 [Sequence]	Forward	1	21	21 [Sequence]	42.1	4e-04	100.00 [Alignment]
ENST00000546010.6	STAT5A	2294	2314	Forward	17:42307668-42307688 [Sequence]	Forward	1	21	21 [Sequence]	42.1	4e-04	100.00 [Alignment]
ENST00000590949.5	STAT5A	2593	2613	Forward	17:42307668-42307688 [Sequence]	Forward	1	21	21 [Sequence]	42.1	4e-04	100.00 [Alignment]
ENST00000345506.8	STAT5A	2493	2513	Forward	17:42307668-42307688 [Sequence]	Forward	1	21	21 [Sequence]	42.1	4e-04	100.00 [Alignment]
ENST00000448238.2	NIPBL	2897	2911	Reverse	5:36985609-36985623 [Sequence]	Forward	6	20	15 [Sequence]	30.2	1.4	100.00 [Alignment]
ENST00000504430.5	NIPBL	2049	2063	Reverse	5:36985609-36985623 [Sequence]	Forward	6	20	15 [Sequence]	30.2	1.4	100.00 [Alignment]
ENST00000282516.12	NIPBL	2928	2942	Reverse	5:36985609-36985623 [Sequence]	Forward	6	20	15 [Sequence]	30.2	1.4	100.00 [Alignment]
ENST00000453658.6	TJP2	1355	1368	Forward	9:69226157-69226170 [Sequence]	Forward	8	21	14 [Sequence]	28.2	5.5	100.00 [Alignment]
ENST00000539225.2	TJP2	1285	1298	Forward	9:69226157-69226170 [Sequence]	Forward	8	21	14 [Sequence]	28.2	5.5	100.00 [Alignment]
ENST00000535702.6	TJP2	1568	1581	Forward	9:69226157-69226170 [Sequence]	Forward	8	21	14 [Sequence]	28.2	5.5	100.00 [Alignment]
ENST00000538247.1	TJP2	1271	1284	Forward	9:69226157-69226170 [Sequence]	Forward	8	21	14 [Sequence]	28.2	5.5	100.00 [Alignment]
ENST00000348208.8	TJP2	1288	1301	Forward	9:69226157-69226170 [Sequence]	Forward	8	21	14 [Sequence]	28.2	5.5	100.00 [Alignment]
ENST00000377245.8	TJP2	1400	1413	Forward	9:69226157-69226170 [Sequence]	Forward	8	21	14 [Sequence]	28.2	5.5	100.00 [Alignment]
ENST00000636438.1	TJP2	1483	1496	Forward	9:69226157-69226170 [Sequence]	Forward	8	21	14 [Sequence]	28.2	5.5	100.00 [Alignment]
ENST00000370994.8	SERBP1	5757	5770	Forward	1:67408716-67408729 [Sequence]	Reverse	5	18	14 [Sequence]	28.2	5.5	100.00 [Alignment]
ENST00000640250.1	FAS	456	469	Forward	10:89014399-89014412 [Sequence]	Forward	7	20	14 [Sequence]	28.2	5.5	100.00 [Alignment]
ENST00000640140.1	FAS	1129	1142	Forward	10:89014399-89014412 [Sequence]	Forward	7	20	14 [Sequence]	28.2	5.5	100.00 [Alignment]
ENST00000355279.2	FAS	932	945	Forward	10:89014399-89014412 [Sequence]	Forward	7	20	14 [Sequence]	28.2	5.5	100.00 [Alignment]
ENST00000492756.5	FAS	785	798	Forward	10:89014399-89014412 [Sequence]	Forward	7	20	14 [Sequence]	28.2	5.5	100.00 [Alignment]
ENST00000479522.5	FAS	672	685	Forward	10:89014399-89014412 [Sequence]	Forward	7	20	14 [Sequence]	28.2	5.5	100.00 [Alignment]
ENST00000488877.5	FAS	873	886	Forward	10:89014399-89014412 [Sequence]	Forward	7	20	14 [Sequence]	28.2	5.5	100.00 [Alignment]
ENST00000357339.6	FAS	993	1006	Forward	10:89014399-89014412 [Sequence]	Forward	7	20	14 [Sequence]	28.2	5.5	100.00 [Alignment]
ENST00000484444.5	FAS	856	869	Forward	10:89014399-89014412 [Sequence]	Forward	7	20	14 [Sequence]	28.2	5.5	100.00 [Alignment]
ENST00000355740.6	FAS	1177	1190	Forward	10:89014399-89014412 [Sequence]	Forward	7	20	14 [Sequence]	28.2	5.5	100.00 [Alignment]
ENST00000612663.5	FAS	1389	1402	Forward	10:89014399-89014412 [Sequence]	Forward	7	20	14 [Sequence]	28.2	5.5	100.00 [Alignment]
ENST00000290607.11	STARD9	6930	6943	Forward	15:42688451-42688464 [Sequence]	Forward	8	21	14 [Sequence]	28.2	5.5	100.00 [Alignment]
ENST00000468496.5	STAT5B	702	715	Forward	17:42210206-42210219 [Sequence]	Reverse	8	21	14 [Sequence]	28.2	5.5	100.00 [Alignment]
ENST00000481253.2	STAT5B	273	286	Forward	17:42210206-42210219 [Sequence]	Reverse	8	21	14 [Sequence]	28.2	5.5	100.00 [Alignment]
ENST00000293328.7	STAT5B	2027	2040	Forward	17:42210206-42210219 [Sequence]	Reverse	8	21	14 [Sequence]	28.2	5.5	100.00 [Alignment]
ENST00000463042.1	SDCCAG8	409	422	Reverse	1:243476147-243476160 [Sequence]	Forward	8	21	14 [Sequence]	28.2	5.5	100.00 [Alignment]
ENST00000336112.8	ASXL2	3096	3109	Forward	2:25743472-25743485 [Sequence]	Reverse	4	17	14 [Sequence]	28.2	5.5	100.00 [Alignment]
ENST00000532485.5	ACER3	7046	7059	Reverse	11:77026465-77026478 [Sequence]	Forward	8	21	14 [Sequence]	28.2	5.5	100.00 [Alignment]

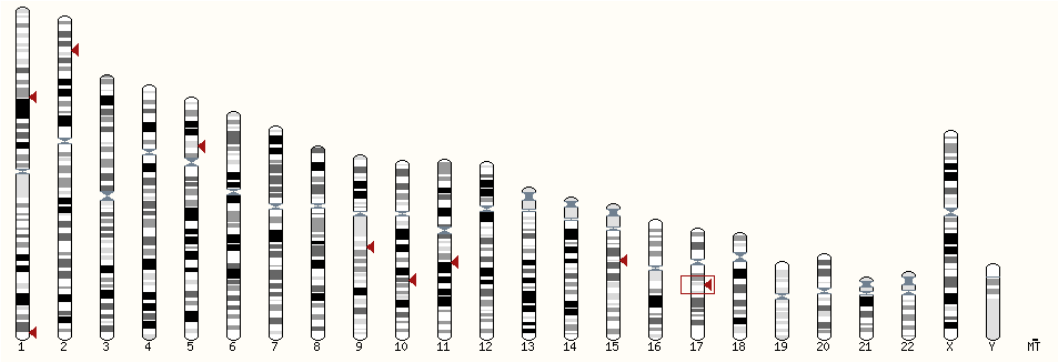

3. TRCN0000232135 described as shSTAT5A3
   Target sequence: ACCATTCACCACGCGGGATTT

Show All entries | Show/hide columns (2 hidden) | Filter

Subject name	Gene hit	Subject start	Subject end	Subject ori	Genomic Location	Orientation	Query start	Query end	Length	Score	E-val	%ID
ENST00000587646.1	STAT5A	530	550	Forward	17:42308203-42308223 [Sequence]	Forward	1	21	21 [Sequence]	42.1	4e-04	100.00 [Alignment]
ENST00000591556.1	STAT5A	584	604	Forward	17:42308203-42308223 [Sequence]	Forward	1	21	21 [Sequence]	42.1	4e-04	100.00 [Alignment]
ENST00000468096.5	STAT5A	586	606	Forward	17:42308203-42308223 [Sequence]	Forward	1	21	21 [Sequence]	42.1	4e-04	100.00 [Alignment]
ENST00000588868.5	STAT5A	1905	1925	Forward	17:42308203-42308223 [Sequence]	Forward	1	21	21 [Sequence]	42.1	4e-04	100.00 [Alignment]
ENST00000546010.6	STAT5A	2375	2395	Forward	17:42308203-42308223 [Sequence]	Forward	1	21	21 [Sequence]	42.1	4e-04	100.00 [Alignment]
ENST00000590949.5	STAT5A	2674	2694	Forward	17:42308203-42308223 [Sequence]	Forward	1	21	21 [Sequence]	42.1	4e-04	100.00 [Alignment]
ENST00000345506.8	STAT5A	2574	2594	Forward	17:42308203-42308223 [Sequence]	Forward	1	21	21 [Sequence]	42.1	4e-04	100.00 [Alignment]
ENST00000622511.1	MUC2	3007	3020	Forward	CHR_HSCHR11_3_CTG1:1097948-1097961 [Sequence]	Forward	5	18	14 [Sequence]	28.2	5.5	100.00 [Alignment]
ENST00000530335.1	ME3	328	341	Forward	11:86672278-86672291 [Sequence]	Reverse	7	20	14 [Sequence]	28.2	5.5	100.00 [Alignment]
ENST00000539359.1	BDKRB2	711	724	Reverse	14:96240718-96240731 [Sequence]	Forward	3	16	14 [Sequence]	28.2	5.5	100.00 [Alignment]
ENST00000542454.2	BDKRB2	3397	3410	Reverse	14:96240718-96240731 [Sequence]	Forward	3	16	14 [Sequence]	28.2	5.5	100.00 [Alignment]
ENST00000613079.4	ELFN2	1915	1928	Forward	22:37374393-37374406 [Sequence]	Reverse	5	18	14 [Sequence]	28.2	5.5	100.00 [Alignment]
ENST00000402918.6	ELFN2	1915	1928	Forward	22:37374393-37374406 [Sequence]	Reverse	5	18	14 [Sequence]	28.2	5.5	100.00 [Alignment]

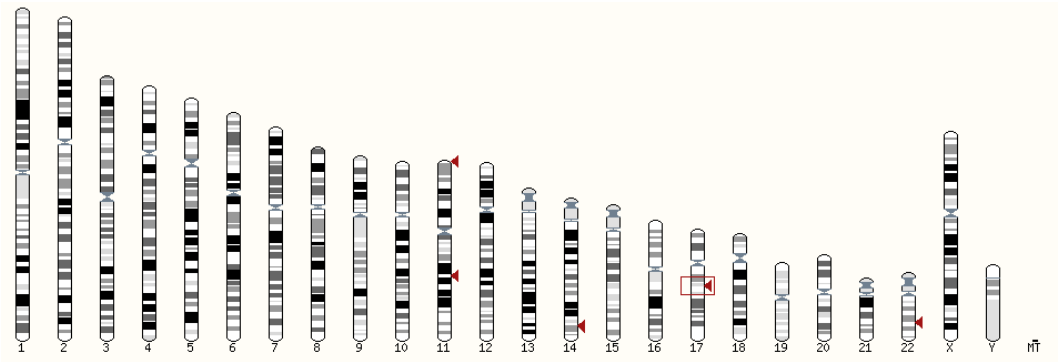

4. TRCN000019358 described as shSTAT5B1

   Target sequence : GCGCTTTAGTGACTCAGAAAT

Show All entries | Show/hide columns (2 hidden) | Filter

Subject name	Gene hit	Subject start	Subject end	Subject ori	Genomic Location	Orientation	Query start	Query end	Length	Score	E-val	%ID
ENST00000415845.1	STAT5B	132	152	Forward	17:42232066-42232086 [Sequence]	Reverse	1	21	21 [Sequence]	42.1	4e-04	100.00 [Alignment]
ENST00000468312.1	STAT5B	211	231	Forward	17:42232066-42232086 [Sequence]	Reverse	1	21	21 [Sequence]	42.1	4e-04	100.00 [Alignment]
ENST00000293328.7	STAT5B	211	231	Forward	17:42232066-42232086 [Sequence]	Reverse	1	21	21 [Sequence]	42.1	4e-04	100.00 [Alignment]
ENST00000444316.2	BANK1	71	85	Reverse	4:101813896-101813910 [Sequence]	Forward	4	18	15 [Sequence]	30.2	1.4	100.00 [Alignment]
ENST00000229708.3	ULBP1	2036	2050	Reverse	6:149972604-149972618 [Sequence]	Forward	1	15	15 [Sequence]	30.2	1.4	100.00 [Alignment]
ENST00000416893.2	ATG4AP1	205	218	Forward	X:82998903-82998916 [Sequence]	Forward	1	14	14 [Sequence]	28.2	5.5	100.00 [Alignment]
ENST00000394892.2	ATG4A	123	136	Forward	X:108131271-108131284 [Sequence]	Forward	1	14	14 [Sequence]	28.2	5.5	100.00 [Alignment]
ENST00000345734.7	ATG4A	364	377	Forward	X:108131271-108131284 [Sequence]	Forward	1	14	14 [Sequence]	28.2	5.5	100.00 [Alignment]
ENST00000372232.7	ATG4A	364	377	Forward	X:108131271-108131284 [Sequence]	Forward	1	14	14 [Sequence]	28.2	5.5	100.00 [Alignment]
ENST00000314319.7	ARHGAP28	4920	4933	Forward	18:6915205-6915218 [Sequence]	Forward	8	21	14 [Sequence]	28.2	5.5	100.00 [Alignment]
ENST00000419673.6	ARHGAP28	4981	4994	Forward	18:6915205-6915218 [Sequence]	Forward	8	21	14 [Sequence]	28.2	5.5	100.00 [Alignment]
ENST00000585734.5	FAM71E2	1091	1104	Reverse	19:55359955-55359968 [Sequence]	Reverse	2	15	14 [Sequence]	28.2	5.5	100.00 [Alignment]
ENST00000486863.1	LACE1	1448	1461	Reverse	6:108520830-108520843 [Sequence]	Forward	1	14	14 [Sequence]	28.2	5.5	100.00 [Alignment]
ENST00000379374.4	PHEX	3425	3438	Reverse	X:22248563-22248576 [Sequence]	Forward	5	18	14 [Sequence]	28.2	5.5	100.00 [Alignment]

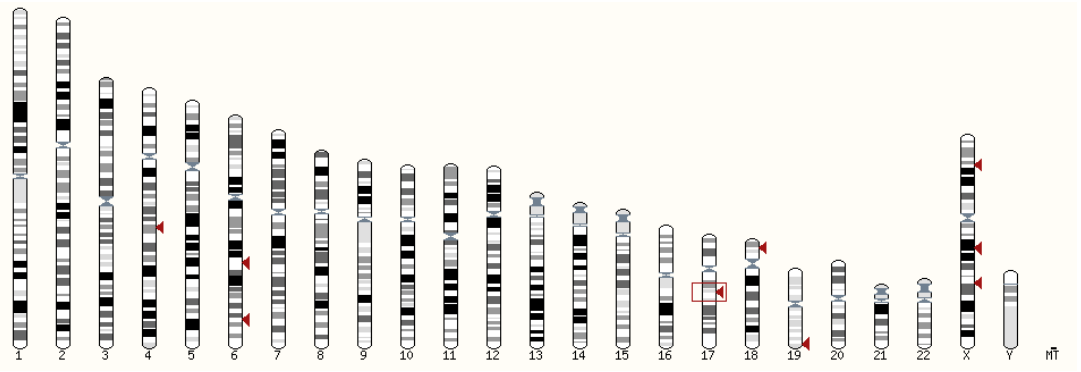

5. TRCN000019355 described as shSTAT5B2

   Target sequence : CGCCATATATTGTACAATGAA

Show All entries | Show/hide columns (2 hidden) | Filter

Subject name	Gene hit	Subject start	Subject end	Subject ori	Genomic Location	Orientation	Query start	Query end	Length	Score	E-val	%ID
ENST00000415845.1	STAT5B	418	438	Forward	17:42224806-42224826 [Sequence]	Reverse	1	21	21 [Sequence]	42.1	4e-04	100.00 [Alignment]
ENST00000468312.1	STAT5B	497	517	Forward	17:42224806-42224826 [Sequence]	Reverse	1	21	21 [Sequence]	42.1	4e-04	100.00 [Alignment]
ENST00000293328.7	STAT5B	497	517	Forward	17:42224806-42224826 [Sequence]	Reverse	1	21	21 [Sequence]	42.1	4e-04	100.00 [Alignment]
ENST00000634773.1	ATAD1	1613	1627	Forward	CHR_HG2334_PATCH:87754429-87754443 [Sequence]	Reverse	2	16	15 [Sequence]	30.2	1.4	100.00 [Alignment]
ENST00000634970.1	ATAD1	1709	1723	Forward	CHR_HG2334_PATCH:87754429-87754443 [Sequence]	Reverse	2	16	15 [Sequence]	30.2	1.4	100.00 [Alignment]
ENST00000274242.9	RPL37	7671	7685	Forward	5:40825263-40825277 [Sequence]	Reverse	7	21	15 [Sequence]	30.2	1.4	100.00 [Alignment]
ENST00000328142.3	ATAD1	1613	1627	Forward	10:87754429-87754443 [Sequence]	Reverse	2	16	15 [Sequence]	30.2	1.4	100.00 [Alignment]
ENST00000308448.11	ATAD1	1709	1723	Forward	10:87754429-87754443 [Sequence]	Reverse	2	16	15 [Sequence]	30.2	1.4	100.00 [Alignment]
ENST00000424296.6	AK9	3983	3996	Reverse	6:109516003-109516016 [Sequence]	Reverse	6	19	14 [Sequence]	28.2	5.5	100.00 [Alignment]
ENST00000470564.5	AK9	419	432	Reverse	6:109516003-109516016 [Sequence]	Reverse	6	19	14 [Sequence]	28.2	5.5	100.00 [Alignment]
ENST00000370793.5	USP33	4113	4126	Forward	1:77696367-77696380 [Sequence]	Reverse	6	19	14 [Sequence]	28.2	5.5	100.00 [Alignment]
ENST00000481579.5	USP33	2477	2490	Forward	1:77696367-77696380 [Sequence]	Reverse	6	19	14 [Sequence]	28.2	5.5	100.00 [Alignment]
ENST00000310389.5	ARL10	10775	10788	Forward	5:176381839-176381852 [Sequence]	Forward	5	18	14 [Sequence]	28.2	5.5	100.00 [Alignment]
ENST00000369002.8	SEC63	6353	6366	Forward	6:107867801-107867814 [Sequence]	Reverse	5	18	14 [Sequence]	28.2	5.5	100.00 [Alignment]
ENST00000352966.9	PKIA	869	882	Reverse	8:78602318-78602331 [Sequence]	Forward	5	18	14 [Sequence]	28.2	5.5	100.00 [Alignment]
ENST00000475187.5	THOC5	1824	1837	Forward	22:29534636-29534649 [Sequence]	Reverse	5	18	14 [Sequence]	28.2	5.5	100.00 [Alignment]
ENST00000420770.6	PAX7	4411	4424	Reverse	1:18747739-18747752 [Sequence]	Forward	8	21	14 [Sequence]	28.2	5.5	100.00 [Alignment]
ENST00000371065.8	LEPROT	2944	2957	Forward	1:65434329-65434342 [Sequence]	Forward	5	18	14 [Sequence]	28.2	5.5	100.00 [Alignment]
ENST00000371065.8	LEPROT	2948	2961	Reverse	1:65434333-65434346 [Sequence]	Forward	5	18	14 [Sequence]	28.2	5.5	100.00 [Alignment]
ENST00000613538.1	LEPROT	2947	2960	Forward	1:65434329-65434342 [Sequence]	Forward	5	18	14 [Sequence]	28.2	5.5	100.00 [Alignment]
ENST00000613538.1	LEPROT	2951	2964	Reverse	1:65434333-65434346 [Sequence]	Forward	5	18	14 [Sequence]	28.2	5.5	100.00 [Alignment]
ENST00000367164.1	RBBP5	3812	3825	Reverse	1:205086607-205086620 [Sequence]	Reverse	4	17	14 [Sequence]	28.2	5.5	100.00 [Alignment]
ENST00000388738.7	KIAA1109	14165	14178	Forward	4:122353832-122353845 [Sequence]	Forward	4	17	14 [Sequence]	28.2	5.5	100.00 [Alignment]
ENST00000306802.8	KIAA1109	3247	3260	Forward	4:122353832-122353845 [Sequence]	Forward	4	17	14 [Sequence]	28.2	5.5	100.00 [Alignment]
ENST00000438707.5	KIAA1109	4127	4140	Forward	4:122353832-122353845 [Sequence]	Forward	4	17	14 [Sequence]	28.2	5.5	100.00 [Alignment]
ENST00000264501.8	KIAA1109	14493	14506	Forward	4:122353832-122353845 [Sequence]	Forward	4	17	14 [Sequence]	28.2	5.5	100.00 [Alignment]
ENST00000334192.8	EML1	2831	2844	Reverse	14:99940304-99940317 [Sequence]	Forward	4	17	14 [Sequence]	28.2	5.5	100.00 [Alignment]
ENST00000262233.10	EML1	2779	2792	Reverse	14:99940304-99940317 [Sequence]	Forward	4	17	14 [Sequence]	28.2	5.5	100.00 [Alignment]
ENST00000327921.13	EML1	3695	3708	Reverse	14:99940304-99940317 [Sequence]	Forward	4	17	14 [Sequence]	28.2	5.5	100.00 [Alignment]

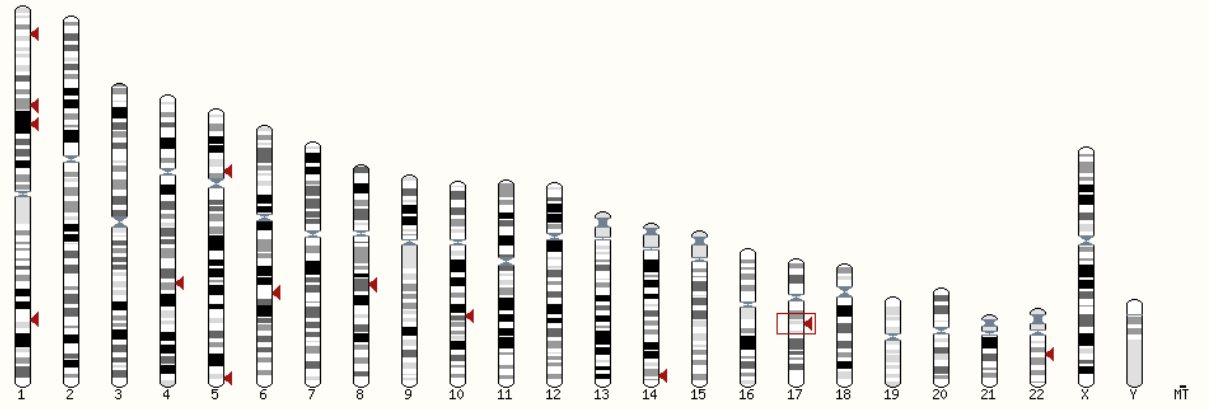

6. TRCN0000222161 described as shSTAT5B3

   Target sequence: CCAGTTCAGTGTTGGTGGAAA

Subject name	Gene hit	Subject start	Subject end	Subject ori	Genomic Location	Orientation	Query start	Query end	Length	Score	E-val	%ID
ENST00000481517.1	STAT5B	576	596	Forward	17:42217182-42217202 [Sequence]	Reverse	1	21	21 [Sequence]	42.1	4e-04	100.00 [Alignment]
ENST00000468496.5	STAT5B	81	101	Forward	17:42217182-42217202 [Sequence]	Reverse	1	21	21 [Sequence]	42.1	4e-04	100.00 [Alignment]
ENST00000293328.7	STAT5B	1507	1527	Forward	17:42217182-42217202 [Sequence]	Reverse	1	21	21 [Sequence]	42.1	4e-04	100.00 [Alignment]
ENST00000630849.1	HSP90AA4P	214	229	Forward	CHR_HSCHR4_7_CTG12:189473360-189473375 [Sequence]	Forward	1	16	16 [Sequence]	32.2	0.35	100.00 [Alignment]
ENST00000631070.1	HSP90AA4P	396	411	Forward	CHR_HSCHR4_7_CTG12:189473360-189473375 [Sequence]	Forward	1	16	16 [Sequence]	32.2	0.35	100.00 [Alignment]
ENST00000378770.1	HSP90AA4P	214	229	Forward	4:189473360-189473375 [Sequence]	Forward	1	16	16 [Sequence]	32.2	0.35	100.00 [Alignment]
ENST00000506915.1	HSP90AA4P	396	411	Forward	4:189473360-189473375 [Sequence]	Forward	1	16	16 [Sequence]	32.2	0.35	100.00 [Alignment]
ENST00000462213.2	KALRN	620	639	Forward	3:124679685-124679704 [Sequence]	Forward	2	21	20 [Sequence]	32.2	0.35	95.00 [Alignment]
ENST00000466110.5	DCTN1	802	820	Forward	2:74371223-74371241 [Sequence]	Reverse	1	19	19 [Sequence]	30.2	1.4	94.74 [Alignment]
ENST00000616231.1	SNX18P1Y	59	72	Reverse	Y:11178364-11178377 [Sequence]	Forward	5	18	14 [Sequence]	28.2	5.5	100.00 [Alignment]
ENST00000630977.2	VPS11	2097	2110	Reverse	CHR_HG2217_PATCH:119081176-119081189 [Sequence]	Forward	7	20	14 [Sequence]	28.2	5.5	100.00 [Alignment]
ENST00000629400.2	VPS11	2709	2722	Reverse	CHR_HG2217_PATCH:119081176-119081189 [Sequence]	Forward	7	20	14 [Sequence]	28.2	5.5	100.00 [Alignment]
ENST00000626621.2	VPS11	2656	2669	Reverse	CHR_HG2217_PATCH:119081176-119081189 [Sequence]	Forward	7	20	14 [Sequence]	28.2	5.5	100.00 [Alignment]
ENST00000373114.4	KLHL4	164	177	Reverse	X:87517977-87517990 [Sequence]	Forward	7	20	14 [Sequence]	28.2	5.5	100.00 [Alignment]
ENST00000373119.8	KLHL4	229	242	Reverse	X:87517977-87517990 [Sequence]	Forward	7	20	14 [Sequence]	28.2	5.5	100.00 [Alignment]
ENST00000614994.4	ZNF285	4316	4329	Forward	19:44383981-44383994 [Sequence]	Reverse	6	19	14 [Sequence]	28.2	5.5	100.00 [Alignment]
ENST00000479417.1	STAT5A	333	346	Forward	17:42304611-42304624 [Sequence]	Forward	2	15	14 [Sequence]	28.2	5.5	100.00 [Alignment]
ENST00000588868.5	STAT5A	1405	1418	Forward	17:42304611-42304624 [Sequence]	Forward	2	15	14 [Sequence]	28.2	5.5	100.00 [Alignment]
ENST00000590949.5	STAT5A	2081	2094	Forward	17:42304611-42304624 [Sequence]	Forward	2	15	14 [Sequence]	28.2	5.5	100.00 [Alignment]
ENST00000345506.8	STAT5A	1981	1994	Forward	17:42304611-42304624 [Sequence]	Forward	2	15	14 [Sequence]	28.2	5.5	100.00 [Alignment]
ENST00000542939.1	PEBP1	453	466	Forward	12:118144854-118144867 [Sequence]	Forward	1	14	14 [Sequence]	28.2	5.5	100.00 [Alignment]
ENST00000261313.2	PEBP1	967	980	Forward	12:118144854-118144867 [Sequence]	Forward	1	14	14 [Sequence]	28.2	5.5	100.00 [Alignment]
ENST00000527181.1	ATM	416	429	Forward	11:108365414-108365427 [Sequence]	Forward	6	19	14 [Sequence]	28.2	5.5	100.00 [Alignment]
ENST00000525178.5	ATM	565	578	Forward	11:108365414-108365427 [Sequence]	Forward	6	19	14 [Sequence]	28.2	5.5	100.00 [Alignment]
ENST00000524792.5	ATM	5292	5305	Forward	11:108365414-108365427 [Sequence]	Forward	6	19	14 [Sequence]	28.2	5.5	100.00 [Alignment]
ENST00000369872.3	SYPL2	1807	1820	Reverse	1:109480320-109480333 [Sequence]	Forward	8	21	14 [Sequence]	28.2	5.5	100.00 [Alignment]
ENST00000620429.4	VPS11	2097	2110	Reverse	11:119081177-119081190 [Sequence]	Forward	7	20	14 [Sequence]	28.2	5.5	100.00 [Alignment]
ENST00000622309.4	VPS11	2709	2722	Reverse	11:119081177-119081190 [Sequence]	Forward	7	20	14 [Sequence]	28.2	5.5	100.00 [Alignment]
ENST00000621676.4	VPS11	2656	2669	Reverse	11:119081177-119081190 [Sequence]	Forward	7	20	14 [Sequence]	28.2	5.5	100.00 [Alignment]
ENST00000337919.9	HEY1	1851	1864	Forward	8:79764445-79764458 [Sequence]	Reverse	8	21	14 [Sequence]	28.2	5.5	100.00 [Alignment]
ENST00000354724.7	HEY1	1845	1858	Forward	8:79764445-79764458 [Sequence]	Reverse	8	21	14 [Sequence]	28.2	5.5	100.00 [Alignment]

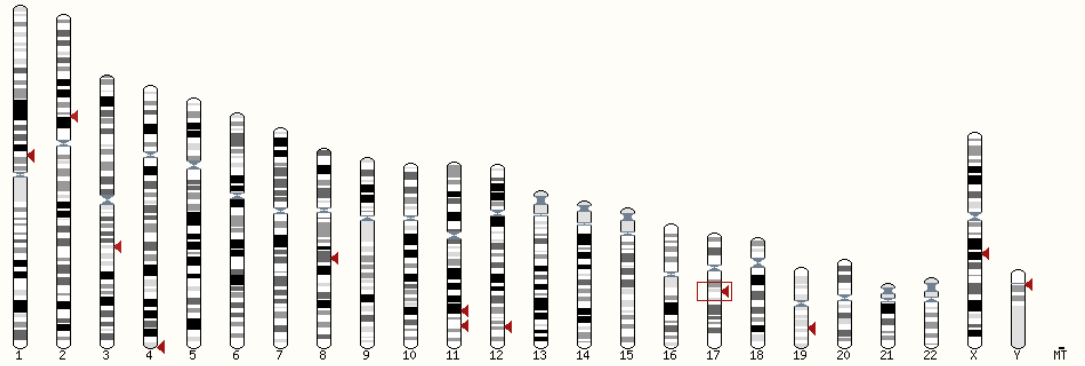

Supplementary Figure 4. Negative control staining for Fluorescence microscopy.

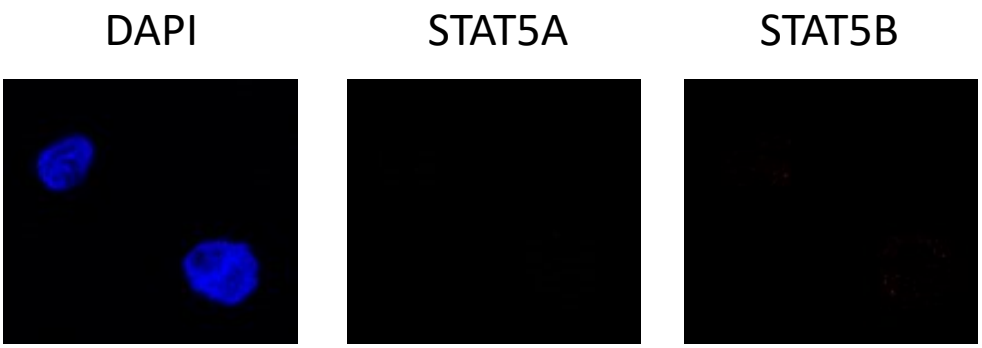

Supplementary Figure 4. Negative control staining for Fluorescence microscopy in THP-1 cells. Cells were incubated with the secondary antibodies coupled with Alexa488 (against rabbit anti-STAT5A antibody) or Alexa546(against mouse anti-STAT5B antibody) fluorophores in the absence of primary antibodies.

Supplementary figure 5. R-Studio script used to perform differential expression analysis of the RNA-seq data.

```
#Import Data
library(edgeR)
library(statmod)

x <- read.table("raw_counts_stat5_samples/gene_expression_table.txt",sep="\t")

colnames(x) <-
c("Symbol,"THP1_S5A1","THP1_S5A2","THP1_S5A3","THP1_S5B1","THP1_S5B2","THP1_S5B3","THP1_C_1","THP1_C_2","THP1_C_3")

x <- x[,c(1,2,4,6,3,5,7,8,9,10,11,12,13,15,17,19,14,16,18)]

group <- factor(c(1,1,1,2,2,2,3,3,3))

#Below example for the differentially expressed genes analysis for the control shSCR transduced cell line vs uSTAT5 down-regulation:

THP1_Control_THP1_S5A1_THP1_S5B1 <- subset(x, select = c(13,14,15,4,5,6,10,11,12))

#Filter according to cpm and values at least 1 in more than a one sample

y <- DGEList(counts=THP1_Control_THP1_S5A1_THP1_S5B1, group=group)

keep <- rowSums(cpm(y)>1) >= 2)

y <- y[keep, , keep.lib.sizes=FALSE]

#Normalization

y <- calcNormFactors(y)

#Check Dispersion

design <- model.matrix(~group)

y <- estimateDisp(y, design)

y$common.dispersion

plotBCV(y)

design <- model.matrix(~group)

fit <- glmFit(y, design)

#Differential Expressed Among All

lrt <- glmLRT(fit, coef=2:3)

topTags(lrt)

differential_expressed_among_all <- lrt$table
```

Quality control performed at the quantification level.

Principle Component Analysis (PCA) plot

To perform the PCA the following R-script was used:

```
library(RColorBrewer)

col<- brewer.pal(length(levels(group)), "Set1")[group]

plotMDS.DGEList(y, col=col)
```

Unsupervised hierarchical clustering

To perform the Unsupervised hierarchical clustering the following R-script was used:

```
m<-cpm(y, prior.count=2, log=T)

dists<- dist(t(m))

mat<- as.matrix(dists)

hmcol <- colorRampPalette(brewer.pal(9,"Blues"))(100)

heatmap.2(mat, trace="none", col=rev(hmcol), dendrogram = "column",
cexRow=1,cexCol=1,margins=c(12,8),srtCol=45)
```

Correlation across the replicates and conditions

```
#correlation between replicates

corr<- function(s1,s2, ...) {

  smoothScatter(s1,s2, ...)

  abline(a=0, b=1, col="black", lwd=4, lty="dotted") #ideal

 lines(lowess(s1,s2),col="red", lwd=4, lty="dotted") #fit

 invisible(0) }

corr(m[,1],m[,2], main="THP1 shSCR replicate1 vs replicate2")
```

```
#correlation between conditions

condshSCR <-apply(m[,1:3], 1, mean)

condshSTAT5A1 <-apply(m[,4:6], 1, mean)

condshSTAT5B3 <-apply(m[,7:9], 1, mean)

corr(condshSCR,condshSTAT5A1, main="THP1 shSCR vs shSTAT5A1")
```

Differential gene expression between conditions

```
#indicating how the replicates are grouped

group <- factor(c(1,1,1,2,2,2,3,3,3))

design <- model.matrix(~group)

fit <- glmFit(y, design)

#Differentially expressed genes between shSCR control and uSTAT5A down-regulation

lrt.2vs1 <- glmLRT(fit, coef=2)

topTags(lrt.2vs1)

differential_THP1_CTRL_Vs_THPS5A <- lrt.2vs1$table

#Filtering the list for the up-regulated genes with a log2FC>= 0.01 and the PValue < 0.01

filtered_differential_THP1_CTRL_Vs_THPS5A <- subset(differential_THP1_CTRL_Vs_THPS5A, logFC
>= 0.01 & PValue < 0.01)

head(filtered_differential_THP1_CTRL_Vs_THPS5A)

#Calculation of the adjusted p-value(FDR) for the up-regulated genes

p.adj <- p.adjust(filtered_differential_THP1_CTRL_Vs_THPS5A$PValue)

filtered_differential_THP1_CTRL_Vs_THPS5A_corrected <-
cbind(filtered_differential_THP1_CTRL_Vs_THPS5A,p.adj)

head(filtered_differential_THP1_CTRL_Vs_THPS5A_corrected)

filtered_differential_THP1_CTRL_Vs_THPS5A_corrected_sort <-
filtered_differential_THP1_CTRL_Vs_THPS5A_corrected[order(filtered_differential_THP1_CTRL_Vs_
THPS5A_corrected$PValue),]
```

```
#Filtering the list for the down-regulated genes with a log2FC<= -0.01 and the PValue < 0.01

filtered_differential_THP1_CTRL_Vs_THPS5A_down <- subset(differential_THP1_CTRL_Vs_THPS5A,
logFC <= -0.01 & PValue < 0.01)

#Calculation of the adjusted p-value(FDR) for the down-regulated genes

p.adj <- p.adjust(filtered_differential_THP1_CTRL_Vs_THPS5A_down$PValue)

filtered_differential_THP1_CTRL_Vs_THPS5A_down_corrected <-
cbind(filtered_differential_THP1_CTRL_Vs_THPS5A_down,p.adj)

filtered_differential_THP1_CTRL_Vs_THPS5A_down_corrected_sort <-
filtered_differential_THP1_CTRL_Vs_THPS5A_down_corrected[order(filtered_differential_THP1_CT
RL_Vs_THPS5A_down_corrected$PValue),]

head(filtered_differential_THP1_CTRL_Vs_THPS5A_down_corrected_sort)



final_THP1_CTRL_Vs_THPS5A <-
rbind(filtered_differential_THP1_CTRL_Vs_THPS5A_corrected_sort,filtered_differential_THP1_CTRL
_Vs_THPS5A_down_corrected_sort)

final_THP1_CTRL_Vs_THPS5A_sort <-
final_THP1_CTRL_Vs_THPS5A[order(final_THP1_CTRL_Vs_THPS5A$PValue),]

write.table(final_THP1_CTRL_Vs_THPS5A_sort,"differential_THP_SCR
cTRL_Vs_THP_shSTAT5A1Kuba",quote=F,row.names=T,col.names=T,sep="\t")



#Fit Control Vs THP1_S5B3

lrt.3vs1 <- glmLRT(fit, coef=3)

topTags(lrt.3vs1)

differential_expressed_THP1_Control <- lrt.3vs1$table

#Filtering the list for the up-regulated genes with a log2FC>= 0.01 and the PValue < 0.01

filtered_differential_expressed_THP1_CTRL_vs_THP1_S5B3 <-
subset(differential_expressed_THP1_Control, logFC >= 0.01 & PValue < 0.01)
```

```
#Calculation of the adjusted p-value(FDR) for the up-regulated genes

p.adj <- p.adjust(filtered_differential_expressed_THP1_CTRL_vs_THP1_S5B3$PValue)

filtered_differential_expressed_THP1_CTRL_vs_THP1_S5B3_corrected <-
cbind(filtered_differential_expressed_THP1_CTRL_vs_THP1_S5B3,p.adj)

filtered_differential_expressed_THP1_CTRL_vs_THP1_S5B3_corrected_sort <-
filtered_differential_expressed_THP1_CTRL_vs_THP1_S5B3_corrected[order(filtered_differential_ex
pressed_THP1_CTRL_vs_THP1_S5B3_corrected$PValue),]

#Filtering the list for the down-regulated genes with a log2FC<= -0.01 and the PValue < 0.01

filtered_differential_expressed_THP1_CTRL_vs_THP1_S5B3_down <-
subset(differential_expressed_THP1_Control, logFC <= -0.01 & PValue < 0.01)

#Calculation of the adjusted p-value(FDR) for the down-regulated genes

p.adj <- p.adjust(filtered_differential_expressed_THP1_CTRL_vs_THP1_S5B3_down$PValue)

filtered_differential_expressed_THP1_CTRL_vs_THP1_S5B3_down_corrected <-
cbind(filtered_differential_expressed_THP1_CTRL_vs_THP1_S5B3_down,p.adj)

final_THP1_CTRL_vs_THP1_S5B3 <-
rbind(filtered_differential_expressed_THP1_CTRL_vs_THP1_S5B3_corrected_sort,filtered_differenti
al_expressed_THP1_CTRL_vs_THP1_S5B3_down_corrected)

final_THP1_CTRL_vs_THP1_S5B3 <-
final_THP1_CTRL_vs_THP1_S5B3[order(final_THP1_CTRL_vs_THP1_S5B3$PValue),]

write.table(final_THP1_CTRL_vs_THP1_S5B3,"differential_expressed_THP1_SCR_CTRL_vs_shSTAT5B-
3.txt",row.names=T,col.names=T,sep="\t",quote=F)
```

Efficacy of STAT5 down-regulation

Figure S6 Efficacy of STAT5 down-regulation in AML cell liens assessed by RT-qPCR analysis.

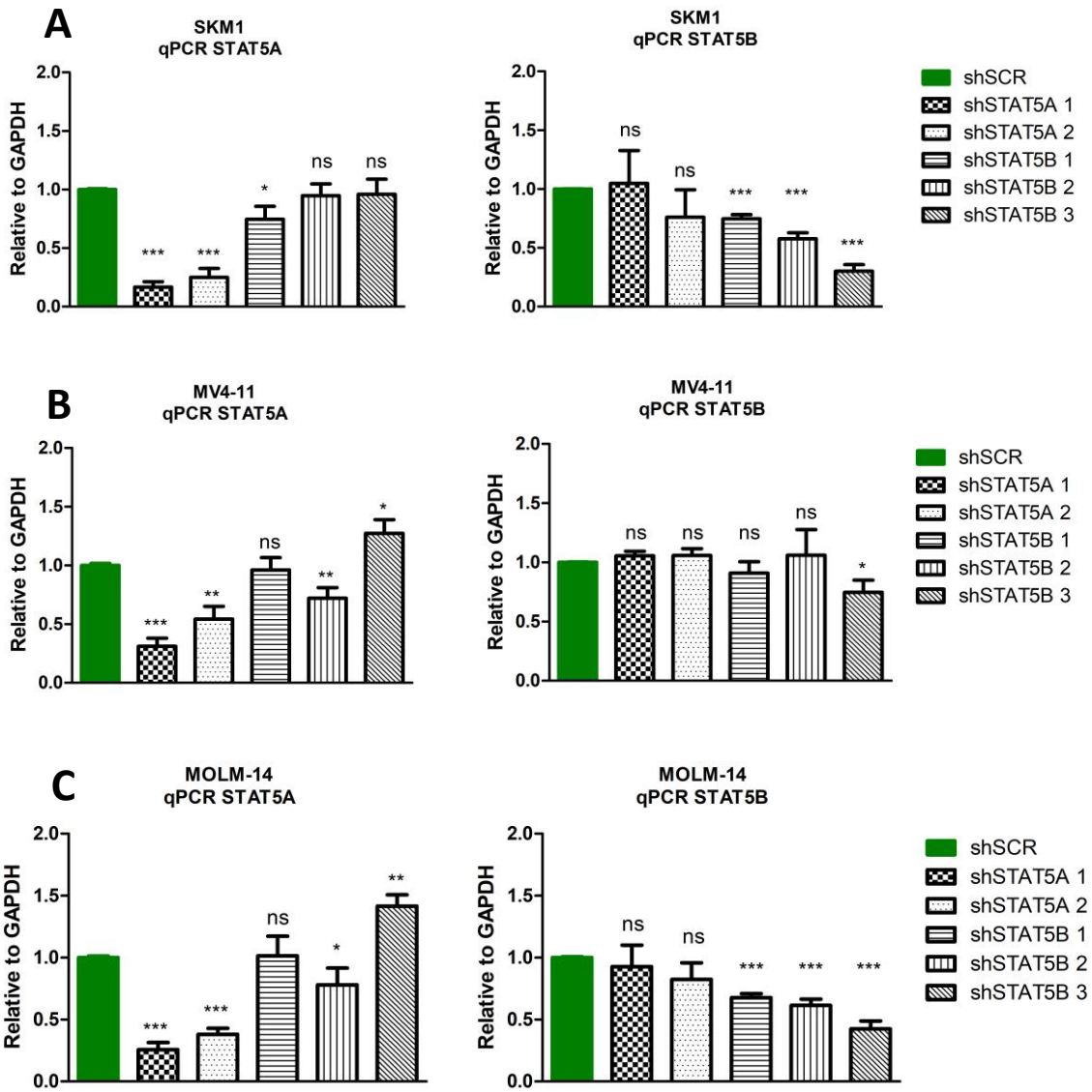

Figure S7. Efficacy of STAT5 down-regulation in SKM-1 (A) and MV4-11 (B) AML cell lines assessed by western-blot analysis.

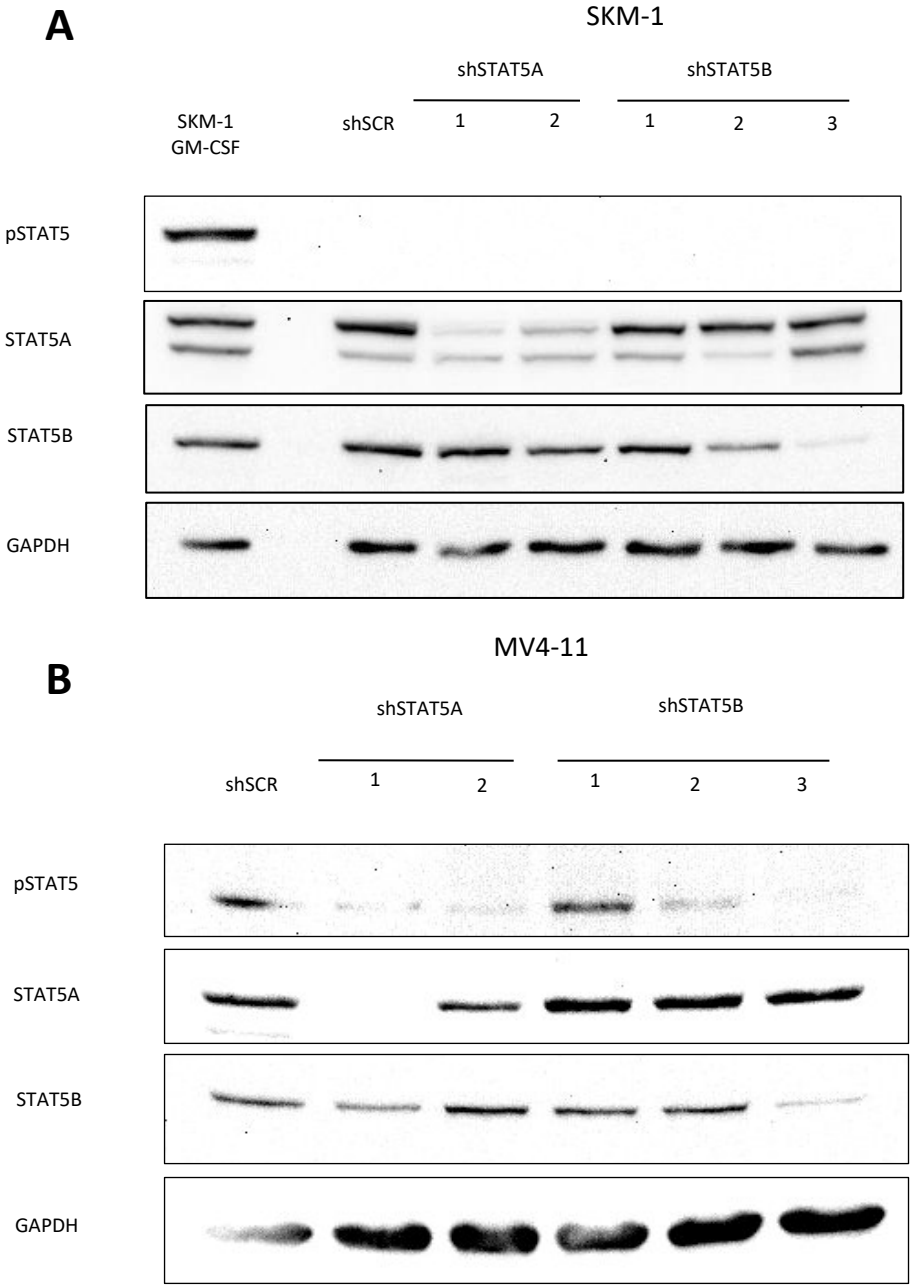

Figure S8. MTT assay

MTT assays were performed after treatment with doxycycline for 5 days to induce of STAT5 knock-down.

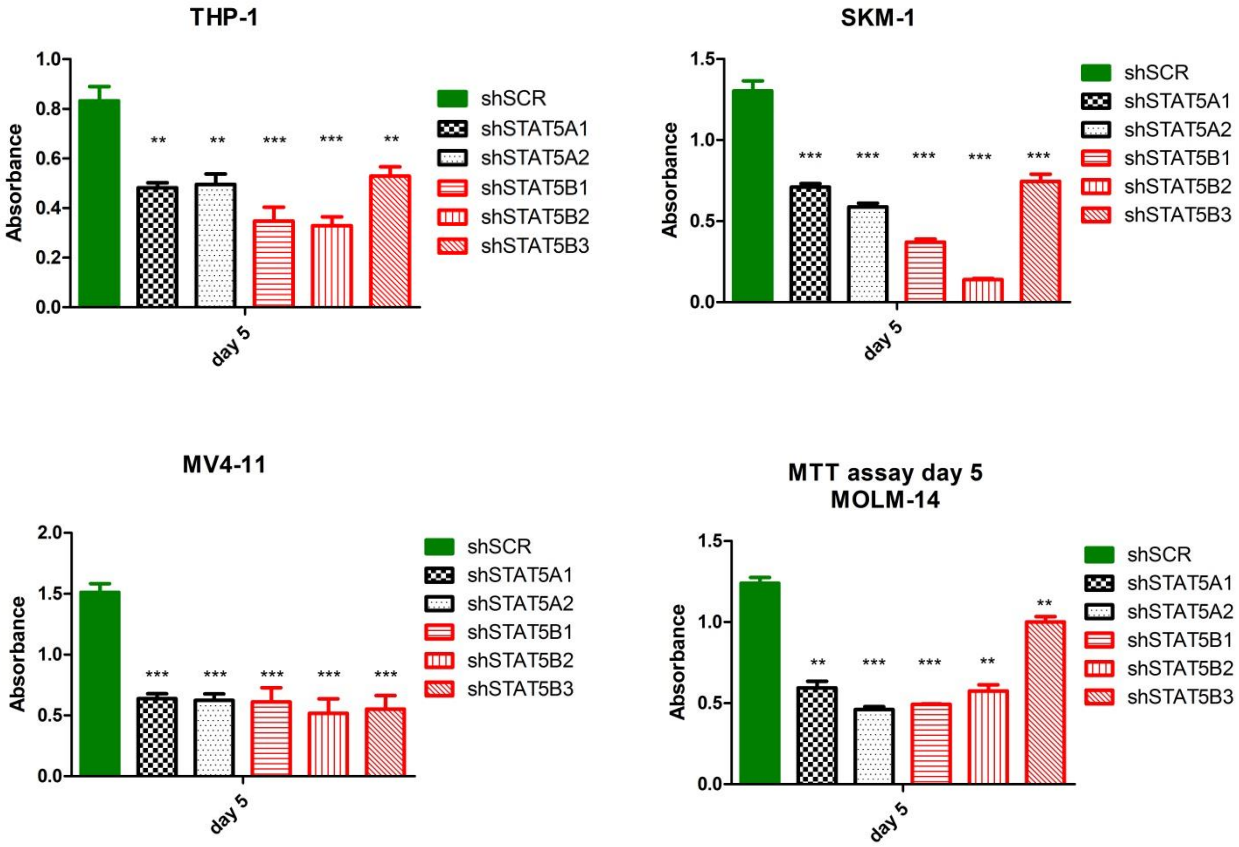

Interacting partners of STAT5 proteins

Table S2. uSTAT5A interacting partners

THP-1		SKM-1		Common	
Interacting partners (171)		Interacting partners (266)		Interacting partners (115)	mean Enrichment
PABPC4	HSPB1	NUP98	EEF1D	RANBP2	165,9093
PCNT	ABHD14B	RANBP2	CLIC1	PABPC4	144,0648
STAT5A;STAT5B	SRM	PCNT	FARSB	PCNT	116,774
ALDH16A1	DDX5	**STAT5A;STAT5B**	TUBB;TUBB3	**STAT5A;STAT5B**	65,77075
PABPC1	HNRNPK	PABPC1	GTF2I	PABPC1	55,31338
CCAR2	ILKAP	PABPC4	ATP5A1	CNST	43,0787
MCM5	HSP90AA1	CNST	MCM6	CCAR2	37,65525
RANBP2	RPS3A	CCAR2	NONO	ASS1	27,2825
RAC2	CCT4	ALDH9A1	SUMO1	VARS	25,85825
SNX27	CLEC11A	ASS1	NPM3	ALDH9A1	24,24683
PFKP	ACTR2	VARS	PSMD3	ALDH16A1	22,23025
PPP1CA	MCM2	BCL9L	COPA	MCM5	18,34005
CDK5RAP2	RPS11	MTHFD1	HNRNPK	MTHFD1	17,546
UBE2M	EIF2S1	LARP1	EEF1G	SNX27	16,69623
ARCN1	CCT8	NCOA5	CAD	GMPS	16,477
PFKL	IDH2	GSPT1;GSPT2	RPLP0;RPLP0P6	PPP1CA	15,15875
GMPS	TUBB4B	SNRPN;SNRPB	SKIV2L2	PDCD6IP	15,11455
VARS	GART	RHOG	GNAI2	PFKL	15,03275
DERA	PCM1	NUP155	COPG1	ARCN1	13,92045
SAMHD1	P4HB	PCNA	CAPN1	SAMHD1	13,80653
PAICS	GNAI2	PDCD6IP	HSP90AA1	NUP155	13,37338
MCM7	FDPS	NUFIP2	WDR1	CDK5RAP2	13,3275
ASS1	PIN1	TIMM23;TIMM23B	ACTR2	MCM7	13,27935
WDR1	BUB3	SLC3A2	FDPS	PRKCD	12,98035
PRKCD	ACAT1	MORC3	MCM2	PAICS	12,89805
ADRBK1	TUFM	SLX4	AARS	CTPS1	12,6385
FERMT3	NANS	CORO1B	RUVBL2	HNRNPL	12,5302
PSMC2	PCBP1	GMPS	GARS	TARS	12,35075
HNRNPL	HNRNPD	PSMC3	FLII	FERMT3	12,2734
ABCF2	PPIA	GFPT1	ARHGDIB	PSMC2	11,9087
PYGL	DYNC1H1	ALDH16A1	HK1	WDR1	11,58195
FARSB	SERPINH1	EIF2S1	RGPD3;RGPD4	MORC3	11,4289
RNH1	EEF1G	NUP214	GART	MCM4	11,19088
CTPS1	RPS15A	NUP54	LRRC47	PSMC1	11,13853
TARS	TUBB	PSMC4	RPS20	FARSB	10,9759
MCM4	ATP5A1	DDX20	TUBA1B;TUBA1C;TUBA1A;TUBA3C;KL	PGD	10,6779
TCP1	SLC25A6;SLC25A4	EIF4A1;EIF4A2	HSPA1A	RPL12	10,38818
CNST	ENO1	CORO7	AFG3L2	PSMC4	10,16533
ARPC4;ARPC4-TTLL3	RPS3	CORO1A	DHX15	CCT5	9,711375
GARS	PHGDH	UPF1	CDK1	PGK1	9,7079
CAPZA1	TRIM21	ANXA11	GEMIN4	GARS	9,6887
PDCD6IP	HADHB	HPRT1	RANGAP1	PFN1	9,6147
WARS	TXNL1	TARS	TARDBP	UPF1	9,568925
RPL12	EFHD2	PGD	VCP	CAPZA1	9,217475
PSMC1	DECR1	PSMC1	ACAA2	FASN	9,14025
PFN1	CORO1A	PFKL	TMCO1	RPL11	9,1234
COPG1	EEF2	CTPS1	PSMC6	TTLL12	9,0279

THP-1		SKM-1		Common	
Interacting partners (171)		Interacting partners (266)		Interacting partners (115)	mean Enrichment
ANXA4	SFXN3	LDHB	RPS3	HSP90AB1	8,9466
TTLL12	ELAVL1	G6PD	NUP93	EIF2S1	8,871475
KARS	PYCRL	ABCE1	HAT1	COPG1	8,8304
AFG3L2	ERLIN2	HNRNPL	PKM	ACTR3	8,812225
PGD	HNRNPM	RAC2;RAC1;RAC3	ARPC5	XRCC5	8,70075
LCP1	LMNB1	PGK1	CAPZA1	HSPD1	8,533525
RPN1	LDHB	SLC25A5	HNRNPH1	RNH1	8,5144
GFM1	HNRNPH1	OGT	RAB7A	SLC25A5	8,4658
RAB7A	LMNA	HSP90AB1	PPIA	AFG3L2	8,391175
CCT5	NNT	FASN	ACTG1;ACTA1;ACTG2;ACTC1;ACTA2	HADHA	8,357375
ALDH9A1	TRIM28	MCM7	COPB2	TCP1	8,31295
RPL11	HNRNPF	PSMD2	HSPH1	MCM3	8,271875
HADHA	SLC25A5	PPIH	TUBA4A	PSMD3	8,162
TBCB	ATIC	CCT3	CFL1	COPA	8,03365
PGK1	SSRP1	PRKCD	PMPCB	CCT7	7,98965
PSMD3	EFTUD2	FARSA	DDX17	RAB7A	7,9577
SUPT16H	ACLY	CCT5	SF3B3	XRCC6	7,83535
ACTR3	SND1	USP14	RAN	PSMD2	7,60925
COPA	ILF3	SAMHD1	CDK5RAP2	CCT3	7,608675
XRCC5	RARS	ADAR	PSMC5	CAPN1	7,510375
STAT1	SYK	MCM4	TRAPPC8	CORO1A	7,393975
CCT7	RPS14	MCM5	ATXN2L	KARS	7,28175
SEC31A	CLTC	RHOA	TRIM21	RPS20	7,217725
FASN	UQCRC2	VPS35	ADSS	ACLY	7,21585
CAPN1	EIF3C;EIF3CL	HSPD1	ACSL4	RPN1	7,18445
LRPPRC	CLIC1	SNX27	CCT6A	PRKDC	7,148775
RPS20	RPS16	FERMT3	EEF1A1P5;EEF1A1	MCM6	7,08335
HSP90AB1	IARS2	UQCRC1	CAPZB	CLTC	6,974625
DIS3	PRKDC	RPL12	PRPF19	LCP1	6,941
XRCC6	CCT3	HADHB	IMMT	CLIC1	6,572225
MCM3	PSMD2	TPP2	DDX5	LDHB	6,4635
HSPD1	GNB2L1	PPP1CB	EIF3C;EIF3CL	PCBP1	6,36915
QARS		ACSL1	AHCY	CCT4	6,353975
PSMC4		PAICS	TRIM28	DDX17	6,2636
PGLS		MCM3	CEP350	CCT6A	6,226175
APEH		PRKDC	GAK	LRPPRC	6,197975
UPF1		XRCC5	DDX3X;DDX3Y	HADHB	6,161425
MTHFD1		TUBB4B;TUBB4A;TUBB3	EEF2	HNRNPK	6,08765
CCT6A		PSMC2	FCGR1C;FCGR1A;FCGR1B	ENO1	6,03125
TRAP1		MSH2	RARS	TUFM	5,94115
MICAL1		ENO1	SND1	TRIM28	5,87085
NUP155		RPL11	EFTUD2	HSP90AA1	5,812125
MORC3		ACTR3	PARK7	ACTR2	5,69575
MCM6		PCBP1	EIF2S3;EIF2S3L	MCM2	5,64595
DDX17		OGDH	SMC3	GNAI2	5,6439
		ARCN1	AMOTL2	FDPS	5,5581
		ARPC4-TTLL3;ARPC4	LRPPRC	EFTUD2	5,5263
		TUBG1;TUBG2	ARHGEF2	SND1	5,4758
		PGM2	RPN1	EEF1G	5,449575
		CPNE1	RRM1	GART	5,447425

THP-1	SKM-1		Common	
Interacting partners (171)	Interacting partners (266)		Interacting partners (115)	mean Enrichment
	CLTC	DDB1	EIF3C;EIF3CL	5,4407
	LDHA	GNB2L1	HNRNPF	5,4066
	CSK	KARS	RARS	5,40205
	ACLY	DPYSL3	ATP5A1	5,35425
	SLC25A3	RPS2	DDX5	5,09875
	CCT4	HNRNPF	PPIA	4,956125
	PFN1	NSUN2	RPS14	4,8258
	RBM14	SIN3A	GNB2L1	4,768825
	XRCC6	RPL23	RPS3	4,730625
	PPP1CA	EPB41L3	HSPB1	4,549675
	TUFM	RAB44	RPS16	4,478175
	EIF4G2	ZC3HAV1	IARS2	4,282725
	ELMO1	PDIA6	TRIM21	4,187425
	TTLL12	YWHAG	HNRNPH1	4,115575
	CCT7	PPA1	CCT8	3,88
	PSMD5	HSPB1	EEF2	3,8492
	DARS	NAA15;NAA16	RPS11	3,6514
	HADHA	RUVBL1	RPS3A	3,62935
	RPS11	TCP1		
	SEC24C	CPSF1		
	UBB;RPS27A;UBC; UBA52;UBBP4	RPS14		
	RPS4X	LCP1		
	HNRNPC	SFPQ		
	RPL10A	KPNB1		
	HSPA6	ERLIN1;ERLIN2		
	RNH1	UBAP2L		
	DDX21	TBK1		
	RPS3A	PLCG2		
	DPYSL2	MNDA		
	IGF2BP1	HK2		
	PDIA3	ANXA6		
	EML4	EIF3D		
	IARS2	RPS16		
	DLD	CCT8		
	HNRNPD;HNRNPD	NPM1		
	PPP3CA;PPP3CC;P PP3CB			
	EWSR1			

Table S3. uSTAT5B interacting partners

THP-1		SKM-1		Common	
Interacting partners (31)		Interacting partners (21)		Interacting partners (11)	mean Enrichment
KDM5C	MCM6	**STAT5B;STAT5A**	RPS20	KDM5C	178,492
CAPRIN1	EEF1G	CAPRIN1	MCM3	CAPRIN1	72,5635
STAT5B;STAT5A	VARS	ETV6	GART	**STAT5B;STAT5A**	68,166
MACF1	EIF3I	KDM5C	PFN1	ETV6	46,533
ETV6	WDR1	SUMO2	WDR1	CCAR1	13,1956
COL18A1	CTPS1	ZBTB7B		SUMO2	11,23665
CCAR1	XRCC5	CBFB		CAPG	4,74735
PRMT1	MCM7	CCAR1		SYNCRIP	3,6334
YLPM1	MCM5	CAPG		TRIM21	4,3041
KIAA0754	SYNCRIP	SYNCRIP		TRIM28	2,20645
MICAL1	TRIM28	TRIM21		WDR1	2,1573
SUMO2	FERMT3	CCAR2			
TRIM21	GNAI3	SAMHD1			
CAPG	XRCC6	MCM4			
FCGR1B	COPA	TRIM28			
FARSB		RHOG			

Table S4. Analysis of un-phosphorylated and phosphorylated STAT5A interacting partners in MV4-11 cells

MV4-11			vehicle vs PKC412			
vehicle only	PKC412 only	common	enriched in vehicle	Score	enriched upon PKC412	Score
RPL30	ASS1	WDR47	TUBB6	0,1009	CHI3L1	19,201
ATP5A1	HNRNPA1	CCAR2	LMNA	0,1622	HNRNPA1	14,467
SLC25A3	HNRNPA2B1	**STAT5A;STAT5B**	KPNB1	0,2171	ALYREF	13,048
TUBA1C;TUBA 1B;TUBA1A;KL	HNRNPAB	KIAA0196	CCDC61	0,23521	RPS19	12,039
SUPT16H	RPS19	PCNT	IGHG1	0,23748	RPL23A	4,2404
LMNA	TRIM21	CCDC61	RPL30	0,24193	RPL13	4,1902
TUBB	RPS18	VARS	CDK5RAP2	0,24507	IGKV2D-24	4,0801
RPN1	RPS25	GEMIN4	**STAT5A;STAT5B**	0,25114	RPS18	3,4802
LMNB1	ATP5O	HELZ	NUP98	0,25342	RPS25	2,9172
	HNRNPU	STRAP	SLC25A3	0,35035	RPS4X;RPS4Y1	2,7315
	RPL23A	RAE1	NMRAL1	0,35351	RPL35	2,7097
	RPS16	SMN1	SUPT16H	0,35943	RPS16	2,5575
	RPL35	UPF1	ATP5A1	0,36975	RPS14	2,4677
	GRB2	GEMIN2	WDR47	0,39009	RPS13	2,4213
	ALYREF	PABPC1	ENO1	0,40513	DDX21	2,3905
	RPS20	CDK5RAP2	HSPB1	0,42967	LARP1	2,261
	DDX21	PFKL	CNST	0,43751	RPL7	2,258
	RPL22	FAM21C	PFKL	0,47056	HNRNPU	2,2533
	RPS14	LDB1	MCM7	0,47302	PABPC4	2,2255
		FAM21A	TRIM21	0,48026	RPS2	2,1931
		TRA2B	LMNB1	0,48172	RPL21	2,1569
		KIAA1033	RAE1	0,48361	RPL4	2,073
		SNRPD3	SLC25A5	0,49538	RPL13A;RPL13a;RPL13AP3	2,0183
		SNRPD1	CCAR2	0,49558	ERP29	2,0103
		CNST			PARP1	1,9739
		CAD				
		SRSF7				

MV4-11			vehicle vs PKC412			
vehicle only	PKC412 only	common	enriched in vehicle	Score	enriched upon PKC412	Score
		RPL11				
		SNRPA				
		HNRNPUL1				
		NMRAL1				
		EFTUD2				
		NUP98				
		HNRNPUL2;HNRNPUL2-BSCL2				
		KHSRP				
		CAPZA1				
		SRSF10;FUSIP1;SR				
		PGAM5				
		MCM7				
		YBX1;YBX3;YBX2				
		CAPZA2				
		PABPC4				
		SF3B3				
		RPS3				
		LARP1				
		MATR3				
		DHX30				
		HSPD1				
		TUFM				
		SRSF3				
		TRA2A				
		SYNCRIP				
		DHX9				

Table S5. Analysis of un-phosphorylated and phosphorylated STAT5B interacting partners in MV4-11 cells

MV4-11			vehicle vs PKC412			
vehicle only	PKC412 only	common	enriched in vehicle	Score	enriched upon PKC412	Score
IGKV2D-24	TPR	PRDX1	IGKV2D-24	0,008671	TPR	9,0282
IGLV2-11	PYGL	NAA50	IGLV2-11	0,021501	PYGL	3,8578
DCD	FAM83H	RPS28	DCD	0,038521	ETV6	3,0436
IGKV2D-29;IGKV2D-40;IGKV2D-30;IGKV2-30;IGKV2D-28	PCMT1	ETV6	IGKV2D-29;IGKV2D-40;IGKV2D-30;IGKV2-30;IGKV2D-28	0,039176		
S100A7;S100A7A	HNRNPM	CFL1	ZNF417	0,061792		
HIST1H2BN;HIST1H2BL;HIST1H2BM;HIST1H2BH;HIST2H2BF;HIST1H2BC;HIST1H2BD;HIST1H2BK;H2BFS	MIF	STAT5B	DSP	0,096262		
HIST1H2AJ;HIST1H2AH;H2AFJ;HIST2H2AC;HIST2H2AA3;HIST1H2AD;HIST1H2AG	EEF2	GSTP1	S100A7;S100A7A	0,12199		

MV4-11			vehicle vs PKC412			
vehicle only	PKC412 only	common	enriched in vehicle	Score	enriched upon PKC412	Score
DSP	RPL11	MACF1	LYZ	0,12593		
HIST3H2BB;HIST2H2BE;HIST1H2BB;HIST1H2BO;HIST1H2BJ;HIST2H2BD;HIST2H2BC	MCM3	MYL1;MYL3	FABP5	0,20615		
HIST1H4A	P4HB	PPIA	MYL1;MYL3	0,25258		
CSE1L		MYH9	PDE6H;MYL6;MYL	0,29481		
KARS		PDE6H;MYL6;MYL	DSG1	0,29525		
TUBB		TXN	DSC1	0,3064		
		TCEB2	H3F3B;H3F3A;HIST2H3A;HIST3H3;HIST1H3A;HIST2H3PS2;H3F3C	0,34629		
		SKP1	HIST1H2BN;HIST1H2BL;HIST1H2BM;HIST1H2BH;HIST2H2BF;HIST1H2BC;HIST1H2BD;HIST1H2BK;H2BFS	0,35803		
		ZC3H12A;ZC3H12	HIST1H4A	0,38435		
		CAPRIN1	HIST3H2BB;HIST2H2BE;HIST1H2BB;HIST1H2BO;HIST1H2BJ;HIST2H2BD;HIST2H2BC	0,39821		
		FLAD1	CSE1L	0,45004		
		EEF1A1P5;EEF1A1	RPL32	0,45554		
		RUVBL1	MYH9	0,45611		
		IARS				
		GRB2				
		UNC13D				
		PDIA3				
		C21orf33				
		NCL				
		CCT2				
		TCEB1				
		CLTC				
		RUVBL2				
		RPL8				
		BOLA2B;BOLA2				
		RPS12				
		EPRS				
		RPL12				
		CAPZA1				
		RPS20				
		KIAA0754				
		EIF5A;EIF5AL1;EIF				
		HSPA1A				
		BIRC6				
		TUBB4B;TUBB4A				
		RPL30				

MV4-11			vehicle vs PKC412			
vehicle only	PKC412 only	common	enriched in vehicle	Score	enriched upon PKC412	Score
		KDM5C ACAP1 RPL10A DDB1 RPS3				

Table S6. Interaction of STAT5 proteins with MCM-family members

	uSTAT5A			pSTAT5A	uSTAT5B			pSTAT5B
	THP-1	SKM-1	MV4-11	MV4-11	THP-1	SKM-1	MV4-11	MV4-11
MCM2	x	x	x					
MCM3	x	x	x			x	x	
MCM4	x	x	x			x		
MCM5	x	x	x		x			
MCM6	x	x	x		x			
MCM7	x	x	x	x	x			

Figure S9. Comparison of uSTAT5A/B and pSTAT5A/B interacting partners in MV4-11 cells.

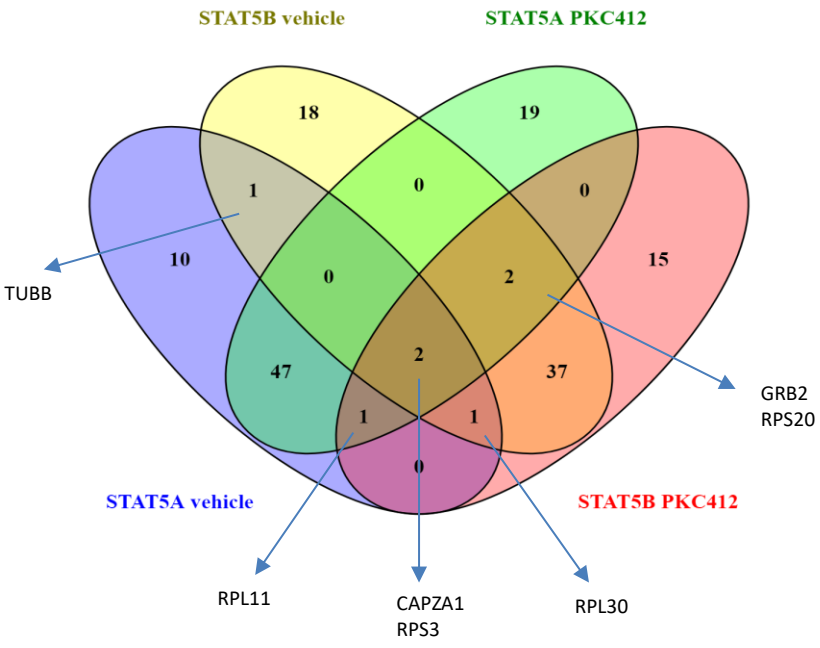

Figure S10. uSTAT5A interacting partners (blue) in SKM-1 and THP-1 cells compared to uSTAT5A (green)/pSTAT5A (orange) in MV4-11.

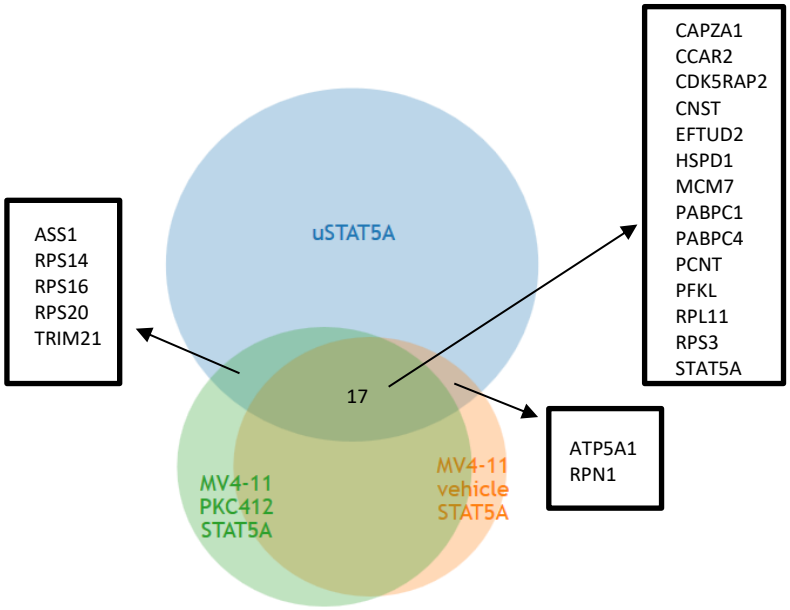

Figure S11. uSTAT5B interacting partners (blue) in SKM-1 and THP-1 cells compared to uSTAT5B (green)/pSTAT5B (orange) in MV4-11.

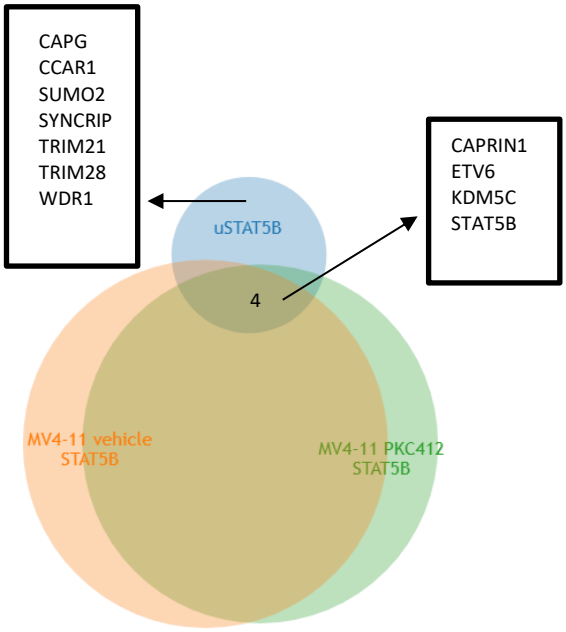

RNA-seq

Table S7. List of top 50 Differentially Expressed Genes upon uSTAT5A KD in THP-1 cells

Up-regulated genes

Ensembl ID	logFC	logCPM	PValue	p.adj	HGNC
ENSG00000218902	3,808684	-0,51529	4,45E-12	3,32E-09	PTMAP3
ENSG00000170381	3,041173	-0,81158	3,32E-05	0,020059	SEMA3E
ENSG00000189157	2,943345	0,11384	1,13E-06	0,000765	FAM47E
ENSG00000133105	2,866799	-0,14665	1,63E-12	1,22E-09	RXFP2
ENSG00000124243	2,86311	0,164439	5,19E-10	3,81E-07	BCAS4
ENSG00000141977	2,733083	-0,31875	2,01E-11	1,49E-08	CIB3
ENSG00000105792	2,71583	1,07273	6,79E-09	4,93E-06	CFAP69
ENSG00000181085	2,573521	-0,01483	1,72E-05	0,010773	MAPK15
ENSG00000182950	2,466271	0,270068	2,06E-08	1,47E-05	ODF3L1
ENSG00000124731	2,35785	2,332759	5,52E-06	0,003597	TREM1
ENSG00000110318	2,264168	1,03208	1,3E-05	0,008198	CEP126
ENSG00000270906	2,256699	-0,17251	4,08E-08	2,9E-05	MTND4P35
ENSG00000124635	2,191403	0,590426	7,56E-06	0,004888	HIST1H2BJ
ENSG00000196684	2,187999	3,423634	8,49E-17	6,39E-14	HSH2D
ENSG00000182809	2,055089	1,628127	2,57E-06	0,001707	CRIP2
ENSG00000111837	1,97113	1,416845	6,5E-12	4,84E-09	MAK
ENSG00000134198	1,970614	0,303183	1,66E-06	0,001112	TSPAN2
ENSG00000187837	1,942415	3,188707	2,16E-07	0,00015	HIST1H1C
ENSG00000186354	1,913567	0,265586	9,96E-07	0,000674	C9ORF47
ENSG00000258846	1,910659	-0,16842	4,39E-08	3,12E-05	EEF1A1P33
ENSG00000256347	1,878582	-0,43304	1,91E-07	0,000134	OR8R1P
ENSG00000235044	1,869631	-0,7558	9,42E-06	0,006058	PPIAP3
ENSG00000148204	1,772582	-0,41898	6,19E-05	0,036145	CRB2
ENSG00000124233	1,755139	4,258991	9,92E-24	7,5E-21	SEMG1
ENSG00000242550	1,752882	3,706234	2,87E-05	0,01754	SERPINB10
ENSG00000188064	1,725011	4,264269	3,16E-11	2,34E-08	WNT7B
ENSG00000010818	1,711268	4,905527	7,74E-06	0,004997	HIVEP2
ENSG00000118997	1,698012	0,430007	1,83E-05	0,011444	DNAH7
ENSG00000233476	1,648144	1,905156	1,37E-12	1,02E-09	EEF1A1P6
ENSG00000102760	1,624997	4,433067	7,2E-11	5,31E-08	RGCC
ENSG00000112246	1,617676	0,944775	1,61E-06	0,001077	SIM1
ENSG00000224116	1,61365	-0,06744	3,14E-05	0,01903	INHBA-AS1
ENSG00000168405	1,611662	1,806259	3,82E-10	2,81E-07	CMAHP
ENSG00000080823	1,61142	1,758399	7,09E-07	0,000484	MOK
ENSG00000057294	1,578899	0,169411	3E-05	0,018316	PKP2
ENSG00000164953	1,555862	2,791959	1,15E-05	0,007358	TMEM67
ENSG00000172403	1,553058	5,652412	2,8E-07	0,000194	SYNPO2
ENSG00000163710	1,551204	1,987128	6,55E-14	4,91E-11	PCOLCE2
ENSG00000245205	1,539199	1,449321	2,62E-11	1,94E-08	EEF1A1P4
ENSG00000075213	1,524169	3,502663	9,7E-13	7,26E-10	SEMA3A
ENSG00000242349	1,491326	0,209432	8,46E-07	0,000575	NPPA-AS1
ENSG00000205592	1,48317	5,056802	2,17E-05	0,013452	MUC19
ENSG00000260876	1,483043	0,421603	1,43E-06	0,000961	LINC01229
ENSG00000147255	1,480011	5,466451	8,57E-17	6,44E-14	IGSF1
ENSG00000242071	1,444276	0,312333	2,3E-05	0,014242	RPL7AP6
ENSG00000198754	1,436861	5,276483	8,32E-07	0,000567	OXCT2
ENSG00000177992	1,422676	-0,16173	3,34E-05	0,020129	SPATA31E1
ENSG00000102554	1,421249	3,233587	1,45E-06	0,000975	KLF5
ENSG00000213694	1,371896	4,091663	3,95E-10	2,9E-07	S1PR3
ENSG00000108622	1,354275	1,529942	2,79E-07	0,000194	ICAM2

Down-regulated genes

Ensembl ID	logFC	logCPM	PValue	p.adj	HGNC
ENSG00000183160	-3,08984	4,508117	7,05E-13	5,88E-10	TMEM119
ENSG00000100385	-2,94193	-0,73087	2,7E-06	0,001971	IL2RB
ENSG00000198842	-2,69761	0,679375	1,17E-10	9,58E-08	DUSP27
ENSG00000129538	-2,29746	0,24644	1,27E-05	0,008667	RNASE1
ENSG00000169548	-2,17115	0,094644	1,55E-08	1,23E-05	ZNF280A
ENSG00000107731	-2,10955	2,85743	9,68E-10	7,84E-07	UNC5B
ENSG00000127533	-2,05717	2,139599	1,39E-06	0,001035	F2RL3
ENSG00000205978	-2,03425	0,861677	1,07E-05	0,007295	NYNRIN
ENSG00000206190	-1,96566	3,749896	1,42E-16	1,2E-13	ATP10A
ENSG00000171724	-1,93824	3,618828	3,53E-13	2,95E-10	VAT1L
ENSG00000205181	-1,92836	0,50395	1,56E-05	0,010512	LINC00654
ENSG00000168329	-1,86122	4,811736	7,68E-10	6,26E-07	CX3CR1
ENSG00000157404	-1,85299	1,587453	1,25E-07	9,74E-05	KIT
ENSG00000171115	-1,84936	2,294692	3,42E-12	2,84E-09	GIMAP8
ENSG00000163449	-1,82508	-0,2354	3,55E-05	0,022677	TMEM169
ENSG00000138172	-1,82144	2,078585	6,68E-08	5,22E-05	CALHM2
ENSG00000178860	-1,81861	4,293198	2,81E-05	0,018213	MSC
ENSG00000152402	-1,79846	0,210216	3,78E-06	0,002724	GUCY1A2
ENSG00000117318	-1,79543	3,386338	5,7E-06	0,004021	ID3
ENSG00000198729	-1,73854	2,206004	3,6E-10	2,95E-07	PPP1R14C
ENSG00000007312	-1,72775	-0,01247	1,96E-06	0,001445	CD79B
ENSG00000087245	-1,70608	4,800471	1,21E-19	1,02E-16	MMP2
ENSG00000160111	-1,70343	0,592507	1,5E-05	0,010106	CPAMD8
ENSG00000108448	-1,701	1,325572	8,48E-06	0,005844	TRIM16L
ENSG00000177383	-1,69006	2,827274	2,9E-09	2,34E-06	MAGEF1
ENSG00000126561	-1,63181	3,779398	2,83E-08	2,24E-05	STAT5A
ENSG00000250510	-1,62124	1,115039	1,2E-09	9,69E-07	GPR162
ENSG00000107719	-1,61853	3,79851	7,95E-10	6,47E-07	PALD1
ENSG00000235531	-1,60427	2,968931	7,03E-05	0,043113	MSC-AS1
ENSG00000180767	-1,6037	2,320824	6,12E-12	5,08E-09	CHST13
ENSG00000101000	-1,56187	1,93868	2,5E-07	0,000193	PROCR
ENSG00000140682	-1,52939	1,837544	9,33E-08	7,27E-05	TGFB1I1
ENSG00000234380	-1,52759	0,924015	4,98E-05	0,031088	LINC01426
ENSG00000198246	-1,51584	2,600462	2,51E-10	2,06E-07	SLC29A3
ENSG00000120833	-1,48811	0,491805	8,2E-05	0,049405	SOCS2
ENSG00000067113	-1,47931	1,096964	1,34E-05	0,009072	PLPP1
ENSG00000178150	-1,44873	1,470555	5,64E-08	4,41E-05	ZNF114
ENSG00000180044	-1,44205	3,493075	2,13E-06	0,001565	C3ORF80
ENSG00000196218	-1,43337	0,754463	7,44E-05	0,045361	RYR1
ENSG00000129195	-1,42266	1,402986	6,85E-05	0,042121	FAM64A
ENSG00000157303	-1,42234	2,423559	8,02E-06	0,005559	SUSD3
ENSG00000116016	-1,42097	5,709949	7,12E-05	0,04355	EPAS1
ENSG00000031081	-1,40964	1,983409	1,18E-05	0,008056	ARHGAP31
ENSG00000064393	-1,39472	6,288334	9,17E-06	0,0063	HIPK2
ENSG00000166848	-1,39009	5,799515	2,45E-28	2,07E-25	TERF2IP
ENSG00000174307	-1,38084	0,341744	2,54E-05	0,016561	PHLDA3
ENSG00000119865	-1,3566	2,444987	1,4E-06	0,001042	CNRIP1
ENSG00000180316	-1,33815	1,062468	3,33E-06	0,002417	PNPLA1
ENSG00000242732	-1,33111	2,0626	4,89E-05	0,030622	RGAG4
ENSG00000114019	-1,30614	0,23805	9,02E-06	0,006208	AMOTL2

Table S8. List of top 50 Differentially Expressed Genes upon uSTAT5B KD in THP-1 cells

Up-regulated genes

Ensembl ID	logFC	logCPM	PValue	p.adj	HGNC
ENSG00000139970	9,09048	-0,40145	9,84E-33	1,26E-29	RTN1
ENSG00000182983	7,922225	0,55569	6,22E-35	8,03E-32	ZNF662
ENSG00000253953	6,875361	0,38007	1,86E-34	2,39E-31	PCDHGB4
ENSG00000115138	6,550814	-0,71872	9,07E-24	1,14E-20	POMC
ENSG00000153930	6,490208	-0,76761	2,62E-24	3,31E-21	ANKFN1
ENSG00000120915	6,068683	0,771285	1,33E-41	1,73E-38	EPHX2
ENSG00000165548	5,995259	-1,17704	9,68E-19	1,2E-15	TMEM63C
ENSG00000135074	5,947275	-0,4651	3,26E-23	4,1E-20	ADAM19
ENSG00000198521	5,943856	1,404609	8,95E-39	1,16E-35	ZNF43
ENSG00000237417	5,764702	0,226209	1,34E-28	1,71E-25	XRCC6P1
ENSG00000100060	5,659994	2,226015	3,53E-51	4,59E-48	MFNG
ENSG00000198286	5,200078	-0,30305	1,1E-24	1,39E-21	CARD11
ENSG00000002726	5,162355	1,329966	1,89E-37	2,44E-34	AOC1
ENSG00000179222	5,060017	1,463768	2,6E-40	3,37E-37	MAGED1
ENSG00000064195	4,95154	1,579604	1,5E-34	1,93E-31	DLX3
ENSG00000148600	4,947247	0,690124	1,47E-25	1,86E-22	CDHR1
ENSG00000072694	4,698558	-0,01947	6,67E-13	7,81E-10	FCGR2B
ENSG00000081803	4,668558	0,582856	2,95E-29	3,77E-26	CADPS2
ENSG00000149054	4,601129	-0,12305	8,25E-26	1,05E-22	ZNF215
ENSG00000241163	4,468966	-0,83519	7,38E-15	8,86E-12	LINC00877
ENSG00000231389	4,433581	-0,9648	2,21E-17	2,71E-14	HLA-DPA1
ENSG00000133169	4,412789	1,157565	3,4E-14	4,05E-11	BEX1
ENSG00000225217	4,359354	-0,69498	3,56E-14	4,23E-11	HSPA7
ENSG00000100181	4,297177	2,457394	2,42E-18	3E-15	TPTEP1
ENSG00000148143	4,280672	-1,17976	1,04E-10	1,15E-07	ZNF462
ENSG00000100228	4,27582	-0,65073	8,3E-11	9,17E-08	RAB36
ENSG00000106236	4,256938	1,105064	3,06E-28	3,9E-25	NPTX2
ENSG00000188153	4,14134	-1,14457	1,93E-13	2,27E-10	COL4A5
ENSG00000137558	4,047065	0,465869	5,84E-31	7,49E-28	PI15
ENSG00000147231	4,022502	2,124523	3,23E-30	4,14E-27	CXORF57
ENSG00000143416	3,970403	-0,86234	2,5E-12	2,88E-09	SELENBP1
ENSG00000088992	3,965856	-0,01469	1,67E-18	2,06E-15	TESC
ENSG00000086548	3,927397	-1,19165	7,55E-12	8,59E-09	CEACAM6
ENSG00000169398	3,854489	3,020337	6,38E-60	8,29E-57	PTK2
ENSG00000132164	3,783809	-0,49182	4,85E-17	5,93E-14	SLC6A11
ENSG00000159164	3,782097	-0,02439	6,42E-14	7,61E-11	SV2A
ENSG00000131042	3,764097	1,1148	2,76E-34	3,55E-31	LILRB2
ENSG00000230453	3,759615	0,354684	6,82E-20	8,51E-17	ANKRD18B
ENSG00000042980	3,748944	2,801709	1,75E-22	2,19E-19	ADAM28
ENSG00000254521	3,728337	0,69791	1,93E-29	2,47E-26	SIGLEC12
ENSG00000204287	3,71639	0,873622	2,72E-13	3,2E-10	HLA-DRA
ENSG00000196581	3,695599	-1,27569	4,73E-09	5,01E-06	AJAP1
ENSG00000154330	3,670103	-0,96374	1,37E-13	1,62E-10	PGM5
ENSG00000114013	3,649898	1,16927	2,59E-29	3,31E-26	CD86
ENSG00000204131	3,649665	1,175212	5,75E-27	7,3E-24	NHSL2
ENSG00000141198	3,538498	0,907713	6,53E-16	7,92E-13	TOM1L1
ENSG00000196368	3,531399	-0,86711	1,14E-12	1,32E-09	NUDT11
ENSG00000166426	3,499236	2,387553	6,76E-28	8,61E-25	CRABP1
ENSG00000165168	3,467925	6,118951	2,36E-46	3,07E-43	CYBB

Down-regulated genes

Ensembl ID	logFC	logCPM	PValue	p.adj	HGNC
ENSG00000165949	-5,28868	4,331246	6,45E-08	7,24E-05	IFI27
ENSG00000177992	-4,42311	-0,16173	1,71E-12	2,07E-09	SPATA31E1
ENSG00000120738	-3,31574	5,561369	2,38E-07	0,000262	EGR1
ENSG00000157601	-3,24184	4,80777	1,5E-05	0,0145	MX1
ENSG00000139364	-3,06089	-0,19982	2,29E-12	2,76E-09	TMEM132B
ENSG00000261192	-2,975	1,170406	4,76E-06	0,004818	RNF126P1
ENSG00000214324	-2,90298	-0,53119	8,48E-08	9,51E-05	C3ORF56
ENSG00000112183	-2,75077	0,712051	6,42E-06	0,006436	RBM24
ENSG00000119922	-2,68653	4,572148	1,29E-16	1,59E-13	IFIT2
ENSG00000151632	-2,65426	6,575091	4,74E-17	5,83E-14	AKR1C2
ENSG00000176381	-2,6486	0,211181	1,73E-08	1,99E-05	PRR18
ENSG00000185745	-2,45884	3,27592	1,34E-05	0,012997	IFIT1
ENSG00000196139	-2,33383	5,397911	1,82E-28	2,26E-25	AKR1C3
ENSG00000163792	-2,30827	2,582758	2,28E-13	2,78E-10	TCF23
ENSG00000188582	-2,25923	-0,57821	3,48E-06	0,003584	PAQR9
ENSG00000142694	-2,08392	2,870786	5,41E-17	6,65E-14	EVA1B
ENSG00000166173	-2,08086	2,695969	4,77E-09	5,56E-06	LARP6
ENSG00000204970	-2,06594	0,478407	7,13E-06	0,007105	PCDHA1
ENSG00000047936	-2,00941	4,635999	1,77E-14	2,16E-11	ROS1
ENSG00000169704	-1,99778	0,598085	7,32E-13	8,88E-10	GP9
ENSG00000187608	-1,99091	4,63416	4,06E-06	0,004142	ISG15
ENSG00000169248	-1,98613	-0,13156	2,57E-05	0,02408	CXCL11
ENSG00000119917	-1,95711	5,069732	4,15E-06	0,004227	IFIT3
ENSG00000172403	-1,867	5,652412	1,51E-09	1,77E-06	SYNPO2
ENSG00000184979	-1,81392	2,360188	1,71E-05	0,016477	USP18
ENSG00000153093	-1,80307	0,4598	3,02E-07	0,000332	ACOXL
ENSG00000204389	-1,77824	3,024292	3,1E-06	0,003202	HSPA1A
ENSG00000177238	-1,77291	0,870408	7,8E-11	9,32E-08	TRIM72
ENSG00000036530	-1,76699	2,479434	1,28E-06	0,001353	CYP46A1
ENSG00000184574	-1,75442	1,930117	1,11E-09	1,31E-06	LPAR5
ENSG00000185070	-1,73602	1,709749	2,74E-07	0,000301	FLRT2
ENSG00000154027	-1,72264	0,227018	9,09E-08	0,000102	AK5
ENSG00000175130	-1,67393	4,000807	6,39E-06	0,006411	MARCKSL1
ENSG00000112186	-1,65171	5,335107	1,59E-08	1,83E-05	CAP2
ENSG00000135919	-1,642	3,790257	6,3E-07	0,000678	SERPINE2
ENSG00000204960	-1,63739	0,471773	5,94E-08	6,69E-05	BLACE
ENSG00000136213	-1,63366	5,220751	3,53E-20	4,37E-17	CHST12
ENSG00000141665	-1,63189	0,563154	3,15E-05	0,029206	FBXO15
ENSG00000232803	-1,62979	0,336282	4,4E-08	5E-05	SLCO4A1-AS1
ENSG00000184985	-1,60775	2,347371	1,73E-08	1,99E-05	SORCS2
ENSG00000100427	-1,60529	7,846896	4,75E-06	0,004818	MLC1
ENSG00000100448	-1,59298	8,824241	2,04E-16	2,51E-13	CTSG
ENSG00000164853	-1,59165	0,452405	1,34E-05	0,013014	UNCX
ENSG00000130675	-1,57195	3,169682	2,59E-06	0,002697	MNX1
ENSG00000145506	-1,56017	5,138568	5,89E-07	0,000636	NKD2
ENSG00000198818	-1,53756	7,580238	3,64E-28	4,52E-25	SFT2D1
ENSG00000182676	-1,53434	6,394383	1,82E-05	0,017339	PPP1R27
ENSG00000164626	-1,5222	4,373788	3,71E-07	0,000405	KCNK5
ENSG00000242600	-1,50197	0,434753	1,62E-05	0,015628	MBL1P
ENSG00000182326	-1,47953	4,0881	2,18E-11	2,62E-08	C1S

Figure S12. List of up-stream regulators that induce changes in gene expression similar to effects of uSTAT5B knock-down (IPA analysis)

Upstream Re...	Expr ...	Molecule Type	Predicted Act...	Activatio...	p-value of ov...
tretinoin		chemical - endogenous mammalian	Activated	4,529	3,57E-17
CSF2		cytokine	Activated	4,275	2,27E-10
ethanol		chemical - endogenous mammalian	Activated	3,499	1,04E-03
cardiotoxin		chemical - other	Activated	3,464	1,45E-05
SPI1		transcription regulator	Activated	3,289	3,74E-09
E. coli B5 lipopolysac		chemical - endogenous non-mammalian	Activated	3,257	1,56E-06
TCF7L2		transcription regulator	Activated	3,176	9,40E-03
cholesterol		chemical - endogenous mammalian	Activated	3,173	1,20E-04
hexachlorobenzene		chemical toxicant	Activated	3,148	4,45E-05
CpG ODN 1826		chemical reagent	Activated	3,081	6,05E-05
E. coli B4 lipopolysac		chemical toxicant	Activated	3,070	1,81E-03
IL1		group	Activated	3,069	1,50E-04
D-glucose		chemical - endogenous mammalian	Activated	3,061	8,20E-03
TGM2	↑1,107	enzyme	Activated	2,974	1,10E-07
bleomycin		chemical drug	Activated	2,926	3,83E-02
BMP2		growth factor	Activated	2,919	6,13E-03
PI3K (complex)		complex	Activated	2,865	7,82E-06
STAT3		transcription regulator	Activated	2,855	1,14E-10
decitabine		chemical drug	Activated	2,842	1,82E-08
CD2		transmembrane receptor	Activated	2,804	1,41E-04

Bibliography

[1] H. J. Park *et al.*, "Cytokine-induced megakaryocytic differentiation is regulated by genome-wide loss of a uSTAT transcriptional program.," *EMBO J.*, vol. 35, no. 6, pp. 580–94, Mar. 2016.

[2] J. Palis, S. Robertson, M. Kennedy, C. Wall, and G. Keller, "Development of erythroid and myeloid progenitors in the yolk sac and embryo proper of the mouse.," *Development*, vol. 126, no. 22, pp. 5073–84, Nov. 1999.

[3] A. Medvinsky and E. Dzierzak, "Definitive Hematopoiesis Is Autonomously Initiated by the AGM Region," *Cell*, vol. 86, no. 6, pp. 897–906, Sep. 1996.

[4] A. Ivanovs, S. Rybtsov, L. Welch, R. A. Anderson, M. L. Turner, and A. Medvinsky, "Highly potent human hematopoietic stem cells first emerge in the intraembryonic aorta-gonad-mesonephros region," *J. Exp. Med.*, vol. 208, no. 12, pp. 2417–2427, Nov. 2011.

[5] E. Dzierzak and N. A. Speck, "Of lineage and legacy: the development of mammalian hematopoietic stem cells," *Nat. Immunol.*, vol. 9, no. 2, pp. 129–136, Feb. 2008.

[6] S. H. Orkin and L. I. Zon, "Hematopoiesis: An Evolving Paradigm for Stem Cell Biology," *Cell*, vol. 132, no. 4, p. 631, 2008.

[7] C. Nombela-Arrieta *et al.*, "Quantitative imaging of haematopoietic stem and progenitor cell localization and hypoxic status in the bone marrow microenvironment," *Nat. Cell Biol.*, vol. 15, no. 5, pp. 533–543, May 2013.

[8] P. Benveniste *et al.*, "Intermediate-term hematopoietic stem cells with extended but time-limited reconstitution potential.," *Cell Stem Cell*, vol. 6, no. 1, pp. 48–58, Jan. 2010.

[9] S. J. Szilvassy, R. K. Humphries, P. M. Lansdorp, A. C. Eaves, and C. J. Eaves, "Quantitative assay for totipotent reconstituting hematopoietic stem cells by a competitive repopulation strategy.," *Proc. Natl. Acad. Sci. U. S. A.*, vol. 87, no. 22, pp. 8736–40, Nov. 1990.

[10] G. J. Spangrude, S. Heimfeld, and I. L. Weissman, "Purification and characterization of mouse hematopoietic stem cells.," *Science*, vol. 241, no. 4861, pp. 58–62, Jul. 1988.

[11] M. J. Kiel, Ö. H. Yilmaz, T. Iwashita, O. H. Yilmaz, C. Terhorst, and S. J. Morrison, "SLAM Family Receptors Distinguish Hematopoietic Stem and Progenitor Cells and Reveal Endothelial Niches for Stem Cells," *Cell*, vol. 121, no. 7, pp. 1109–1121, Jul. 2005.

[12] A. Larochelle *et al.*, "Human and rhesus macaque hematopoietic stem cells cannot be purified based only on SLAM family markers," *Blood*, vol. 117, no. 5, pp. 1550–1554, Feb. 2011.

[13] H. J. Sutherland, C. J. Eaves, A. C. Eaves, W. Dragowska, and P. M. Lansdorp, "Characterization and partial purification of human marrow cells capable of initiating long-term hematopoiesis in vitro.," *Blood*, vol. 74, no. 5, pp. 1563–70, Oct. 1989.

[14] Q. L. Hao, F. T. Thiemann, D. Petersen, E. M. Smogorzewska, and G. M. Crooks, "Extended long-term culture reveals a highly quiescent and primitive human hematopoietic progenitor population.," *Blood*, vol. 88, no. 9, pp. 3306–13, Nov. 1996.

[15] J. M. McCune, R. Namikawa, H. Kaneshima, L. D. Shultz, M. Lieberman, and I. L. Weissman, "The SCID-hu mouse: murine model for the analysis of human hematolymphoid differentiation and function.," *Science*, vol. 241, no. 4873, pp. 1632–9, Sep. 1988.

[16] M. Bhatia, J. C. Wang, U. Kapp, D. Bonnet, and J. E. Dick, "Purification of primitive human

hematopoietic cells capable of repopulating immune-deficient mice.," *Proc. Natl. Acad. Sci. U. S. A.*, vol. 94, no. 10, pp. 5320–5, May 1997.

[17] R. Majeti, C. Y. Park, and I. L. Weissman, "Identification of a hierarchy of multipotent hematopoietic progenitors in human cord blood.," *Cell Stem Cell*, vol. 1, no. 6, pp. 635–45, Dec. 2007.

[18] N. N. Iscove and K. Nawa, "Hematopoietic stem cells expand during serial transplantation in vivo without apparent exhaustion.," *Curr. Biol.*, vol. 7, no. 10, pp. 805–8, Oct. 1997.

[19] J. E. Till, E. A. McCulloch, and L. Siminovitch, "A stochastic model of stem cell proliferation, based on the growth of spleen colony-forming cells.," *Proc. Natl. Acad. Sci. U. S. A.*, vol. 51, pp. 29–36, Jan. 1964.

[20] K. Akashi, D. Traver, T. Miyamoto, and I. L. Weissman, "A clonogenic common myeloid progenitor that gives rise to all myeloid lineages," *Nature*, vol. 404, no. 6774, pp. 193–197, Mar. 2000.

[21] R. E. Mebius *et al.*, "The fetal liver counterpart of adult common lymphoid progenitors gives rise to all lymphoid lineages, CD45+CD4+CD3- cells, as well as macrophages.," *J. Immunol.*, vol. 166, no. 11, pp. 6593–601, Jun. 2001.

[22] H. Kawamoto, K. Ohmura, and Y. Katsura, "Direct evidence for the commitment of hematopoietic stem cells to T, B and myeloid lineages in murine fetal liver.," *Int. Immunol.*, vol. 9, no. 7, pp. 1011–9, Jul. 1997.

[23] J. Adolfsson *et al.*, "Identification of Flt3+ Lympho-Myeloid Stem Cells Lacking Erythro-Megakaryocytic Potential," *Cell*, vol. 121, no. 2, pp. 295–306, Apr. 2005.

[24] F. Notta *et al.*, "Distinct routes of lineage development reshape the human blood hierarchy across ontogeny.," *Science*, vol. 351, no. 6269, p. aab2116, Jan. 2016.

[25] H. Döhner *et al.*, "Diagnosis and management of acute myeloid leukemia in adults: recommendations from an international expert panel, on behalf of the European LeukemiaNet.," *Blood*, vol. 115, no. 3, pp. 453–74, Jan. 2010.

[26] J. W. Vardiman *et al.*, "The 2008 revision of the World Health Organization (WHO) classification of myeloid neoplasms and acute leukemia: rationale and important changes," *Blood*, vol. 114, no. 5, pp. 937–951, Jul. 2009.

[27] D. A. Arber *et al.*, "The 2016 revision to the World Health Organization classification of myeloid neoplasms and acute leukemia.," *Blood*, vol. 127, no. 20, pp. 2391–405, May 2016.

[28] K. Mrózek *et al.*, "Prognostic Significance of the European LeukemiaNet Standardized System for Reporting Cytogenetic and Molecular Alterations in Adults With Acute Myeloid Leukemia," *J. Clin. Oncol.*, vol. 30, no. 36, pp. 4515–4523, Dec. 2012.

[29] E. H. Estey, "Acute myeloid leukemia: 2014 Update on risk-stratification and management," *Am. J. Hematol.*, vol. 89, no. 11, pp. 1063–1081, Nov. 2014.

[30] H. Döhner, D. J. Weisdorf, and C. D. Bloomfield, "Acute Myeloid Leukemia," *N. Engl. J. Med.*, vol. 373, no. 12, pp. 1136–1152, Sep. 2015.

[31] T. Büchner *et al.*, "Acute Myeloid Leukemia (AML): Different Treatment Strategies Versus a Common Standard Arm—Combined Prospective Analysis by the German AML Intergroup," *J.*

Clin. Oncol., vol. 30, no. 29, pp. 3604–3610, Oct. 2012.

[32] R. A. Larson, K. Kondo, J. W. Vardiman, A. E. Butler, H. M. Golomb, and J. D. Rowley, "Evidence for a 15;17 translocation in every patient with acute promyelocytic leukemia.," *Am. J. Med.*, vol. 76, no. 5, pp. 827–41, May 1984.

[33] F. Grignani *et al.*, "The acute promyelocytic leukemia-specific PML-RAR alpha fusion protein inhibits differentiation and promotes survival of myeloid precursor cells.," *Cell*, vol. 74, no. 3, pp. 423–31, Aug. 1993.

[34] J. Bernard, M. Weil, M. Boiron, C. Jacquillat, G. Flandrin, and M. F. Gemon, "Acute promyelocytic leukemia: results of treatment by daunorubicin.," *Blood*, vol. 41, no. 4, pp. 489–96, Apr. 1973.

[35] M. E. Huang *et al.*, "Use of all-trans retinoic acid in the treatment of acute promyelocytic leukemia.," *Blood*, vol. 72, no. 2, pp. 567–72, Aug. 1988.

[36] P. Fenaux *et al.*, "A randomized comparison of all transretinoic acid (ATRA) followed by chemotherapy and ATRA plus chemotherapy and the role of maintenance therapy in newly diagnosed acute promyelocytic leukemia. The European APL Group.," *Blood*, vol. 94, no. 4, pp. 1192–200, Aug. 1999.

[37] Cancer Genome Atlas Research Network *et al.*, "Genomic and Epigenomic Landscapes of Adult De Novo Acute Myeloid Leukemia," *N. Engl. J. Med.*, vol. 368, no. 22, pp. 2059–2074, May 2013.

[38] R. M. Stone *et al.*, "Phase IB study of the FLT3 kinase inhibitor midostaurin with chemotherapy in younger newly diagnosed adult patients with acute myeloid leukemia," *Leukemia*, vol. 26, no. 9, pp. 2061–2068, Sep. 2012.

[39] K. W. Pratz *et al.*, "A pharmacodynamic study of sorafenib in patients with relapsed and refractory acute leukemias," *Leukemia*, vol. 24, no. 8, pp. 1437–1444, Aug. 2010.

[40] A.-M. O'Farrell *et al.*, "An innovative phase I clinical study demonstrates inhibition of FLT3 phosphorylation by SU11248 in acute myeloid leukemia patients.," *Clin. Cancer Res.*, vol. 9, no. 15, pp. 5465–76, Nov. 2003.

[41] C. Röllig *et al.*, "Sorafenib Versus Placebo in Addition to Standard Therapy in Younger Patients with Newly Diagnosed Acute Myeloid Leukemia: Results from 267 Patients Treated in the Randomized Placebo-Controlled SAL-Soraml Trial," *Blood*, vol. 124, no. 21, 2014.

[42] R. M. Stone *et al.*, "Patients with acute myeloid leukemia and an activating mutation in FLT3 respond to a small-molecule FLT3 tyrosine kinase inhibitor, PKC412," *Blood*, vol. 105, no. 1, pp. 54–60, Jan. 2005.

[43] R. M. Stone *et al.*, "Midostaurin plus Chemotherapy for Acute Myeloid Leukemia with a *FLT3* Mutation," *N. Engl. J. Med.*, vol. 377, no. 5, pp. 454–464, Aug. 2017.

[44] M. J. Levis *et al.*, "Final Results of a Phase 2 Open-Label, Monotherapy Efficacy and Safety Study of Quizartinib (AC220) in Patients with FLT3-ITD Positive or Negative Relapsed/Refractory Acute Myeloid Leukemia After Second-Line Chemotherapy or Hematopoietic Stem Cell Transp…," *Blood*, vol. 120, no. 21, 2012.

[45] C. C. Smith *et al.*, "Crenolanib is a selective type I pan-FLT3 inhibitor," *Proc. Natl. Acad. Sci.*, vol. 111, no. 14, pp. 5319–5324, Apr. 2014.

[46] F. Wang *et al.*, “Targeted Inhibition of Mutant IDH2 in Leukemia Cells Induces Cellular Differentiation,” *Science (80-.).*, vol. 340, no. 6132, pp. 622–626, May 2013.

[47] S. H. Petersdorf *et al.*, “A phase 3 study of gemtuzumab ozogamicin during induction and postconsolidation therapy in younger patients with acute myeloid leukemia,” *Blood*, vol. 121, no. 24, pp. 4854–4860, Jun. 2013.

[48] R. K. Hills *et al.*, “Addition of gemtuzumab ozogamicin to induction chemotherapy in adult patients with acute myeloid leukaemia: a meta-analysis of individual patient data from randomised controlled trials,” *Lancet Oncol.*, vol. 15, no. 9, pp. 986–996, Aug. 2014.

[49] S. S. Kenderian *et al.*, “CD33-specific chimeric antigen receptor T cells exhibit potent preclinical activity against human acute myeloid leukemia,” *Leukemia*, vol. 29, no. 8, pp. 1637–1647, Aug. 2015.

[50] R. C. Lynn *et al.*, “Targeting of folate receptor on acute myeloid leukemia blasts with chimeric antigen receptor-expressing T cells,” *Blood*, vol. 125, no. 22, pp. 3466–3476, May 2015.

[51] C. Schindler, K. Shuai, V. Prezioso, and J. Darnell, “Interferon-dependent tyrosine phosphorylation of a latent cytoplasmic transcription factor,” *Science (80-.).*, vol. 257, no. 5071, pp. 809–813, Aug. 1992.

[52] K. Shuai, C. M. Horvath, L. H. T. Huang, S. A. Qureshi, D. Cowburn, and J. E. Darnell, “Interferon activation of the transcription factor Stat91 involves dimerization through SH2-phosphotyrosyl peptide interactions,” *Cell*, vol. 76, no. 5, pp. 821–828, Mar. 1994.

[53] Z. Zhong, Z. Wen, and J. E. Darnell, “Stat3: a STAT family member activated by tyrosine phosphorylation in response to epidermal growth factor and interleukin-6.,” *Science*, vol. 264, no. 5155, pp. 95–8, Apr. 1994.

[54] Z. Zhong, Z. Wen, and J. E. Darnell, “Stat3 and Stat4: members of the family of signal transducers and activators of transcription.,” *Proc. Natl. Acad. Sci. U. S. A.*, vol. 91, no. 11, pp. 4806–10, May 1994.

[55] A. L. Mui, H. Wakao, A. M. O’Farrell, N. Harada, and A. Miyajima, “Interleukin-3, granulocyte-macrophage colony stimulating factor and interleukin-5 transduce signals through two STAT5 homologs.,” *EMBO J.*, vol. 14, no. 6, pp. 1166–75, Mar. 1995.

[56] X. Liu, G. W. Robinson, F. Gouilleux, B. Groner, and L. Hennighausen, “Cloning and expression of Stat5 and an additional homologue (Stat5b) involved in prolactin signal transduction in mouse mammary tissue.,” *Proc. Natl. Acad. Sci. U. S. A.*, vol. 92, no. 19, pp. 8831–5, Sep. 1995.

[57] J. Hou, U. Schindler, W. J. Henzel, T. C. Ho, M. Brasseur, and S. L. McKnight, “An interleukin-4-induced transcription factor: IL-4 Stat.,” *Science*, vol. 265, no. 5179, pp. 1701–6, Sep. 1994.

[58] M. Azam *et al.*, “Interleukin-3 signals through multiple isoforms of Stat5.,” *EMBO J.*, vol. 14, no. 7, pp. 1402–11, Apr. 1995.

[59] N. G. Copeland *et al.*, “Distribution of the mammalian Stat gene family in mouse chromosomes.,” *Genomics*, vol. 29, no. 1, pp. 225–8, Sep. 1995.

[60] J. X. Lin, J. Mietz, W. S. Modi, S. John, and W. J. Leonard, “Cloning of human Stat5B. Reconstitution of interleukin-2-induced Stat5A and Stat5B DNA binding activity in COS-7 cells.,” *J. Biol. Chem.*, vol. 271, no. 18, pp. 10738–44, May 1996.

[61] X. Liu, G. W. Robinson, K. U. Wagner, L. Garrett, A. Wynshaw-Boris, and L. Hennighausen, “Stat5a is mandatory for adult mammary gland development and lactogenesis.,” *Genes Dev.*, vol. 11, no. 2, pp. 179–86, Jan. 1997.

[62] G. B. Udy *et al.*, “Requirement of STAT5b for sexual dimorphism of body growth rates and liver gene expression.,” *Proc. Natl. Acad. Sci. U. S. A.*, vol. 94, no. 14, pp. 7239–44, Jul. 1997.

[63] F. Gouilleux, H. Wakao, M. Mundt, and B. Groner, “Prolactin induces phosphorylation of Tyr694 of Stat5 (MGF), a prerequisite for DNA binding and induction of transcription.,” *EMBO J.*, vol. 13, no. 18, pp. 4361–9, Sep. 1994.

[64] M. Onishi *et al.*, “Identification and characterization of a constitutively active STAT5 mutant that promotes cell proliferation.,” *Mol. Cell. Biol.*, vol. 18, no. 7, pp. 3871–9, Jul. 1998.

[65] T. Nosaka, T. Kawashima, K. Misawa, K. Ikuta, A. L. Mui, and T. Kitamura, “STAT5 as a molecular regulator of proliferation, differentiation and apoptosis in hematopoietic cells,” *EMBO J.*, vol. 18, no. 17, pp. 4754–4765, Sep. 1999.

[66] S. John, U. Vinkemeier, E. Soldaini, J. E. Darnell, and W. J. Leonard, “The significance of tetramerization in promoter recruitment by Stat5.,” *Mol. Cell. Biol.*, vol. 19, no. 3, pp. 1910–8, Mar. 1999.

[67] E. Soldaini, S. John, S. Moro, J. Bollenbacher, U. Schindler, and W. J. Leonard, “DNA binding site selection of dimeric and tetrameric Stat5 proteins reveals a large repertoire of divergent tetrameric Stat5a binding sites.,” *Mol. Cell. Biol.*, vol. 20, no. 1, pp. 389–401, Jan. 2000.

[68] R. Moriggl *et al.*, “Stat5 tetramer formation is associated with leukemogenesis.,” *Cancer Cell*, vol. 7, no. 1, pp. 87–99, Jan. 2005.

[69] R. A. Kirken *et al.*, “Two discrete regions of interleukin-2 (IL2) receptor beta independently mediate IL2 activation of a PD98059/rapamycin/wortmannin-insensitive Stat5a/b serine kinase.,” *J. Biol. Chem.*, vol. 272, no. 24, pp. 15459–65, Jun. 1997.

[70] H. Yamashita, J. Xu, R. A. Erwin, W. L. Farrar, R. A. Kirken, and H. Rui, “Differential control of the phosphorylation state of proline-juxtaposed serine residues Ser725 of Stat5a and Ser730 of Stat5b in prolactin-sensitive cells.,” *J. Biol. Chem.*, vol. 273, no. 46, pp. 30218–24, Nov. 1998.

[71] A. Berger *et al.*, “PAK-dependent STAT5 serine phosphorylation is required for BCR-ABL-induced leukemogenesis.,” *Leukemia*, vol. 28, no. 3, pp. 629–41, Mar. 2014.

[72] K. Friedbichler *et al.*, “Stat5a serine 725 and 779 phosphorylation is a prerequisite for hematopoietic transformation,” *Blood*, vol. 116, no. 9, pp. 1548–1558, Sep. 2010.

[73] L. Ma *et al.*, “Acetylation modulates prolactin receptor dimerization,” *Proc. Natl. Acad. Sci.*, vol. 107, no. 45, pp. 19314–19319, Nov. 2010.

[74] U. H. Beier, L. Wang, and W. W. Hancock, “Combination of isoform-selective histone/protein deacetylase inhibitors improves Foxp3+ T-regulatory cell function,” *Cell Cycle*, vol. 11, no. 18, pp. 3351–3352, Sep. 2012.

[75] S. Pinz, S. Unser, D. Buob, P. Fischer, B. Jobst, and A. Rascle, “Deacetylase inhibitors repress STAT5-mediated transcription by interfering with bromodomain and extra-terminal (BET) protein function.,” *Nucleic Acids Res.*, vol. 43, no. 7, pp. 3524–45, Apr. 2015.

[76] T. Van Nguyen *et al.*, “SUMO-Specific Protease 1 Is Critical for Early Lymphoid Development through Regulation of STAT5 Activation,” *Mol. Cell*, vol. 45, no. 2, pp. 210–221, Jan. 2012.

[77] R. Geiss-Friedlander and F. Melchior, “Concepts in sumoylation: a decade on,” *Nat. Rev. Mol. Cell Biol.*, vol. 8, no. 12, pp. 947–956, Dec. 2007.

[78] C. Küçük *et al.*, “Activating mutations of STAT5B and STAT3 in lymphomas derived from γδ-T or NK cells,” *Nat. Commun.*, vol. 6, no. 1, p. 6025, Dec. 2015.

[79] P. Freund *et al.*, “O-GlcNAcylation of STAT5 controls tyrosine phosphorylation and oncogenic transcription in STAT5-dependent malignancies,” *Leukemia*, vol. 31, no. 10, pp. 2132–2142, Oct. 2017.

[80] Y. Cui *et al.*, “Inactivation of Stat5 in Mouse Mammary Epithelium during Pregnancy Reveals Distinct Functions in Cell Proliferation, Survival, and Differentiation,” *Mol. Cell. Biol.*, vol. 24, no. 18, pp. 8037–8047, Sep. 2004.

[81] A. Hoelbl *et al.*, “Clarifying the role of Stat5 in lymphoid development and Abelson-induced transformation,” *Blood*, vol. 107, no. 12, pp. 4898–4906, Jun. 2006.

[82] Z. Yao *et al.*, “Nonredundant roles for Stat5a/b in directly regulating Foxp3,” *Blood*, vol. 109, no. 10, pp. 4368–4375, May 2007.

[83] K. D. Bunting, H. L. Bradley, T. S. Hawley, R. Moriggl, B. P. Sorrentino, and J. N. Ihle, “Reduced lymphomyeloid repopulating activity from adult bone marrow and fetal liver of mice lacking expression of STAT5.,” *Blood*, vol. 99, no. 2, pp. 479–87, Jan. 2002.

[84] G. Li *et al.*, “STAT5 requires the N-domain to maintain hematopoietic stem cell repopulating function and appropriate lymphoid-myeloid lineage output,” *Exp. Hematol.*, vol. 35, no. 11, pp. 1684–1694, Nov. 2007.

[85] Z. Wang, G. Li, W. Tse, and K. D. Bunting, “Conditional deletion of STAT5 in adult mouse hematopoietic stem cells causes loss of quiescence and permits efficient nonablative stem cell replacement,” *Blood*, vol. 113, no. 20, pp. 4856–4865, May 2009.

[86] Y. Kato *et al.*, “Selective activation of STAT5 unveils its role in stem cell self-renewal in normal and leukemic hematopoiesis.,” *J. Exp. Med.*, vol. 202, no. 1, pp. 169–179, 2005.

[87] Y. Cui *et al.*, “Loss of signal transducer and activator of transcription 5 leads to hepatosteatosis and impaired liver regeneration,” *Hepatology*, vol. 46, no. 2, pp. 504–513, Aug. 2007.

[88] S. Teglund *et al.*, “Stat5a and Stat5b proteins have essential and nonessential, or redundant, roles in cytokine responses.,” *Cell*, vol. 93, no. 5, pp. 841–50, May 1998.

[89] J. Woelfle, J. Billiard, and P. Rotwein, “Acute Control of Insulin-like Growth Factor-I Gene Transcription by Growth Hormone through Stat5b,” *J. Biol. Chem.*, vol. 278, no. 25, pp. 22696–22702, Jun. 2003.

[90] E. M. Kofoed *et al.*, “Growth Hormone Insensitivity Associated with a *STAT5b* Mutation,” *N. Engl. J. Med.*, vol. 349, no. 12, pp. 1139–1147, Sep. 2003.

[91] D. Gotthardt *et al.*, “STAT5 Is a Key Regulator in NK Cells and Acts as a Molecular Switch from Tumor Surveillance to Tumor Promotion.,” *Cancer Discov.*, vol. 6, no. 4, pp. 414–29, Apr. 2016.

[92] K. Schönberg *et al.*, “JAK Inhibition Impairs NK Cell Function in Myeloproliferative

Neoplasms.," *Cancer Res.*, vol. 75, no. 11, pp. 2187–99, Jun. 2015.

[93] A. C. Cohen *et al.*, "Cutting edge: Decreased accumulation and regulatory function of CD4+ CD25(high) T cells in human STAT5b deficiency.," *J. Immunol.*, vol. 177, no. 5, pp. 2770–4, Sep. 2006.

[94] A. Bernasconi *et al.*, "Characterization of Immunodeficiency in a Patient With Growth Hormone Insensitivity Secondary to a Novel STAT5b Gene Mutation," *Pediatrics*, vol. 118, no. 5, pp. e1584–e1592, Nov. 2006.

[95] S. Zhang *et al.*, "Essential role of signal transducer and activator of transcription (Stat)5a but not Stat5b for Flt3-dependent signaling.," *J. Exp. Med.*, vol. 192, no. 5, pp. 719–28, Sep. 2000.

[96] S. Fatrai, A. T. J. Wierenga, S. M. G. J. Daenen, E. Vellenga, and J. J. Schuringa, "Identification of HIF2 as an important STAT5 target gene in human hematopoietic stem cells," *Blood*, vol. 117, no. 12, pp. 3320–3330, Mar. 2011.

[97] B. Basham *et al.*, "In vivo identification of novel STAT5 target genes," *Nucleic Acids Res.*, vol. 36, no. 11, pp. 3802–3818, May 2008.

[98] A. Nanou *et al.*, "The dual role of LSD1 and HDAC3 in STAT5-dependent transcription is determined by protein interactions, binding affinities, motifs and genomic positions," *Nucleic Acids Res.*, vol. 45, no. 1, pp. 142–154, Jan. 2017.

[99] K. Kang, D. Yamaji, K. H. Yoo, G. W. Robinson, and L. Hennighausen, "Mammary-Specific Gene Activation Is Defined by Progressive Recruitment of STAT5 during Pregnancy and the Establishment of H3K4me3 Marks," *Mol. Cell. Biol.*, vol. 34, no. 3, pp. 464–473, Feb. 2014.

[100] W. Liao, J.-X. Lin, L. Wang, P. Li, and W. J. Leonard, "Modulation of cytokine receptors by IL-2 broadly regulates differentiation into helper T cell lineages," *Nat. Immunol.*, vol. 12, no. 6, pp. 551–559, Jun. 2011.

[101] Y. Zhang, E. V. Laz, and D. J. Waxman, "Dynamic, Sex-Differential STAT5 and BCL6 Binding to Sex-Biased, Growth Hormone-Regulated Genes in Adult Mouse Liver," *Mol. Cell. Biol.*, vol. 32, no. 4, pp. 880–896, Feb. 2012.

[102] X. Zeng, M. Willi, H. Y. Shin, L. Hennighausen, and C. Wang, "Lineage-Specific and Non-specific Cytokine-Sensing Genes Respond Differentially to the Master Regulator STAT5," *Cell Rep.*, vol. 17, no. 12, pp. 3333–3346, Dec. 2016.

[103] D. Neculai *et al.*, "Structure of the Unphosphorylated STAT5a Dimer," *J. Biol. Chem.*, vol. 280, no. 49, pp. 40782–40787, Dec. 2005.

[104] H. Y. Shin and N. C. Reich, "Dynamic trafficking of STAT5 depends on an unconventional nuclear localization signal.," *J. Cell Sci.*, vol. 126, no. Pt 15, pp. 3333–43, Aug. 2013.

[105] S. Shi *et al.*, "Drosophila STAT is required for directly maintaining HP1 localization and heterochromatin stability.," *Nat. Cell Biol.*, vol. 10, no. 4, pp. 489–496, 2008.

[106] S.-J. Yan, S. J. Lim, S. Shi, P. Dutta, and W. X. Li, "Unphosphorylated STAT and heterochromatin protect genome stability.," *FASEB J.*, vol. 25, pp. 232–241, 2011.

[107] X. Hu *et al.*, "Unphosphorylated STAT5A stabilizes heterochromatin and suppresses tumor growth.," *Proc. Natl. Acad. Sci. U. S. A.*, vol. 110, no. 14, pp. 10213–8, 2013.

[108] M. Mandal *et al.*, "Epigenetic repression of the Igk locus by STAT5-mediated recruitment of

the histone methyltransferase Ezh2," *Nat. Immunol.*, vol. 12, no. 12, pp. 1212–1220, Oct. 2011.

[109] J. E. Lee, Y.-M. Yang, F.-X. Liang, D. J. Gough, D. E. Levy, and P. B. Sehgal, "Nongenomic STAT5-dependent effects on Golgi apparatus and endoplasmic reticulum structure and function," *Am. J. Physiol. Physiol.*, vol. 302, no. 5, pp. C804–C820, Mar. 2012.

[110] C. FENG and S. CAO, "Activation of STAT5 contributes to proliferation in U87 human glioblastoma multiforme cells," *Mol. Med. Rep.*, vol. 10, no. 1, pp. 203–210, Jul. 2014.

[111] S. Xi, Q. Zhang, W. E. Gooding, T. E. Smithgall, and J. R. Grandis, "Constitutive activation of Stat5b contributes to carcinogenesis in vivo.," *Cancer Res.*, vol. 63, no. 20, pp. 6763–71, Oct. 2003.

[112] Q. Yang, M. Li, T. Wang, H. Xu, W. Zang, and G. Zhao, "Effect of STAT5 silenced by siRNA on proliferation apoptosis and invasion of esophageal carcinoma cell line Eca-109," *Diagn. Pathol.*, vol. 8, no. 1, p. 803, Dec. 2013.

[113] I. Matsumura *et al.*, "Transcriptional regulation of the cyclin D1 promoter by STAT5: its involvement in cytokine-dependent growth of hematopoietic cells," *EMBO J.*, vol. 18, no. 5, pp. 1367–1377, Mar. 1999.

[114] A. Slupianek *et al.*, "Fusion tyrosine kinases induce drug resistance by stimulation of homology-dependent recombination repair, prolongation of G(2)/M phase, and protection from apoptosis.," *Mol. Cell. Biol.*, vol. 22, no. 12, pp. 4189–201, Jun. 2002.

[115] S. Dumon *et al.*, "IL-3 dependent regulation of Bcl-xL gene expression by STAT5 in a bone marrow derived cell line," *Oncogene*, vol. 18, no. 29, pp. 4191–4199, Jul. 1999.

[116] H. Xiong *et al.*, "Inhibition of STAT5 induces G1 cell cycle arrest and reduces tumor cell invasion in human colorectal cancer cells," *Lab. Investig.*, vol. 89, no. 6, pp. 717–725, Jun. 2009.

[117] L. Gu *et al.*, "Stat5 promotes metastatic behavior of human prostate cancer cells in vitro and in vivo," *Endocr. Relat. Cancer*, vol. 17, no. 2, pp. 481–493, May 2010.

[118] A. Weber *et al.*, "The Inhibition of Stat5 by a Peptide Aptamer Ligand Specific for the DNA Binding Domain Prevents Target Gene Transactivation and the Growth of Breast and Prostate Tumor Cells," *Pharmaceuticals*, vol. 6, no. 8, pp. 960–987, Aug. 2013.

[119] R. L. Ilaria and R. A. Van Etten, "P210 and P190(BCR/ABL) induce the tyrosine phosphorylation and DNA binding activity of multiple specific STAT family members.," *J. Biol. Chem.*, vol. 271, no. 49, pp. 31704–10, Dec. 1996.

[120] V. Sexl *et al.*, "Stat5a/b contribute to interleukin 7-induced B-cell precursor expansion, but abl- and bcr/abl-induced transformation are independent of stat5.," *Blood*, vol. 96, no. 6, pp. 2277–83, Sep. 2000.

[121] D. Ye, N. Wolff, L. Li, S. Zhang, and R. L. Ilaria, "STAT5 signaling is required for the efficient induction and maintenance of CML in mice," *Blood*, vol. 107, no. 12, pp. 4917–4925, Jun. 2006.

[122] M. Schaller-Schönitz *et al.*, "BCR-ABL Affects STAT5A and STAT5B Differentially," *PLoS One*, vol. 9, no. 5, p. e97243, May 2014.

[123] A. Weber *et al.*, “Stat5 Exerts Distinct, Vital Functions in the Cytoplasm and Nucleus of Bcr-Abl+ K562 and Jak2(V617F)+ HEL Leukemia Cells.,” *Cancers (Basel).*, vol. 7, no. 1, pp. 503–37, Mar. 2015.

[124] M. Nakao *et al.*, “Internal tandem duplication of the flt3 gene found in acute myeloid leukemia.,” *Leukemia*, vol. 10, no. 12, pp. 1911–8, Dec. 1996.

[125] M. Funakoshi-Tago, K. Tago, M. Abe, Y. Sonoda, and T. Kasahara, “STAT5 Activation Is Critical for the Transformation Mediated by Myeloproliferative Disorder-associated JAK2 V617F Mutant,” *J. Biol. Chem.*, vol. 285, no. 8, pp. 5296–5307, Feb. 2010.

[126] C. Walz *et al.*, “Essential role for Stat5a/b in myeloproliferative neoplasms induced by BCR-ABL1 and JAK2V617F in mice,” *Blood*, vol. 119, no. 15, pp. 3550–3560, Apr. 2012.

[127] J. Schwaller *et al.*, “Stat5 is essential for the myelo- and lymphoproliferative disease induced by TEL/JAK2.,” *Mol. Cell*, vol. 6, no. 3, pp. 693–704, Sep. 2000.

[128] O. Hantschel *et al.*, “BCR-ABL uncouples canonical JAK2-STAT5 signaling in chronic myeloid leukemia,” *Nat. Chem. Biol.*, vol. 8, no. 3, pp. 285–293, Mar. 2012.

[129] W. Warsch *et al.*, “STAT5 triggers BCR-ABL1 mutation by mediating ROS production in chronic myeloid leukaemia,” *Oncotarget*, vol. 3, no. 12, pp. 1669–87, Dec. 2012.

[130] J. E. Ferrell, “Bistability, Bifurcations, and Waddington’s Epigenetic Landscape,” *Curr. Biol.*, vol. 22, no. 11, pp. R458–R466, Jun. 2012.

[131] P. A. Jones, “Functions of DNA methylation: islands, start sites, gene bodies and beyond,” *Nat. Rev. Genet.*, vol. 13, no. 7, pp. 484–492, Jul. 2012.

[132] A. Bird, “DNA methylation patterns and epigenetic memory.,” *Genes Dev.*, vol. 16, no. 1, pp. 6–21, Jan. 2002.

[133] O. Abdel-Wahab and R. L. Levine, “Mutations in epigenetic modifiers in the pathogenesis and therapy of acute myeloid leukemia,” *Blood*, vol. 121, no. 18, pp. 3563–3572, May 2013.

[134] M. J. Walter *et al.*, “Recurrent DNMT3A mutations in patients with myelodysplastic syndromes,” *Leukemia*, vol. 25, no. 7, pp. 1153–1158, Jul. 2011.

[135] T. J. Ley *et al.*, “*DNMT3A* Mutations in Acute Myeloid Leukemia,” *N. Engl. J. Med.*, vol. 363, no. 25, pp. 2424–2433, Dec. 2010.

[136] L. I. Shlush *et al.*, “Identification of pre-leukaemic haematopoietic stem cells in acute leukaemia,” *Nature*, vol. 506, no. 7488, pp. 328–333, Feb. 2014.

[137] C. Quivoron *et al.*, “TET2 Inactivation Results in Pleiotropic Hematopoietic Abnormalities in Mouse and Is a Recurrent Event during Human Lymphomagenesis,” *Cancer Cell*, vol. 20, no. 1, pp. 25–38, Jul. 2011.

[138] A. H. Shih, O. Abdel-Wahab, J. P. Patel, and R. L. Levine, “The role of mutations in epigenetic regulators in myeloid malignancies,” *Nat. Rev. Cancer*, vol. 12, no. 9, pp. 599–612, Sep. 2012.

[139] McGraw-Hill, *McGraw-Hill encyclopedia of science and technology.* McGraw-Hill, 1997.

[140] M. a. Dawson and T. Kouzarides, “Cancer epigenetics: From mechanism to therapy,” *Cell*, vol. 150, no. 1, pp. 12–27, 2012.

[141] T. Kouzarides, “Chromatin modifications and their function.,” *Cell*, vol. 128, no. 4, pp. 693–705, Feb. 2007.

[142] M. G. Guenther, S. S. Levine, L. A. Boyer, R. Jaenisch, and R. A. Young, “A chromatin landmark and transcription initiation at most promoters in human cells.,” *Cell*, vol. 130, no. 1, pp. 77–88, Jul. 2007.

[143] B. E. Bernstein *et al.*, “Methylation of histone H3 Lys 4 in coding regions of active genes.,” *Proc. Natl. Acad. Sci. U. S. A.*, vol. 99, no. 13, pp. 8695–700, Jun. 2002.

[144] H. Santos-Rosa *et al.*, “Active genes are tri-methylated at K4 of histone H3,” *Nature*, vol. 419, no. 6905, pp. 407–411, Sep. 2002.

[145] S. D. Briggs *et al.*, “Histone H3 lysine 4 methylation is mediated by Set1 and required for cell growth and rDNA silencing in Saccharomyces cerevisiae,” *Genes Dev.*, vol. 15, no. 24, pp. 3286–3295, Dec. 2001.

[146] H. H. Ng, F. Robert, R. A. Young, and K. Struhl, “Targeted recruitment of Set1 histone methylase by elongating Pol II provides a localized mark and memory of recent transcriptional activity.,” *Mol. Cell*, vol. 11, no. 3, pp. 709–19, Mar. 2003.

[147] B. E. Bernstein *et al.*, “A Bivalent Chromatin Structure Marks Key Developmental Genes in Embryonic Stem Cells,” *Cell*, vol. 125, no. 2, pp. 315–326, Apr. 2006.

[148] S. Rea *et al.*, “Regulation of chromatin structure by site-specific histone H3 methyltransferases,” *Nature*, vol. 406, no. 6796, pp. 593–599, Aug. 2000.

[149] L. Aagaard *et al.*, “Functional mammalian homologues of the Drosophila PEV-modifier Su(var)3-9 encode centromere-associated proteins which complex with the heterochromatin component M31,” *EMBO J.*, vol. 18, no. 7, pp. 1923–1938, Apr. 1999.

[150] A. J. Bannister *et al.*, “Selective recognition of methylated lysine 9 on histone H3 by the HP1 chromo domain,” *Nature*, vol. 410, no. 6824, pp. 120–124, Mar. 2001.

[151] X. Hu *et al.*, “Unphosphorylated STAT5A stabilizes heterochromatin and suppresses tumor growth,” *Proc. Natl. Acad. Sci.*, vol. 110, no. 25, pp. 10213–10218, Jun. 2013.

[152] C. R. Vakoc, S. A. Mandat, B. A. Olenchock, and G. A. Blobel, “Histone H3 Lysine 9 Methylation and HP1γ Are Associated with Transcription Elongation through Mammalian Chromatin,” *Mol. Cell*, vol. 19, no. 3, pp. 381–391, Aug. 2005.

[153] E. Metzger *et al.*, “LSD1 demethylates repressive histone marks to promote androgen-receptor-dependent transcription,” *Nature*, vol. 437, no. 7057, pp. 436–439, Sep. 2005.

[154] L. Berglund *et al.*, “A Genecentric Human Protein Atlas for Expression Profiles Based on Antibodies,” *Mol. Cell. Proteomics*, vol. 7, no. 10, pp. 2019–2027, Oct. 2008.

[155] S. Hayami *et al.*, “Overexpression of LSD1 contributes to human carcinogenesis through chromatin regulation in various cancers,” *Int. J. Cancer*, vol. 128, no. 3, pp. 574–586, Feb. 2011.

[156] D. Niebel, J. Kirfel, V. Janzen, T. Höller, M. Majores, and I. Gütgemann, “Lysine-specific demethylase 1 (LSD1) in hematopoietic and lymphoid neoplasms.,” *Blood*, vol. 124, no. 1, pp. 151–2, Jul. 2014.

[157] P. Pozarowski and Z. Darzynkiewicz, “Analysis of cell cycle by flow cytometry.,” *Methods Mol.*

Biol., vol. 281, pp. 301–311, 2004.

[158] K. J. Livak and T. D. Schmittgen, “Analysis of Relative Gene Expression Data Using Real-Time Quantitative PCR and the 2−ΔΔCT Method,” *Methods*, vol. 25, no. 4, pp. 402–408, Dec. 2001.

[159] D. Wiederschain *et al.*, “Single-vector inducible lentiviral RNAi system for oncology target validation,” *Cell Cycle*, vol. 8, no. 3, pp. 498–504, Feb. 2009.

[160] A. Kimura *et al.*, “The transcription factors STAT5A/B regulate GM-CSF-mediated granulopoiesis,” *Blood*, vol. 114, no. 21, pp. 4721–4728, Nov. 2009.

[161] E. Cerami *et al.*, “The cBio cancer genomics portal: an open platform for exploring multidimensional cancer genomics data.,” *Cancer Discov.*, vol. 2, no. 5, pp. 401–4, May 2012.

[162] S.-E. Ong and M. Mann, “Stable Isotope Labeling by Amino Acids in Cell Culture for Quantitative Proteomics,” in *Methods in molecular biology (Clifton, N.J.)*, vol. 359, 2007, pp. 37–52.

[163] S.-E. Ong and M. Mann, “A practical recipe for stable isotope labeling by amino acids in cell culture (SILAC),” *Nat. Protoc.*, vol. 1, no. 6, pp. 2650–2660, Jan. 2007.

[164] A. Dobin *et al.*, “STAR: ultrafast universal RNA-seq aligner,” *Bioinformatics*, vol. 29, no. 1, pp. 15–21, Jan. 2013.

[165] V. K. Mootha *et al.*, “PGC-1α-responsive genes involved in oxidative phosphorylation are coordinately downregulated in human diabetes,” *Nat. Genet.*, vol. 34, no. 3, pp. 267–273, Jul. 2003.

[166] A. Subramanian *et al.*, “Gene set enrichment analysis: a knowledge-based approach for interpreting genome-wide expression profiles.,” *Proc. Natl. Acad. Sci. U. S. A.*, vol. 102, pp. 15545–50, 2005.

[167] M. Yoo *et al.*, “DSigDB: Drug signatures database for gene set analysis,” *Bioinformatics*, vol. 31, no. May, pp. 3069–3071, 2015.

[168] J. Lamb *et al.*, “The Connectivity Map : Using Gene-Expression Signatures to Connect Small Molecules, Genes, and Disease,” *Science (80-.).*, vol. 313, no. September, pp. 1929–1935, 2006.

[169] E. G. van Lochem, V. H. J. van der Velden, H. K. Wind, J. G. te Marvelde, N. A. C. Westerdaal, and J. J. M. van Dongen, “Immunophenotypic differentiation patterns of normal hematopoiesis in human bone marrow: Reference patterns for age-related changes and disease-induced shifts,” *Cytometry*, vol. 60B, no. 1, pp. 1–13, Jul. 2004.

[170] J. Wo?niak and J. Kope?-Szl?zak, “C-Kit receptor (CD117) expression on myeloblasts and white blood cell counts in acute myeloid leukemia,” *Cytometry*, vol. 58B, no. 1, pp. 9–16, Mar. 2004.

[171] P. Montesinos *et al.*, “Differentiation syndrome in patients with acute promyelocytic leukemia treated with all-trans retinoic acid and anthracycline chemotherapy: characteristics, outcome, and prognostic factors,” vol. 20.

[172] T. Wang *et al.*, “Gene Essentiality Profiling Reveals Gene Networks and Synthetic Lethal Interactions with Oncogenic Ras,” *Cell*, vol. 168, no. 5, p. 890–903.e15, Feb. 2017.

[173] M. Hamaguchi *et al.*, “DBC2, a candidate for a tumor suppressor gene involved in breast cancer.,” *Proc. Natl. Acad. Sci. U. S. A.*, vol. 99, no. 21, pp. 13647–52, Oct. 2002.

[174] R. Sundararajan, G. Chen, C. Mukherjee, and E. White, “Caspase-dependent processing activates the proapoptotic activity of deleted in breast cancer-1 during tumor necrosis factor-alpha-mediated death signaling,” *Oncogene*, vol. 24, no. 31, pp. 4908–4920, Jul. 2005.

[175] B. Qin *et al.*, “DBC1 Functions as a Tumor Suppressor by Regulating p53 Stability,” *Cell Rep.*, vol. 10, no. 8, pp. 1324–1334, Mar. 2015.

[176] W. Zhao, J.-P. Kruse, Y. Tang, S. Y. Jung, J. Qin, and W. Gu, “Negative regulation of the deacetylase SIRT1 by DBC1,” *Nature*, vol. 451, no. 7178, pp. 587–590, Jan. 2008.

[177] J.-E. Kim, J. Chen, and Z. Lou, “DBC1 is a negative regulator of SIRT1,” *Nature*, vol. 451, no. 7178, pp. 583–586, Jan. 2008.

[178] A. Jacobson and M. Favreau, “Possible involvement of poly(A) in protein synthesis.,” *Nucleic Acids Res.*, vol. 11, no. 18, pp. 6353–68, Sep. 1983.

[179] I. Behm-Ansmant, D. Gatfield, J. Rehwinkel, V. Hilgers, and E. Izaurralde, “A conserved role for cytoplasmic poly(A)-binding protein 1 (PABPC1) in nonsense-mediated mRNA decay.,” *EMBO J.*, vol. 26, no. 6, pp. 1591–601, Mar. 2007.

[180] N. Hosoda, F. Lejeune, and L. E. Maquat, “Evidence that poly(A) binding protein C1 binds nuclear pre-mRNA poly(A) tails.,” *Mol. Cell. Biol.*, vol. 26, no. 8, pp. 3085–97, Apr. 2006.

[181] H. K. Kini, J. Kong, and S. A. Liebhaber, “Cytoplasmic Poly(A) Binding Protein C4 Serves a Critical Role in Erythroid Differentiation,” *Mol. Cell. Biol.*, vol. 34, no. 7, pp. 1300–1309, Apr. 2014.

[182] H. Yang, C. S. Duckett, and T. Lindsten, “iPABP, an inducible poly(A)-binding protein detected in activated human T cells.,” *Mol. Cell. Biol.*, vol. 15, no. 12, pp. 6770–6, Dec. 1995.

[183] A. Tibelius *et al.*, “Microcephalin and pericentrin regulate mitotic entry via centrosome-associated Chk1,” *J. Cell Biol.*, vol. 185, no. 7, pp. 1149–1157, Jun. 2009.

[184] A. Rauch *et al.*, “Mutations in the Pericentrin (PCNT) Gene Cause Primordial Dwarfism,” *Science (80-.).*, vol. 319, no. 5864, pp. 816–819, Feb. 2008.

[185] B. K. Tye, “MCM Proteins in DNA Replication,” *Annu. Rev. Biochem.*, vol. 68, no. 1, pp. 649–686, Jun. 1999.

[186] S. Hutten, A. Flotho, F. Melchior, and R. H. Kehlenbach, “The Nup358-RanGAP Complex Is Required for Efficient Importin / -dependent Nuclear Import,” *Mol. Biol. Cell*, vol. 19, no. 5, pp. 2300–2310, May 2008.

[187] S. Hutten, S. Walde, C. Spillner, J. Hauber, and R. H. Kehlenbach, “The nuclear pore component Nup358 promotes transportin-dependent nuclear import,” *J. Cell Sci.*, vol. 122, no. 8, pp. 1100–1110, Apr. 2009.

[188] R. Bernad, H. van der Velde, M. Fornerod, and H. Pickersgill, “Nup358/RanBP2 attaches to the nuclear pore complex via association with Nup88 and Nup214/CAN and plays a supporting role in CRM1-mediated nuclear protein export.,” *Mol. Cell. Biol.*, vol. 24, no. 6, pp. 2373–84, Mar. 2004.

[189] J. Joseph, S.-T. Liu, S. A. Jablonski, T. J. Yen, and M. Dasso, “The RanGAP1-RanBP2 Complex Is Essential for Microtubule-Kinetochore Interactions In Vivo,” *Curr. Biol.*, vol. 14, no. 7, pp. 611–617, Apr. 2004.

[190] R. D. Kortschak, P. W. Tucker, and R. Saint, “ARID proteins come in from the desert,” *Trends Biochem. Sci.*, vol. 25, no. 6, pp. 294–299, Jun. 2000.

[191] R. J. Klose, E. M. Kallin, and Y. Zhang, “JmjC-domain-containing proteins and histone demethylation,” *Nat. Rev. Genet.*, vol. 7, no. 9, pp. 715–727, Sep. 2006.

[192] S. Iwase *et al.*, “The X-Linked Mental Retardation Gene SMCX/JARID1C Defines a Family of Histone H3 Lysine 4 Demethylases,” *Cell*, vol. 128, no. 6, pp. 1077–1088, Mar. 2007.

[193] L. R. Jensen *et al.*, “Mutations in the JARID1C Gene, Which Is Involved in Transcriptional Regulation and Chromatin Remodeling, Cause X-Linked Mental Retardation,” *Am. J. Hum. Genet.*, vol. 76, no. 2, pp. 227–236, Feb. 2005.

[194] M. Vashishtha *et al.*, “Targeting H3K4 trimethylation in Huntington disease.,” *Proc. Natl. Acad. Sci. U. S. A.*, vol. 110, no. 32, pp. E3027-36, Aug. 2013.

[195] B. Rondinelli *et al.*, “Histone demethylase JARID1C inactivation triggers genomic instability in sporadic renal cancer,” *J. Clin. Invest.*, vol. 125, no. 12, pp. 4625–4637, Nov. 2015.

[196] I. A. Hendriks, L. W. Treffers, M. Verlaan-de Vries, J. V. Olsen, and A. C. O. Vertegaal, “SUMO-2 Orchestrates Chromatin Modifiers in Response to DNA Damage,” *Cell Rep.*, vol. 10, no. 10, pp. 1778–1791, Mar. 2015.

[197] N. S. Outchkourov *et al.*, “Balancing of Histone H3K4 Methylation States by the Kdm5c/SMCX Histone Demethylase Modulates Promoter and Enhancer Function,” *Cell Rep.*, vol. 3, no. 4, pp. 1071–1079, Apr. 2013.

[198] L. C. Wang, F. Kuo, Y. Fujiwara, D. G. Gilliland, T. R. Golub, and S. H. Orkin, “Yolk sac angiogenic defect and intra-embryonic apoptosis in mice lacking the Ets-related factor TEL,” *EMBO J.*, vol. 16, no. 14, pp. 4374–4383, Jul. 1997.

[199] L. C. Wang *et al.*, “The TEL/ETV6 gene is required specifically for hematopoiesis in the bone marrow,” *Genes Dev.*, vol. 12, no. 15, pp. 2392–2402, Aug. 1998.

[200] E. De Braekeleer, N. Douet-Guilbert, F. Morel, M.-J. Le Bris, A. Basinko, and M. De Braekeleer, “ETV6 fusion genes in hematological malignancies: A review,” *Leuk. Res.*, vol. 36, no. 8, pp. 945–961, Aug. 2012.

[201] T. Jaatinen *et al.*, “Global gene expression profile of human cord blood-derived CD133+ cells.,” *Stem Cells*, vol. 24, no. 3, pp. 631–41, Mar. 2006.

[202] B. Schaerlinger, P. Hickel, N. Etienne, L. Guesnier, and L. Maroteaux, “Agonist actions of dihydroergotamine at 5-HT2B and 5-HT2C receptors and their possible relevance to antimigraine efficacy.,” *Br. J. Pharmacol.*, vol. 140, pp. 277–84, 2003.

[203] R. Noiva, “Protein disulfide isomerase: The multifunctional redox chaperone of the endoplasmic reticulum,” *Semin. Cell Dev. Biol.*, vol. 10, no. 5, pp. 481–493, Oct. 1999.

[204] S. Elsasser *et al.*, “Proteasome subunit Rpn1 binds ubiquitin-like protein domains,” *Nat. Cell Biol.*, vol. 4, no. 9, pp. 725–730, Sep. 2002.

[205] R. Rosenzweig, V. Bronner, D. Zhang, D. Fushman, and M. H. Glickman, “Rpn1 and Rpn2 Coordinate Ubiquitin Processing Factors at Proteasome,” *J. Biol. Chem.*, vol. 287, no. 18, pp. 14659–14671, Apr. 2012.

[206] S. Lewis, G. Tian, and N. Cowan, “The α- and β-tubulin folding pathways,” *Trends Cell Biol.*, vol.

7, no. 12, pp. 479–484, Dec. 1997.

[207] G. Tian *et al.*, “Tubulin subunits exist in an activated conformational state generated and maintained by protein cofactors.,” *J. Cell Biol.*, vol. 138, no. 4, pp. 821–32, Aug. 1997.

[208] D. Kortazar *et al.*, “Role of cofactors B (TBCB) and E (TBCE) in tubulin heterodimer dissociation,” *Exp. Cell Res.*, vol. 313, no. 3, pp. 425–436, Feb. 2007.

[209] A. M. Krasinskas, M. A. Wasik, M. Kamoun, R. Schretzenmair, J. Moore, and K. E. Salhany, “The usefulness of CD64, other monocyte-associated antigens, and CD45 gating in the subclassification of acute myeloid leukemias with monocytic differentiation.,” *Am. J. Clin. Pathol.*, vol. 110, no. 6, pp. 797–805, Dec. 1998.

[210] R. F. Todd, L. M. Nadler, and S. F. Schlossman, “Antigens on human monocytes identified by monoclonal antibodies.,” *J. Immunol.*, vol. 126, no. 4, pp. 1435–42, Apr. 1981.

[211] Motorin YuA, A. D. Wolfson, A. F. Orlovsky, and K. L. Gladilin, “Mammalian valyl-tRNA synthetase forms a complex with the first elongation factor.,” *FEBS Lett.*, vol. 238, no. 2, pp. 262–4, Oct. 1988.

[212] F. O. Bagger *et al.*, “BloodSpot: a database of gene expression profiles and transcriptional programs for healthy and malignant haematopoiesis,” *Nucleic Acids Res.*, vol. 44, no. D1, pp. D917–D924, Jan. 2016.

[213] S. R. Frankel, A. Eardley, G. Lauwers, M. Weiss, and R. P. Warrell, “The "Retinoic Acid Syndrome" in Acute Promyelocytic Leukemia,” *Ann. Intern. Med.*, vol. 117, no. 4, p. 292, Aug. 1992.

[214] C. Dubois *et al.*, “Modulation of IL-8, IL-1 beta, and G-CSF secretion by all-trans retinoic acid in acute promyelocytic leukemia.,” *Leukemia*, vol. 8, no. 10, pp. 1750–7, Oct. 1994.

[215] L. Degos and Z. Y. Wang, “All trans retinoic acid in acute promyelocytic leukemia,” *Oncogene*, vol. 20, no. 49, pp. 7140–7145, Oct. 2001.

[216] K. Asano, H. P. Vornlocher, N. J. Richter-Cook, W. C. Merrick, A. G. Hinnebusch, and J. W. Hershey, “Structure of cDNAs encoding human eukaryotic initiation factor 3 subunits. Possible roles in RNA binding and macromolecular assembly.,” *J. Biol. Chem.*, vol. 272, no. 43, pp. 27042–52, Oct. 1997.

[217] R. Pincheira, Q. Chen, and J.-T. Zhang, “Identification of a 170-kDa protein over-expressed in lung cancers,” *Br. J. Cancer*, vol. 84, no. 11, pp. 1520–1527, Jun. 2001.

[218] F. Bachmann, R. Bänziger, and M. M. Burger, “Cloning of a novel protein overexpressed in human mammary carcinoma.,” *Cancer Res.*, vol. 57, no. 5, pp. 988–94, Mar. 1997.

[219] A. Dellas, J. Torhorst, F. Bachmann, R. Bänziger, E. Schultheiss, and M. M. Burger, “Expression of p150 in cervical neoplasia and its potential value in predicting survival,” *Cancer*, vol. 83, no. 7, pp. 1376–1383, Oct. 1998.

[220] L. Zhang, X. Pan, and J. W. B. Hershey, “Individual Overexpression of Five Subunits of Human Translation Initiation Factor eIF3 Promotes Malignant Transformation of Immortal Fibroblast Cells,” *J. Biol. Chem.*, vol. 282, no. 8, pp. 5790–5800, Feb. 2007.

[221] G. Liu *et al.*, “Knockdown of eukaryotic translation initiation factor 3 subunit D (eIF3D) inhibits proliferation of acute myeloid leukemia cells,” *Mol. Cell. Biochem.*, vol. 438, no. 1–2, pp. 191–

198, Jan. 2018.

[222] D. Sasca *et al.*, “SIRT1 prevents genotoxic stress-induced p53 activation in acute myeloid leukemia,” *Blood*, vol. 124, no. 1, pp. 121–133, Jul. 2014.

[223] J. J. Zhang *et al.*, “Ser727-dependent recruitment of MCM5 by Stat1alpha in IFN-gamma-induced transcriptional activation.,” *EMBO J.*, vol. 17, no. 23, pp. 6963–71, Dec. 1998.

[224] C. Zeng, W. Wang, X. Yu, L. Yang, S. Chen, and Y. Li, “Pathways related to PMA-differentiated THP1 human monocytic leukemia cells revealed by RNA-Seq,” *Sci. China Life Sci.*, vol. 58, no. 12, pp. 1282–1287, Dec. 2015.

[225] H. Nishitani, Z. Lygerou, T. Nishimoto, and P. Nurse, “The Cdt1 protein is required to license DNA for replication in fission yeast,” *Nature*, vol. 404, no. 6778, pp. 625–628, Apr. 2000.

[226] J. H. Cocker, S. Piatti, C. Santocanale, K. Nasmyth, and J. F. X. Diffley, “An essential role for the Cdc6 protein in forming the pre-replicative complexes of budding yeast,” *Nature*, vol. 379, no. 6561, pp. 180–182, Jan. 1996.

[227] M. Lei, I. H. Cheng, L. A. Roberts, M. A. McAlear, and B. K. Tye, “Two mcm3 mutations affect different steps in the initiation of DNA replication.,” *J. Biol. Chem.*, vol. 277, no. 34, pp. 30824–31, Aug. 2002.

[228] Z. You, Y. Komamura, and Y. Ishimi, “Biochemical analysis of the intrinsic Mcm4-Mcm6-mcm7 DNA helicase activity.,” *Mol. Cell. Biol.*, vol. 19, no. 12, pp. 8003–15, Dec. 1999.

[229] B. Durand, F. B. Gao, and M. Raff, “Accumulation of the cyclin-dependent kinase inhibitor p27/Kip1 and the timing of oligodendrocyte differentiation,” *EMBO J.*, vol. 16, no. 2, pp. 306–317, Jan. 1997.

[230] M. L. Fero *et al.*, “A Syndrome of Multiorgan Hyperplasia with Features of Gigantism, Tumorigenesis, and Female Sterility in p27Kip1-Deficient Mice,” *Cell*, vol. 85, no. 5, pp. 733–744, May 1996.

[231] A. Dimberg, F. Bahram, I. Karlberg, L.-G. Larsson, K. Nilsson, and F. Oberg, “Retinoic acid-induced cell cycle arrest of human myeloid cell lines is associated with sequential down-regulation of c-Myc and cyclin E and posttranscriptional up-regulation of p27(Kip1).,” *Blood*, vol. 99, no. 6, pp. 2199–206, Mar. 2002.

[232] A. P. Feinberg, M. A. Koldobskiy, and A. Göndör, “Epigenetic modulators, modifiers and mediators in cancer aetiology and progression,” *Nat. Rev. Genet.*, vol. 17, no. 5, pp. 284–299, May 2016.

[233] W. A. Whyte *et al.*, “Enhancer decommissioning by LSD1 during embryonic stem cell differentiation,” *Nature*, Feb. 2012.

[234] J. Fang *et al.*, “Upregulation of CD11b and CD86 through LSD1 inhibition promotes myeloid differentiation and suppresses cell proliferation in human monocytic leukemia cells.,” *Oncotarget*, vol. 8, no. 49, pp. 85085–85101, Oct. 2017.

[235] G. L. Dalgliesh *et al.*, “Systematic sequencing of renal carcinoma reveals inactivation of histone modifying genes,” *Nature*, vol. 463, no. 7279, pp. 360–363, Jan. 2010.

[236] Z. Liang, M. Diamond, J. A. Smith, M. Schnell, and R. Daniel, “Proliferating cell nuclear antigen is required for loading of the SMCX/KMD5C histone demethylase onto chromatin,”

Epigenetics Chromatin, vol. 4, no. 1, p. 18, Oct. 2011.

[237] C. Alabert *et al.*, "Nascent chromatin capture proteomics determines chromatin dynamics during DNA replication and identifies unknown fork components," *Nat. Cell Biol.*, vol. 16, no. 3, pp. 281–291, Mar. 2014.

[238] C.-F. Pereira *et al.*, "Induction of a hemogenic program in mouse fibroblasts.," *Cell Stem Cell*, vol. 13, no. 2, pp. 205–18, Aug. 2013.

[239] P. Rasighaemi, S. M. N. Onnebo, C. Liongue, and A. C. Ward, "ETV6 (TEL1) regulates embryonic hematopoiesis in zebrafish.," *Haematologica*, vol. 100, no. 1, pp. 23–31, Jan. 2015.

[240] H. Hock *et al.*, "Tel/Etv6 is an essential and selective regulator of adult hematopoietic stem cell survival.," *Genes Dev.*, vol. 18, no. 19, pp. 2336–41, Oct. 2004.

[241] W. Takahashi, K. Sasaki, N. Komatsu, and K. Mitani, "TEL/ETV6 accelerates erythroid differentiation and inhibits megakaryocytic maturation in a human leukemia cell line UT-7/GM," *Cancer Sci.*, vol. 96, no. 6, pp. 340–348, Jun. 2005.

[242] M. Eguchi-Ishimae *et al.*, "Leukemia-related transcription factor TEL/ETV6 expands erythroid precursors and stimulates hemoglobin synthesis," *Cancer Sci.*, vol. 100, no. 4, pp. 689–697, Apr. 2009.

[243] R. G. Lopez, C. Carron, C. Oury, P. Gardellin, O. Bernard, and J. Ghysdael, "TEL is a sequence-specific transcriptional repressor.," *J. Biol. Chem.*, vol. 274, no. 42, pp. 30132–8, Oct. 1999.

[244] P. Boccuni, D. MacGrogan, J. M. Scandura, and S. D. Nimer, "The Human L(3)MBT Polycomb Group Protein Is a Transcriptional Repressor and Interacts Physically and Functionally with TEL (ETV6)," *J. Biol. Chem.*, vol. 278, no. 17, pp. 15412–15420, Apr. 2003.

[245] I. Nordentoft and P. Jørgensen, "The acetyltransferase 60 kDa trans-acting regulatory protein of HIV type 1-interacting protein (Tip60) interacts with the translocation E26 transforming-specific leukaemia gene (TEL) and functions as a transcriptional co-repressor.," *Biochem. J.*, vol. 374, no. Pt 1, pp. 165–73, Aug. 2003.

[246] T. Sakurai *et al.*, "Effects of overexpression of the Ets family transcription factor TEL on cell growth and differentiation of K562 cells.," *Int. J. Oncol.*, vol. 22, no. 6, pp. 1327–33, Jun. 2003.

[247] R. Fenrick *et al.*, "TEL, a putative tumor suppressor, modulates cell growth and cell morphology of ras-transformed cells while repressing the transcription of stromelysin-1.," *Mol. Cell. Biol.*, vol. 20, no. 16, pp. 5828–39, Aug. 2000.

[248] B. J. Irvin *et al.*, "TEL, a Putative Tumor Suppressor, Induces Apoptosis and Represses Transcription of Bcl-X $_L$," *J. Biol. Chem.*, vol. 278, no. 47, pp. 46378–46386, Nov. 2003.

[249] T. Yamagata, K. Maki, K. Waga, and K. Mitani, "TEL/ETV6 induces apoptosis in 32D cells through p53-dependent pathways," *Biochem. Biophys. Res. Commun.*, vol. 347, no. 2, pp. 517–526, Aug. 2006.

[250] G. Boily, J. Larose, S. Langlois, and D. Sinnett, "Identification of transcripts modulated by ETV6 expression," *Br. J. Haematol.*, vol. 136, no. 1, pp. 48–62, Jan. 2007.

[251] L. Van Rompaey, M. Potter, C. Adams, and G. Grosveld, "Tel induces a G1 arrest and suppresses Ras-induced transformation," *Oncogene*, vol. 19, no. 46, pp. 5244–5250, Nov. 2000.

[252] A. Unnikrishnan *et al.*, “A quantitative proteomics approach identifies ETV6 and IKZF1 as new regulators of an *ERG* -driven transcriptional network,” *Nucleic Acids Res.*, vol. 44, no. 22, pp. 10644–10661, Dec. 2016.